

MATHEMATICAL MODELLING OF BLAST FURNACE

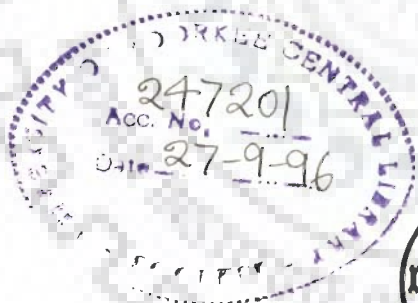
A THESIS

*submitted in fulfilment of the
requirements for the award of the degree*

of
DOCTOR OF PHILOSOPHY
in
CHEMICAL ENGINEERING

By

SMT. SHASHI



DEPARTMENT OF CHEMICAL ENGINEERING
UNIVERSITY OF ROORKEE
ROORKEE-247 667, INDIA

JULY, 1993



TO

MY PARENTS

In whom courage, devotion, and earnest efforts for intellectual pursuits of their children, beautifully combined to form the quintessence of life

Their inspiration

sustained me through the protracted evolution of this work.

CANDIDATE'S DECLARATION

I hereby certify that the work which is being presented in the thesis entitled **MATHEMATICAL MODELLING OF BLAST FURNACE** in fulfilment of the requirement for the award of the **Degree of Doctor of Philosophy** and submitted in the Department of Chemical Engineering of the University is an authentic record of my own work carried out during a period from September 1987 to July 1993 under the supervision of **Dr. M.L. Kapoor and Dr. S.D. Bhattacharya.**

The matter presented in this thesis has not been submitted by me for the award of any other degree of this or any other University.

Shashi
(Smt. Shashi)

This is to certify that the above statement made by the candidate is correct to the best of our knowledge.

S.D. Bhattacharya
(Dr. S.D. Bhattacharya)
Professor
Deptt. of Chemical Engg.
University of Roorkee

M.L. Kapoor
(Dr. M.L. Kapoor)
Professor
Deptt. of Metallurgical Engg.
University of Roorkee

Date : July 30, 1993

The Ph.D. Viva-Voce examination of Smt. Shashi, Research Scholar, has been held on *May 12, 1994*.

S.D. Bhattacharya
Signatures of
Supervisors

M.L. Kapoor
Signature of
Head, CHED

B.P. Chakraborty
Signature of
External Examiner

ABSTRACT

Blast furnace is a moving bed noncatalytic reactor, used widely for producing pig iron. Burden feed consisting of iron ore, coke and flux enters the furnace from top and moves downwards. While the hot air blast introduced through the tuyeres at the bottom of furnace, moves upwards. Many transfer and rate processes take place during the countercurrent sojourn of gas and solids in the furnace. Overall process of making pig iron requires large amount of heat, which is supplied by the hot gases produced during the combustion of coke with hot air blast. Due to the increasing emphasis on energy conservation and pollution control, there is a need to understand and analyse the blast furnace process so that the problems associated with its operation, design and control could be solved.

Mathematical modelling is an attractive tool for the analysis and simulation of systems as the models are based upon fundamental laws of conservation of mass, momentum and energy. Properly formulated models provide sufficient insight about the processes occurring in the system and also assist in quantifying them. Thus, it is desirable to develop a mathematical model of the complex blast furnace process.

In the present thesis, a One-dimensional mathematical model of the shaft region of blast furnace has been developed. The shaft encompasses stack, belly and bosh. Its model consists of ten nonlinear partial differential equations (time-dependent convection equations), one ordinary differential equation and four algebraic equations. In the model eight chemical reactions have been considered, which also include the reaction of SiO gas with carbon dissolved in molten pig iron. This model is capable of predicting the behaviour and performance under

unsteady state as well as steady state operations. For its numerical solution, initial and boundary conditions, and appropriate constitutive relationships are required.

In view of the above, a procedure for computing the material and energy balances of a blast furnace has been developed and programmed. The program calculates the boundary conditions of the proposed mathematical model by using the generally available plant data and also computes the parameters of streams, which are difficult to measure and are normally not known. During the process few significant results and relationships have also been obtained, which are mentioned below.

- A methodology for computing the molar flow rate of SiO gas formed in the combustion zone.
- An empirical relationship for calculating the melting temperature of coke ash for the specified Al_2O_3 and SiO_2 contents.
- Simplified relationships for the direct calculation of adiabatic flame temperature, tuyere gas temperature, and top gas temperature.

Besides, it has been clearly demonstrated by computations that the tuyere gas temperature is approximately 250 K less than the adiabatic flame temperature. Hence, it is not advisable to use adiabatic flame temperature in place of tuyere gas temperature in modelling studies.

Constitutive relationships play an important role in modelling and simulation of engineering systems. For blast furnace process, their number is quite large. Correlations for various parameters used in the model have been discussed and derived. Their limitations have also been pointed out. Further, the heat of reaction varies with temperature, and there exists wide variation in temperature within the furnace. Therefore, the correlations for heats of reactions as a function of temperature have been derived so that the effect of variation in heats

of reactions on the behaviour of furnace could be studied.

The model has been transformed into steady state model by setting time derivatives equal to zero. Resulting model equations consist of eleven nonlinear ordinary differential equations. In the present work, it was decided to obtain the numerical solution of the model under steady state conditions only. These model equations constitute a Boundary Value Problem (BVP), which is generally difficult to solve in comparison to an Initial Value Problem (IVP). Since developed model consists of many adjustable parameters pertaining to the maldistribution of gas and solids, and uncertainties associated with the constitutive relationships, therefore, the model equations have been solved as an IVP and the iterations have been stopped by matching the calculated and given boundary conditions at one of the end. A computer program has been developed for the simulation of steady state model. It has been our experience that the numerical solution of the model is very sensitive to the adjustable parameters and slight variation in their values might lead to nonconvergence of the numerical scheme adapted to solve it as a BVP.

An industrial blast furnace was selected for testing the model predictions. Its dimensions and four sets of operating data were taken from the literature. In order to ascertain the correctness of the proposed model, longitudinal profiles of all the process variables, namely compositions, fractional conversions, temperatures and pressure have been computed, and are in accordance with those reported in the literature. These have also been explained on the basis of assumptions underlying the model.

It has been observed that the change in heats of reactions as a result of variation in temperature has appreciable effect on the model predictions in higher temperature zones (1000 K or above). Therefore, it is necessary to account for this effect in the model. This conclusion is in contrast to most of the earlier modelling studies in

which heats of reactions were considered constant and taken at the reference temperature (298 K).

It is our view that the proposed model may be used for the analysis of blast furnace process and optimization of its productivity, provided actual plant data could be made available for estimating the adjustable parameters of the model. Then the model may also be used for studying its dynamic behaviour and developing suitable control strategies.



ACKNOWLEDGEMENTS

I express my profound sense of gratitude to my supervisors, Dr. M. L. Kapoor, Professor, Department of Metallurgical Engineering, and Dr. S. D. Bhattacharya, Professor, Department of Chemical Engineering, University of Roorkee, for their constant inspiration, encouragement and guidance throughout the course of this research work. Their personal involvement at difficult stages of the work helped me greatly in completing the thesis.

It is my privilege to express my gratitude and respect to Dr. I. M. Mishra, Professor and Head, Department of Chemical Engineering, University of Roorkee, for his constant encouragement, moral support and providing all necessary research facilities.

I am deeply indebted to my friends Mrs. Surekha Bhanot and Mr. R. K. Vyas for their assistance, constructive suggestions, discussions and above all the affection rendered in the completion of this work. Many times in assisting me, they had foregone their own research work, which was necessary and at a critical stage. Their patience in going through the typed manuscript leave me in short of words to acknowledge. I would ever remain grateful to them.

I express my sincere thanks to Mr. Akhilesh Kumar Sharma and Mr. Rakesh Kumar for their regular assistance and untiring efforts in typing and xeroxing the manuscript.

I am also grateful to all those who assisted me directly or indirectly in the completion of thesis.

The University Grants Commission, New Delhi, had awarded me a Senior Research Fellowship for carrying out this research work. Their financial support is gratefully acknowledged.

Shashi
(Smt. Shashi)



CONTENTS

ABSTRACT	i
ACKNOWLEDGEMENTS	v
CONTENTS	vii
LIST OF FIGURES	xv
LIST OF TABLES	xix
NOMENCLATURE	xxi
CHAPTER I INTRODUCTION	1
1.1 Objectives	5
1.2 Organization of Thesis	7
CHAPTER II LITERATURE REVIEW	9
2.0 Introduction	9
2.1 Blast Furnace	9
2.1.1 Raw Materials	10
2.1.1.1 Iron Ores	11
2.1.1.2 Fuel	12
2.1.1.3 Fluxes	13
2.1.1.4 Manganese Ore	14
2.1.1.5 Hot Air Blast	15
2.1.2 Blast Furnace Operation	16
2.1.2.1 Combustion Zone	17
2.1.2.2 Direct Reduction and Melting Zone	23
2.1.2.3 Thermal Reserve Zone	26
2.1.2.4 Preheating Zone	28

2.2	Blast Furnace Models	29
2.2.1	Thermodynamic Models	30
2.2.2	Kinetic Models	32
2.2.3	Transport Control Models	33
2.2.3.1	Steady State Models	34
2.2.3.2	Unsteady State Models	39
2.3	Motivation for the Present Study	41
2.4	Concluding Remarks	42
CHAPTER III	MATERIAL AND ENERGY BALANCE COMPUTATIONS	45
3.0	Introduction	45
3.1	Material Balance	46
3.1.1	Overall Material Balance	46
3.1.1.1	Component Material Balance	49
3.1.1.2	Solution Methodology	54
3.1.1.3	Results and Discussion	56
3.1.2	Rate of SiO Gas Generation in Combustion Zone	56
3.1.2.1	Methodology	61
3.1.2.2	Results and Discussion	66
3.1.3	Material Balance Around Combustion Zone	71
3.1.3.1	Methodology	72
3.1.3.2	Results	75
3.2	Energy Balance	75

	ix
3.2.1 Adiabatic Flame Temperature	75
3.2.1.1 Solution Methodology and Results	82
3.2.2 Tuyere Gas Temperature	86
3.2.2.1 Results	92
3.2.3 Top Gas Temperature	93
3.2.3.1 Solution Methodology and Results	103
3.3 Computer Program	105
3.4 Concluding Remarks	105
CHAPTER IV DEVELOPMENT OF MATHEMATICAL MODEL OF BLAST FURNACE	109
4.0 Introduction	109
4.1 Premises for Modelling	109
4.1.1 Assumptions	110
4.1.2 Chemical Reactions	114
4.2 Dynamic Model Equations	116
4.2.1 Differential Component Mass Balance Equations	117
4.2.1.1 Component Mass Balance for Solid Fe_2O_3	118
4.2.1.2 Component Mass Balance for CO Gas	119
4.2.1.3 Other Component Mass Balances	121

4.2.2	Differential Energy Balance Equations	123
4.2.2.1	Energy Balance for Gas Phase	124
4.2.2.2	Energy Balance for Solid Phase	127
4.2.3	Differential Pressure Drop Equation	130
4.2.4	Algebraic Equations	131
4.2.4.1	Equation for Volumetric Flow Rate of Gas (F_g)	132
4.2.4.2	Equation for Density of Gas (ρ_g)	132
4.2.4.3	Equation for Density of Solids (ρ_b)	133
4.2.4.4	Equation for Diameter (D_z) and Cross-sectional Area (A_z) of the Furnace	133
4.2.4.5	Equation for Mole Fraction of H_2O (y_{H_2O})	134
4.2.4.6	Initial Concentration of FeO (C_{wo})	135
4.2.5	Initial and Boundary Conditions	135
4.2.6	Constitutive Relationships	136
4.3	Steady State Model	136
4.4	Concluding Remarks	138
CHAPTER V	CORRELATIONS FOR PARAMETERS USED IN THE MODEL	139
5.0	Introduction	139
5.1	Properties of Solids	139
5.1.1	Volumetric Flow Rate of Burden Feed	139
5.1.2	Average Diameter of Solid Particles	140
5.1.3	Average Shape Factor for Solid Particles	141

5.1.4	Average Porosity of Iron Bearing Solid Particles	141
5.1.5	Total Surface Area of Iron Bearing Solid Particles in Unit Volume of Bed	142
5.1.6	Number of Solid Particles in Unit Volume of Bed	142
5.1.7	Initial Concentration of Components in Solids	142
5.1.8	Heat Capacities of Solids in Burden Feed	143
5.2	Properties of Gas Mixture	144
5.2.1	Viscosity of Gas Mixture	145
5.2.2	Thermal Conductivity of Gas Mixture	145
5.2.3	Average Heat Capacity of Gas Mixture	146
5.3	Heat Transfer Coefficient Between Solid and Gas	147
5.4	Overall Heat Transfer Coefficient for Heat Loss Through Furnace Wall	148
5.5	Heats of Reactions	148
5.5.1	Indirect Reduction of Fe_2O_3 by CO	150
5.5.2	Solution Loss Reaction	150
5.5.3	Direct Reduction of Molten FeO	151
5.5.4	Decomposition of CaCO_3	151
5.5.5	Indirect Reduction of Fe_2O_3 by H_2	152
5.5.6	Water Gas Reaction	153
5.5.7	Water Gas Shift Reaction	153
5.5.8	Reduction of SiO Gas	153
5.6	Overall Reaction Rates	154
5.6.1	Gas-Solid Reactions	154
5.6.2	Indirect Reduction of Iron Ore by CO	158

5.6.3	Solution Loss Reaction	161
5.6.4	Direct Reduction of Molten FeO	163
5.6.5	Decomposition of Limestone	165
5.6.6	Indirect Reduction of Iron Ore by H ₂	167
5.6.7	Water Gas Reaction	170
5.6.8	Water Gas Shift Reaction	173
5.6.9	Reduction of SiO Gas	173
5.7	Concluding Remarks	176
CHAPTER VI NUMERICAL SOLUTION OF THE MODEL, RESULTS AND DISCUSSION		177
6.0	Introduction	177
6.1	Numerical Solution of the Model	177
6.1.1	Runge-Kutta-Fehlberg Formulas	181
6.1.2	Procedure	183
6.1.3	Computer Program	183
6.1.4	Selection of Step-size	185
6.2	Results and Discussion	185
6.2.1	Experiences with Numerical Simulation and Necessity of Adjustable Parameters	186
6.2.2	Longitudinal Distribution of Process Variables	193
6.2.2.1	Profiles of Temperature of Gas and Solid	193
6.2.2.2	Profiles of Fractional Conversion of Fe ₂ O ₃ , Lime, Coke Carbon and FeO	220

6.2.2.3	Profiles of Mole Fraction of CO, CO ₂ and H ₂	221
6.2.2.4	Profiles of Per Cent Conversion of SiO Gas	224
6.2.2.5	Profiles of Gas Pressure	229
6.2.3	Effect of Variation in Heat of Reaction(due to change in temperature) on the Behaviour of Blast Furnace	230
6.3	Concluding Remarks	248
CHAPTER VII CONCLUSIONS AND RECOMMENDATION		253
7.1	Conclusions	253
7.1.1	Model Equations	253
7.1.2	Boundary and Initial Conditions	254
7.1.3	Constitutive Relationships	258
7.1.4	Numerical Solution of Model Equations and Computer Programs	258
7.1.5	Validation of the Model	259
7.1.6	Effect of Variation in Heat of Reaction on the Behaviour of Blast Furnace	260
7.1.7	Final Remark	260
7.2	Recommendations for Future Work	260
	REFERENCES	263
APPENDIX A	PHYSICAL PROPERTIES AND DIMENSIONS	273
APPENDIX B	RUNGE-KUTTA-FEHLBERG FORMULAS FOR SYSTEM OF ORDINARY DIFFERENTIAL EQUATIONS	285

LIST OF FIGURES

1.1	A Schematic Diagram of Blast Furnace	3
2.1	Thermal and Chemical Process Zones with Temperature Distribution of Gas and Solids along the Height of Blast Furnace	19
2.2	A Schematic Plan View of the Combustion Zone at the Tuyere Level of a Blast Furnace	21
3.1	Block Diagram of Simplified Blast Furnace Process Showing Input and Output Streams at Different Heights	47
3.2	Variation of Melting Temperature of Coke Ash with SiO_2 and Al_2O_3 Contents	63
3.3	Comparison of Observed and Predicted Melting Temperatures of Coke Ash [Equation (3.13)]	67
4.1	Schematic Diagram of the Shaft Used in Modelling	111
6.1	Longitudinal Profiles of Temperature of Gas and Solid (Operating Data Set-1)	195
6.2	Longitudinal Profiles of Fractional Conversion of Fe_2O_3 , Lime, Coke Carbon and FeO (Operating Data Set-1)	197
6.3	Longitudinal Profiles of Mole Fraction of CO , CO_2 and H_2 (Operating Data Set-1)	199
6.4	Longitudinal Profiles of Temperature of Gas and Solid (Operating Data Set-2)	201

6.5	Longitudinal Profiles of Fractional Conversion of Fe_2O_3 , Lime, Coke Carbon and FeO (Operating Data Set-2)	203
6.6	Longitudinal Profiles of Mole Fraction of CO , CO_2 and H_2 (Operating Data Set-2)	205
6.7	Longitudinal Profiles of Temperature of Gas and Solid (Operating Data Set-3)	207
6.8	Longitudinal Profiles of Fractional Conversion of Fe_2O_3 , Lime, Coke Carbon and FeO (Operating Data Set-3)	209
6.9	Longitudinal Profiles of Mole Fraction of CO , CO_2 and H_2 (Operating Data Set-3)	211
6.10	Longitudinal Profiles of Temperature of Gas and Solid (Operating Data Set-4)	213
6.11	Longitudinal Profiles of Fractional Conversion of Fe_2O_3 , Lime, Coke Carbon and FeO (Operating Data Set-4)	215
6.12	Longitudinal Profiles of Mole Fraction of CO , CO_2 and H_2 (Operating Data Set-4)	217
6.13	Comparison of Longitudinal Profiles of Per Cent Conversion of SiO Gas, Obtained with Variable Heat of Reaction for All the Four Operating Data Sets	225
6.14	Longitudinal Profiles of Gas Pressure for All the Four Operating Data Sets	231

6.15	Longitudinal Profiles of Temperature of Gas and Solid with Constant Heat of Reaction (Operating Data Set-1)	233
6.16	Longitudinal Profiles of Fractional Conversion of Fe_2O_3 , Lime, Coke Carbon and FeO with Constant Heat of Reaction (Operating Data Set-1)	235
6.17	Longitudinal Profiles of Mole Fraction of CO , CO_2 and H_2 with Constant Heat of Reaction (Operating Data Set-1)	237
6.18	Comparison of Longitudinal Profiles of Temperatures of Gas and Solid, Obtained with Constant and Variable Heat of Reaction (Operating Data Set-1)	241
6.19	Comparison of Longitudinal Profiles of Fractional Conversions of $\text{Fe}_2\text{O}_3 / \text{FeO}$ and Coke Carbon, Obtained with Constant and Variable Heat of Reaction (Operating Data Set-1)	243
6.20	Comparison of Longitudinal Profiles of Mole Fractions of CO and CO_2 , Obtained with Constant and Variable Heat of Reaction (Operating Data Set-1)	245
6.21	Comparison of Longitudinal Profiles of Per Cent Conversion of SiO Gas, Obtained with Constant and Variable Heat of Reaction (Operating Data Set-1)	249
6.22	Comparison of Longitudinal Profiles of Gas Pressure, Obtained with Constant and Variable Heat of Reaction (Operating Data Set-1)	251

LIST OF TABLES

3.1	Composition of Materials in Solid Feed	51
3.2	Composition of Flue Dust, Pig Iron and Slag	51
3.3	Process Variables for Blast Furnace at B.S.P.	57
3.4	Comparison of Computed Results by Material Balance Program with Observed Data	59
3.5	Computed Results for SiO Gas Formation at Tuyere Level	69
3.6	Computed Results for Flow Conditions at the Bottom of Bosh	77
3.7	Comparison of Adiabatic Flame Temperature Computed by Newton Raphson Method and Approximate Relationship	83
3.8	Average Heat Capacities of Substances	87
3.9	Computed Results for Tuyere Gas Temperature	95
3.10	Comparison of Top Gas Temperature Computed by Newton Raphson Method and Approximate Relationship	95
3.11	Subroutines for Material and Energy Balance Computations	107

6.1	Boundary Conditions for the Mathematical Model	187
6.2	Adjustable Parameter (β_5) and Residence Time of Solids for Operating Data Sets	191
6.3	Per Cent Si Content in Metal	227
6.4	Heats of Reactions at Reference Temperature (298 K)	239
7.1	Summary of Model Equations	255
A.1	Specific Heats of Substances	273
A.2	Heats of Fusion of Substances	277
A.3	Heats of Formation of Substances	279
A.4	Molecular Weights of Substances	281
A.5	Characteristics and Properties of Materials	283
A.6	Dimensions of the Shaft of Blast Furnace	283

NOMENCLATURE

A_{gm}	effective interfacial area for reduction of SiO gas, (m^2/m^3 (bed))
A_w	inner surface area between top of burden bed and tuyere level, (m^2)
A_z	cross sectional area of furnace at height z, (m^2)
a_2	parameter defined by equation (3.58a)
B	parameter used in equation (3.13)
b_2	parameter defined by equation (3.58b)
b_i	mass fraction of component i in coke ash, (-)
C	parameter used in equation (3.13)
C_{co}	initial concentration of carbon, ($kmol/m^3$ (bed))
C_{FeO}	molar concentration of FeO at any level in bosh, ($kcal/m^3$ (slag))
C_g	average heat capacity of gas mixture, ($kcal/kmol.K$)
C_h	molar concentration of Fe_2O_3 at any level, ($kmol/m^3$ (bed))
C_{ho}	initial concentration of Fe_2O_3 in solids, ($kmol/m^3$ (bed))
C_{Lo}	initial concentration of $CaCO_3$ in solids, ($kmol/m^3$ (bed))
CO2	CO ₂ used in Figures 6.3, 6.6, 6.9, 6.12, 6.17 and 6.20
C_s	average heat capacity of solid particles, ($kcal/kg.K$)
C_{wo}	initial concentration of FeO in bosh, ($kmol/m^3$ (bed))

c_2	parameter defined by equation (3.58c)
$(C)_i$	heat capacity of component i in solid used in Section 5.1.8, (kcal/kg.K)
$(C_p)_i$	heat capacity of component i , (kcal/kmol.K)
$(C_p)_{\text{pig}}$	heat capacity of pig iron, (kcal/kg.K)
$(C_p)_{\text{slag}}$	heat capacity of slag, (kcal/kg.K)
$(C_s)_B$	heat capacity of solid burden, (kcal/kg.K)
$(C_s)_C$	heat capacity of coke, (kcal/kg.K)
$(C_s)_L$	heat capacity of limestone, (kcal/kg.K)
$(C_s)_O$	heat capacity of iron ore, (kcal/kg.K)
$(C_s)_{OM}$	heat capacity of manganese ore, (kcal/kg.K)
$(C_s)_{OP}$	heat capacity of pellets, (kcal/kg.K)
$(C_s)_{OS}$	heat capacity of sinter, (kcal/kg.K)
D_b	inner diameter of belly, (m)
D_h	inner diameter of hearth, (m)
D_i	diffusion coefficient of component i in blast furnace gas, (m^2/hr)
D_o	inner diameter of throat, (m)
D_{s1}	intraparticle diffusion coefficient of CO in reduced iron phase, (m^2/hr)
D_{s2}	intraparticle diffusion coefficient of CO_2 in coke, (m^2/hr)

D_{s4}	intraparticle diffusion coefficient of CO_2 in decomposed phase of limestone, (m^2/hr)
D_{s5}	intraparticle diffusion coefficient of H_2 in reduced iron phase, (m^2/hr)
D_{s6}	intraparticle diffusion coefficient of H_2O in coke, (m^2/hr)
D_z	inner diameter of furnace at height z , (m)
d_c	average diameter of coke particles, (m)
d_i	average diameter of particles of solid i , (m)
d_L	average diameter of limestone particles, (m)
d_o	average diameter of iron ore particles, (m)
d_{oa}	average diameter of iron bearing solid particles, (m)
d_p	average diameter of solid particles, (m)
Ef_2	effectiveness factor for solution loss reaction, (-)
Ef_6	effectiveness factor for water gas reaction, (-)
F_0	volumetric flow rate of gas at top of furnace, (Nm^3/hr)
F_1	volumetric flow rate of gas at bottom of bosh, (Nm^3/hr)
$F_{\text{CO},2}$	volumetric flow rate of CO gas after coke combustion in front of tuyeres, (Nm^3/hr)
F_b	volumetric flow rate of blasted air, (Nm^3/min)
Fe203	Fe_2O_3 used in Figures 6.2, 6.5, 6.8, 6.11, 6.16 and 6.19
F_g	volumetric flow rate of gaseous mixture at any level in furnace, (Nm^3/hr)

$F_{i,1}$	volumetric flow rate of component i at bottom of bosh, (Nm^3/hr)
$F_{\text{FeO},m}$	molar flow rate of molten FeO, (kmol/hr)
F_{m_i}	molar flow rate of component i , (kmol/hr)
$F_{m_{i,1}}$	molar flow rate of component i at bottom of bosh, (kmol/hr)
F_s	volumetric flow rate of solid burden, (m^3/hr)
f_c	fractional conversion of coke carbon, (-)
f_L	fractional conversion of CaCO_3 , (-)
f_s	fractional conversion of Fe_2O_3 , (-)
f_{sn}	fractional conversion of FeO, (-)
G_g	mass velocity of gas at any level in furnace { $= F_g \rho_g / A_z$ }, ($\text{kg}/\text{m}^2 \cdot \text{hr}$)
g	acceleration due to gravity { $= 127.1376 \times 10^6$ }, (m/hr^2)
g_i	mass fraction of component i in manganese ore, (-)
H2	H_2 used in Figures 6.3, 6.6, 6.9, 6.12 and 6.17
H_L	fraction of heat energy lost through wall, (-)
$(\Delta H_R)_1$	heat of reaction of indirect reduction of Fe_2O_3 by CO, (kcal/kmol (CO))
$(\Delta H_R)_2$	heat of reaction of solution loss reaction, (kcal/kmol (CO_2))
$(\Delta H_R)_3$	heat of reaction of direct reduction of molten FeO, (kcal/kmol (FeO))

- $(\Delta H_R)_4$ heat of reaction of decomposition of lime
 (kcal/kmol (CaCO_3))
- $(\Delta H_R)_5$ heat of reaction of indirect reduction of Fe_2O_3 by H_2 ,
 (kcal/kmol (H_2))
- $(\Delta H_R)_6$ heat of reaction of water gas reaction,
 (kcal/kmol (H_2O))
- $(\Delta H_R)_7$ heat of reaction of water gas shift reaction,
 (kcal/kmol (H_2O))
- $(\Delta H_R)_8$ heat of reaction of reduction of SiO gas,
 (kcal/kmol (SiO))
- $(\Delta H_R)_{i,T}$ heat of reaction i at temperature T, (kcal/kmol)
- $(\Delta H)_i$ enthalpy change of reaction i, (kcal/kmol)
- h_{gs} heat transfer coefficient between solid and gas,
 (kcal/ $\text{m}^2 \cdot \text{hr} \cdot \text{K}$)
- j_i mass fraction of component i in flue dust, (-)
- K_1 equilibrium constant for indirect reduction of
 iron ore by CO, (-)
- K_4 equilibrium constant of decomposition of limestone, (atm)
- K_5 equilibrium constant of indirect reduction of
 iron ore by H_2 , (-)
- k_1 reaction rate constant of indirect reduction of
 iron ore by CO, (m/hr)
- k_2 reaction rate constant of solution loss reaction,
 ($\text{m}^3/\text{kg} \cdot \text{hr}$)

- k_3 reaction rate constant of direct reduction of molten FeO,
($m^4/kmol (FeO).hr$)
- k_4 reaction rate constant of decomposition of limestone,
($kmol (CO_2)/m^2.hr$)
- k_5 reaction rate constant of indirect reduction of
iron ore by H_2 , (m/hr)
- k_6 reaction rate constant of water gas reaction, ($m^3/kg.hr$)
- k_8 reaction rate constant of reduction of SiO gas,
($kmol/m^2 atm.hr$)
- kf_1 gas film mass transfer coefficient in indirect
reduction of iron ore by CO, (m/hr)
- kf_2 gas film mass transfer coefficient in
solution loss reaction, (m/hr)
- kf_4 gas film mass transfer coefficient in
decomposition of limestone, (m/hr)
- kf_5 gas film mass transfer coefficient in indirect
reduction of iron ore by H_2 , (m/hr)
- kf_6 gas film mass transfer coefficient in
water gas reaction, (m/hr)
- k_g thermal conductivity of blast furnace gas, (kcal/m.hr.K)
- L height between top of stack and tuyere level,
i.e. height of shaft, (m)
- L_b combined height of stack and belly, (m)
- L_s height of stack, (m)

l_i	mass fraction of component i in limestone, (-)
Lf_i	latent heat of fusion of component i , (kcal/kmol)
M_i	molecular weight of component i
M_g	molecular weight of gas mixture
m_2	Thiele modulus for solution loss reaction, (-)
m_6	Thiele modulus for water gas reaction, (-)
N_C	number of coke particles per unit volume of bed, ($1/m^3$ (bed))
N_L	number of limestone particles per unit volume of bed, ($1/m^3$ (bed))
P	pressure of gas in furnace, (atm)
P_i	mass fraction of component i in pellets, (-)
Pr	Prandtl number $\{ = C_g \mu_g / k_g M_g \}$, (-)
p_{SiO}	partial pressure of SiO gas, (atm)
Q_B	rate of input of sensible energy through solid burden, (kcal/hr)
Q_D	rate of output of sensible energy through flue dust, (kcal/hr)
Q_G	rate of total heat transfer from gas in combustion zone, (kcal/hr)
Q_M	rate of energy consumption for melting solid components in bosh, (kcal/hr)
Q_{MA}	rate of energy consumption for melting coke ash in combustion zone, (kcal/hr)

Q_R	rate of total heat of reaction in shaft, (kcal/hr)
Q_{RI}	rate of heat of reaction of direct reduction of Fe_2O_3 in combustion zone, (kcal/hr)
Q_S	rate of output of sensible energy through solids from bottom of bosh, (kcal/hr)
Q_{SA}	rate of heat of formation of slag from coke ash in combustion zone, (kcal/hr)
Q_{SL}	rate of heat of formation of slag in bosh, (kcal/hr)
Q_{SM}	rate of heat transfer from gas to molten materials in combustion zone, (kcal/hr)
Q_{SP}	rate of output of sensible energy through slag and pig iron, (kcal/hr)
Q_T	rate of output of sensible energy through top gas, (kcal/hr)
Q_{TG}	rate of input of sensible energy through tuyere gas, (kcal/hr)
Q_{VSI}	rate of heat of reaction of SiO gas formation in combustion zone, (kcal/hr)
Q_W	rate of heat losses through wall of furnace, (kcal/hr)
R	universal gas constant { = 1.987 }, (kcal/kmol.K)
R'	universal gas constant { = 0.08206 }, (atm. m^3 /kmol.K)
R_1	overall reaction rate of indirect reduction of iron ore by CO, (kmol (CO)/ m^3 (bed).hr)

- R_2 overall reaction rate of solution loss reaction,
($\text{kmol (CO}_2\text{)}/\text{m}^3(\text{bed}).\text{hr}$)
- R_3 overall reaction rate of direct reduction of molten FeO,
($\text{kmol (FeO)}/\text{m}^3(\text{bed}).\text{hr}$)
- R_4 overall reaction rate of decomposition of limestone,
($\text{kmol (CaCO}_3\text{)}/\text{m}^3(\text{bed}).\text{hr}$)
- R_5 overall reaction rate of indirect reduction of
iron ore by H_2 , ($\text{kmol (H}_2\text{)}/\text{m}^3(\text{bed}).\text{hr}$)
- R_6 overall reaction rate of water gas reaction
($\text{kmol (H}_2\text{O)}/\text{m}^3(\text{bed}).\text{hr}$)
- R_7 overall reaction rate of water gas shift reaction,
($\text{kmol (H}_2\text{O)}/\text{m}^3(\text{bed}).\text{hr}$)
- R_8 overall reaction rate of reduction of SiO gas,
($\text{kmol (SiO)}/\text{m}^3(\text{bed}).\text{hr}$)
- Re_p Reynolds number based on particle diameter $\{ = d_p G_g / \mu_g \}$,
(-)
- r_{Fe} mass fraction of Fe in slag, (-)
- S_3 specific surface area of coke available for direct reduction
of molten FeO ($\text{m}^2/\text{m}^3(\text{bed})$)
- Sc Schmidt number $\{ = \mu_g / \rho_g D_i \}$, (-)
- S_o total surface area of iron bearing solid particles in bed,
($\text{m}^2/\text{m}^3(\text{bed})$)
- s_i mass fraction of component i in sinter, (-)
- T_1 adiabatic flame temperature of gas, (K)

xxx

T_b	temperature of blasted air, (K)
T_c	temperature of coke entering the combustion zone, (K)
T_g	temperature of gas at any level in furnace, (K)
$T_{g,0}$	temperature of gas at top of furnace, (K)
$T_{g,1}$	temperature of gas at bottom of bosh, (K)
T_{gm}	arithmetic mean of gas and solid temperatures [$(T_g + T_s) / 2$], (K)
T_m	melting temperature of ash, (K)
T'_m	melting temperature of ash, ($^{\circ}\text{C}$)
T_o	reference temperature, (K)
T_p	temperature of pig iron, (K)
T_s	temperature of solids at any level in furnace, (K)
$T_{s,0}$	temperature of burden feed, (K)
T_{sl}	temperature of slag, (K)
T_{st}	temperature of steam injected with air, (K)
T_{wc}	temperature of cooling water, (K)
t	time, (hr)
t_a	mass fraction of ash in coke, (-)
t_c	mass fraction of carbon in coke, (-)
U	overall coefficient for heat transfer through furnace wall based on inner surface area, ($\text{kcal}/\text{m}^2 \cdot \text{hr} \cdot \text{K}$)

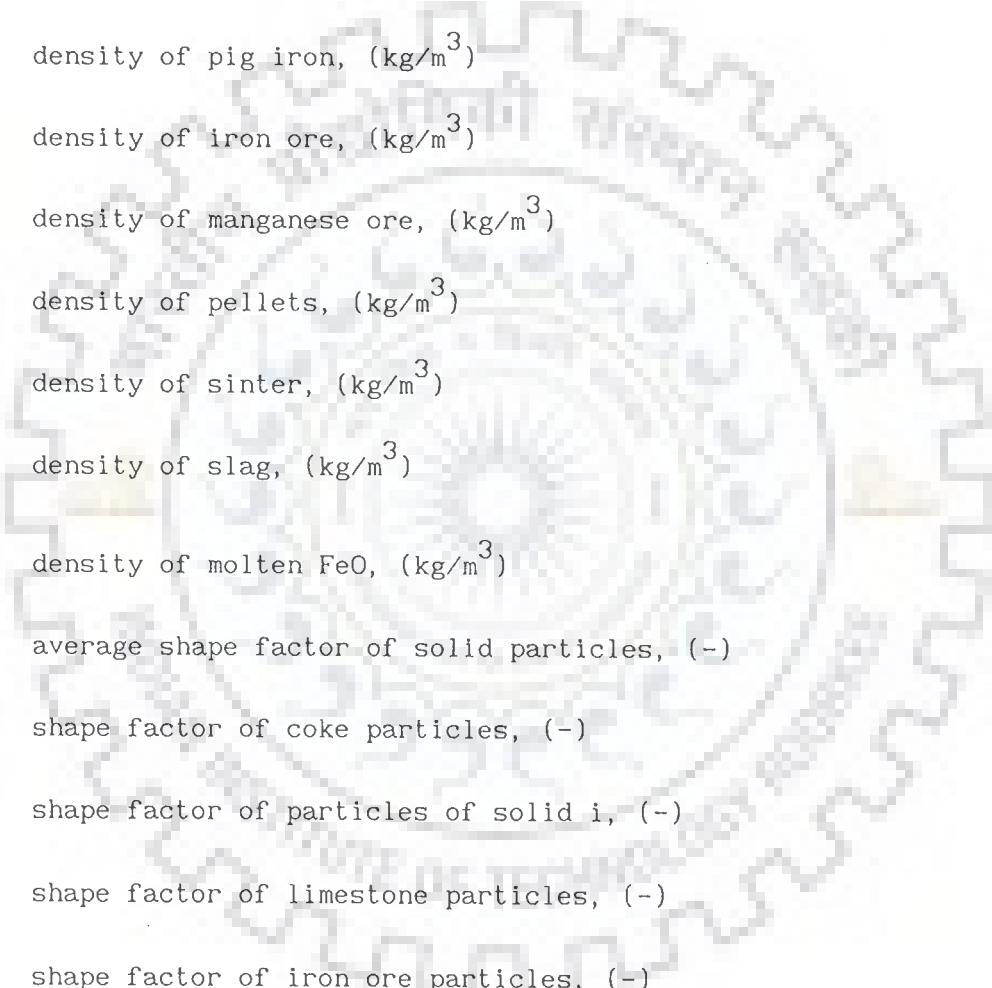
V_B	combined volume of bosh and belly which contains fused and molten materials, (m^3)
v_i	mass fraction of component i in iron ore, (-)
W_C	mass flow rate of coke, (kg/hr)
$W_{C,1}$	mass flow rate of solids at bottom of bosh, (kg/hr)
W_D	mass flow rate of flue dust, (kg/hr)
W_i	mass flow rate of component i in solids, (kg/hr)
W_L	mass flow rate of limestone, (kg/hr)
W_O	mass flow rate of iron ore, (kg/hr)
W_{OM}	mass flow rate of manganese ore, (kg/hr)
W_{OP}	mass flow rate of pellets, (kg/hr)
W_{OS}	mass flow rate of sinter, (kg/hr)
W_P	mass flow rate of pig iron, (kg/hr)
$W_{P,1}$	mass flow rate of pig iron at bottom of bosh, (kg/hr)
W_S	mass flow rate of slag, (kg/hr)
W_{st}	mass of steam in blasted air, (g/Nm^3 (blast))
$W_{S,1}$	mass flow rate of slag at bottom of bosh, (kg/hr)
X_A	mass fraction of SiO_2 in ash defined by equation (3.14), (-)
$X_{Al_2O_3}$	mass fraction of Al_2O_3 in ash defined by equation (3.15), (-)
X_{O_2}	ratio of oxygen enrichment, ($Nm^3(O_2)/Nm^3$ (blast))

X_{SiO_2}	mass fraction of SiO_2 in ash defined by equation (3.14a), (-)
Y_{CO}	y_{CO} used in Figures 6.3, 6.6, 6.9, 6.12 and 6.17
Y_{CO_2}	y_{CO_2} used in Figures 6.3, 6.6, 6.9, 6.12 and 6.17
Y_{H_2}	y_{H_2} used in Figures 6.3, 6.6, 6.9, 6.12 and 6.17
y_i	mole fraction of component i in gas at any level in furnace, (-)
$y_{i,0}$	mole fraction of component i in gas at top of furnace, (-)
$y_{i,1}$	mole fraction of component i in gas at bottom of bosh, (-)
y_{CO}^*	equilibrium mole fraction of CO for indirect reduction of iron ore by CO , (-)
$y_{\text{CO}_2}^*$	equilibrium mole fraction of CO_2 for decomposition of limestone, (-)
$y_{\text{H}_2}^*$	equilibrium mole fraction of H_2 for indirect reduction of iron ore by H_2 , (-)
z	axial distance from top of the shaft, (m)

GREEK LETTERS

α_{Fe}	mass fraction of Fe in pig iron, (-)
α_i	mass fraction of component i in pig iron, (-)
β_1	stack angle (degree)
β_2	bosh angle (degree)

β_3	conditional parameter for fusion of solids, (-)
β_4	adjustable parameter for heat transfer coefficient used in equation (5.16), (-)
β_5	adjustable parameter for D_z , (-)
β_8	adjustable parameter for rate constant k_8 , (-)
ϵ	porosity of bed, (-)
ϵ_c	average porosity of coke particles, (-)
ϵ_i	average porosity of particles of solid i , (-)
ϵ_L	average porosity of limestone particles, (-)
ϵ_o	average porosity of iron ore particles, (-)
ϵ_p	average porosity of iron bearing particles, (-)
ϵ_{VL}	porosity of decomposed layer of CaO, (-)
ϵ_{vo}	porosity of reduced iron layer, (-)
θ	a dimensionless variable $\{= T_1/1000\}$, (-)
θ_1	a dimensionless variable $\{= T_{g,0}/100\}$, (-)
μ_g	viscosity of gas mixture, (kg/m.hr)
ξ_c	labyrinth factor of coke, (-)
ξ_L	labyrinth factor of limestone for decomposed CaO layer, (-)
ξ_o	labyrinth factor of iron ore for reduced iron layer, (-)
ρ_b	bulk density of solids in bed at any level in furnace, (kg/m ³ (bed))



ρ_C	density of coke, (kg/m^3)
ρ_g	density of gas mixture at any level in furnace, (kg/Nm^3)
ρ_i	density of solid i, (kg/m^3)
ρ_L	density of limestone, (kg/m^3)
ρ_m	density of pig iron, (kg/m^3)
ρ_O	density of iron ore, (kg/m^3)
ρ_{OM}	density of manganese ore, (kg/m^3)
ρ_{OP}	density of pellets, (kg/m^3)
ρ_{OS}	density of sinter, (kg/m^3)
ρ_{s1}	density of slag, (kg/m^3)
ρ_w	density of molten FeO , (kg/m^3)
ϕ	average shape factor of solid particles, (-)
ϕ_C	shape factor of coke particles, (-)
ϕ_i	shape factor of particles of solid i, (-)
ϕ_L	shape factor of limestone particles, (-)
ϕ_O	shape factor of iron ore particles, (-)

INTRODUCTION

Noncatalytic gas-solid reactions constitute an important class of heterogeneous reactions. Examples of these can be abundantly found in chemical and metallurgical processes such as sponge iron making, pig iron making, calcination of limestone, roasting of ores, coal gasification etc. Doraiswamy and Sharma (1984) have excellently summarized and discussed a variety of gas-solid reactions encountered in industry in their classical monograph on heterogeneous reactions. The importance of these reactions in the context of the increasing emphasis on pollution control and of the need to develop fuels from coal and to design metallurgical units with high efficiency cannot be overemphasized.

Most important and best known noncatalytic reactor is the blast furnace, which is used for producing pig iron. A schematic diagram of blast furnace is shown in Figure 1.1. In general, blast furnace is a vertical moving bed reactor. A mixture of solid materials, namely iron ore, coke and flux, is fed from the top of the furnace and hot air blast (along with auxiliary fuels, if any) is introduced through the tuyeres located on the sides above the hearth at the bottom of furnace. As the solids move down through the furnace, all of them except the coke melt and the resulting molten iron and slag drip slowly to the hearth. Most of the coke carbon combusts in front of tuyeres on contact with the incoming hot air blast. The product molten pig iron and molten slag come out of the spouts provided on the sides just above the bottom of the furnace. Slag is the product of the reaction of flux with unwanted gangue materials in the ores and coke ash. The gases produced leave the furnace from the top.

It is obvious from the above description of the blast furnace process that many exothermic and endothermic heterogeneous chemical reactions, phase transformations and exchange of heat from gases to solids and liquids take place simultaneously in the reactor. Occurrence of all these phenomena together make the blast furnace process complicated. Thus, there is a need to understand the blast furnace process so that the problems associated with its operation, design and control could be solved. In order to achieve these objectives, many models of the blast furnace have been developed by research workers. These may be broadly classified into the following three groups :

Thermodynamic Models

In these models blast furnace is divided into several zones and the chemical equilibrium is assumed in each zone. The models proposed by Reichardt (1927), Ridgion (1962), and Staib and Michard (1965) fall in this group.

Kinetic Models

Like models of first group, in the kinetic models the furnace is also divided into several zones and the temperatures in individual zones are assumed to be invariant. The reaction rates are also considered in the model. Such a model was developed by Flierman and Langen (1966).

Transport Control Models

Basic equations of models of this group are derived by taking energy and mass balances around a differential height of bed at any arbitrary level in the furnace. The rate of heat transfer between the fluid and solid particles, and the reaction rates are taken into account in these balances. These models are large in number and most of them have been reviewed and described in detail by Omori (1987). It is necessary to mention that Transport Control Models are also referred to as Transport Phenomena Models in the literature.

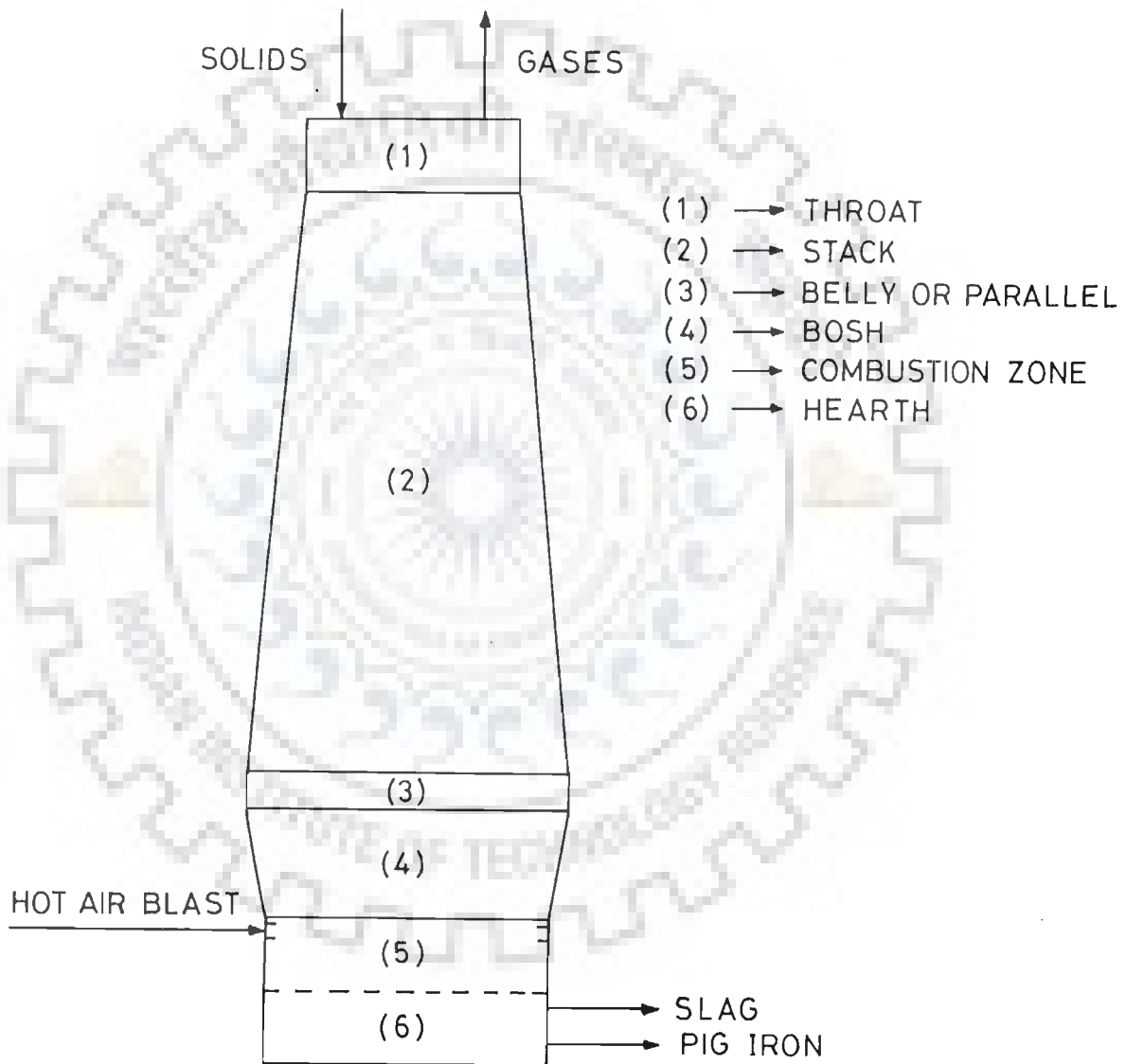


FIGURE 1:1 A SCHEMATIC DIAGRAM OF BLAST FURNACE

Beside these models, few models were proposed, which were totally based on the statistical analysis of observed data involving multivariant regression analysis. These models predict the internal situation of only that blast furnace for which data are collected.

Out of the above group of models, mostly transport phenomena or transport control models have been the subject of study in the past three decades as these could explain the blast furnace process significantly, and their predictions were quite reasonable, but they possess one or other limitation. Few authors have considered the furnace with invariant diameter, i.e. the furnace of cylindrical shape. But in the downward direction, diameter of furnace in stack region increases continuously while in bosh region it decreases. A large number of chemical reactions take place in the furnace; number of reactions considered varies from model to model. Heat of chemical reaction has been assumed to be constant in the models; in fact it varies appreciably with the temperature, particularly, when the range of temperature variation is large as is the case with the blast furnace, where temperature varies from 300 to 2200 K. Proposed models are one- or two-dimensional, steady state or dynamic in nature, and explain that aspect of the blast furnace process, for which they have been developed. Besides, models are specific to one of the two modes of feeding the solid burden, viz. mixed burden and layered burden. Improved theory of silica reduction in furnace is also available, which could not yet be included in a comprehensive model.

In view of the above, it is proposed to develop a mathematical model of the blast furnace process in the present thesis.

1.1 OBJECTIVES

The main objectives of the thesis are as follows :

(a) **Development of Mathematical Models**

To develop one-dimensional steady and unsteady state mathematical models of the blast furnace process for its shaft region, which consists of stack, belly and bosh.

(b) **Estimation of Boundary Conditions at the Inlet and Outlet Boundaries of the Shaft Region**

- (i) To develop a computational procedure for carrying out the overall material balance around the blast furnace, so that the consistency of available plant data could be checked.
- (ii) To determine the composition and flow rate of streams (which are not known), entering and leaving the shaft region.
- (iii) To develop the algorithms for estimating the temperatures of tuyere gas entering into the bosh and top gas leaving the stack.
- (iv) To develop an algorithm for estimating the rate of formation of SiO gas from coke ash in the combustion zone, which is required for SiO gas reduction in the bosh.

(c) **Development of Constitutive Relationships of the Model**

- (i) To develop the relationships for calculating the heat of reaction of different chemical reactions at any temperature in the furnace.
- (ii) To find out and develop the constitutive relationships for various other parameters used in the model.

(d) **Solution of Steady State Model Equations**

- (i) To obtain the numerical solution of steady state model equations for given sets of input data.
- (ii) To predict the longitudinal distribution of temperature, pressure and composition of gas, temperature of solids, and fractional conversions of iron oxide, lime, coke carbon and SiO gas.

- (iii) To analyse the model predictions vis-a-vis results reported in the literature and validate the model with the plant data.

1.2 ORGANIZATION OF THE THESIS

The thesis has been organized into seven chapters. Chapter II describes the blast furnace process and reviews the available literature on its modelling. Chapter III presents the development of material and energy balance equations to compute the required boundary conditions around the shaft region and check the consistency of observed data of an Indian blast furnace. Chapter IV presents the development of one-dimensional unsteady state mathematical model for the blast furnace process of shaft region. Unsteady state model has been reduced to steady state model by setting the time derivative terms equal to zero. There are various constitutive parameters used in the mathematical models such as overall kinetic rate of reactions, heat of reactions, heat transfer coefficients etc. The correlations for all these parameters along with the derivation of few of them are described in Chapter V. The numerical solution of the steady state model, its results and validation have been discussed in Chapter VI. Finally, the Chapter VII highlights the main conclusions of the thesis and provides recommendations for future work.

LITERATURE REVIEW

2.0 INTRODUCTION

Blast furnace is the heart of an integrated steel plant and has been in use since long for the production of pig iron from iron ore. From time to time it has undergone several modifications with the aim of improving its productivity, fuel efficiency and also for reducing coke rate by means of injections and high top pressure. Hence, enormous literature is available on various aspects of blast furnace. This makes the task of writing a detailed literature review on all aspects of blast furnace extremely difficult. Therefore, only those aspects of blast furnace have been described and reviewed here, which elucidate its operation and constructional details and are required for its modelling and simulation. A brief description of blast furnace is given for the sake of general description of the process.

2.1 BLAST FURNACE

Blast furnace looks like a combination of huge conical frustums and cylinders arranged in a specific pattern. Figure 1.1 depicts a schematic diagram of the blast furnace. It consists of six portions. The cylindrical topmost portion is called the throat. The portion below the throat, which has the shape of a truncated cone, is called the stack. Below the stack there is again a cylindrical portion which is called belly or parallel. It is followed by an inverted truncated cone shaped portion known as bosh, which is further connected with the bottom of furnace called hearth. Few centimetres below the upper rim of the hearth there are series of water cooled cylindrical holes which are uniformly spaced around the hearth periphery. Tuyeres are put in

these holes, and are used to introduce hot blast into the furnace. The zone in front of tuyeres is known as combustion zone.

The dimension and shape of each portion, which have undergone modifications from time to time, depend upon many factors such as working methods, types of feed etc. The angles of stack and bosh are chosen in such a way so that the burden can descend smoothly and ascending gases can be distributed almost uniformly over the entire cross-section of the furnace. The cylindrical belly has the largest diameter in the furnace. As the fusion of solids starts in this region, its large cross-sectional area helps in upward movement of gases through semi-molten materials. The large height of the furnace helps the ascending gases in transferring their sensible heat to solids and molten materials, and simultaneously affect the chemical reactions in a controlled manner.

Complete operation of the blast furnace can be visualized as the combination of three basic steps or processes, namely reduction, fusion and combustion. Iron oxides are reduced to produce metallic iron. The oxides of few other elements such as SiO_2 , MnO_2 and CaCO_3 etc, which are present as impurities or added as fluxes, are also reduced. Unwanted oxides react with the charged fluxes such as limestone to form slag. All the solid components except coke get fused so that the molten pig iron and slag can be easily separated. Thus, the processing of solid feed into molten pig iron and slag requires reducing agents as well as heat for fusion and reactions. Both of them are supplied predominantly by the partial combustion of coke. The quality, quantity and mixing of ingredients of feed are so adjusted that the process is performed smoothly to yield a product of desired composition.

2.1.1 Raw Materials

The raw materials required for iron making are iron ore as source

of iron, coke as fuel, limestone, manganese ore and quartzite as fluxes. Hot air and auxiliary injections also form a part of total requirement of materials. In early times when the furnaces were small, the raw materials for blast furnace were mainly iron ore, limestone, coke and air blast. During last four decades, an increasing demand of low cost iron and steel led to the necessity of improving the blast furnace operation. Therefore, the efforts were made to increase the production rate with minimum fuel consumption and also to obtain better quality of pig iron with desired silicon and low sulphur contents. Bates (1973) has shown that the properties of raw materials affect the furnace productivity greatly. Therefore, in order to achieve these objectives, the characteristics of raw materials have been significantly modified by various treatments. Natural iron ore has been partially replaced by sinter, pellets and beneficiated iron ore. Auxiliary solid, liquid and gaseous fuels are being used as a part replacement of universal fuel coke. Hot blast is being humidified and enriched with oxygen. A detailed description of various raw materials are given in the following subsections.

2.1.1.1 Iron Ores

The iron ore contains iron mainly in the form of its oxides, viz. hematite (Fe_2O_3) and magnetite (Fe_3O_4). The iron ore for blast furnace is prepared from mined ores and the operation is commonly known as preparation of ore. This includes crushing, grinding, screening, washing, blending, concentrating, agglomerating etc. The purpose of ore preparation is to improve the quality of raw ore so that it can enhance the blast furnace productivity. During ore mining and preparation, sufficient amount of fines is generated. A few decades ago these fines used to be considered as waste. The fines in the furnace decrease the voidage of the bed, which results in increased resistance to flow of ascending gases. Thus, they cause the adverse effects on the blast furnace operation.

In view of the above, it is necessary to agglomerate the fines into porous lumps of required strength. The agglomeration is done by sintering and pelletizing processes, which increase the reducibility and strength of ore lumps. The lumps thus formed are named as sinters and pellets. These porous lumps provide good bed permeability for the flow of gas in the furnace. Agarwal and Davis (1963) discussed the chemical engineering aspects of sintering and pelletizing processes together with the resulting improvements in blast furnace performance.

The mixture of prepared ore, sinters and pellets is known as iron ore burden. This is the main solid burden, which is charged from the top with other solids into the furnace.

2.1.1.2 Fuel

Coke is used universally as fuel in blast furnace and it is charged with ore in the burden. It provides major portion of the thermal energy requirements of the furnace and the reducing agents. Coke is made from special grades of natural coal called coking coals. Coal as such is not very strong and unable to provide the mechanical support and bed porosity to the large charge column in the furnace. Hence, coal cannot be used in its raw form. To overcome these drawbacks coking is done. This is the process of heating certain specific grades of coals to a temperature of around 1273 K in the absence of air. This leads to the expulsion of gases from coal in the form of coke oven gas and provides strength to the residue for use in the blast furnace. Although use of coke is advantageous in many ways, it forms a significant portion of the production cost of iron. It is not only costly, but a good quality coking coal is becoming scarce day by day. Hence, attempts are being made to find out ways to reduce the consumption of coke. Use of auxiliary fuels as part replacement of coke is one way to reduce the coke consumption. This is achieved by

using solid, liquid and gaseous fuels as given below.

Gaseous fuels : Coke oven gas, reformed gas, natural gas etc.

Liquid fuels : Fuel oil, naphtha, oil-coal slurry, tar etc.

Solid fuels : Pulverized coal, form coke, anthracite, lignite etc.

These fuels are generally injected into the furnace through the tuyeres along with the blast. They can neither provide bed permeability in the dry zone nor the mechanical support like coke to the charge column in the wet zone, i.e. bosh, but they perform same chemical and thermal functions as coke. Therefore, they reduce the consumption of coke.

The choice of the type of fuel for injection depends upon its availability and economy. It varies from place to place. India does not have sufficient amount of oil and natural gas. Also, the coking coals in India are of poor quality. Ash content of coke is high. That is why Indian blast furnaces have poor productivity. Therefore, several processes are being developed to produce coke, which is suitable for blast furnace, from inferior, weak and noncoking coals. 'Form coke' and 'Ferro coke' are of these types. These cokes as part replacement of fuel coke are most suitable fuels according to Indian conditions. This is the recent development in the field of fuels for blast furnace and experiments are being carried out on this aspect [Tupkari (1985)].

2.1.1.3 Fluxes

The impurities are also associated with the ore and coke, which contain mainly the oxides of silicon (Si) and aluminium (Al) in large amounts and manganese (Mn), phosphorous (P), sulphur (S), tin (Sn), lead (Pb), Nickel (Ni), chromium (Cr), copper (Cu) and alkali metals like sodium (Na), potassium (K) etc in small amounts. As long as these

impurities or gangue materials remain in solid state, their extraction from metal is very difficult. But in liquid state, gangue is insoluble in molten iron, so it can be separated completely. Therefore, the viscosity or fluidity of molten gangue materials should be such that they can flow out freely and rapidly over the molten iron at the operating temperature in the hearth. But silica (SiO_2) and alumina (Al_2O_3), which are present in gangue, are acidic and amphoteric in nature respectively, and possess very high melting points as compared to furnace operating temperatures. Hence, in order to bring gangue materials to liquid state, limestone, manganese ore, dolomite and some times quartzite are added to the ore and coke mixture as fluxes. In presence of these fluxes the gangue materials fuse at lower temperature. The molten product thus formed with the combination of flux and gangue materials is known as slag.

The quantity of flux in solid mixture is decided on the basis of basicity of slag. Basicity is the ratio of bases and acids in slag and is expressed generally as $(\% \text{CaO} + \% \text{MgO}) / (\% \text{SiO}_2 + \% \text{Al}_2\text{O}_3)$. It has been suggested that for proper operation of blast furnace basicity of slag should be between 0.9 and 1.2 [Biswas (1981)].

2.1.1.4 Manganese Ore

In iron and steel making, manganese in iron has beneficial effect. It acts as a desulphurizer as well as a flux. In order to introduce manganese in pig iron, manganese ore is deliberately added to the solid burden. Manganese ore contains oxide of Mn as MnO_2 . In slag it is present as MnO. Its fluxing action is similar to that of lime and MgO. MnO keeps the slag in molten form during its passage upto the hearth because MnO is reduced at very high temperature. Therefore, its presence in slag helps to broaden the range of fluidity of slag. MnO also stabilizes the viscosity of the primary slag formed in the bosh,

so that the burden descends smoothly and the lime dissolution rate is improved.

It is known that sulphur in blast furnace is carried predominantly by coke ash in the form of its sulphides and sulphates. During the descent of the burden, this sulphur is absorbed by the metal in the stack and bosh regions. Sulphur in pig iron is present in the form of dissolved sulphur and beyond a certain limit, it has adverse effects in steel making. Its presence in finished steel causes hot-shotness. Therefore, it is necessary to control the sulphur content in the pig iron. Towards this, MnO plays a substantial role as it is a very good desulphuriser.

2.1.1.5 Hot Air Blast

The air blast is needed for the combustion of coke and is introduced into the furnace through the tuyeres. In order to improve productivity and fuel efficiency, it is desirable to preheat the blasted air. This leads to increase in tuyere gas temperature, i.e. flame temperature. The increase in the flame temperature upto a certain value has advantageous effect and beyond this it has disadvantageous effect. The upper limit of temperature depends upon the burden characteristics and furnace profiles. Raising the flame temperature beyond certain limit, causes many irregularities in the blast furnace operation. Important ones among them are described below :

(i) Bosh hanging or Burden hanging :

As a result of very high temperature, the reaction zone in bosh becomes relatively narrow due to which semifused slag restricts the flow of ascending gases. This makes the movement of descending material sluggish and leads to bosh hanging.

(ii) Choking of the voids of burden :

Higher flame temperature causes the vapourization of volatile impurities, which may condense in the voids of the moving burden resulting in the choking. As a consequence, resistance to the flow of ascending gases increases. This causes the adverse effect on the blast furnace operation.

In order to avoid these irregularities in blast furnace, it is necessary to avoid unduly high flame temperature. The flame temperature may be regulated by injecting additional substances with the hot air blast. The steam is injected with hot air blast as a coolant. The reaction of steam with carbon is endothermic in nature and thus reduces the flame temperature. Hence, in the presence of steam, the blast temperature can be increased without any increase in flame temperature. Another advantage of steam injection with the air blast is the generation of a potent reducing agent such as H_2 gas. The steam after reacting with coke produces carbon monoxide as well as hydrogen gas. Thus, the tuyere gas is also enriched with reducing gases. The injection of steam with air blast is also known as humidification of blast.

As steam is added to reduce the flame temperature, the oxygen enrichment of the blast is used for raising the flame temperature. The increase in the flame temperature is due to lower production of tuyere gas per kg of coke and not due to increase in heat input. From thermal point of view, furnace efficiency will be better if the flame temperature is kept constant by combining the oxygen enrichment and humidification of blast. It is noticed that the coke burning rate, hence the furnace productivity, increases considerably from such a combination.

2.1.2 Blast Furnace Operation

In the blast furnace, a mixture of solid materials is charged from

the top of furnace, which gets heated by the ascending gases. Iron oxides and the oxides of some impurities, which are present in the descending burden, are reduced by hot reducing gases. After reduction, solid materials take heat from the gases and get melted. Thus, all the components of solid burden except coke are converted into pig iron and slag, which are tapped near the hearth bottom. Coke is the only component of solid burden, which descends as solid upto the tuyere level, where it reacts with hot air blast leading to the production of hot reducing gases. These hot gases have sufficient thermal energy to provide the total thermal requirement of the furnace. From the tuyere level, gases ascend through molten, semi-molten, and solid materials present in bosh and stack regions.

Throughout the furnace process, hot rising gases impart their heat to the descending materials. Depending upon the thermal and chemical processes occurring in the furnace, blast furnace can be divided into four zones. Starting from the bottom, these zones are as follows :

- (i) Combustion zone
- (ii) Direct reduction and melting zone
- (iii) Indirect reduction or thermal reserve zone
- (iv) Preheating or preparation zone

Figure 2.1 shows these zones along with the temperature profiles. The processes in each zone are described in the following subsections.

2.1.2.1 Combustion Zone

The combustion zone lies in front of tuyeres. The combustion of coke and other fuels take place in this zone. Coke descends to tuyeres in solid state. Therefore, the packed bed which is present in front of tuyeres, contains solid coke and fused materials. The temperature of solid coke remains in between 1673 and 1773 K . The oxygen required for burning of coke and fuels is supplied by the hot air blast, which

is introduced through the tuyeres at a pressure of 2.5 - 3.5 atm and at a velocity of 150 - 300 m/s. The blasted air penetrates radially into the packed bed of coke and molten materials upto a certain depth. The penetration depth depends upon the kinetic energy of the blasted air and is normally 1 - 2 m. Therefore, a ring of 1 - 2 m is formed around the hearth periphery in front of tuyeres as shown in Figure 2.2. This ring is known as raceway or active zone because the combustion takes place here. The continuous consumption of coke creates empty spaces in the raceway, which helps in downward flow of molten materials.

Beyond the raceway, there remains a column of unreacted coke. Since no reaction takes place in this portion, it is known as inactive or dead man zone. Therefore, the depth of raceway as well as dimensions of the hearth and tuyeres play an important role in the improvement of furnace productivity and in smooth and rapid descent of materials. Following reactions take place in this zone :

Exothermic combustion reaction of carbon with air



Endothermic carbon gasification reaction



Endothermic combustion reaction of coke carbon with steam



The net heat of all reactions maintains the temperature of produced gases, which is generally in the range of 2073 - 2273 K. This temperature is sufficient to fulfill the heat requirement of the blast

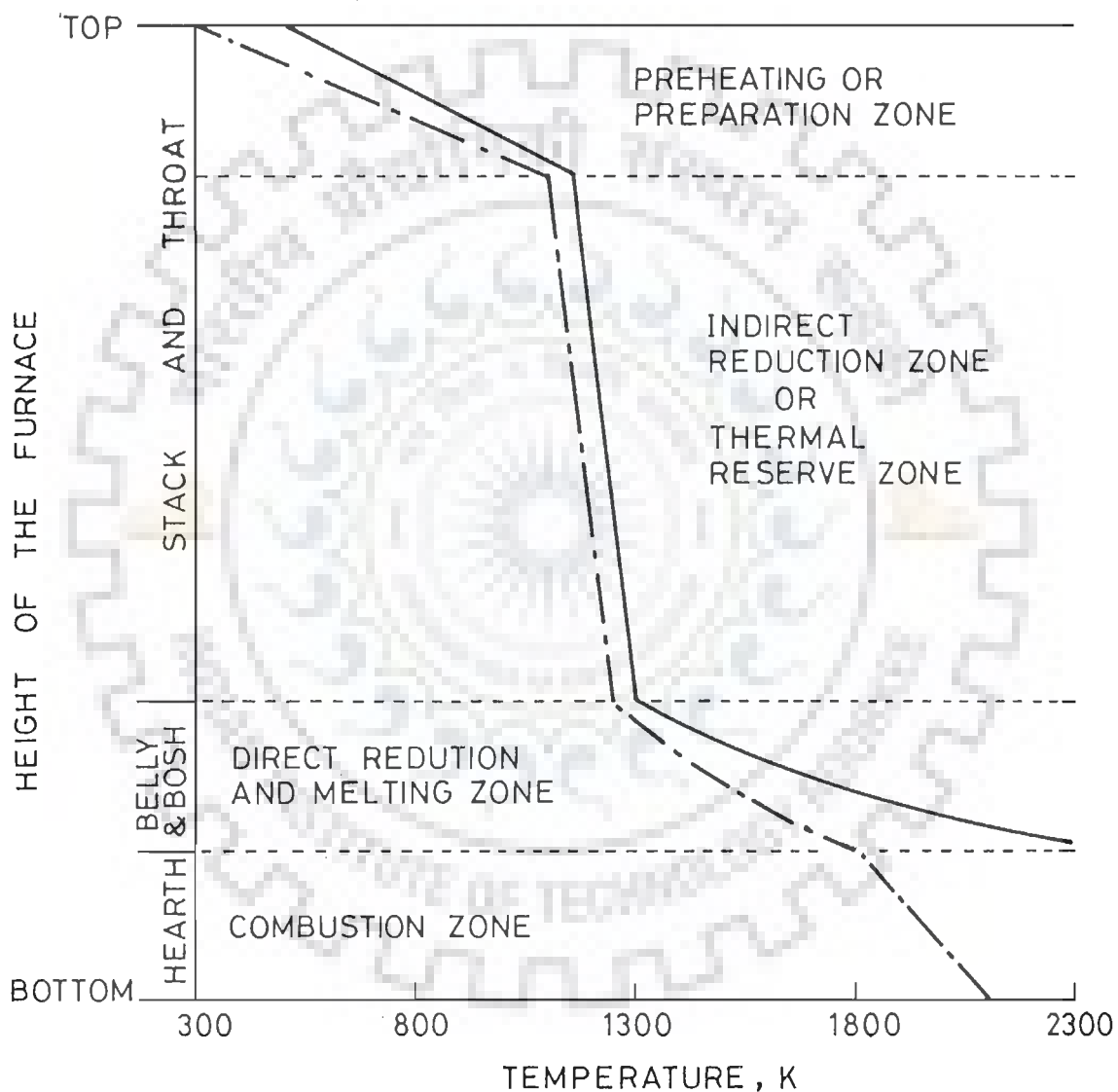


FIGURE 21 THERMAL AND CHEMICAL PROCESS ZONES WITH TEMPERATURE DISTRIBUTION OF GAS AND SOLIDS ALONG THE HEIGHT OF BLAST FURNACE

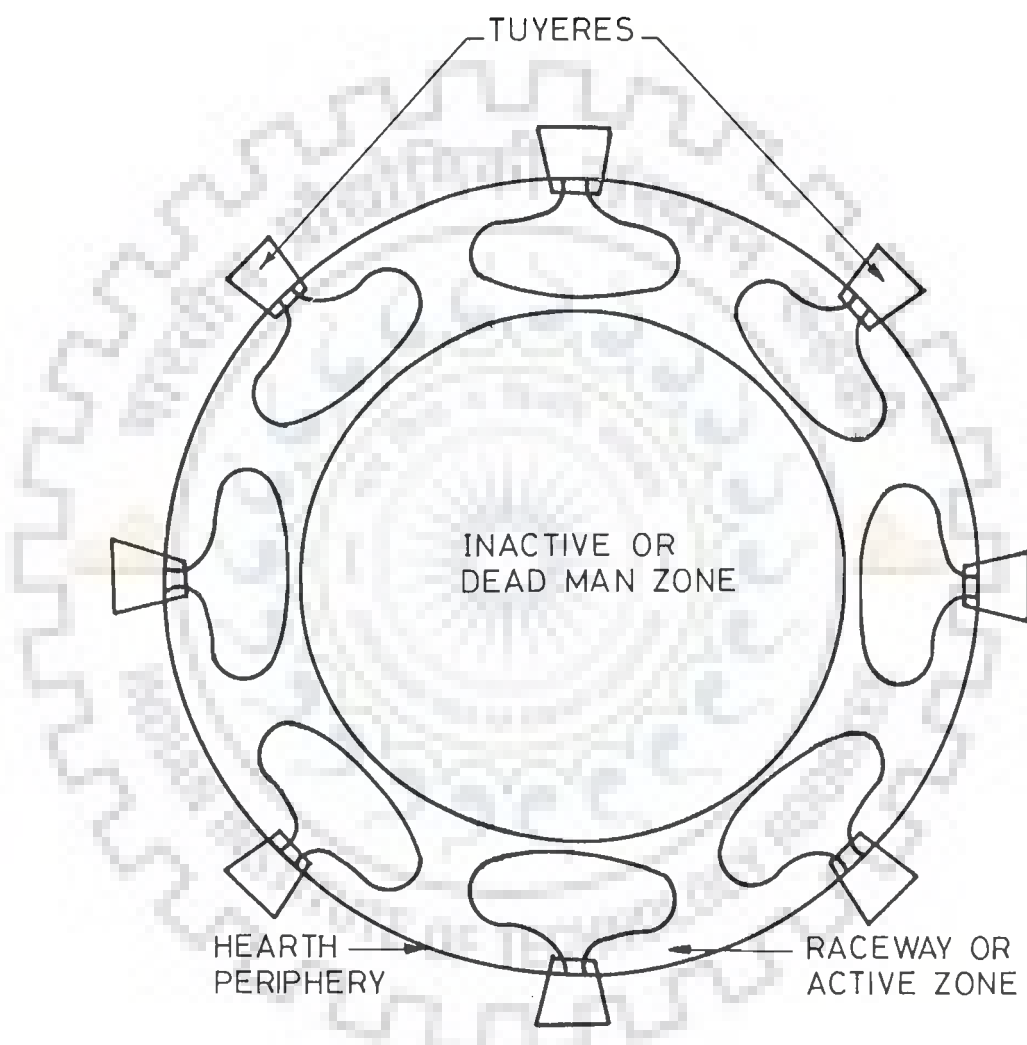


FIGURE 2-2 A SCHEMATIC PLAN VIEW OF THE COMBUSTION ZONE AT THE TUYERE LEVEL OF A BLAST FURNACE

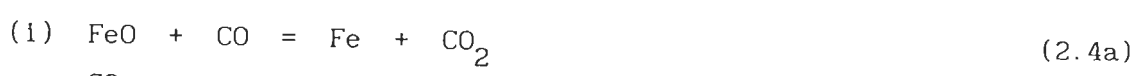
furnace operation. The gases from combustion zone, generally named as tuyere gas, enter the bosh region that lies just above the combustion zone.

The coke ash, released after combustion of coke, combines with the bosh slag and lime, and forms hearth slag. The hearth slag flows to the hearth with the molten iron and unreacted solid coke. The temperature in the hearth is sufficiently high, generally in the range of 1973 - 2073 K. As the molten iron passes through the slag to settle down, the slag reacts with the metal. This results into the exchange of few elements like Si, Mn, S between slag and metal.

2.1.2.2 Direct Reduction and Melting Zone

Direct reduction and melting zone starts from belly region and extends upto the bottom of bosh region. The temperature in this zone is above 1173 K. The gases from the combustion zone enter the bosh at the temperature of 2073 - 2273 K and cool down to 1173 - 1273 K at belly. The solid materials from indirect reduction zone enter this zone at a temperature of about 1173 K. This is the zone where various chemical as well as physical changes take place. All the solids except coke melt here. Thus, the fused materials and solid coke leave this zone at temperature of 1673 - 1773 K. Some of the important chemical reactions, which occur in this zone, are as follows :

Endothermic direct reduction of FeO



Overall reaction





Overall reaction



Endothermic decomposition of CaCO_3



Endothermic decomposition of MgCO_3 in dolomite



Endothermic direct reduction of MnO_2



Endothermic direct reduction of SiO_2



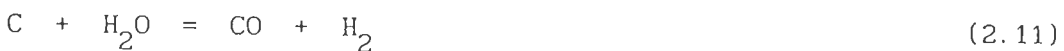
Endothermic reduction of CO_2

(Carbon gasification reaction or Solution loss reaction)



Endothermic reduction of H_2O

(Water gas reaction)



It is interesting to note that all the above reactions are endothermic in nature. Besides, melting of solids also occurs in this zone. Therefore, the processes in bosh region mainly determine the thermal requirement of the blast furnace and affect its efficiency.

The unreduced iron oxide from indirect reduction zone descends here in the form of FeO, which gets reduced by direct reduction at temperature above 1273 K according to reactions (2.4) and (2.5). Basically, the direct reduction of FeO by carbon is not itself a single reaction. This is a combination of two reduction reactions, viz. indirect reduction of FeO by CO or H₂ and solution loss reaction or water gas reaction. The overall reaction gives the direct consumption of carbon and thus stated as direct reduction by carbon. The unreduced iron oxide is expected to be reduced completely in this zone; otherwise on entering the hearth it will consume heat and will disturb the thermal state there.

The limestone, which is used for fluxing the acidic gangue, contains mainly CaCO₃. Decomposition of CaCO₃ is according to the reaction (2.6). The evolution of CO₂ makes the limestone particles porous. The increased porosity helps in transferring the heat to the solids for reaction. The porous product CaO gets melted and becomes one of the components of slag.

MgCO₃ and CaCO₃ are the main components of dolomite. The decomposition of MgCO₃ via reaction (2.7), takes place at lower temperature than the decomposition of CaCO₃. Product MgO thus formed also acts as a flux. It helps in maintaining the fluidity of slag.

The CO₂ gas is unstable above 1273 K in presence of carbon. Therefore, CO₂ evolved during the decomposition of limestone and dolomite gets consumed through carbon gasification reaction (2.10). Hence, CO gas is produced.

Reduction of SiO_2 to silicon by carbon is a slow reaction and proceeds according to the reaction (2.9). It occurs at temperature above 1573 K and is endothermic in nature. After reduction, the product silicon enters the molten iron. The concentration of silicon in iron must be low as it is not suitable for steel making process. The rate of reduction and so the silicon in iron increases with the increasing metal temperature. Since the quality measurements of pig iron are given on the basis of its silicon content, therefore, the reduction mechanism of silica, and silicon transfer to iron lead to various investigations. A number of mechanisms have been suggested by several research workers. These mechanisms are discussed in Chapter V.

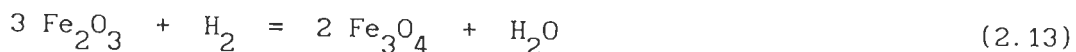
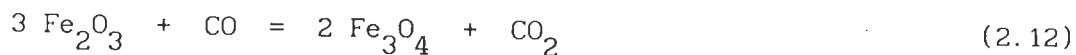
The softening of solid materials which is primary stage of melting, starts in belly region. The molten part of solid materials is supposed to reduce the void spaces in the bed and make the upward flow of gases difficult. As the belly has largest diameter in furnace, bed of solids has more void spaces in this region. Therefore, the large cross-sectional area of belly helps in upward movement of gases through semi-molten materials.

2.1.2.3 Thermal Reserve Zone

In this zone temperatures of both the solids and gases do not change significantly and remain almost constant. However, the temperature of gases differs marginally with that of solids. Hence, the zone is known as thermal reserve zone.

Further, most of the indirect reductions occur in this zone. The word indirect is used because the iron oxides are reduced by CO and H_2 and not by carbon directly. Therefore, the zone is also known as indirect reduction zone. The important reactions occurring in this zone are as follows :

Exothermic indirect reduction of Fe_2O_3 by CO and H_2



Endothermic indirect reduction of Fe_3O_4 by CO and H_2



Exothermic indirect reduction of FeO by CO

[Reaction (2.4a)]

Endothermic indirect reduction of FeO by H_2

[Reaction (2.5a)]

Exothermic water gas shift reaction



A chemically inactive zone may be present within this zone. This is the zone where the concentrations of CO and CO_2 approach towards equilibrium with iron oxide, and the exchange of oxygen between iron oxide and gas is very little. In other words, the gas composition does not change appreciably. This zone generally appears when the coke consumption per tonne of hot metal is low. The low consumption gives just sufficient amount of CO to reduce iron oxide. This results in the creation of chemically inactive zone.

2.1.2.4 Preheating Zone

This is the topmost zone in the blast furnace and is known as preparation zone . In this zone the burden is charged to the furnace and the gases come out from its top. The charging of burden may be done by many devices, viz. double bell type charging system, Paul Wurth bell-less top charging system, etc. The purpose of charging is to distribute the charged materials uniformly around its whole cross-sectional area. Uniform distribution of burden is essential to have good and uniform bed permeability, which makes the uniform distribution of gases through the burden. This in turn improves the contact time of gases with burden and results in the efficient reduction and energy exchange processes occurring there.

The burden enters the furnace from top at ambient temperature, while the ascending gases enter this zone at a temperature between 1073 - 1273 K from the indirect reduction zone. In this zone, heat exchange between gases and solids takes place. This results in the heating of burden in the temperature range of 1073 - 1273 K and the cooling of gases in the temperature range of 373 - 523 K. Due to heating of the burden, vaporization of moisture and hydrated water in the burden also takes place here. However, few chemical reactions occur in this zone. These are listed below.

Exothermic indirect reduction of Fe_2O_3 by CO and H_2

[Reactions (2.12) and (2.13)]

Endothermic indirect reduction of Fe_3O_4 by CO and H_2

[Reactions (2.14) and (2.15)]

Exothermic carbon deposition reaction



2.2 BLAST FURNACE MODELS

During the last three decades or so the development of mathematical models has served as an invaluable tool for better understanding of complicated physical and chemical processes occurring simultaneously in the blast furnace. A mathematical model is merely a mathematical representation of the conceptual view of a process [Aris (1977)]. A number of attempts have been made to develop the mathematical models of blast furnace. These models are comprised of many equations derived for each phenomena occurring in the furnace and provide a great deal of information on the internal situation of the blast furnace. These models have also been found to be very useful for the improvement, optimization and the stabilization of the blast furnace operation [Tate (1972), Yagi et al. (1974), Bradley et al. (1981), Hatano et al. (1982a), Takenaka et al. (1986), Omori (1987)].

This section reviews the literature on mathematical models of the blast furnace. At this juncture, it is pertinent to point out that the literature on this subject is so vast that it is not possible to prepare an exhaustive review. However, every possible effort has been made in this writing to include all the literature available to us.

Early workers used the furnace input and output measurements to develop meaningful relationships between operating variables with the aim of yielding practical furnace control criteria. Although this approach is useful in establishing some basic relationships, it does not give an insight into the process as such and so does not lead to the effective furnace control schemes.

The researchers then proposed the mathematical models for the furnace process, which were based upon the fundamental physical and chemical mechanisms involved, and conservation laws. These models may be classified into following three categories.

- (i) Thermodynamic models
- (ii) Kinetic models
- (iii) Transport Phenomena models

2.2.1 Thermodynamic Models

In these models, blast furnace was divided into several zones based upon the temperature. The sequence of reactions and the temperature range for each reaction were both known. For each zone, the chemical equilibrium was assumed and overall heat and mass balances between solid and gaseous species were taken. Therefore, these models were generalized as stage-wise heat and mass balance models. Reichardt (1927), Ridgion (1962), Staib and Michard (1965) presented these type of models.

Reichardt (1927) divided the blast furnace into five zones and the chemical reactions occurring in each zone were specified. The function of each zone was also defined as follows :

- (i) 0 - 400°C ; preheating of solid burden
- (ii) 400 - 900°C ; indirect reduction
- (iii) 900 - 1200°C ; direct reduction
- (iv) 1200 - 1400°C ; fusion of reduced iron and direct reduction
- (v) > 1400°C ; formation of slag, reduction of metalloids
(SiO₂ , MnO, P₂O₅ etc)

According to the concept that heat exchange between the gas and solid or molten phase took place in each zone, the heat requirement of the

solids was calculated for 100 kg production of hot metal with the assumption that the blast at 600°C reacted with coke at 1400°C in the tuyere zone. The calculated results were presented in the form of two plots. The first plot was between the solid temperature and the heat requirement. The curves on this plot represented the heat requirement of different processes, namely heating up and fusion of iron, heating up and fusion of slag, decomposition of limestone and formation of slag, direct reduction of iron oxide and reduction of MnO , SiO_2 and P_2O_5 . The overall heat requirement for the whole process was obtained by summing up the heat requirements of each zone. The second plot was between the temperatures of gas and burden, and heat requirement. From these studies Reichardt (1927) concluded that the heat requirement of the burden descending in the stack of the furnace must be provided by the ascending gases only in order to raise its temperature and also to sustain the reactions going on there. Even a small amount of heat supplied by the gas must always be available at a temperature higher than that of the contacting solid for stable operation of the furnace. On the basis of this criteria, Reichardt (1927) proposed a method to determine the optimum coke requirement for the furnace.

Ridgion (1962) developed a computer program for the calculation procedure proposed by Reichardt (1927), so that the relatively precise calculations of the heat requirement of the furnace could be made. In the computer program, variation in specific heat of the gases with temperature and the changes in mass flow rate of the gas stream due to interchange of gaseous component with the solid phase were also included. This program computed the heat requirement of solid phase in steps of 50°C , when solid temperature varied from 0 to 1500°C . In this study, the longitudinal distributions of solid and gas temperatures were presented. The effect of changes in operating parameters, namely the temperature and composition of the blast, on coke rate were also evaluated, which keeps the system in balance in relation to a defined pattern of difference in gas and solid temperatures.

Staib and Michard (1965) proposed a simple quantitative model of the blast furnace. They pointed out existence of a thermal reserve zone in the furnace, where the temperature of solid particles was almost equal to that of gas. They also proposed the existence of a chemical reserve zone in the lower part of the thermal reserve zone, when the operation of the blast furnace was ideal with uniform distribution of burden. In this zone, the reduction of iron oxide might not occur due to the equilibrium of reduction reaction. On the basis of above proposition, Staib and Michard (1965) divided the furnace into two zones. The dividing boundary was within the thermal reserve zone at the level of the chemical reserve zone. In the upper zone, the burden was preheated and reduced to wustite phase. The gas was in equilibrium with the wustite phase and left the zone at 100°C . This zone was named as conditioning zone. In lower zone large amount of heat exchange was involved due to chemical reactions. This zone was called as processing zone. By application of laws of conservation of mass and energy to the lower zone, a mathematical model was developed for calculating the coke rate and the production rate of pig iron for the given composition of the top gas.

Although these models provided the criterion for the stable operation of the furnace, approximate procedures for calculating the heat requirement and coke consumption rate, but could not predict the reduction behaviour of iron oxide, which plays an important role for the determination of the heat requirement in the higher temperature region. These models could also not predict correctly the temperature of solids and gases at the boundaries. To overcome the limitations associated with the above models, kinetic models were developed.

2.2.2 Kinetic Models

In the kinetic model, the blast furnace was again divided into

several zones. The temperatures prevailing in the individual zones were assumed to be invariant and the reaction rates were included in the model. The model reported by Flierman and Langen (1966) belongs to this category.

Flierman and Langen (1966) divided the blast furnace into five zones, namely shaft zone, melting zone, zone containing molten materials, tuyere zone and the hearth. The reaction rates of indirect reduction of iron ore by CO and H₂, solution loss reaction and decomposition of limestone were taken into account. The rate constants were measured in the laboratory for the burden material fed to the blast furnace. The expressions for these reaction rates were simple. However, these did not include the effect of wide variations in blast furnace conditions. This model reasonably described the longitudinal distributions of gas and solid temperatures as well as of mole fractions of CO and CO₂.

Although the development of above kinetic model was appreciated, but this did not include the energy balance equations with reaction rate expressions, therefore, its predictions were not as accurate as desired.

2.2.3 Transport Control Models

Transport control models, were found most successful in predicting the behaviour of blast furnace [Tate (1972) and Omori (1987)]. In these models, the blast furnace was considered as a series of counter current heterogeneous chemical reactors involving gas, solid and liquid phases. The basic model equations were derived by using the laws of conservation of mass, momentum and energy. Transport control models were proposed for steady state as well as for unsteady state operations.

2.2.3.1 Steady State Models

Koump et al. (1964) presented an idealized physical model of the blast furnace, which consisted of three reactors and one accumulator. Reactor-1 comprised the stack region of the blast furnace, where only indirect reduction of iron ore by CO, and solution loss reaction were considered to take place along with the heat exchange between gas and solid. Reactor-2 comprised the cohesive zone and dead man zone in which phase transformation from solid to liquid phases occurred. Thus, the important characteristic of this reactor was the coexistence of gas, liquid and solid phases. Reactor-3 included the raceway region. Accumulator corresponded to the hearth region, utilized to store the hot metal and slag. Koump et al. (1964) developed a steady state one-dimensional model for reactor-1, i.e for stack region.

They considered the stack as heterogeneous moving bed system in which heat exchange and chemical reactions occurred between the countercurrently moving gas and solid streams. Reaction rates were taken into account. The model consisted of six ordinary differential equations. The longitudinal distributions of gas and solid temperatures, fractional reduction of iron ore and partial pressures of CO and CO₂ were obtained in the stack region of the blast furnace.

This model by Koump et al. (1964) was the first model in which the blast furnace process was formulated mathematically in the form of six ordinary differential equations. Due to this reason it could predict the essential characteristics of the blast furnace operation. Since this model was proposed for the stack region only, therefore, it could not predict the overall performance of the blast furnace.

Yagi and Muchi (1970b) also presented a one-dimensional mathematical model for estimating the longitudinal distribution of process variables in the upper part of the blast furnace, i.e. in the stack and bosh.

The model considered overall reaction rates of eight reactions, viz. indirect reduction of iron ore by CO and H₂, solution loss reaction, direct reduction of molten wustite by solid coke, decomposition of limestone, reaction between coke and steam, water gas shift reaction and direct reduction of silica in slag by solid coke. The heat transfer between fluid and solid particles and the overall heat transfer through furnace wall were also included in the model. The model consisted of ten ordinary differential equations and three algebraic equations along with overall heat and material balance equations to give the solid temperature at tuyere level and the theoretical flame temperature. Behaviour of the blast furnace was obtained under the wide range of operating conditions such as top pressure, diameter of iron ore particles, blast volume, blast temperature, rate of steam injection, ratio of oxygen enrichment and pre-reduction of iron ore. The effects of such operating conditions and parameters on the production rate of pig iron, carbon ratio and longitudinal distribution of process variables were also estimated.

This model by Yagi and Muchi (1970b) is quite attractive because it estimates the operational results as well as the longitudinal distribution of every process variable.

Togino et al. (1980) developed a mathematical model for estimating the fuel rate when the operating conditions of a blast furnace were given. This model was established on the basis of the concept of Yagi and Muchi (1970) by taking account of the softening-melting zone, dropping of melts through a dead man zone and reaction of silicates by gas-metal reactions. The smallest value of carbon rate was obtained with the assumption that no heavy oil was injected and blast and top gas temperatures were 1350°C and 130°C respectively. In the next step the smallest value of carbon rate was obtained when heavy oil was injected with the assumption that the top gas ratio (CO/CO₂), hydrogen utilization ratio and direct reduction ratio did not change after the heavy oil injection. The estimated fuel rate was found higher than the

actual value whereas the longitudinal distribution of temperature of gas and solid showed a satisfactory performance.

All the above models were one-dimensional models. Naturally, these models do not include the radial distribution of variables. In the actual blast furnaces, radial distribution of variables is also responsible for controlling the gas flow and other process variables. Therefore, the attention was also focussed on the two-dimensional distribution of process variables along with the progress in operating techniques for blast furnace.

The earliest attempt at two-dimensional analysis of a blast furnace was made by Lahiri and Seshadri (1969). They extended the work of Koump et al. (1964) and developed a two-dimensional model for blast furnace stack corresponding to the reactor-1 of Koump's model. They accounted the diffusion of gas in radial direction and the heat conduction through the burden. The mathematical formulation led to seven simultaneous partial differential equations, which were solved by using the finite difference method. The model predicted both the longitudinal and radial distributions of temperatures of gas and solid particles, mole fractions of CO and CO₂ and fractional reduction of iron ore in stack region. This model possesses serious limitations. First, it deals with the gas-solid reaction region only. Secondly, it requires radial gas flow and temperature distributions at the top of the furnace for its numerical solution. Due to this reason, it cannot be used to obtain the radial distributions for a given set of input data on a operating blast furnace.

Chon and Tate (1975) also considered the radial distribution of variables in their model. In order to represent the radial nonuniformity of the process variables, they divided the blast furnace into three coaxial annular zones, namely central zone, intermediate zone and peripheral zone, and considered them as independent reactors. The ore to coke ratio for these three zones were taken as 0.6, 0.99 and

1.10 respectively. These three reactors had different gas flow rates according to the permeability. The proposed model estimated the longitudinal distribution of temperature of gas and solid in three zones and made comparative study of these three profiles. In this way the model was able to examine the effect of uneven distribution of the burden in the furnace on the temperature of solid and gas upto some extent. The computed results compared well with those obtained in an experimental furnace. The positive point of this model was that the operating conditions of the furnace were used as the input data.

The models, discussed above, were for mixed burden mode of feeding, i.e. the solids were uniformly mixed throughout the furnace. Another mode of feeding the solids into the blast furnace is the layered burden. In this mode, coke and ore are charged alternatively into the top of the furnace.

The layered burden structure in reality is a highly complex packed bed structure, which consists of a number of distinct zones. These zones are characterized by the physical states of the solids (i.e. size and voidage) moving down through the furnace. There are six zones, which exist in the furnace. The granular zone is located in the highest part of the stack where both the ore and coke layers retain their structures as formed at the level of charging. The cohesive zone consists of alternate layers of coke and semi-molten reduced iron ore particles. Semi-molten iron greatly decreases the local voidage and thus, increases the flow resistance. The active coke zone, i.e. the third zone, consists of loosely packed coke through which molten iron and slag flow. The fourth zone is the raceway, which has a very small void space, generated by the displacement of coke due to the momentum of the hot air blast gas at the tuyeres. In the stagnant coke zone, the coke is densely packed and thus forms a region of high flow resistance. The sixth zone is hearth itself. The hearth is packed with uncombusted solid coke, slag and molten iron where fluid components are tapped. The physical properties of ore and coke layers and kind of reactions taking

place in these layers are different from each other. Therefore, at any level in the furnace the process variables such as temperature of gas and particles, velocity and composition of gas would change periodically with the alternate passage of ore and coke layers.

Many research workers proposed the models of blast furnace with layered burdens. Kuwabara and Muchi (1977) developed a mathematical model in which inclined layers of ore and coke burdens were assumed from the top to the melting level of the furnace. The thickness of each layer was assumed to change in the radial direction. The model was based on the equation of continuity and motion. These equations were numerically solved to find out the longitudinal and radial distributions of the process variables, namely temperature, gas composition, gas velocity and the fractional reduction of iron ore. From the results, it was observed that the estimated process variables, and the softening layer of iron ores (over the region from 1200° to 1400°C) changed remarkably in the radial direction. In this model, the distribution of process variables were estimated on the basis of the operating conditions and measurable data at the furnace top. However, model was not complete as it did not include the heat exchange, mass transfer with noncatalytic reaction, and flow of gas, liquid and solid.

Hatano and Kurita (1982) considered the existence of cohesive zone. They proposed a model, which included the transport equations concerning momentum, mass and energy, and noncatalytic chemical reactions and the vectorial form of Ergun's equation. This model was able to predict two-dimensional profiles of temperature, fractional reduction of iron ore, flow rate of gas, liquid and solids. The model was solved numerically by the characteristic method. The results were in good agreement with the values observed in the actual furnace. The computed results concluded that the distribution of the temperatures, mass fractions and the velocities of the gas and the solid in the stack region depended remarkably on ore to coke ratio at the top of the furnace. Further, it was concluded that the stagnant region in the

lower part of the furnace, which played the role of a heat reservoir, had a remarkable influence on the shape of the cohesive zone and due to which this zone assumed the inverted V-shape.

Yagi et al. (1982) presented a model where the raceway and cohesive zone were also considered for estimating the two-dimensional gas flow and heat transfer in blast furnace with layered structure. Finite element method was used for solving the model equations. For the purpose of analysis and simulation, a computer program was written to compute the gas flow, pressure of gas, solid flow, temperatures of gas and solid by assuming the potential flow for solid bed movement. Computed results demonstrated that the flow pattern of gas was principally governed by the bed structure including the size distribution of particles and it was having significant effect on the temperature distribution. Finally, the model concluded that the charging method and the profile of cohesive zone were the important factors for blast furnace operation. Regarding the radial distribution of temperature, the computed results showed an almost uniform distribution in radial direction in shaft region, whereas actual measurements of temperature in operating blast furnaces resulted in appreciable nonuniformity in the temperature distribution in radial direction.

2.2.3.2 Unsteady State Models

Unsteady state models of blast furnace were also proposed, which might be used for control purposes. These models predicted the responses to the step change in operating conditions and unsteady state operation of blast furnace such as shut down, the blow in, and the blow out.

Fielden and Wood (1968) proposed a one-dimensional unsteady state model. The model included the tuyere and hearth zones too. The blast furnace was divided into five zones on the basis of temperature. The

chemical reactions occurring in the individual zones were specified. The working volume was subdivided into a number of horizontal zones of height 1.0 m. The model equations were constructed by taking heat and material balances. The amount and composition of the material, and the temperature of gas and solid within each zone were assumed to be the average of their values at the boundaries of zone. Every zone was assumed to move below instantly after some retention time in a stepwise manner. The computed results predicted the transitional variations of few process variables such as temperature and composition of pig iron and of top gas for the step changes in blast temperature, ore/coke ratio and injected oil. It was noted that the unsteady state responses of process variables compared favorably with the trends observed in the actual furnace.

Hatano and Yamoaka (1977 and 1979) presented a one-dimensional unsteady state model for describing the transitional behaviour of process variables for the case of step changes in blast and charge parameters as well as for unsteady state blast furnace operation. The model equations were formulated for stack and bosh regions by using the conservation equations of heat and mass together with heat exchange and chemical reactions. The model was solved by using finite difference method. It was concluded that for the step change in blast temperature and blast moisture, furnace took smaller time to reach the new steady state as compared to the changes in ore/coke ratio, oxygen enrichment, oil injection and volumetric flow rate of blast. In case of shutdown, ore to coke ratio should be optimized in order to get smooth recovery. The blow in operation could be simulated according to the schedule of the increase in blast rate and blast temperature. The model also predicted the schedule for blow out operation where the inner volume was blown out with the decrease of stock level from the top to the upper bosh. The computed results showed good agreement with the actual results.

Hatano et al. (1982) developed an unsteady state mathematical

model by dividing the blast furnace into five zones and taking material and energy balances around each zone. This model was presented for the purpose of the automatic computer control of the hot metal temperature. For this, the response characteristics of the solution loss reaction rate and the hot metal production rate had been investigated experimentally and theoretically for the step change in operational variables such as blast temperature, the moisture content, the oil injection rate and the coke ratio. On the basis of this response, the reaction rate equations were formulated as function of the operational variables and were used in the model. The solid temperature at the tuyere level calculated by this model corresponds well with the measured hot metal temperature.

For the purpose of clarifying transient behaviour of the furnace, Kubo et al. (1982) presented an unsteady state one-dimensional simulation model. By means of this model, the variations in gas components, temperatures of solid and top gas during the blowing out and blowing in operations were predicted. The predictions were in good agreement with the actual results.

2.3 MOTIVATION FOR THE PRESENT STUDY

It is evident from the earlier discussion that the blast furnace is a critical unit of a steel plant and its performance would have marked effect on its overall productivity. Therefore, it is essential to understand the complex processes occurring in the furnace, and also to quantify them. Mathematical modelling appears an attractive tool for the analysis and simulation of blast furnace. Besides, complexity of the blast furnace process also compels a chemical engineer for its modelling and simulation as it is simply a noncatalytic moving bed gas-solid reactor, where one can use effectively one's knowledge of transport phenomena, heat and mass transfer, reaction engineering, thermodynamics, and modelling and simulation.

It is obvious from the review in Section 2.2, that a large number of mathematical models have been developed for the blast furnace during the past 30 to 35 years. These models include one- and two-dimensional models of the various sections of the blast furnace, which may be used to obtain its behaviour under steady or unsteady state operations for both the mixed and layered type of burdens. They are limited in their applications and differ from each other in terms of their complexity and the objectives of the studies carried out.

According to Denn (1986), a mathematical model may be defined as follows :

A mathematical model of a process is a system of equations whose solution, given specified input data, is representative of the response of the process to a corresponding set of inputs.

Beside the model equations, which are based upon conservation laws, constitutive relationships of the system being modelled play a crucial role. It is essential to determine them with as much accuracy as possible. Another equally important aspect associated with a model is the boundary conditions with which it is solved to obtain its behaviour. Generally, the boundary conditions are either given or easy to determine. But for the blast furnace, these also require special consideration, and computational strategies are needed for their determination. In view of the above, studies on mathematical modelling of blast furnace has been undertaken to achieve the objectives, mentioned in Section 1.1.

2.4 CONCLUDING REMARKS

In this chapter blast furnace process has been briefly described. Besides, mathematical models of blast furnace proposed by various

research workers have been critically reviewed. Generally, these models may be classified into three groups, viz. thermodynamic models, kinetic models and transport phenomena models. Amongst them, the transport phenomena models have been found to be most successful in understanding and predicting the behaviour of blast furnace. Models of this group also vary in their complexity depending upon the objectives of the modelling engineer/scientist. Lastly, the motivation for the proposed study has been explained.



MATERIAL AND ENERGY BALANCE COMPUTATIONS

3.0 INTRODUCTION

In the present work, a mathematical model has been developed which addresses itself to the behaviour of the process in the shaft region of the furnace. As mentioned earlier, the shaft is the region between the top of the stack and the bottom of the bosh. It constitutes three regions of the furnace, namely stack, belly and bosh as shown in Figure 3.1. In order to solve the model equations, one requires a set of conditions at the boundaries of the shaft, i.e. at the top and at the bottom of the shaft. These conditions comprise the mass flow rate and the temperature of solids, gases and molten materials entering and leaving the shaft region. The boundary conditions, therefore, may be obtained by material and energy balance computations around appropriate regions of the furnace. The operating data on the blast furnace are also needed for these computations. These data are generally available in the steel plants but cannot be used as such, because the measurements are prone to various types of errors. Therefore, it is necessary to check the consistency of measured input and output data prior to their use. This is also done with the help of material and energy balance calculations. This chapter deals with the estimation of boundary conditions by computing the material and energy balances.

The flow rate and composition of different materials entering and leaving the shaft as well as the furnace, are estimated by taking material balances around whole furnace and around combustion zone. The equations thus formed, are then solved for given operating conditions, which include charging rate of raw materials and their compositions, air blast rate with steam and excess oxygen, dust rate and its composition, and pig iron composition. Solution of these equations

gives volumetric flow rates and compositions of gases at the top of the furnace and at the bottom of the bosh, mass flow rate of pig iron and slag, and the solids flow rate at the bottom of the bosh. These will lead to boundary conditions for their use in the model.

In order to determine the temperatures at boundaries, energy balances are taken around the combustion zone and shaft region. Thus, the temperatures of gases at the top of the furnace and the bottom of the bosh are calculated.

The details of material and energy balance computations are described in the following sections.

3.1 MATERIAL BALANCE

Material balance for the blast furnace has been carried out in three stages. In the first stage, an overall material balance is taken around whole furnace. It estimates the mass flow rates and compositions of gaseous products at the top, and pig iron and slag at the bottom of the furnace. In the second stage, efforts have been made to calculate the flow rate of SiO gas entering the bosh from combustion zone. Lastly, the material balance is taken around the combustion zone to calculate the mass flow rate of gases, solids and molten materials at the bottom of bosh.

3.1.1 Overall Material Balance

A material flow diagram of a blast furnace is shown in Figure 3.1. A solid mixture of iron ore, sinter, pellet, limestone, manganese ore, quartzite and coke enters from the top of the furnace. The hot air blast with additives like steam, excess oxygen and oil is supplied from the bottom of the furnace. The pig iron and slag with some unreacted

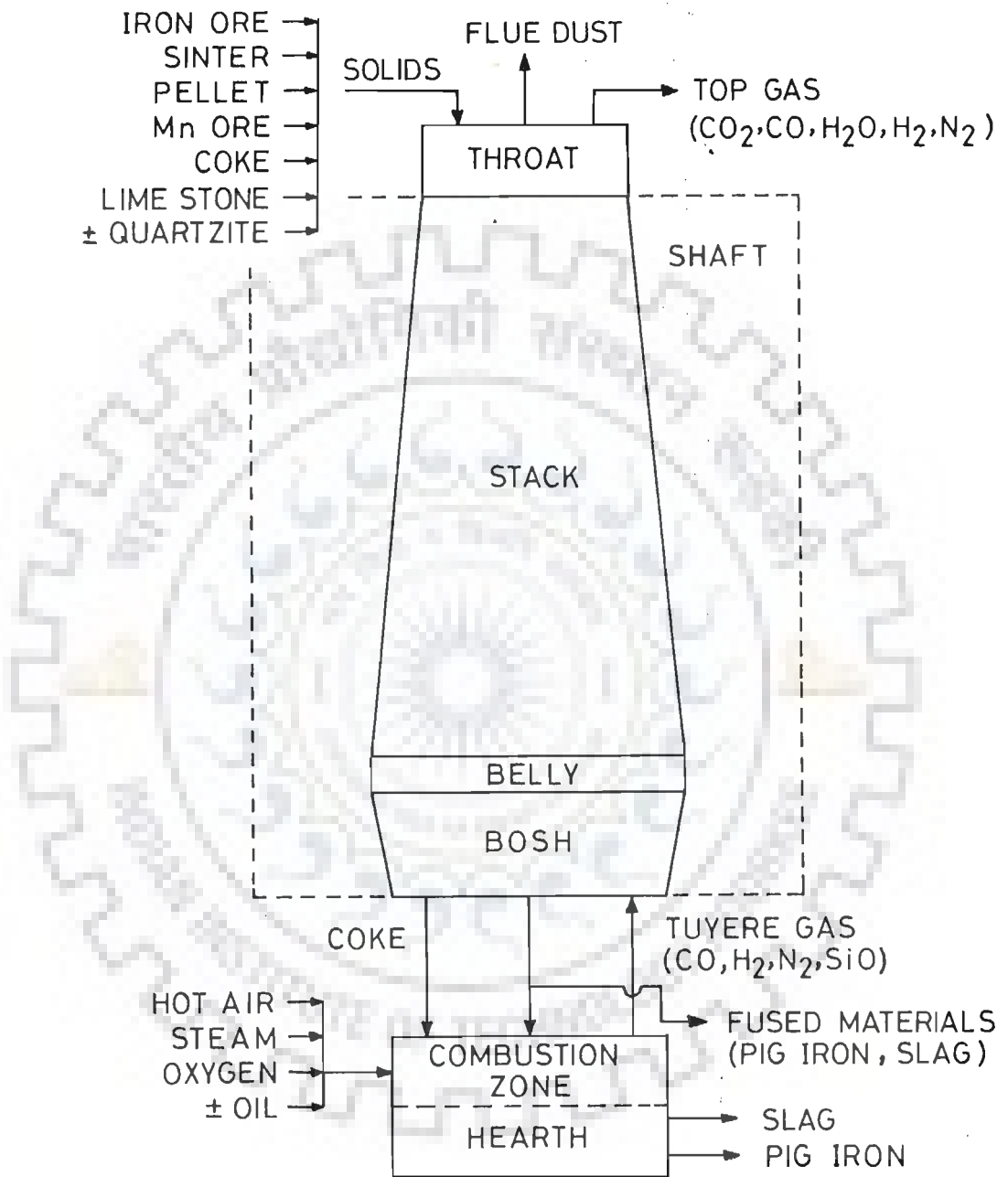


FIGURE 3-1 BLOCK DIAGRAM OF SIMPLIFIED BLAST FURNACE PROCESS SHOWING INPUT AND OUTPUT STREAMS AT DIFFERENT HEIGHTS

coke are collected from the bottom of the furnace. The gaseous products, namely CO , CO_2 , H_2 , H_2O , and N_2 come out from the top of the furnace. Some fines of solid feed also come out with the gases in the form of dust.

The flow rate and composition of the top gas, production rate of hot metal, and the discharge rate of slag have been estimated by taking overall component material balances around the whole furnace. The following assumptions are made during the formulation of component material balance equations.

- (i) Iron ore, sinter, pellets, manganese ore, limestone and coke contain only those components, which are mentioned in Table 3.1. It has been assumed for the present case that no quartzite is added to the burden.
- (ii) Dust contains only oxides of iron and carbon as mentioned in Table 3.2.
- (iii) Pig iron contains carbon, silicon, manganese and iron.
- (iv) The oxides of iron are completely converted into metallic iron, except those accompanying flue gases as dust.
- (v) There is no unreacted coke coming out of the furnace.
- (vi) In slag MnO_2 is present as MnO .
- (vii) Hot air blast is blown along with the steam and oxygen. Other fuel additives, e.g. oil etc, are not considered.
- (viii) The gases coming out from the top are CO , CO_2 , H_2 , H_2O and N_2 .

With the above assumptions, the overall component material balances have been written.

3.1.1.1 Component Material Balance

The overall material balances for different components are as follows :

Material balance for Fe

$$\begin{aligned}
 W_S r_{Fe} + W_P \alpha_{Fe} + W_D j_{Fe} = & 0.6994 \left[W_O v_{Fe_2O_3} + W_{OS} s_{Fe_2O_3} \right. \\
 & + W_{OP} p_{Fe_2O_3} + W_{OM} g_{Fe_2O_3} \\
 & \left. + W_C t_{a b_{Fe_2O_3}} \right] \\
 & + 0.7773 \left[W_{OS} s_{FeO} \right. \\
 & \left. + W_{OP} p_{FeO} \right] \quad (3.1)
 \end{aligned}$$

Material balance for C

$$\begin{aligned}
 \frac{W_C t_c}{12} + \frac{W_L l_{CO_2}}{44} = & \frac{W_P \alpha_C}{12} + \frac{W_D j_C}{12} \\
 & + \frac{F_0}{22.4} \left[y_{CO,0} + y_{CO_2,0} \right] \quad (3.2)
 \end{aligned}$$

Material balance for N₂

$$F_0 y_{N_2,0} = 0.79 \times 60 \times F_b \quad (3.3)$$

Material balance for H₂

$$\frac{F_0}{22.4} \left[y_{H_2,0} + y_{H_2O,0} \right] = \frac{60 \times F_b W_{st}}{18000} \quad (3.4)$$

247201



Table 3.1 Composition of Materials in Solid Feed

S.N.	Material	Composition, weight per cent							
		Fe ₂ O ₃	FeO	SiO ₂	Al ₂ O ₃	CaO	MgO	MnO ₂	CO ₂
1	Iron ore	92.93	-	2.57	4.50	-	-	-	-
2	Sinter	67.70	8.0	5.50	4.40	11.70	2.70	-	-
3	Pellet	91.45	0.50	2.57	4.50	0.54	0.44	-	-
4	Manganese ore	40.48	-	3.63	0.46	-	-	55.43	-
5	Limestone	-	-	5.00	3.00	57.00	2.00	-	33.00
6	Coke ash	5.50	-	55.00	32.00	5.00	2.50	-	-

Table 3.2 Composition of Flue Dust, Pig Iron and Slag

S.N.	Material	Composition, weight per cent				
		Fe	C	Si	Mn	O
1	Flue dust	52.00	25.66	-	-	22.34
2	Pig iron	94.30	4.00	1.00	0.70	-
3	Slag	0.30	-	-	-	-

Material balance for O_2

$$\begin{aligned}
 & \frac{1.5}{159.70} \left[W_0 v_{Fe_2O_3} + W_{OS} s_{Fe_2O_3} + W_{OP} p_{Fe_2O_3} + W_{OM} g_{Fe_2O_3} \right. \\
 & \quad \left. + W_C t_{Fe_2O_3} \right] + \frac{1}{2 \times 71.85} \left[W_{OS} s_{FeO} + W_{OP} p_{FeO} \right] \\
 & \quad + \frac{W_{OM} g_{MnO_2}}{2 \times 86.9} + \frac{W_L l_{CO_2}}{44} \\
 & \quad + \frac{60 \times F_b}{22.4} \left[0.21 + \frac{22.4 \times W_{st}}{36000} + X_{O_2} \right] \\
 & = \frac{F_0}{22.4} \left[\frac{y_{CO,0}}{2} + y_{CO_2,0} + \frac{y_{H_2O,0}}{2} \right] + \frac{W_D j_O}{32} \\
 & \quad - W_P \left[\frac{\alpha_{Mn}}{2 \times 54.9} + \frac{\alpha_{Si}}{28.09} \right] \tag{3.5}
 \end{aligned}$$

Material balance for slag

The material balance for other components present in the slag such as Mn, Si, Al, Ca and Mg, are not being given separately. On combining the material balance equations on Mn, Si, Al, Ca and Mg, we get the following equation for slag flow rate (W_S).

$$\begin{aligned}
 & W_0 \left[v_{SiO_2} + v_{Al_2O_3} \right] + W_{OS} \left[s_{SiO_2} + s_{Al_2O_3} + s_{CaO} + s_{MgO} \right] \\
 & + W_{OP} \left[p_{SiO_2} + p_{Al_2O_3} + p_{CaO} + p_{MgO} \right]
 \end{aligned}$$

$$\begin{aligned}
& + W_C t_a \left[b_{\text{SiO}_2} + b_{\text{Al}_2\text{O}_3} + b_{\text{CaO}} + b_{\text{MgO}} \right] \\
& + W_L \left[l_{\text{SiO}_2} + l_{\text{Al}_2\text{O}_3} + l_{\text{CaO}} + l_{\text{MgO}} \right] \\
& + W_{\text{OM}} \left[g_{\text{SiO}_2} + g_{\text{Al}_2\text{O}_3} + \frac{70.9 \times g_{\text{MnO}_2}}{86.9} \right] \\
& - W_P \left[\frac{60.09 \times \alpha_{\text{Si}}}{28.09} + \frac{70.9 \times \alpha_{\text{Mn}}}{54.9} \right] = W_S \left[1 - r_{\text{Fe}} \right] \quad (3.6)
\end{aligned}$$

Material balance for gas at the top

$$y_{\text{CO},0} + y_{\text{CO}_2,0} + y_{\text{H}_2,0} + y_{\text{H}_2\text{O},0} + y_{\text{N}_2,0} = 1 \quad (3.7)$$

Equations (3.1 - 3.7) are material balance equations and are solved simultaneously for estimating the volumetric flow rate of gas and its composition at the top, production rate of pig iron, and the discharge rate of slag. The solution methodology of these equations is discussed in the next section.

3.1.1.2 Solution Methodology

The seven equations (3.1 - 3.7) are to be solved for estimating the unknown parameters. In solving these equations, the charging rate of raw materials, flow rate of hot blasted air, steam injection and oxygen enrichment are considered as given operating parameters. Further, the compositions of dust and hot metal, and the composition of Fe in slag are assumed to be prespecified. The Fe is assumed to be present in suspended form in the slag. However, there are eight unknown

variables, which are to be estimated by solving seven equations (3.1 - 3.7). As the number of variables is more than the number of equations, it is necessary to find out one more condition. The observed results of Indian blast furnaces as mentioned by Batra (1988), indicate that the concentration of water vapour in the top gas is very very low, almost equal to zero, whereas other gases are in appreciable quantities. Therefore, the observed top gas analysis does not contain H_2O vapours. This observation may also be supported by considering the equilibrium constant for water gas shift reaction. The temperature of gas at the top of the furnace is generally around 500 K. According to Miyasaka et al. (1975), the equilibrium constant for water gas shift reaction (K_7) at 500 K is 132.7145 and is expressed as follows :

$$K_7 = (y_{CO_2} y_{H_2}) / (y_{CO} y_{H_2O})$$

Thus, $y_{H_2O,0}$ can be written as follows :

$$y_{H_2O,0} = y_{H_2,0} \left[\frac{y_{CO,0}}{y_{CO_2,0}} \right]^{-1} / 132.7145$$

For Indian blast furnaces, the ratio ($y_{CO,0} / y_{CO_2,0}$) varies from 1.0 to 2.0 and the maximum amount of H_2 gas is 5% (i.e. $y_{H_2,0} = 0.05$). This implies that the maximum amount of H_2O vapours in top gas is 0.0377 % (i.e. $y_{H_2O,0} = 0.0377 \times 10^{-2}$) which is negligibly small.

With the above observations and facts, concentration of H_2O vapours in the top gas is assumed to be zero. Thus, we have

$$y_{H_2O,0} = 0 \quad (3.8)$$

With the above assumptions and operating conditions, the flow rates of pig iron (W_p) and slag (W_s) are determined from the equations (3.1) and

(3.6). The volumetric flow rate of top gas (F_0) and its composition ($y_{CO,0}$, $y_{CO_2,0}$, $y_{N_2,0}$, $y_{H_2,0}$ and $y_{H_2O,0}$) are determined by solving equations (3.2 - 3.5), (3.7) and (3.8) simultaneously.

3.1.1.3 Results and Discussion

Four sets of operating conditions and the corresponding observed output conditions are collected from the report by Batra (1988) on the blast furnaces operating at Bokaro Steel Plant, India. These sets are mentioned in Table 3.3. The components and their compositions in different solid feeds, pig iron, dust and slag are collected from the literature and reports on blast furnaces by Gupta et al. (1990) and Batra (1988), and are listed in Tables 3.1 and 3.2. These data are in accordance with the Indian conditions. The compositions of pig iron and dust are assumed to be independent of operating conditions and are same for all the four data sets. The iron content in slag is assumed to be 0.3% by weight. On the basis of these compositions, all the data of four sets of Table 3.3 are processed according to the material balance equations (3.1 - 3.8). The results obtained by using the computer program, developed in the present work, are compared with observed data and are given in Table 3.4. It may be seen that these results are quite close to each other and variation is within permissible limits of $\pm 5\%$. Hence, a good agreement between calculated and observed data indicates accuracy and good reliability of the overall material balance computations.

3.1.2 Rate of SiO Gas Generation in Combustion Zone

In the combustion zone where the temperature is very high, generation of white gaseous product SiO is observed. This is produced by the reaction of SiO_2 with carbon at high temperature. There are two

Table 3.3 Process Variables for Blast Furnace at B.S.P. [Batra (1988)]

Process Variable	Set number				
	1	2	3	4	
Pig iron , kg/hr	76125.0	87250.0	71540.0	66300.0	
Slag , kg/hr	36015.0	42143.0	34410.0	32550.0	
Iron ore , kg/hr	43984.0	50000.0	43500.0	40180.0	
Coke , kg/hr	57030.0	68000.0	56800.0	51700.0	
Sinter , kg/hr	79922.0	90650.0	72400.0	67500.0	
Mn ore , kg/hr	2578.0	3840.0	3220.0	2520.0	
Lime , kg/hr	1641.0	1745.0	2075.0	1525.0	
Dust , kg/hr	1641.0	1134.0	1073.0	1392.0	
Pellets , kg/hr	0.0	0.0	0.0	0.0	
Blast , Nm ³ /min	2083.0	2477.0	2027.0	1879.0	
Steam , gm/Nm ³ (blast)	29.6	47.6	49.50	49.50	
Oxygen enrichment , Nm ³ /Nm ³ (blast)	0.0	0.0	0.0	0.0	
Blast temperature, K	1163.0	1176.0	1213.0	1199.0	
Blast pressure, kg/cm ²	2.2	2.36	2.03	2.31	
Composition of top gas, vol. per cent	CO	24.8	24.8	24.9	25.2
	CO ₂	17.0	16.7	16.8	16.6
	N ₂	55.3	54.7	53.9	53.9
	H ₂	2.7	4.1	4.2	4.2

Table 3.4 Comparison of Computed Results by Material Balance Program with Observed Data

Set number	Value	Pig iron, kg/hr	Slag, kg/hr	Composition of top gas, Vol. %			
				CO	CO ₂	H ₂	N ₂
1	Observed	76125.0	36015.0	24.80	17.00	2.70	55.30
	Computed	76072.9	36708.9	24.73	16.53	2.62	56.12
	% variation	0.0685	-1.8903	0.2831	2.8433	3.0534	-1.4611
2	Observed	87250.0	42143.0	24.80	16.70	4.10	54.70
	Computed	87068.9	42812.2	24.38	16.48	4.13	55.02
	% variation	0.2080	-1.5631	1.7227	1.3350	-0.7264	-0.5816
3	Observed	71540.0	34410.0	24.9	16.8	4.20	53.9
	Computed	71973.7	35518.9	25.36	15.95	4.25	54.44
	% variation	-0.6026	-3.1220	-1.8139	5.3292	-1.1765	-0.9919
4	Observed	66300.0	32550.0	25.20	16.60	4.20	53.90
	Computed	66472.1	32284.4	23.90	16.85	4.29	54.96
	% variation	-0.2589	0.8227	5.4393	-1.4837	-2.0979	-1.9287

major sources of SiO_2 in the blast furnace, namely coke, ash and slag. The Indian coke contains ash as high as 20 - 26 % , and the SiO_2 content in the ash is around 50 % . Since almost all the coke flows into the combustion zone and the total coke ash is processed there, therefore, the coke ash becomes a potential source of SiO gas formation in the combustion zone.

3.1.2.1 Methodology

The formation of SiO gas takes place according to the following reaction, which is endothermic in nature.



It has been reported by Taguchi et al. (1982) that the evolution of SiO gas from SiO_2 of ash does not take place until the ash melts. SiO_2 of ash reacts with carbon in coke to produce SiO gas. This results in the continuous decrease in SiO_2 content of ash. Since the melting point of ash depends upon its SiO_2 content and varies inversely with it, therefore, the melting point of residual ash increases gradually. The laboratory studies reported by Omori (1987), have demonstrated that the formation of SiO vapours takes place till the melting point of residual ash reaches 1700°C .

On the basis of these laboratory studies, a method is proposed for calculating the formation rate of SiO gas. The detailed description is given in the following paragraphs.

First of all, it is necessary to find out the relationship between melting temperature of coke ash and its SiO_2 content. For this, $\text{CaO} - \text{Al}_2\text{O}_3 - \text{SiO}_2$ phase diagram is used to find out the melting temperature of ash at different ash compositions [Muan and Osborn (1965)]. Thus, plots (Figure 3.2) between melting temperature of ash

(T'_m) and mass fraction of SiO_2 in ash (X_A) have been constructed for four different values of mass per cent of Al_2O_3 ($X_{\text{Al}_2\text{O}_3}$) in ash. In these plots amount of MgO present in ash has been included in CaO , because MgO is relatively in small amounts in coke ash. The plots show that T'_m varies linearly with SiO_2 content of ash for specified Al_2O_3 content. Therefore, method of least squares has been used to obtain the line of best fit.

The linear relationships thus obtained for four different values of $X_{\text{Al}_2\text{O}_3}$ in ash are as follows :

For $X_{\text{Al}_2\text{O}_3} = 81.0$:

$$T'_m = 1799.721 - 235.963 X_A \quad (3.9)$$

For $X_{\text{Al}_2\text{O}_3} = 85.0$:

$$T'_m = 1847.063 - 266.0434 X_A \quad (3.10)$$

For $X_{\text{Al}_2\text{O}_3} = 90.0$:

$$T'_m = 1957.186 - 380.5155 X_A \quad (3.11)$$

For $X_{\text{Al}_2\text{O}_3} = 95.0$:

$$T'_m = 2060.860 - 489.1946 X_A \quad (3.12)$$

It is seen that the slopes and intercepts of equations (3.9 - 3.12) increase with the increasing Al_2O_3 content. Further trials by means of regression analysis were undertaken to represent T'_m by a single linear relationship. After making some trials, it became possible to arrive at such a relationship. The equation (3.13) represents this relationship.

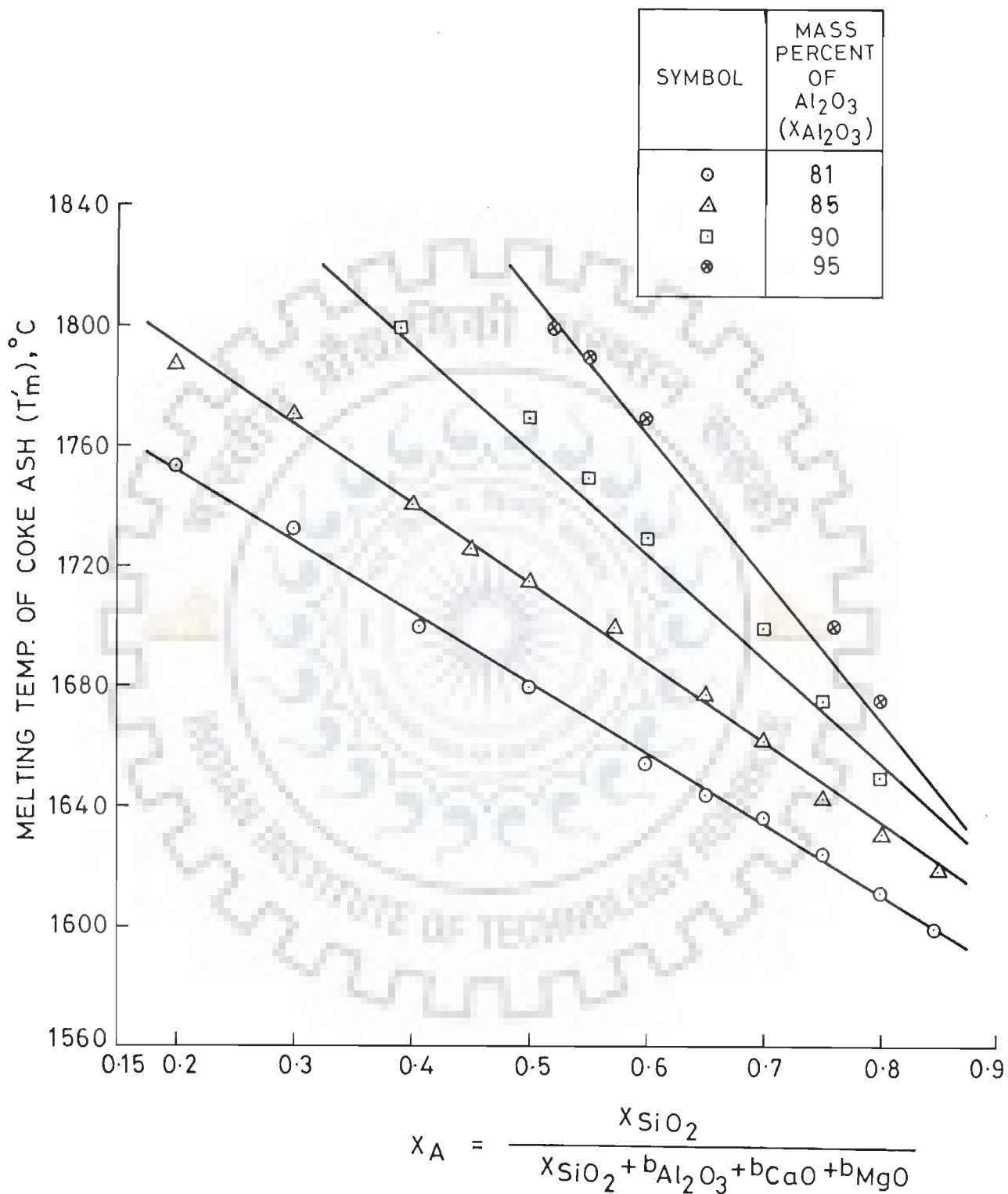


FIGURE 3.2 VARIATION OF MELTING TEMPERATURE OF COKE ASH WITH SiO_2 AND Al_2O_3 CONTENTS

$$T'_m = B X_A + C \quad (3.13)$$

Where

$$B = 3.73.1661 - 7.5201 X_{Al_2O_3} \quad ; \quad 80.0 \leq X_{Al_2O_3} \leq 85.0$$

$$B = 1629.794 - 22.31531 X_{Al_2O_3} \quad ; \quad 85.0 \leq X_{Al_2O_3} \leq 95.0$$

$$C = 800.6885 \exp (9.9288 \times 10^{-3} X_{Al_2O_3})$$

and

$$X_A = \frac{X_{SiO_2}}{X_{SiO_2} + b_{Al_2O_3} + b_{CaO} + b_{MgO}} \quad (3.14)$$

X_{SiO_2} is the mass fraction of SiO_2 in ash at any time. It reduces continuously due to SiO gas formation and is defined as follows :

$$X_{SiO_2} = \frac{\text{weight of } SiO_2 \text{ in ash at any time}}{W_C t_a} \quad (3.14a)$$

$$X_{Al_2O_3} = \frac{b_{Al_2O_3} \times 100}{b_{Al_2O_3} + b_{CaO} + b_{MgO}} \quad (3.15)$$

Figure 3.3 indicates the variation of actual melting temperature obtained from phase diagram with the melting temperature calculated from equation (3.13) for the four values of $X_{Al_2O_3}$. The variation in these two temperatures is within $\pm 2\%$, which is acceptable. Hence, equation (3.13) can be used to determine the relationship between melting temperature of ash and its SiO_2 content for the compositions under consideration.

In order to find out the formation rate of SiO gas, the value of X_A is calculated at 1700°C from equation (3.13) as the formation of SiO gas stops at around 1700°C. Thus, we get

$$X_A = \frac{C - 1700}{B}$$

On substituting the value of X_A in equation (3.14), we get

$$X_{SiO_2} = \frac{X_A}{1 - X_A} (b_{Al_2O_3} + b_{CaO} + b_{MgO})$$

Therefore, the molar flow rate of SiO gas formed, will be as follows :

$$F_{m_{SiO,1}} = W_C t_a (b_{SiO_2} - X_{SiO_2}) / 60.09 \quad (3.16)$$

3.1.2.2 Results and Discussion

Regarding SiO gas formation, following practical observations are mentioned in the literature. Firstly, since the formation of SiO gas is endothermic, so the temperature of tuyere gas is reduced due to this reaction. In Indian blast furnaces this reduction in tuyere gas temperature is of the order of 100 - 200°C [Batra (1988)]. Secondly, SiO gas ascends alongwith tuyere gas with a partial pressure in the range of $10^{-1} - 10^{-2}$ atm under Indian conditions where ash content of coke is very high [Biswas (1981)]. On the basis of above observations, the validity of equation (3.16) has been ascertained.

The molar flow rate of SiO gas, calculated from equation (3.16), is mentioned in Table 3.5 for all four data sets given in Table 3.3. Table 3.5 also indicates the reduction in tuyere gas temperature, $\Delta T_{g,1}$, due to SiO gas formation and the partial pressure of SiO gas, $p_{a_{SiO}}$, in ascending gases from tuyere level. Both $p_{a_{SiO}}$ and $\Delta T_{g,1}$ are

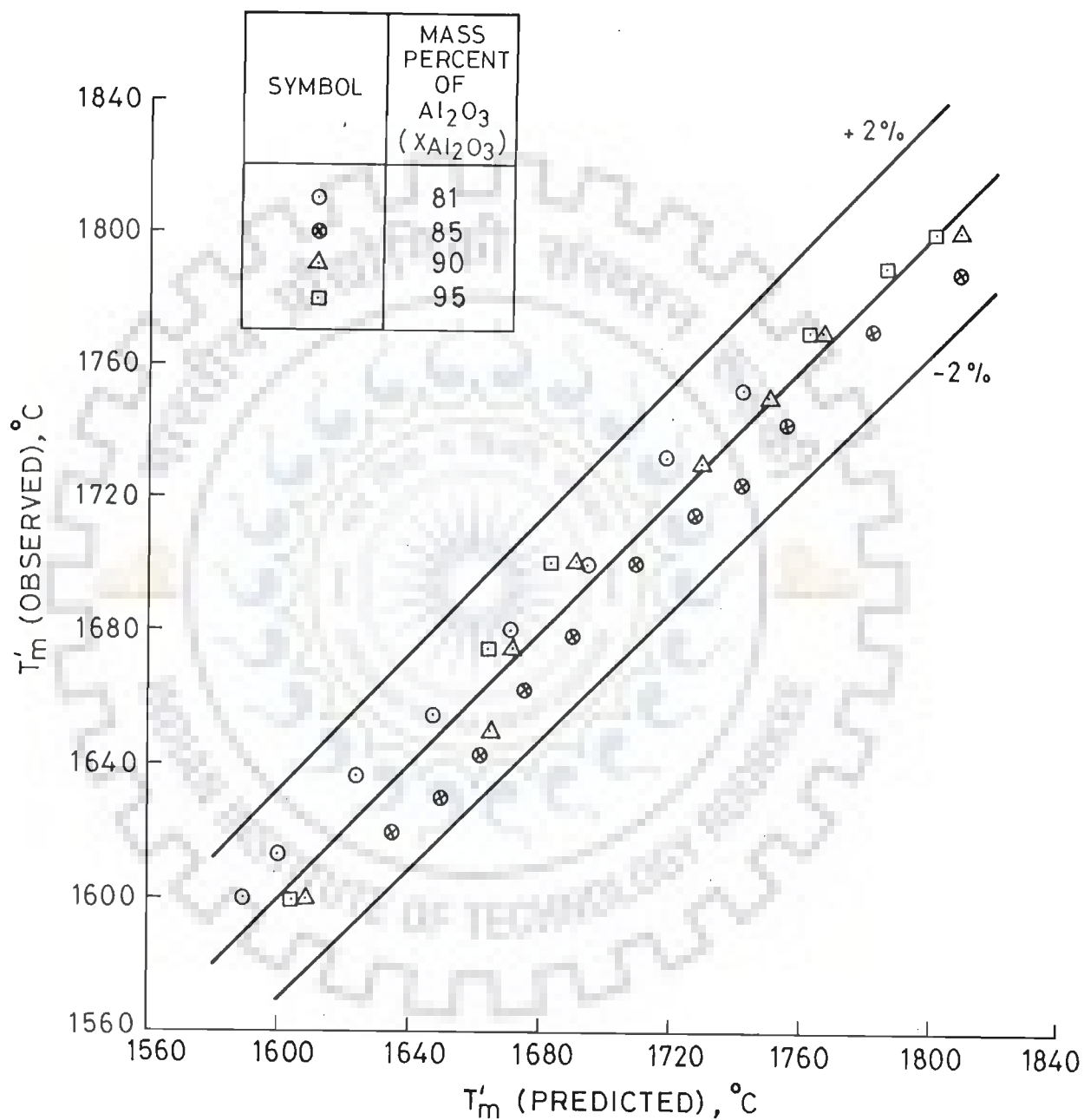


FIGURE 3-3 COMPARISON OF OBSERVED AND PREDICTED MELTING TEMPERATURES OF COKE ASH [EQUATION (3-13)]

Table 3.5 Computed Results for SiO Gas Formation at Tuyere Level

Set number	Molar flow rate of SiO gas, kmol/hr	Temperature of tuyere gas, K		Temperature drop due to SiO gas formation K	Mole per cent of SiO gas in tuyere gas	Partial pressure of SiO gas, atm
		With SiO gas formation	Without SiO gas formation			
1	75.9351	2099.088	2263.425	164.337	0.0104	3.12×10^{-2}
2	90.5416	2032.608	2190.865	158.257	0.0100	3.00×10^{-2}
3	75.6289	2046.379	2207.656	161.277	0.0102	3.06×10^{-2}
4	68.8382	2040.616	2198.865	158.249	0.0100	3.00×10^{-2}

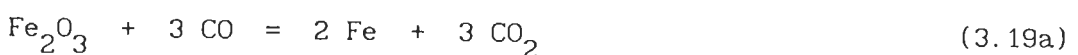
within their normal range of values as reported in the literature for various blast furnaces, i.e. $\Delta T_{g,1}$ is in the range of 100 - 200°C and $p_{a_{SiO}}$ is in the range of 10^{-1} to 10^{-2} atm. In the calculation of $p_{a_{SiO}}$, total pressure of gases at tuyere level has been taken to be 3.0 atm, which is generally kept in Indian blast furnaces.

Hence, the calculated results lead to good reliability of the equation (3.16) to determine the molar rate of formation of SiO gas.

3.1.3 Material Balance around Combustion Zone

The incoming and outgoing streams of solids, liquids and gases around combustion zone are shown in Figure 3.1. The coke is the only material, which enters as solid. Pig iron and slag that are formed in bosh, enter in molten state. The hot air with steam and excess oxygen, is blown into this zone through the tuyeres. The gases produced after reactions in combustion zone, enter the bosh. The pig iron and slag are collected into the hearth from the bottom of this zone.

The main chemical reaction, which takes place in the combustion zone in front of tuyeres, is combustion of coke. The other chemical reactions considered here are the reduction of steam, and the reduction of SiO_2 and Fe_2O_3 , which are present in coke ash. These reactions may be described as follows :



Combination of reactions (3.19a) and (3.19b) yields



Due to above reactions H_2 , CO and SiO gases are produced. These gaseous products along with inert N_2 of air form tuyere gas enter the bosh from combustion zone. The ash present in the coke melts and forms slag.

On the basis of reactions (3.17 - 3.21) one can estimate the volumetric flow rate and composition of tuyere gas. The mass flow rate of coke, pig iron and slag, which are entering the combustion zone from the bosh can be estimated by taking mass balance around combustion zone. These estimations will provide us the boundary conditions at the bottom of bosh, which are obviously essential for the solution of proposed mathematical model.

3.1.3.1 Methodology

In order to determine the required flow rate and compositions at the bottom of bosh, the following assumptions are made.

- (i) The reactions (3.17 - 3.20) proceed to completion. This implies that the tuyere gas does not contain H_2O , CO_2 and O_2 and there is no unreacted Fe_2O_3 present in coke ash.
- (ii) Total coke ash in the furnace is considered to form the slag in the combustion zone only. Thus, the ash present in the coke which is consumed in shaft region, will leave the bosh as solid along with the unreacted solid coke.

By considering above assumptions, the volumetric flow rates, i.e.

$F_{CO,1}$, $F_{H_2,1}$, $F_{N_2,1}$ and $F_{SiO,1}$ of gases CO, H_2 , N_2 and SiO respectively, are expressed by the following equations.

$$F_{CO,1} = 60 F_b \left[0.42 + 2 X_{O_2} + \frac{22.4 W_{st}}{18000} \right] + 22.4 F_{mSiO,1} + 3 \times 22.4 W_C t_a b_{Fe_2O_3} / 159.70 \quad (3.22)$$

$$F_{H_2,1} = 22.4 \times 60 F_b W_{st} / 18000 \quad (3.23)$$

$$F_{N_2,1} = 0.79 \times 60 F_b \quad (3.24)$$

$$F_{SiO,1} = 22.4 F_{mSiO,1} \quad (3.25)$$

The molar flow rate of SiO gas entering the bosh ($F_{mSiO,1}$) can be calculated by equation (3.16). The total flow rate of gas (F_1) can be expressed by adding equations (3.22) to (3.25). Thus, we obtain

$$F_1 = F_b (72.6 + 120.0 X_{O_2} + 149.3334 \times 10^{-3} W_{st}) + 0.4208 W_C t_a b_{Fe_2O_3} + 44.8 F_{mSiO,1} \quad (3.26)$$

The mole fractions of CO, H_2 , N_2 and SiO gas in tuyere gas at the bottom of bosh can be represented as follows :

$$y_{CO,1} = \frac{F_{CO,1}}{F_1} \quad (3.27a)$$

$$y_{H_2,1} = \frac{F_{H_2,1}}{F_1} \quad (3.27b)$$

$$y_{N_2,1} = \frac{F_{N_2,1}}{F_1} \quad (3.27c)$$

$$y_{SiO,1} = \frac{F_{SiO,1}}{F_1} \quad (3.27d)$$

Equation (3.26) and equations (3.27a - 3.27d) represent the volumetric flow rate of gas and its composition, and thus, provide us a set of required boundary conditions for gas phase at the bottom of bosh.

The solids leaving the bosh, contain the unreacted coke as well as the solid ash, which is released from coke after reactions in shaft region. Since it is already assumed in Section 3.1.1 that there is no unreacted coke coming out from the furnace, therefore, the coke consumption rate in combustion zone represents the mass flow rate of coke leaving the bosh. Rest of the coke is considered to be consumed in shaft region. Thus, the mass flow rate of solids leaving the bosh ($W_{C,1}$) is expressed by the following equation.

$$W_{C,1} = (W_C t_a) (0.6994 \alpha_C b_{Fe_2O_3} + \alpha_{Fe}) / \alpha_{Fe} + 0.5357 F_{CO,1} \quad (3.28)$$

The mass flow rate of slag ($W_{S,1}$) and pig iron ($W_{P,1}$) at the bottom of bosh can be obtained from equations (3.29) and (3.30) respectively.

$$W_{S,1} = W_S - W_C t_a (1 - b_{Fe_2O_3}) \quad (3.29)$$

$$W_{P,1} = W_P - 0.6994 W_C t_a b_{Fe_2O_3} / \alpha_{Fe} \quad (3.30)$$

3.1.3.2 Results

The calculations are carried out for four different data sets as given in Table 3.3 by using equations (3.26), (3.27a - 3.27d), and (3.28 - 3.30) to find out the boundary conditions concerning the flow rate and compositions at the bottom of bosh. The calculated results are reported in Table 3.6 . Since the practically observed conditions at the bottom of bosh are not available, therefore, the correctness of calculated boundary conditions at the bottom of bosh cannot be ascertained. However, these appear to be correct.

3.2 ENERGY BALANCE

In order to find out the temperatures of tuyere and top gases, energy balances around appropriate regions of the blast furnace are required. The tuyere gas temperature ($T_{g,1}$) has been estimated according to the following two steps.

- (i) Determination of adiabatic flame temperature of gases produced by combustion of coke in front of tuyeres.
- (ii) Energy balance around combustion zone.

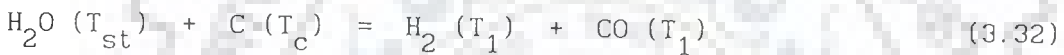
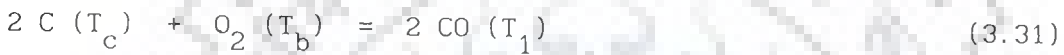
Temperature of gases leaving the furnace from the top ($T_{g,0}$) , has been calculated by taking overall energy balance around the shaft region. In these computations, the temperatures of solids leaving the bosh have been assumed, as reported by Batra (1988) and Gupta et al. (1990) for Indian blast furnaces.

3.2.1 Adiabatic Flame Temperature

If the combustion of coke in front of tuyeres proceeds

adiabatically, i.e. no heat is exchanged with the surroundings, then the gaseous products will attain a temperature known as adiabatic flame temperature (T_1). Hence, for adiabatic system the sum of enthalpies of the reactants must equal the sum of standard heats of reactions and the enthalpies of all the products [Hougen et al. (1964)]. The products must include all materials actually present ; inerts and excess reactants as well as new compounds formed. This is the basis for calculating the adiabatic flame temperature (T_1).

Following combustion reactions take place in front of tuyeres.



It may be noted that the temperatures are mentioned in the brackets.

Coke enters the combustion zone at temperature T_c . The carbon of coke reacts with oxygen and steam, injected with air. The combustion of coke with oxygen [reaction (3.31)] is exothermic while the reaction of steam with the carbon of coke [reaction (3.32)] is endothermic. Nitrogen in air acts as an inert gas. T_b and T_{st} are the temperatures of the blasted air and steam respectively. T_1 is the adiabatic flame temperature, which is to be calculated. The temperature T_o is selected as reference temperature for calculating the enthalpies.

The enthalpy change for any reaction can be written as follows :

$$(\Delta H)_j = (\Delta H_R)_{j, T_o} + \int_{T_o}^T \sum_P (C_p)_P dT - \sum_i \int_{T_o}^{T_i} (C_p)_i dT \quad (3.33)$$

Where

$$(\Delta H)_j = \text{enthalpy change of reaction } j$$

Table 3.6 Computed Results for Flow Conditions at the Bottom of Bosh

S.N.	Process Variable	Set Number				
		1	2	3	4	
1	Flow rate of solids, kg/hr	46534.06	57170.40	47260.89	43543.74	
2	Flow rate of pig iron, kg/hr	75468.05	86347.68	71371.29	65923.76	
3	Flow rate of slag, kg/hr	22696.63	26104.58	21563.12	19581.71	
4	Flow rate of tuyere gas, Nm ³ /hr	164180.0	201904.8	165875.3	153701.5	
5	Composition of tuyere gas, mole fraction	$y_{CO,1}$	0.3602	0.3648	0.3654	0.3653
		$y_{H_2,1}$	0.0280	0.0436	0.0452	0.0452
		$y_{N_2,1}$	0.6014	0.5815	0.5792	0.5795
		$y_{SiO,1}$	0.0104	0.0100	0.0102	0.0100

$(\Delta H_R)_{j, T_0}$ = heat of reaction j at temperature T_0

$\sum_P (C_p)_P$ = sum of heat capacities of products

$(C_p)_i$ = heat capacity of reactant i

T = temperature at which the products are formed.

T_i = temperature at which the reactant i reacts.

On applying equation (3.33) to reactions (3.31) and (3.32), we obtain the following equations.

The enthalpy change for reaction (3.31), $(\Delta H)_1$

$$\begin{aligned}
 (\Delta H)_1 = & (\Delta H_R)_{1, T_0} + 2 \int_{T_0}^{T_1} (C_p)_{CO} dT - 2 \int_{T_0}^{T_c} (C_p)_C dT \\
 & - \int_{T_0}^{T_b} (C_p)_{O_2} dT
 \end{aligned} \tag{3.34}$$

The enthalpy change for reaction (3.32), $(\Delta H)_2$

$$\begin{aligned}
 (\Delta H)_2 = & (\Delta H_R)_{2, T_0} + \int_{T_0}^{T_1} \left\{ (C_p)_{CO} + (C_p)_{H_2} \right\} dT \\
 & - \int_{T_0}^{T_{st}} (C_p)_{H_2O} dT - \int_{T_0}^{T_c} (C_p)_C dT
 \end{aligned} \tag{3.35}$$

Since the temperature of nitrogen gas changes from T_b to T_1 , therefore, the corresponding change in its enthalpy, $(\Delta H)_3$, is as follows :

$$(\Delta H)_3 = \int_{T_b}^{T_1} (C_p)_{N_2} dT \quad (3.36)$$

Let A_1 , A_2 and A_3 be the new parameters, which represent the moles of O_2 consumed, mole of steam consumed and moles of N_2 entering with the air per unit time respectively. On writing enthalpy balance for the adiabatic system, we get

$$A_1 (\Delta H)_1 + A_2 (\Delta H)_2 + A_3 (\Delta H)_3 = 0 \quad (3.37)$$

On substituting the equations (3.34) to (3.36) into the equation (3.37), we obtain

$$\begin{aligned} & A_1 (\Delta H_{R1, T_0}) + A_1 (\Delta H_{R2, T_0}) + (2A_1 + A_2) \int_{T_0}^{T_1} (C_p)_{CO} dT \\ & - (2A_1 + A_2) \int_{T_0}^{T_c} (C_p)_C dT - A_1 \int_{T_0}^{T_b} (C_p)_{O_2} dT + A_2 \int_{T_0}^{T_1} (C_p)_{H_2} dT \\ & - A_2 \int_{T_0}^{T_{st}} (C_p)_{H_2O} dT + A_3 \int_{T_b}^{T_1} (C_p)_{N_2} dT = 0 \end{aligned} \quad (3.38)$$

Using the expressions for heat capacities as a function of temperature from Table A.1 and integrating equation (3.38), we obtain following nonlinear equation for adiabatic flame temperature (T_1).

$$A_9 T_1^3 + A_{10} T_1^2 + A_{15} T_1 + A_{11} = 0 \quad (3.39)$$

Where

$$A_9 = 10^{-3} (0.98 A_1 + 0.88 A_2 + 0.51) / A_3$$

$$A_{10} = (13.58 A_1 + 13.31 A_2 + 6.66) / A_3$$

$$A_{11} = 10^3 (22 A_1 - A_2) / A_3$$

$$A_{15} = A_8 - A_7 - A_{14} - [2 A_1 A_{12} + A_2 (A_{12} + A_{13})] / A_3$$

$$A_1 = 2.6786 F_b (0.21 + X_{O_2})$$

$$A_2 = 3.3333 \times 10^{-3} F_b W_{st}$$

$$A_3 = 2.1161 F_b$$

$$A_4 = 2.93 + 10^{-3} (T_c + T_o) - \frac{1.1 \times 10^5}{T_c \times T_o}$$

$$A_5 = 7.16 + 0.5 \times 10^{-3} (T_b + T_o) - \frac{0.40 \times 10^5}{T_b \times T_o}$$

$$A_6 = 7.17 + 1.28 \times 10^{-3} (T_{st} + T_o) - \frac{0.08 \times 10^5}{T_{st} \times T_o}$$

$$A_7 = [A_4 (2A_1 + A_2) (T_c - T_o) + A_1 A_5 (T_b - T_o) + A_2 A_6 (T_{st} - T_o)] / A_3$$

$$A_8 = \left[A_1 (\Delta H_R)_{1, T_o} + A_2 (\Delta H_R)_{2, T_o} \right] / A_3$$

$$A_{12} = 6.79 T_o + 0.49 \times 10^{-3} T_o^2 + \frac{0.11 \times 10^5}{T_o}$$

$$A_{13} = 6.52 T_o + 0.39 \times 10^{-3} T_o^2 - \frac{0.12 \times 10^5}{T_o}$$

and

$$A_{14} = 6.66 T_b + 0.51 \times 10^{-3} T_b^2$$

The solution of equation (3.39) gives the adiabatic flame temperature. The methodology is described in the following section.

3.2.1.1 Solution Methodology and Results

In order to find out the solution of equation (3.39), it is necessary to calculate its coefficients. During their calculations the reference temperature (T_o) and temperature of coke in combustion zone (T_c) are considered as 298 and 1773 K respectively. The temperature of steam (T_{st}) is taken same as the temperature of air blast (T_b). The heats of reactions at 298 K, used in equations (3.34) and (3.35), are calculated by using the heats of formations as given in Table A.3.

Thus, the coefficients of equation (3.39), i.e. A_9 , A_{10} , A_{11} and A_{15} , are calculated for all the four data sets of Table 3.3 and are mentioned in Table 3.7.

Equation (3.39) can be easily solved numerically by Newton Raphson method and the values of T_1 thus obtained with tolerance 1×10^{-4} have been reported in Table 3.7 for all the data sets.

However, there exists a possibility to obtain an analytical expression for approximate value of T_1 . For the first data set, equation (3.39) is as follows :

$$0.80157 \times 10^{-3} T_1^3 + 10.891 T_1^2 - 30078.0 T_1 + 5802.3 = 0 \quad (3.39a)$$

Table 3.7 Comparison of Adiabatic Flame Temperatures Computed by Newton Raphson Method and Approximate Relationship

Set Number	Coefficients of equation (3.39)				Adiabatic flame temperature (T_1), K		Per cent variation
	A_9	A_{10}	A_{11}	A_{15}	Solution of equation (3.39) by Newton Raphson Method	Approximate relationship, equation (3.42)	
1	0.8016×10^{-3}	10.891	5802.3	-30078.0	2353.7510	2353.9190	7.138×10^{-3}
2	0.8265×10^{-3}	11.268	5773.9	-29944.0	2276.8880	2277.0570	7.422×10^{-3}
3	0.8292×10^{-3}	11.308	5770.9	-30319.0	2294.7810	2294.9470	7.277×10^{-3}
4	0.8292×10^{-3}	11.308	5770.9	-30166.0	2284.668	2284.835	7.310×10^{-3}

Since the value of adiabatic flame temperature is generally more than 1000 K, therefore, a dimensionless variable θ ($= T_1/1000$), shall scale down the magnitude of unknown variable in the above equation. Writing the equation (3.39a) in terms of θ , we obtain

$$0.80157 \theta^3 + 10.891 \theta^2 - 30078.0 \times 10^{-3} \theta + 5802.3 \times 10^{-6} = 0 \quad (3.39b)$$

or

$$A_9 \times 10^3 \theta^3 + A_{10} \theta^2 + A_{15} \times 10^{-3} \theta + A_{11} \times 10^{-6} = 0 \quad (3.40a)$$

Coefficient $A_{11} \times 10^{-6}$ is very small for all the data sets and may be neglected for approximation purposes. This results in the quadratic equation

$$A_9 \times 10^3 \theta^2 + A_{10} \theta + A_{15} \times 10^{-3} = 0 \quad (3.40b)$$

whose solution is given by the following equation .

$$\theta = \frac{-A_{10} \pm \sqrt{A_{10}^2 - 4 A_{15} A_9}}{2 A_9 \times 10^3} \quad (3.41)$$

As adiabatic flame temperature cannot be negative, therefore,

$$T_1 = \frac{-A_{10} + \sqrt{A_{10}^2 - 4 A_{15} A_9}}{2 A_9} \quad (3.42)$$

where A_{10} , A_{15} and A_9 are same as defined for equation (3.39).

The values of T_1 were also calculated using equation (3.42) and reported in Table 3.7. It may be observed that these two values of T_1

are quite close to each other. Value of T_1 by equation (3.42) differs only by 7.422×10^{-3} per cent with respect to the value obtained numerically by Newton Raphson method. Therefore, it may be concluded that equation (3.42) provides sufficiently accurate value of T_1 and can be used for the computation of adiabatic flame temperature.

3.2.2 Tuyere Gas Temperature

The temperature of gases entering the bottom of bosh from combustion zone, is known as tuyere gas temperature. It depends upon the adiabatic flame temperature of gases produced after combustion of coke and various other processes occurring in the combustion zone, viz. melting of ash, formation of SiO gas, reduction of Fe_2O_3 , formation of slag from ash etc. Due to these additional processes, the tuyere gas temperature differs from the adiabatic flame temperature. As discussed in Section 3.2.1 for the determination of adiabatic flame temperature, it has been assumed that heat released is used to increase the gas temperature only. Thus, ash formed after combustion remains at the temperature of coke, T_c . Further, it is necessary to mention here that during the estimation of tuyere gas temperature, the average values of heat capacities of solids, liquids and gases have been taken because of small variations in their temperatures. These average values of heat capacities are given in Table 3.8. The involved heat energies in various processes and their computation have been described below.

Heat consumed for raising the temperature of bosh slag and metal, Q_{SM}

The bosh slag and pig iron formed in bosh are assumed to be at the same temperature T_c as the solid coke, and leave the combustion zone at temperatures T_{sl} and T_p respectively.

Therefore, heat energy is required to raise the temperatures of

Table 3.8 Average Heat Capacities of Substances

S.N.	Substance	Heat capacity, kcal / kmol.K	Temperature range, K
1	Al ₂ O ₃ (s)	20.7246 38.2758	298 - 373 1673 - 1973
2	C (s)	2.6114 6.1339	298 - 373 1473 - 1773
3	CaCO ₃ (s)	21.1602	298 - 373
4	CaO (s)	10.7289 13.0113	298 - 373 1177 - 1973
5	CO (g)	9.0910	2200 - 2500
6	Fe (l)	10.00	1803 - 1873
7	FeO (s)	11.7282	298 - 373
8	Fe ₂ O ₃ (s)	26.5650 34.5362	298 - 373 1473 - 1750
8	H ₂ (g)	8.3552	2200 - 2500
9	MgO (s)	9.3840 12.9789	298 - 373 1673 - 1973
10	MnO ₂ (s)	13.9280	298 - 373
11	N ₂ (g)	9.5270	2200 - 2500
12	SiO (g)	9.0853	2200 - 2500
13	SiO ₂ (s)	11.9584 17.6458	298 - 373 1673 - 1973
14	Pig Iron (l)	0.2030 kcal/kg.K	1673 - 1973
15	Slag (l)	0.2750 kcal/kg.K	1673 - 1973

bosh slag and pig iron from T_c to T_{sl} and T_p respectively. Thus, we obtain the following relationship.

$$Q_{SM} = W_{P,1} (C_p)_{pig} (T_p - T_c) + W_{S,1} (C_p)_{slag} (T_{sl} - T_c) \quad (3.43)$$

$W_{S,1}$ and $W_{P,1}$ are given by equations (3.29) and (3.30) respectively.

Heat consumed for melting ash, Q_{MA}

The melting of ash starts at temperature T_m . Since ash is released at temperature T_c , therefore, heat energy will be needed to raise the temperature of ash from T_c to T_m . The heat required to melt the ash depends upon the constituents of ash and their latent heats of fusion, and thus, can accordingly be calculated. Therefore, we have

$$Q_{MA} = W_C t_a \sum_i \left[\frac{b_i}{M_i} \left\{ (C_p)_i (T_m - T_c) + Lf_i \right\} \right], \quad (3.44)$$

where $i = Al_2O_3, SiO_2, CaO$ and MgO .

The melting temperature of ash (T_m) is given by the equation (3.13)

Heat energy given out for forming slag from ash, Q_{SA}

Q_{SA} can be calculated by using the equation given by Ufret et al. (1981) as mentioned below.

$$Q_{SA} = W_C t_a \left\{ 297.2 (b_{CaO} + 297.14 b_{MgO}) - 17.0 (b_{Al_2O_3} + b_{SiO_2}) \right\} \quad (3.45)$$

In the present computations, it has been assumed that the total SiO_2 of coke ash forms slag at tuyere level only. Thus, the effect of formation of SiO vapours from SiO_2 in coke ash has not been included.

Heat energy consumed for reducing Fe_2O_3 into pig iron, Q_{RI}

Iron oxide (Fe_2O_3) in the ash reduces into pig iron according to the reaction (3.20). This is an endothermic reaction and the energy required is given as follows :

$$Q_{RI} = \frac{W_C t_a b_{\text{Fe}_2\text{O}_3} Q_{RI1}}{159.70} \quad (3.46)$$

Where

$$Q_{RI1} = 132.1350 \times 10^3 - \left[(C_p)_{\text{Fe}_2\text{O}_3} + 3(C_p)_C \right] (T_c - 1473) \\ - 2(C_p)_{\text{Fe}(l)} (1803 - T_c) + 3(C_p)_{\text{CO}} (T_{g,1} - 2200)$$

Heat consumed for forming SiO gas, Q_{VSI}

SiO gas forms by the reaction of molten SiO_2 present in ash with solid carbon according to the reaction (3.21). It is an endothermic reaction and its heat requirement can be calculated by the following relation.

$$Q_{VSI} = F_{m_{\text{SiO},1}} \left[153.1747 \times 10^3 - (C_p)_C (T_c - 1473) \right. \\ \left. + (T_{g,1} - 2200) \left\{ (C_p)_{\text{SiO}} + (C_p)_{\text{CO}} \right\} \right. \\ \left. - (C_p)_{\text{SiO}_2} (T_m - 1673) \right] \quad (3.47)$$

The molar flow rate of SiO gas formed ($F_{m_{SiO,1}}$), is given by equation (3.16).

Heat given out by gases, Q_G

After the combustion of coke in front of tuyeres, the gases are produced at adiabatic flame temperature T_1 and provide the energy requirement of the above processes. Therefore, the temperature of gases is reduced from T_1 to $T_{g,1}$. The produced gases are CO, H_2 and N_2 .

The heat energy given out by the gases, Q_G , can be expressed as follows :

$$Q_G = (T_1 - T_{g,1}) \left\{ F_{N_2,1} (C_p)_{N_2} + F_{H_2,1} (C_p)_{H_2} + F_{CO,2} (C_p)_{CO} \right\} / 22.4 \quad (3.48)$$

Where

$$F_{CO,2} = 60 F_b \left[0.42 + 2 X_{O_2} + 1.2444 \times 10^{-3} W_{st} \right]$$

$F_{H_2,1}$ and $F_{N_2,1}$ can be calculated by equations (3.23) and (3.24) respectively.

On the basis of above heat energies involved in various processes, energy balance around combustion zone gives the following expression for tuyere gas temperature $T_{g,1}$.

$$T_{g,1} = \frac{B_6 T_1 + B_9}{B_8 + B_6} \quad (3.49)$$

Where

$$B_1 = Q_{SM} + Q_{MA} - Q_{SA}$$

$$B_2 = (W_C t_a b_{Fe_2O_3}) / 159.70$$

$$B_3 = 132.1350 \times 10^3 - \left\{ (C_p)_{Fe_2O_3} + 3(C_p)_C \right\} (T_c - 1473) \\ - 2(C)_{Fe(l)} (1803 - T_c)$$

$$B_4 = F_{m_{SiO_2,1}} \left\{ 153.1747 \times 10^3 - (C_p)_C (T_c - 1473) \right. \\ \left. - (C_p)_{SiO_2} (T_m - 1673) \right\}$$

$$B_5 = F_{m_{SiO_2,1}} \left\{ (C_p)_{SiO} + (C_p)_{CO} \right\}$$

$$B_6 = \left\{ F_{N_2,1} (C_p)_{N_2} + F_{H_2,1} (C_p)_{H_2} + F_{CO,2} (C_p)_{CO} \right\} / 22.4$$

$$B_7 = B_1 + B_2 + B_3 + B_4$$

$$B_8 = 3.0 B_2 (C_p)_{CO} + B_5$$

$$B_9 = 2200.0 B_8 - B_7$$

3.2.2.1 Results

The tuyere gas temperature $T_{g,1}$ was calculated by equation (3.49) for all the data sets of Table 3.3. The temperature of coke (T_c), pig iron (T_p) and slag (T_{s1}) are taken as 1773, 1873 and 1973 K

respectively. The latent heats of fusion of substances is taken from Table A.2.

The results are reported in Table 3.9, in which set number refers to Table 3.3. It has been reported in the literature [Strassburger (1969), Biswas (1981)] that the tuyere gas temperature should be more than 2000 K. Thus, the calculated temperatures are in conformity with the literature. However, it is noted that the tuyere gas temperature is about 250 K less than the corresponding adiabatic flame temperature. This reduction in temperature is significant and is naturally due to various energy consuming processes occurring in the combustion zone, which have been already considered in the formulation of equation (3.49). Further, it has been assumed in the present work that the total quantity of coke entering the combustion zone, is consumed there. But it is very likely that a portion of this quantity remains unreacted, which depends upon the penetration depth caused by the blast. An approximate calculation with the information provided by Biswas (1981) on inactive zone, has shown that the unreacted core leaving the combustion zone, shall reduce the tuyere gas temperature by about 10°C only, which can be neglected.

In view of the above, it is obvious that the adiabatic flame temperature should not be taken as the tuyere gas temperature for Indian blast furnaces, which is in contrast to the suggestion made by Strassburger (1969) for selecting the appropriate boundary conditions.

3.2.3 Top Gas Temperature

The temperature of gas coming out of the furnace from its top, is generally called as top gas temperature.

The tuyere gas at temperature $T_{g,1}$, enters the shaft region from the bottom of bosh. The solids fed from the top of the furnace are

processed in the shaft. The tuyere gas provides reducing gases as well as heat for processing the solids into finished products. Thus, tuyere gas cools down from $T_{g,1}$ to $T_{g,0}$ at exit at the top and the solid feed is heated up from temperature $T_{s,0}$ to T_c . The incoming and outgoing streams of solids, liquids and gases around the shaft of the furnace are shown in Figure 3.1. Further, various chemical reactions take place in the shaft but only eight chemical reactions are taken into consideration for modelling. These are mentioned in Section 4.1.2.

In the derivation of top gas temperature $T_{g,0}$, the assumptions, which follows, are made about the occurrence of chemical reactions. Indirect reduction by H_2 and water gas reaction together result into the same reaction equation as obtained by combining the indirect reduction by CO and solution loss reaction. Therefore, in either case net heat of consumption/production would be the same. In view of this, indirect reduction by CO and solution loss reaction have been considered for taking over all energy balance around shaft. Both the reactions have been assumed to occur at complete conversion. It is reported in the literature [Biswas (1981)] that water gas shift reaction takes place in lower temperature region. Since the gases entering the shaft region do not contain water vapour and there is also no source of production of water vapour in the shaft region as the indirect reduction by H_2 has been neglected, therefore, water gas shift reaction has also been neglected. These assumptions are in conformity with the studies of Yagi and Muchi (1970a). Keeping the above assumptions in view, the energy balance is taken around the shaft region. The various energy terms involved in energy balance, are discussed and derived below.

Energy input with solid burden, Q_B

The solid burden enters the furnace at the temperature $T_{s,0}$, which is very close to reference temperature. Therefore, the heat capacity of each solid component of burden is averaged and mentioned in Table 3.8.

Table 3.9 Computed Results for Tuyere Gas Temperature

Set Number	Adiabatic flame temperature (T_1), K	Tuyere Gas Temperature ($T_{g,1}$), K	($T_1 - T_{g,1}$)
1	2353.9190	2099.088	254.8310
2	2277.0570	2032.608	244.4490
3	2294.9470	2046.379	248.5680
4	2284.8350	2040.616	244.2190

Table 3.10 Comparison of Top Gas Temperature Computed by Newton Raphson Method and Approximate Relationship

Set number	Coefficients of equation (3.60)			Top gas temperature ($T_{g,0}$), K		Per cent variation
	E_4	E_5	E_6	Solution of equation (3.60) by Newton Raphson Method	Approximate relationship, equation (3.64)	
1	12.3630	-6.0351	-6.0612×10^{-2}	460.3742	470.2782	2.1513
2	12.3700	-6.9345	-6.0258×10^{-2}	528.7785	537.2598	1.6039
3	12.4120	-6.5640	-5.8950×10^{-2}	499.2415	508.0406	1.7625
4	12.3730	-7.1096	-6.1210×10^{-2}	541.7361	550.1272	1.5489

On the basis of these average values, the heat capacity of solid burden, $(C_s)_B$, is calculated as given in Chapter V. Thus, the rate of input of sensible energy with solid burden is as follows :

$$Q_B = W_B (C_s)_B (T_{s,0} - T_o) \quad (3.50)$$

Where

$$W_B = W_O + W_{OS} + W_{OP} + W_{OM} + W_C + W_L$$

Energy going out with flue dust, Q_D

The flue dust comes out of the furnace with the top gas. Therefore, the temperature of flue dust is assumed to be equal to the top gas temperature, $T_{g,0}$. The heat capacity of dust is also assumed to be equal to that of solid burden, $(C_s)_B$. Thus,

$$Q_D = W_D (C_s)_B (T_{g,0} - T_o) \quad (3.51)$$

Energy going out with slag and pig iron, Q_{SP}

The slag and pig iron formed in bosh, leave this zone at the temperature of solid coke, T_c . Thus,

$$Q_{SP} = \left\{ W_{P,1} (C_p)_{\text{pig}} + W_{S,1} (C_p)_{\text{slag}} \right\} (T_c - T_o) \quad (3.52)$$

$W_{S,1}$ and $W_{P,1}$ are given by equations (3.29) and (3.30) respectively.

Energy going out with solids leaving from bottom, Q_S

The solids leave the shaft from the bottom of bosh and contain the

unreacted coke and the ash released in the shaft. The heat capacity of these solids is assumed to be same as that of coke in the burden, $(C_s)_C$. Thus,

$$Q_S = W_{C,1} (C_s)_C (T_c - T_o) \quad (3.53)$$

$W_{C,1}$ is given by equation (3.28) and calculation of $(C_s)_C$ has been described in Chapter V.

Energy input with tuyere gas, Q_{TG}

The tuyere gas at temperature $T_{g,1}$ enters the bottom of bosh. It contains CO , H_2 , N_2 and SiO gases. Since there is wide difference between the temperatures T_o and $T_{g,1}$, therefore, the heat capacities of these gases are considered as a function of temperature and are taken from Table A.1. Thus, we get

$$Q_{TG} = \frac{1}{22.4} \int_{T_o}^{T_{g,1}} \left[\sum_i F_{i,1} (C_p)_i \right] dT, \quad i = N_2, H_2, CO, SiO$$

or

$$Q_{TG} = \frac{(T_{g,1} - T_o)}{22.4} \left[a_1 + \frac{b_1}{2000} (T_{g,1} + T_o) + \frac{c_1 \times 10^5}{T_{g,1} \times T_o} \right], \quad (3.54)$$

where

$$a_1 = 6.79 F_{CO,1} + 6.66 F_{N_2,1} + 6.52 F_{H_2,1} + 7.755 F_{SiO,1}$$

$$b_1 = 0.98 F_{CO,1} + 1.02 F_{N_2,1} + 0.78 F_{H_2,1} + 0.57 F_{SiO,1}$$

$$c_1 = 0.12 F_{H_2,1} - 0.11 F_{CO,1} - 0.505 F_{SiO,1}$$

$$F_{SiO,1} = 22.4 F_{mSiO,1}$$

$F_{CO,1}$, $F_{N_2,1}$, $F_{H_2,1}$ and $F_{SiO_2,1}$ are expressed by equations (3.22-3.25).

Energy consumed in fusion, Q_M

The melting of solids starts in the bosh region. The metallic iron formed after complete reduction of iron oxides, melts as pig iron. The $CaCO_3$ and MnO_2 charged, melt as CaO and MnO respectively. The other oxides, namely SiO_2 , Al_2O_3 and MgO , melt in the same form as charged. The coke ash does not melt in the shaft region and is assumed to remain as solid. Thus,

$$Q_M = \sum_i (w_i Lf_i / M_i) \quad (3.55)$$

$$i = Fe, SiO_2, Al_2O_3, CaO, MnO, MgO$$

where

$$w_{Fe} = w_S r_{Fe} + w_P \alpha_{Fe} - 0.6994 w_C t_a b_{Fe_2O_3}$$

$$w_{SiO_2} = w_O v_{SiO_2} + w_{OS} s_{SiO_2} + w_{OP} p_{SiO_2} + w_{OM} g_{SiO_2} + w_L l_{SiO_2}$$

$$w_{Al_2O_3} = w_O v_{Al_2O_3} + w_{OS} s_{Al_2O_3} + w_{OP} p_{Al_2O_3} + w_{OM} g_{Al_2O_3} + w_L l_{Al_2O_3}$$

$$w_{CaO} = w_{OS} s_{CaO} + w_{OP} p_{CaO} + w_L l_{CaO}$$

$$w_{MgO} = w_{OS} s_{MgO} + w_{OP} p_{MgO} + w_L l_{MgO}$$

$$w_{MnO} = 0.8159 w_{OM} g_{MnO_2}$$

Energy released in slag formation, Q_{SL}

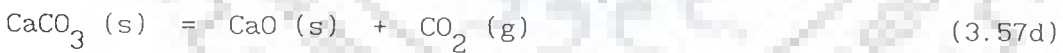
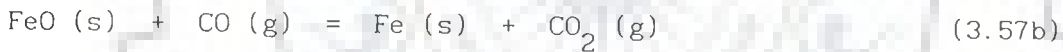
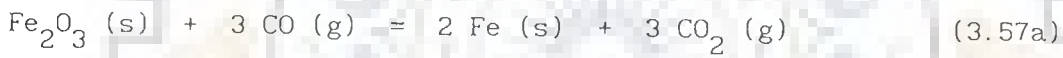
Q_{SL} is calculated on the basis of equation given by Ufret et al. (1981). Accordingly, we get

$$Q_{SL} = 314.2 (W_{CaO} + W_{MgO}) - 17 W_{S,1} \quad (3.56)$$

The expressions for W_{CaO} and W_{MgO} are same as used in equation (3.55), while $W_{S,1}$ is given by equation (3.29).

Net heat consumed in reactions, Q_R

As per above discussion, the following four reactions are considered for calculating Q_R .



The iron in dust is assumed to be present as Fe_2O_3 . If $(\Delta H_R)_{3,T_0}$, $(\Delta H_R)_{4,T_0}$, $(\Delta H_R)_{5,T_0}$ and $(\Delta H_R)_{6,T_0}$ are the heat of reactions at reference temperature T_0 for reactions (3.57a), (3.57b), (3.57c) and (3.57d) respectively, then

$$Q_R = Fm_{Fe_2O_3} (\Delta H_R)_{3,T_0} + Fm_{FeO} (\Delta H_R)_{4,T_0} + Fm_C (\Delta H_R)_{5,T_0} + Fm_{CaCO_3} (\Delta H_R)_{6,T_0} \quad (3.57e)$$

where

$$Fm_{Fe_2O_3} = \left\{ W_O^v Fe_2O_3 + W_{OS}^s Fe_2O_3 + W_{OP}^p Fe_2O_3 + W_{OM}^g Fe_2O_3 \right.$$

$$+ W_D J_{Fe} / 0.6994 \} / 159.70 \quad (3.57f)$$

$$Fm_{FeO} = (W_{OS} s_{FeO} + W_{OP} p_{FeO}) / 71.85 \quad (3.57g)$$

$$Fm_C = (W_C - W_{C,1}) / 12.0$$

$$Fm_{CaCO_3} = W_L l_{CO_2} / 44.0$$

Energy going out with the top gas, Q_T

The top gas leaves the furnace at a temperature $T_{g,0}$. Its component gases are CO , CO_2 , H_2 and N_2 . Since there is an appreciable difference between the temperatures T_o and $T_{g,0}$, therefore, the heat capacities of gases are considered as a function of temperature as given in Table A.1. Thus,

$$Q_T = \frac{F_0}{22.4} \int_{T_o}^{T_{g,0}} \left(\sum_i y_{i,0} (C_p)_i \right) dT, \quad i = CO, CO_2, H_2, N_2$$

or

$$Q_T = \frac{F_0 (T_{g,0} - T_o)}{22.4} \left[a_2 + \frac{b_2}{2000} (T_{g,0} + T_o) + \frac{c_2 \times 10^5}{T_{g,0} \times T_o} \right] \quad (3.58)$$

where

$$a_2 = 6.79 y_{CO,0} + 10.55 y_{CO_2,0} + 6.52 y_{H_2,0} + 6.66 y_{N_2,0} \quad (3.58a)$$

$$b_2 = 0.98 y_{CO,0} + 2.16 y_{CO_2,0} + 0.78 y_{H_2,0} + 1.02 y_{N_2,0} \quad (3.58b)$$

$$c_2 = 0.12 y_{H_2,0} - 0.11 y_{CO,0} - 2.04 y_{CO_2,0} \quad (3.58c)$$

The estimation of mole fractions of gases in top gas ($y_{CO,0}$, $y_{CO_2,0}$, $y_{H_2,0}$, and $y_{N_2,0}$) has already been described in Section 3.1.1.

Energy lost through the wall of furnace, Q_w

Some part of heat energy is lost through the wall of the furnace. It consists of the heat taken off by cooling water and the heat lost from the surface of furnace wall to the ambient air. Therefore, the heat loss from the furnace wall is expected to change considerably with the change in the external conditions. That is why in Indian steel plants this loss of energy is mentioned as per cent heat loss through the wall and is fixed for estimation of variables. It is generally considered between 5 to 10% of energy input for Indian blast furnaces. Therefore, in order to calculate Q_w , a fixed value of heat loss through wall (H_L) has been considered. Thus,

$$Q_w = (Q_B + Q_{TG} + Q_{SL}) \times H_L \quad (3.59)$$

Q_B , Q_{TG} and Q_{SL} are expressed by equations (3.50), (3.54) and (3.56) respectively.

Equations (3.50 - 3.59) represent the energy associated with various streams and processes in the shaft region of the furnace. On the basis of these energies, the energy balance around shaft region gives the following nonlinear equation for top gas temperature $T_{g,0}$.

$$T_{g,0}^3 + E_4 T_{g,0}^2 + E_5 T_{g,0} - E_6 = 0 \quad (3.60)$$

Where

$$E_4 = 44.8 \times 10^3 E_3 / (F_0 b_2)$$

$$E_5 = E_4 (E_2 - E_1) / E_3$$

$$E_6 = 2 \times 10^8 c_2 / b_2$$

$$E_1 = Q_B + Q_{TG} + Q_{SL} - Q_{SP} - Q_S - Q_M - Q_R - Q_W$$

$$E_2 = \frac{F_0}{22.4} \left(\frac{c_2 \times 10^5}{T_o} - \frac{b_2 T_o^2}{2000} - a_2 T_o \right) - W_D (C_S)_B T_o$$

$$E_3 = W_D (C_S)_B + F_0 a_2 / 22.4$$

The solution of equation (3.60) gives the top gas temperature $T_{g,0}$. The solution methodology and results are given in the following section.

3.2.3.1 Solution Methodolgy and Results

The coefficients of equation (3.60), i.e. E_4 , E_5 and E_6 , are determined for all the four data sets of Table 3.3 and are mentioned in Table 3.10. For this, the average heat capacities of solid components in feed, pig iron and slag are taken from Table 3.8. The latent heats of fusion, L_f , and molecular weights for different solid components are taken from Tables A.2 and A.4 respectively. The heats of reactions used in equation (3.57) are calculated by using the heats of formation of different substances given in Table A.3. The reference temperature T_o is taken as 298 K. The percent heat loss through wall of the furnace is taken as 10% .

The equation (3.60) is solved numerically by Newton Raphson method and the values of top gas temperature $T_{g,0}$ thus obtained with tolerance 1×10^{-4} , are reported in Table 3.10 for all the data sets.

Equation (3.60) can be reduced to a quadratic equation to obtain an analytical expression for approximate value of $T_{g,0}$. Since the top gas temperature is generally less than 1000 K, therefore, a dimensional variable $\theta_1 (= T_{g,0} / 100)$ has been used to scale down the magnitude of

unknown variable $T_{g,0}$. Writing equation (3.60) in terms of θ_1 , we obtain

$$10^2 \theta_1^3 + E_4 \theta_1^2 + E_5 \times 10^{-2} \theta_1 - E_6 \times 10^{-4} = 0 \quad (3.61)$$

On observing Table 3.10, it appears that the coefficient $E_6 \times 10^{-4}$ is very small for all the four data sets and so, may be neglected for approximation purposes.

Thus, equation (3.61) transforms to the following quadratic equation.

$$10^2 \theta_1^2 + E_4 \theta_1 + E_5 \times 10^{-2} = 0 \quad (3.62)$$

Whose solution is given below.

$$\theta_1 = \frac{-E_4 \pm \sqrt{E_4^2 - 4E_5}}{2 \times 10^2} \quad (3.63)$$

Since the top gas temperature cannot be negative, therefore, we write equation (3.63) in terms of $T_{g,0}$ as follows :

$$T_{g,0} = \left\{ -E_4 + \sqrt{E_4^2 - 4E_5} \right\} / 2.0 \quad (3.64)$$

The values of $T_{g,0}$ are calculated for all the four data sets by using equation (3.64) and are reported in Table 3.10. The value of $T_{g,0}$ by equation (3.64) differs at the most by 2.1513 per cent with respect to the value obtained numerically by Newton Raphson method. Therefore, it may be concluded that equation (3.64) provides the value of top gas temperature within permissible limit of error of $\pm 5\%$ and hence, it can be used for the computation of top gas temperature $T_{g,0}$.

3.3 COMPUTER PROGRAM

On the basis of descriptions and derivations in the preceding sections, a computer program has been developed in FORTRAN 77 to compute the material and energy balances and required boundary conditions. The computer program has been executed on the NEXUS 3500 (APOLLO 3500) CAD Workstation. It contains about 1050 lines in a main programme and seven subroutines, which are mentioned in Table 3.11 with their purposes.

Input data for the Computer program are as follows :

- Mass flow rate and composition of solids in burden feed
- Volumetric flow rate of hot air blast
- Weight of steam injected per Nm^3 of blast
- Oxygen enrichment per Nm^3 of blast
- Composition of pig iron
- Temperature of burden feed
- Temperature of pig iron and slag
- Temperature of air blast
- Temperature of steam

Output results include the unknown mass flow rate and composition of streams, all the boundary conditions needed for the solution of mathematical model, and many more intermediate results, which help in analysing the blast furnace process. The program also reports the values of all the constitutive parameters used in the computation. A typical output for a data set runs in about five pages.

3.4 CONCLUDING REMARKS

In this chapter, procedures for computing the material and energy balances of a blast furnace have been developed and programmed. The computer program calculates the boundary conditions of the proposed

mathematical model by using the generally available operating data on blast furnaces, and thus, enhances the utility of the model. Besides, the program also computes mass flow rates, compositions, and temperatures of streams, which are normally not known. This would assist greatly in carrying out the routine checks on the blast furnace performance in the steel plants.

Three outcomes of the study reported in this chapter need special mention. First is the methodology developed for the computation of molar flow rate of SiO gas formed in the combustion zone. Other two are the simplified relationships, viz. equations (3.42) and (3.64), developed for computing the adiabatic flame temperature and top gas temperature respectively by utilizing the method of scaling the variables in polynomial equations. These simplifications could be possible due to the magnitude of coefficients in the polynomial equations, developed for these temperatures. This supports the common belief that the nature always takes care of its own creations.

Further, it has been clearly demonstrated that the adiabatic flame temperature is approximately 250 K more than the tuyere gas temperature. Therefore, it is pertinent to mention that the adiabatic flame temperature should not be used in place of tuyere gas temperature in the modelling studies.

Table 3.11 Subroutines for Material and Energy Balance Computations

S.N.	Subroutine	Purpose
1	MATBAL	To Calculate material balances and compositions
2	SILICA	To compute rate of formation of SiO gas
3	FT	To calculate adiabatic flame temperature
4	GAST	To calculate tuyere gas temperature
5	BOSH	To compute top gas temperature
6	R1 and R2	To present input data and output results in the desired format

DEVELOPMENT OF MATHEMATICAL MODEL OF BLAST FURNACE

4.0 INTRODUCTION

This chapter describes the development of one-dimensional mathematical model of the shaft region of blast furnace to predict the longitudinal distribution of process variables. As stated earlier, the shaft region constitutes three main portions of the furnace, viz. stack, belly and bosh. The blast furnace has been visualized as a moving bed countercurrent gas-solid noncatalytic reactor. The major transfer and rate processes including the chemical reactions occur in this reactor between the ascending gases and descending bed of solid and molten substances. The basis of modelling studies is the fundamental conservation equations of mass, momentum, and energy [Bird et al. (1960), Aris (1979), Denn (1986)]. Besides, model requires constitutive relationships pertaining to the phases present in the furnace so that the solution of model equations may be obtained.

4.1 PREMISES FOR MODELLING

A schematic diagram describing the process of blast furnace is shown in Figure 3.1. For modelling, the shaft is divided into two regions, upper one is stack and the lower one is bosh. Belly is adjusted in between these two portions. The bosh region starts at the plane from where the process of fusion of solids begins. Chemical and transport processes occurring in both the regions are almost similar. Formation of molten iron and slag phases is the additional process in the bosh region.

4.1.1 Assumptions

In order to formulate a one-dimensional mathematical model of the shaft region of blast furnace, the major assumptions used are listed and discussed below.

- (i) For developing the model, the bed height is divided into small elemental heights. Each of these consists of a small volume of bed between two horizontal planes perpendicular to the longitudinal axis of the shaft. The temperatures, compositions, fractional conversions and all other properties of solid, molten and gaseous phases are assumed to be uniform inside the elemental volume. Thus, reaction rates, mass and heat transfer rates at a given time and height, are the same throughout the elemental volume. Therefore, the shaft can be visualized as a series of stirred tank reactors through which the solid and gas move successively, but countercurrently. Thus, the small elemental volume provides the basis for model formation. Figure 4.1 shows the shaft with a small elemental volume.
- (ii) Particles of different types of solids in burden are considered to be uniformly distributed throughout the bed.
- (iii) The voidage in the bed is independent of the location of elemental height. It implies that the voidage in stack will not change, even though there is disintegration of particles. In bosh region, where the fusion process starts and the fused materials cover a portion of the bed, the bed voidage must be different from the voidage in stack. According to the studies of Sugiyama et al. (1980), the change in voidage in packed bed due to fusion depends upon the degree of shrinkage of fused bed and the voidage does not show a large change when the degree of shrinkage ranges from 0 to 0.47. In blast furnace, the degree of

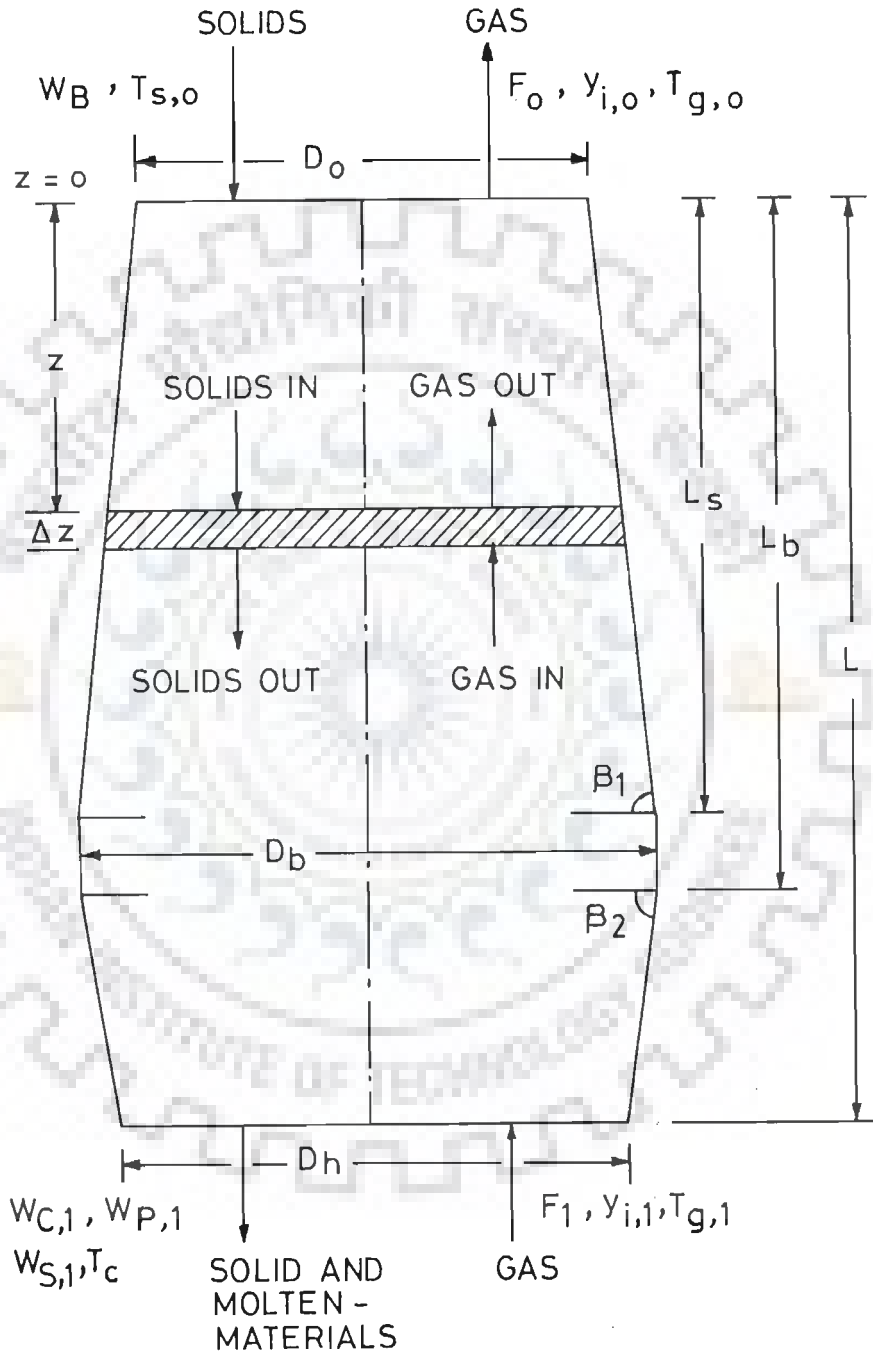


FIGURE 4-1 SCHEMATIC DIAGRAM OF THE SHAFT USED IN MODELLING

shrinkage is upto approximately 0.5. Therefore, the bed voidage in bosh region is considered to be same as that in the stack.

- (iv) The diffusion term is neglected in the mass conservation equations because of the following reason :

According to Hatano and Kurita (1982), the gas velocity in the furnace is about 1.0 m/s, the diffusion coefficient for gases is around $10^{-4} \text{ m}^2/\text{s}$ and concentration gradient is about $3 \times 10^{-3} \text{ kmol/m}^4$. On the basis of these information the diffusion term comes out to be much smaller than the convection term by a factor of about 10^4 . Therefore, it is not usually necessary to consider the diffusion term unless the gas velocity is extremely low.

- (V) During the chemical reaction, the volume of solid particles remains unchanged; only the weight of particles is changed by the reaction.
- (vi) The temperatures of solid and molten phases in the bosh are same. This assumption is quite logical as there is intimate contact of solids and molten materials.
- (vii) Although several chemical reactions occur in the blast furnace, but it is assumed that only eight chemical reactions are taking place in the shaft of the furnace, which are mentioned in Section 4.1.2. Desulphurization and phosphorus reduction do not take place, since they are not present in the feed (Tables 3.1 and 3.2). Manganese reduction is neglected as it takes place in combustion zone and hearth. The kinetic model by Yagi and Muchi (1970a) has been considered to determine the overall reaction rates. In their kinetic model, solution loss reaction is assumed to be irreversible. Thus, the carbon deposition reaction, which is reverse of the solution loss reaction, is assumed negligible.

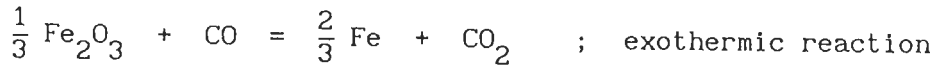
Also, according to Strassburger (1969), the carbon deposition reaction does not occur to any appreciable extent. Therefore, this reaction is neglected in the present work.

- (viii) For gas-solid reactions, it is assumed that the heat of reaction is released to the solid phase only, as these reactions take place at solid interface. For gas phase reactions, the heat of reaction is obviously assumed to be released into the gas phase.
- (ix) Formation of pig iron and slag is assumed to take place completely in the bosh region. The total amount of heat required for melting of solids and formation of slag is considered to be distributed uniformly over the whole volume of bed in the bosh, i.e. heat required per unit time per unit bed volume is assumed to be constant.
- (x) The direction of movement of solids in the furnace, i.e. the downward direction or z direction, is assumed to be positive. Therefore, the gases move up in negative z direction.
- (xi) Since the operating pressure is moderate (1-3 atm) and the temperature of gases is high in the blast furnace, the ideal gas law is assumed to be applicable.
- (xii) Each solid particle is assumed to be homogeneous in temperature and concentration gradients.

4.1.2 Chemical Reactions

Eight chemical reactions have been assumed to occur in the blast furnace. These are described below.

Indirect reduction of Fe_2O_3 ore by CO



R_1 = Rate of reaction, kmol of CO /m³(bed).hr

Solution loss reaction



R_2 = Rate of reaction, kmol of CO₂ /m³(bed).hr

Direct reduction of molten FeO



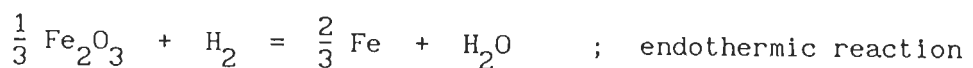
R_3 = Rate of reaction, kmol of FeO /m³(bed).hr

Decomposition of CaCO₃



R_4 = Rate of reaction, kmol of CaCO₃ /m³(bed).hr

Indirect reduction of Fe_2O_3 ore by H_2



R_5 = Rate of reaction , kmol of H₂ /m³(bed).hr

Water gas reaction

R_6 = Rate of reaction, kmol of $\text{H}_2\text{O} / \text{m}^3(\text{bed}).\text{hr}$

Water gas shift reaction

R_7 = Rate of reaction, kmol of $\text{H}_2\text{O} / \text{m}^3(\text{bed}).\text{hr}$

Reduction of SiO gas

R_8 = Rate of reaction, kmol of $\text{SiO} / \text{m}^3(\text{bed}).\text{hr}$

The kinetic expressions for the above chemical reactions are given in Chapter V.

Within the framework of above premises, a mathematical model of the shaft of blast furnace has been proposed. In the following sections, the development of model is described in detail.

4.2 DYNAMIC MODEL EQUATIONS

For the derivation of mathematical model, the schematic representation of shaft of the blast furnace is shown in Figure 4.1. An elemental volume of differential height Δz is considered at an height z from the top level of the bed. The cross-sectional area and diameter of the furnace at height z are represented by A_z and D_z respectively. The

mass and energy balances based on conservation laws are taken around this elemental volume to formulate the model equations.

4.2.1 Differential Component Mass Balance Equations

The basic component mass conservation equation is transformed into a general form of the unsteady state component material balance equation for blast furnace and is represented as follows :

$$\begin{aligned}
 \left[\begin{array}{l} \text{rate of accumul-} \\ \text{ation of compon-} \\ \text{ent } i \text{ inside} \\ \text{the elemental} \\ \text{volume} \end{array} \right] &= \left[\begin{array}{l} \text{rate of flow} \\ \text{of component} \\ i \text{ into the} \\ \text{elemental} \\ \text{volume} \end{array} \right] - \left[\begin{array}{l} \text{rate of flow} \\ \text{of component} \\ i \text{ out of the} \\ \text{elemental} \\ \text{volume} \end{array} \right] \\
 &+ \left[\begin{array}{l} \text{net rate of generat-} \\ \text{ion of component } i \\ \text{by chemical reaction} \\ \text{in the elemental} \\ \text{volume} \end{array} \right] \quad (4.1)
 \end{aligned}$$

The net rate of generation of component i by chemical reaction is obtained by subtracting its rate of consumption from its rate of formation.

Equation (4.1) is applied around the elemental volume of height Δz for every reacting solid and gaseous component. The derivation of these equations in detail is described below.

4.2.1.1 Component Mass Balance for Solid Fe_2O_3

The concentration of Fe_2O_3 in the elemental volume (C_h) can be expressed as follows :

$$C_h = C_{ho} (1 - f_s) \quad (4.2)$$

The application of equation (4.1) for component mass balance of Fe_2O_3 yields :

Accumulation = In - Out + Generation - Consumption

$$A_z \Delta z \frac{\Delta C_h}{\Delta t} = \left[C_h \frac{F_s}{1-\epsilon} \right] \Big|_z - \left[C_h \frac{F_s}{1-\epsilon} \right] \Big|_{z+\Delta z} + 0 - \left[\frac{R_1}{3} + \frac{R_5}{3} \right] A_z \Delta z \quad (4.3)$$

Dividing equation (4.3) by Δz and taking the limits $\Delta z \rightarrow 0$ and $\Delta t \rightarrow 0$, the equation assumes the following form.

$$A_z \frac{\partial C_h}{\partial t} = - \frac{\partial}{\partial z} \left[C_h \frac{F_s}{1-\epsilon} \right] - \left[\frac{R_1}{3} + \frac{R_5}{3} \right] A_z$$

Since F_s and ϵ are both assumed to be fixed for stack and bosh region, $\left[\frac{F_s}{1-\epsilon} \right]$ will be independent of height z .

Therefore, we get

$$A_z \frac{\partial C_h}{\partial t} = - \left[\frac{F_s}{1-\epsilon} \right] \frac{\partial C_h}{\partial z} - \left[R_1 + R_5 \right] \frac{A_z}{3} \quad (4.4)$$

With the help of equation (4.2), the equation (4.4) becomes

$$\frac{\partial f_s}{\partial t} + \left[\frac{F_s}{(1-\epsilon)A_z} \right] \frac{\partial f_s}{\partial z} = \left[\frac{R_1 + R_5}{3 C_{ho}} \right] \quad (4.5)$$

Equation (4.5) represents the differential mass balance equation for solid Fe_2O_3 .

4.2.1.2 Component Mass Balance for CO Gas

On the basis of reactions, which produce or consume CO, the molar flow rates of CO in the elemental volume may be expressed as follows :

$$\text{molar flow rate of CO produced} = (2R_2 + R_3 + R_6 + R_8) A_z \Delta z$$

$$\text{molar flow rate of CO consumed} = (R_1 + R_7) A_z \Delta z$$

The use of equation (4.1) for gaseous component CO leads to the following differential mass balance equation.

$$\text{Accumulation} = \text{In} - \text{Out} + \text{Generation} - \text{Consumption}$$

$$\left(\frac{A_z \Delta z \epsilon}{22.4} \right) \frac{\Delta y_{CO}}{\Delta t} = \left[\frac{y_{CO} F_g}{22.4} \right] \Big|_{z+\Delta z} - \left[\frac{y_{CO} F_g}{22.4} \right] \Big|_z + (2R_2 + R_3 + R_6 + R_8) A_z \Delta z - (R_1 + R_7) A_z \Delta z \quad (4.6)$$

Here, $\left[\frac{F_g}{22.4} \right] \Big|_z$ represents the molar flow rate of gases leaving the elemental volume, which can be written as the sum of the molar flow rates of gases entering the elemental volume and the net molar rate of gases produced by chemical reactions in the elemental volume.

Therefore,

$$\left[\frac{F_g}{22.4} \right] \Big|_z = \left[\frac{F_g}{22.4} \right] \Big|_{z+\Delta z} + \left[\frac{\Delta F_g}{22.4} \right] \quad (4.7)$$

Where $\frac{\Delta F_g}{22.4}$ is the net molar flow rate of production of gases in the elemental volume and is calculated by subtracting the molar flow rate of consumption of gases from the total molar flow rate of production of gases. Therefore, we get

$$\frac{\Delta F_g}{22.4} = (R_2 + R_3 + R_4 + R_6) A_z \Delta z \quad (4.8)$$

By substituting equations (4.7) and (4.8) into equation (4.6), we obtain

$$\begin{aligned} \left[\frac{A_z \Delta z \epsilon}{22.4} \right] \frac{\Delta y_{CO}}{\Delta t} &= \left[\frac{F_g}{22.4} \right] \Big|_{z+\Delta z} \left[\left[y_{CO} \right] \Big|_{z+\Delta z} - \left[y_{CO} \right] \Big|_z \right] \\ &\quad - \left[y_{CO} \right] \Big|_z A_z \Delta z (R_2 + R_3 + R_4 + R_6) \\ &\quad + A_z \Delta z (2R_2 + R_3 + R_6 + R_8 - R_1 - R_7) \end{aligned}$$

Dividing this equation by Δz and taking the limits $\Delta z \rightarrow 0$ and $\Delta t \rightarrow 0$, we obtain

$$\begin{aligned} \frac{A_z \epsilon}{22.4} \frac{\partial y_{CO}}{\partial t} &= \frac{F_g}{22.4} \left[\frac{\partial y_{CO}}{\partial z} \right] - y_{CO} A_z (R_2 + R_3 + R_4 + R_6) \\ &\quad + A_z (2R_2 + R_3 + R_6 + R_8 - R_1 - R_7) \end{aligned}$$

or

$$\frac{\partial y_{CO}}{\partial t} - \left[\frac{F_g}{A_z \epsilon} \right] \frac{\partial y_{CO}}{\partial z} = \frac{22.4}{\epsilon} \left[R_2(2 - y_{CO}) + R_3(1 - y_{CO}) + R_4 y_{CO} + R_6(1 - y_{CO}) + R_8 - R_1 - R_7 \right] \quad (4.9)$$

Equation (4.9) represents the differential mass balance equation for gaseous component CO.

4.2.1.3 Other Component Mass Balances

By proceeding in the similar way, the component mass balances for each reacting component in solid, liquid and gaseous phases have been derived. The final forms of their differential mass balance equations are as follows :

Component mass balance for solid carbon

$$\frac{\partial f_c}{\partial t} + \left[\frac{F_s}{(1-\epsilon) A_z} \right] \frac{\partial f_c}{\partial z} = (R_2 + R_3 + R_6 + R_8) / C_{CO} \quad (4.10)$$

Component mass balance for solid CaCO₃

$$\frac{\partial f_L}{\partial t} + \left[\frac{F_s}{(1-\epsilon) A_z} \right] \frac{\partial f_L}{\partial z} = \frac{R_4}{C_{Lo}} \quad (4.11)$$

Component mass balance for molten FeO

$$\frac{\partial f_{sn}}{\partial t} + \left[\frac{F_s}{(1-\epsilon) A_z} \right] \frac{\partial f_{sn}}{\partial z} = \frac{R_3}{C_{wo}} \quad (4.12)$$

Component mass balance for CO₂ gas

$$\frac{\partial y_{\text{CO}_2}}{\partial t} - \left[\frac{F_g}{A_z \epsilon} \right] \frac{\partial y_{\text{CO}_2}}{\partial z} = \frac{22.4}{\epsilon} \left[R_1 - R_2 (1 + y_{\text{CO}_2}) - y_{\text{CO}_2} (R_3 + R_6) + R_4 (1 - y_{\text{CO}_2}) + R_7 \right] \quad (4.13)$$

Component mass balance for H₂ gas

$$\frac{\partial y_{\text{H}_2}}{\partial t} - \left[\frac{F_g}{A_z \epsilon} \right] \frac{\partial y_{\text{H}_2}}{\partial z} = \frac{22.4}{\epsilon} \left[R_7 - R_5 + R_6 (1 - y_{\text{H}_2}) - y_{\text{H}_2} (R_2 + R_3 + R_4) \right] \quad (4.14)$$

Component mass balance for SiO gas

$$\frac{\partial y_{\text{SiO}}}{\partial t} - \left[\frac{F_g}{A_z \epsilon} \right] \frac{\partial y_{\text{SiO}}}{\partial z} = - \frac{22.4}{\epsilon} \left[y_{\text{SiO}} (R_2 + R_3 + R_4 + R_6) + R_8 \right] \quad (4.15)$$

Equations (4.5) and (4.9 - 4.15) represent the differential mass balance equations. Thus, one set of governing equations for the model has been formulated. The another set of equations will be based on energy balances.

4.2.2 Differential Energy Balance Equations

The general form of the energy balance equation can be written as follows :

$$\begin{aligned}
 & \left[\begin{array}{l} \text{Rate of accu-} \\ \text{mulation of} \\ \text{energy in the} \\ \text{elemental} \\ \text{volume} \end{array} \right] = \left[\begin{array}{l} \text{Rate of energy} \\ \text{in due to mass} \\ \text{flow of mater-} \\ \text{ials into the} \\ \text{elemental volume} \end{array} \right] - \left[\begin{array}{l} \text{Rate of energy} \\ \text{out due to mass} \\ \text{flow of mater-} \\ \text{ials from the} \\ \text{elemental volume} \end{array} \right] \\
 & \quad \quad \quad - \left[\begin{array}{l} \text{Net rate of en-} \\ \text{ergy consumed} \\ \text{in chemical} \\ \text{reactions in} \\ \text{the elemental} \\ \text{volume} \end{array} \right] - \left[\begin{array}{l} \text{Rate of energy} \\ \text{consumed for} \\ \text{phase change, i.e.} \\ \text{solid to liquid} \\ \text{in the elemental} \\ \text{volume} \end{array} \right] \\
 & \quad \quad \quad - \left[\begin{array}{l} \text{Rate of loss} \\ \text{of energy th-} \\ \text{rough wall of} \\ \text{furnace from} \\ \text{the elemental} \\ \text{volume} \end{array} \right] - \left[\begin{array}{l} \text{Rate of energy} \\ \text{transfer to} \\ \text{other phases,} \\ \text{i.e. gas to} \\ \text{solid in the} \\ \text{elemental volume} \end{array} \right] \quad (4.16)
 \end{aligned}$$

Where net rate of energy consumed in chemical reactions is calculated by subtracting the exothermic heats of reactions from the endothermic heats of reactions.

Equation (4.16) is applied on the elemental volume of height Δz and diameter D_z for gas and solid phases. Thus, the differential energy balance equations for gas and solid phases are derived.

4.2.2.1 Energy Balance for Gas Phase

In blast furnace, gases are at higher temperature than the solids, so, the energy is transferred from gases to solids. Also some energy of gases is lost through wall. Since there is no phase change associated with the gaseous phase, the term corresponding to rate of energy consumed in phase change in equation (4.16), is zero. Thus, equation (4.16) for gas phase can be written as follows :

$$\text{Accumulation} = \text{In} - \text{Out} - \text{Consumed in reaction} - \text{Lost through wall} \\ - \text{Transferred to solids}$$

Thus,

$$\left[\frac{A_z \Delta z \varepsilon}{22.4} \right] \frac{\Delta(C_g T_g)}{\Delta t} = \left[\frac{F_g}{22.4} C_g T_g \right] \Big|_{z+\Delta z} - \left[\frac{F_g}{22.4} C_g T_g \right] \Big|_z \\ - \sum_i \left[(\Delta H_R)_i R_i \right] A_z \Delta z \\ - \pi D_z \Delta z U (T_g - T_{wc}) \\ - S (T_g - T_s) h_{gs} \quad (4.17)$$

The surface area of solids (S) in elemental volume is given by the following equation.

$$S = \frac{6.0 (1 - \varepsilon)}{d_p \phi} A_z \Delta z \quad (4.18)$$

Since only water gas shift reaction takes place in gas phase (Section 4.1.2), we have

$$\sum_i (\Delta H_R)_i R_i = (\Delta H_R)_7 R_7 \quad (4.19)$$

Use of equations (4.7), (4.18) and (4.19) modifies equation (4.17) in the following form.

$$\begin{aligned}
 \left[\frac{A_z \Delta z \epsilon}{2} \right] \frac{\Delta(C_g T_g)}{\Delta t} &= \left[\frac{F_g}{22.4} \right] \Big|_{z+\Delta z} \left[(C_g T_g) \Big|_{z+\Delta z} \right. \\
 &\quad \left. - (C_g T_g) \Big|_z \right] - \frac{\Delta F_g}{22.4} (C_g T_g) \Big|_z \\
 &\quad - \pi D_z \Delta z U (T_g - T_{wc}) \\
 &\quad - \frac{6(1-\epsilon)}{d_p \phi} A_z \Delta z (T_g - T_s) h_{gs} \\
 &\quad - (\Delta H_R)_7 R_7 A_z \Delta z
 \end{aligned} \tag{4.20}$$

From equation (4.8) the value of $\frac{\Delta F_g}{22.4}$ is substituted into equation (4.20). Now, equation (4.20) is divided by Δz and the limits $\Delta z \rightarrow 0$ and $\Delta t \rightarrow 0$ are taken. This results in the following form of equation.

$$\begin{aligned}
 \left[\frac{A_z \epsilon}{22.4} \right] \frac{\partial(C_g T_g)}{\partial t} &= \frac{F_g}{22.4} \frac{\partial(C_g T_g)}{\partial z} \\
 &\quad - A_z C_g T_g (R_2 + R_3 + R_4 + R_6) \\
 &\quad - \pi D_z U (T_g - T_{wc}) \\
 &\quad - \frac{6}{d_p \phi} A_z (T_g - T_s) h_{gs} \\
 &\quad - (\Delta H_R)_7 R_7 A_z
 \end{aligned} \tag{4.21}$$

In order to make the equation concise, we assume that

$$q_1 = R_2 + R_3 + R_4 + R_6 \quad (4.22)$$

$$q_2 = \frac{6(1-\epsilon)}{d_p \phi} h_{gs} \quad (4.23)$$

$$q_3 = (\Delta H_R)_7 R_7 \quad (4.24)$$

and

$$q_4 = \frac{\pi D_z U}{A_z} \quad (4.25)$$

Since the heat capacity of gas depends upon its temperature, we can write

$$\begin{aligned} \frac{\partial(C_g T_g)}{\partial z} &= \left[T_g \frac{\partial C_g}{\partial T_g} + C_g \right] \frac{\partial T_g}{\partial z} \\ &= q_5 \frac{\partial T_g}{\partial z} \end{aligned} \quad (4.26)$$

$$\begin{aligned} \text{and } \frac{\partial(C_g T_g)}{\partial t} &= \left[T_g \frac{\partial C_g}{\partial T_g} + C_g \right] \frac{\partial T_g}{\partial t} \\ &= q_5 \frac{\partial T_g}{\partial t} \end{aligned} \quad (4.27)$$

where

$$q_5 = \left[T_g \frac{\partial C_g}{\partial T_g} + C_g \right] \quad (4.28)$$

Using equations (4.22 - 4.27), equation (4.21) is modified in the following form.

$$\frac{\partial T_g}{\partial t} - \left[\frac{F_g}{A_z \epsilon} \right] \frac{\partial T_g}{\partial z} = - \frac{22.4}{q_5 \epsilon} \left[q_1 C_g T_g + q_2 (T_g - T_s) + q_3 + q_4 (T_g - T_{wc}) \right] \quad (4.29)$$

Equation (4.29) is the desired differential energy balance equation for gas phase.

4.2.2.2 Energy Balance for Solid Phase

Since the energy loss through wall of the furnace is from gases only, the term corresponding to this energy loss is omitted from the equation (4.16) for solids. The solid phase starts to melt into the liquid phase in the bosh region. Therefore, the term, energy consumed for the phase change in equation (4.16) will be applicable only in bosh region. Hence, for solid phase, equation (4.16) shall be written in the following form.

Accumulation = In - Out - Consumed in chemical reaction
- Consumed in melting - Taken from gases

$$\begin{aligned} A_z \Delta z \frac{\Delta(\rho_b C_s T_s)}{\Delta t} &= \left[\frac{F_s}{1 - \epsilon} \rho_b C_s T_s \right] \Bigg|_z \\ &\quad - \left[\frac{F_s}{1 - \epsilon} \rho_b C_s T_s \right] \Bigg|_{z+\Delta z} \\ &\quad - \left[\sum_i (\Delta H_R)_i R_i \right] A_z \Delta z - \beta_3 \frac{q_7}{V_B} A_z \Delta z \\ &\quad + \frac{6(1-\epsilon)}{d_p \phi} h_{gs} (T_g - T_s) A_z \Delta z \end{aligned} \quad (4.30)$$

Where

$$\beta_3 = 0 \quad ; \quad \text{for stack region}$$

$$\beta_3 = 1 \quad ; \quad \text{for bosh region from where the melting starts.}$$

q_7 = heat required to form slag and pig iron per hour

$$\left[\frac{F_s}{1-\epsilon} \rho_b \right] \Big|_{z+\Delta z} = \text{kg of solid coming out of the elemental volume per hour}$$

$$= (\text{kg of solids entering} - \text{net kg of solids consumed}) \text{ in the elemental volume per hour}$$

Therefore,

$$\left[\frac{F_s}{1-\epsilon} \rho_b \right] \Big|_{z+\Delta z} = \left[\frac{F_s}{1-\epsilon} \rho_b \right] \Big|_z - q_6 A_z \Delta z \quad (4.31)$$

Where q_6 is the net weight of solids consumed per unit volume of bed per hour. Substituting equations (4.23) and (4.31) in equation (4.30), we obtain

$$A_z \Delta z \frac{\Delta(\rho_b C_s T_s)}{\Delta t} = \left[\frac{F_s}{1-\epsilon} \rho_b \right] \Big|_z \left[(C_s T_s) \Big|_z - (C_s T_s) \Big|_{z+\Delta z} \right]$$

$$+ q_6 \Delta z A_z (C_s T_s) \Big|_{z+\Delta z}$$

$$+ q_2 (T_g - T_s) A_z \Delta z$$

$$- \left[\sum_i (\Delta H_R)_i R_i \right] A_z \Delta z - \beta_3 \frac{q_7}{V_B} A_z \Delta z$$

Dividing this equation by Δz and taking limits $\Delta z \rightarrow 0$ and $\Delta t \rightarrow 0$, we get

$$\begin{aligned}
 A_z \frac{\partial(\rho_b C_s T_s)}{\partial t} &= - \left[\frac{F_s \rho_b}{(1-\epsilon)} \right] \frac{\partial(C_s T_s)}{\partial z} + q_6 A_z C_s T_s \\
 &\quad + q_2 (T_g - T_s) A_z - \left[\sum_i (\Delta H_R)_i R_i \right] A_z \\
 &\quad - \beta_3 \frac{q_7}{V_B} A_z
 \end{aligned} \tag{4.32}$$

Heat capacity of solids depends upon the temperature, and the density of solids in bed (ρ_b) varies with the height and time. Therefore, we expand the derivative terms as follows :

$$\begin{aligned}
 \frac{\partial(\rho_b C_s T_s)}{\partial t} &= \rho_b \left[\left(C_s + T_s \frac{\partial C_s}{\partial T_s} \right) \frac{\partial T_s}{\partial t} \right] \\
 &\quad + C_s T_s \frac{\partial \rho_b}{\partial t} \\
 &= q_g \rho_b \frac{\partial T_s}{\partial t} + C_s T_s \frac{\partial \rho_b}{\partial t} \\
 \frac{\partial(C_s T_s)}{\partial z} &= \left[C_s + T_s \frac{\partial C_s}{\partial T_s} \right] \frac{\partial T_s}{\partial z} \\
 &= q_g \frac{\partial T_s}{\partial z}
 \end{aligned}$$

By substituting these derivatives into equation (4.32) and rearranging the terms further, equation (4.32) takes the following final form.

$$\frac{\partial T_s}{\partial t} + \frac{F_s}{A_z (1-\epsilon)} \frac{\partial T_s}{\partial z} = \frac{1}{q_g \rho_b} \left[q_6 C_s T_s + q_2 (T_g - T_s) \right]$$

$$\left. - q_8 - \frac{\beta_3 q_7}{V_B} - q_{10} \right] \quad (4.33)$$

Where

$$q_6 = 16 (R_1 + R_5) + 12 (R_2 + R_6) + 28 R_3 + 44 R_4 - 16.09 R_8 \quad (4.34a)$$

$$q_8 = \sum_{\substack{i=1 \\ i \neq 7}}^8 (\Delta H_{R_i}) R_i \quad (4.34b)$$

$$q_9 = C_s + T_s \frac{\partial C_s}{\partial T_s} \quad (4.35a)$$

$$q_{10} = C_s T_s \frac{\partial \rho_b}{\partial t} \quad (4.35b)$$

q_7 is calculated by combining equations (3.55) and (3.56), while equation (4.23) gives q_2 .

Equation (4.33) is the differential energy balance equation for solid phase.

4.2.3 Differential Pressure Drop Equation

The momentum balance equation describes the relationship between the pressure and the velocity. But in its rigorous form, it is difficult to solve this equation for the complicated system like blast furnace. However, the pressure drop in the blast furnace can be calculated by Ergun's formula [Lahiri and Seshadri (1969)].

Ergun's equation [Bird et al. (1960)] is as follows :

$$\frac{dP}{dz} = \frac{(1-\epsilon)}{1.31352 \times 10^{12} \epsilon^3} \left[\frac{150 (1-\epsilon) \mu_g}{d_p G_g} + 1.75 \right] \frac{G_g^2}{\rho'_g d_p} \quad (4.36)$$

In this equation, ρ'_g is the density of gas in kg/m^3 . But the density of gas, ρ_g , which is used in the modelling equations in the preceding sections, is in kg/Nm^3 .

Therefore,

$$\rho'_g = 273 P \rho_g / T_g \quad (4.37)$$

On putting the value of ρ'_g from equation (4.37) into equation (4.36), we obtain

$$\frac{dP}{dz} = 2.7887 \times 10^{-15} f_p \left[\frac{1-\epsilon}{\epsilon^3} \right] \left[\frac{G_g^2 T_g}{d_p P \rho_g} \right] \quad (4.38)$$

where

$$f_p = \frac{150 (1-\epsilon) \mu_g}{d_p G_g} + 1.75$$

Equation (4.38) represents the differential pressure drop equation.

4.2.4 Algebraic Equations

The process variables, namely volumetric flow rate of gas (F_g), densities of gas (ρ_g) and solid phase (ρ_b), mole fraction of H_2O vapour in gas ($y_{\text{H}_2\text{O}}$) etc, depend upon the mole fraction of gases and

fractional conversion of solids. Since the mole fraction of different gases and fractional conversion of solids have already been taken into consideration in the model equations in Section 4.2.1, therefore, the process variables, i.e. F_g , ρ_g , ρ_b , y_{H_2O} and C_{wo} , can be expressed as a function of model parameters by simple material balance and stoichiometry of chemical reactions. The derived algebraic equations for these process variables are discussed in the following subsections.

4.2.4.1 Equation for Volumetric Flow Rate of Gas (F_g)

Gaseous phase in the furnace contains CO, CO₂, H₂, H₂O, N₂ and SiO. The nitrogen gas acts as an inert gas. Therefore, at any level total moles of N₂ gas will remain the same. It is considered that the only source of nitrogen is the blasted air. Hence, by taking the component material balance for N₂ at any level z in the furnace, we obtain

$$F_g = F_b \left[\frac{47.4 + 74.6667 \times 10^{-3} w_{st}}{1 - y_{CO} - y_{CO_2} - y_{SiO}} \right] \quad (4.39)$$

SiO gas enters the bosh with the tuyere gas. Below the temperature of 1673 K, SiO gas is converted into SiO₂ and gets mixed up with the bosh slag [Biswas (1981)]. So, y_{SiO} term in equation (4.39) will effectively become zero for temperatures less than 1673 K.

4.2.4.2 Equation for Density of Gas (ρ_g)

The density of gas ρ_g at any level in the furnace can be expressed in terms of mole fractions of gases at that level. The equation derived is as follows :

$$\rho_g = 1.25 + 0.7143 y_{\text{CO}_2} - 1.1607 y_{\text{H}_2} - 0.4464 y_{\text{H}_2\text{O}} + 0.7183 y_{\text{SiO}} \quad (4.40)$$

As stated earlier, y_{SiO} is zero for temperatures below 1673 K.

4.2.4.3 Equation for Density of Solids (ρ_b)

The density of solids, ρ_b , can be expressed in terms of fractional conversions of different reacting solid components. Therefore, the density of solids at any level z in the furnace is given by the following equation.

$$\rho_b = \frac{W_B}{F_S} (1-\epsilon) - 4.0 \left[11.0 C_{\text{Lo}} f_L + 3.0 C_{\text{co}} f_c + 12.0 C_{\text{ho}} f_s + 4.0 f_{\text{sn}} C_{\text{wo}} \right] \quad (4.41)$$

Where

$$W_B = W_O + W_{\text{OS}} + W_{\text{OP}} + W_C + W_{\text{OM}} + W_L$$

4.2.4.4 Equation for Diameter (D_z) and Cross-Sectional Area (A_z) of the Furnace

The geometry of the blast furnace is not cylindrical, but is a combination of conical frustums as shown in Figure 4.1. The diameter (D_z) and cross-sectional area (A_z) of the furnace at any level z are expressed as follows :

$$D_z = D_o \quad ; \quad \text{for } z = 0 \quad , \quad (4.42a)$$

$$D_z = D_o + \frac{2z}{\tan \beta_1} \quad ; \quad \text{for } 0 < z \leq L_s \quad , \quad (4.42b)$$

$$D_z = D_b \quad ; \quad \text{for } L_s \leq z \leq L_b \quad , \quad (4.42c)$$

$$D_z = D_b - \frac{2(z - L_b)}{\tan \beta_2} \quad ; \quad \text{for } L_b \leq z \leq L \quad , \quad (4.42d)$$

$$D_z = D_h \quad ; \quad \text{for } z = L \quad (4.42e)$$

and

$$A_z = \pi D_z^2 / 4 \quad (4.43)$$

4.2.4.5 Equation for Mole Fraction of H_2O (y_{H_2O})

Water vapours enter the furnace only with the air blast as steam. The solid feed does not contain any moisture and any component of hydrogen. Therefore, steam in the blast is the only source of hydrogen gas and water vapour. The reaction with H_2 gas or with H_2O vapour as reactants or products indicates that one mole of hydrogen produces one mole of H_2O gas and vice versa. This shows that the total moles of hydrogen plus water vapours will remain same at any level z in the furnace. On this basis, following equation for mole fraction of H_2O in gas is written.

$$y_{H_2O} = 74.6667 \times 10^{-3} \frac{F_b W_{st}}{F_g} - y_{H_2} \quad (4.44)$$

4.2.4.6 Initial Concentration of FeO (C_{wo})

The reduction of molten FeO starts in melting zone. It is assumed that all unreacted Fe_2O_3 in melting zone exist as molten FeO, dissolved homogeneously in slag. Thus, the initial concentration of FeO is expressed in terms of the fractional conversion of Fe_2O_3 as given below.

$$C_{wo} = \left[3 (1 - f_s) F_{m_{Fe_2O_3}} + F_{m_{FeO}} \right] \frac{(1 - \epsilon)}{F_s} \quad (4.45)$$

Where $F_{m_{Fe_2O_3}}$ and $F_{m_{FeO}}$ are calculated from equations (3.57f) and (3.57g) respectively.

4.2.5 Initial and Boundary Conditions

As discussed above, the model equations constitute a set of partial differential equations and algebraic equations. Mathematically speaking, these form a boundary value problem. In order to solve them by a suitable numerical method, we require initial and boundary conditions. For the dynamic model equations, initial conditions shall be obtained by solving the steady state model equations, while the boundary conditions shall include the change in input parameters at either end of the shaft. Values of parameters in the streams entering the shaft at the top or bottom are assumed to be known. The initial estimates for remaining parameters have to be provided so that the numerical solution may be initiated. Values of parameters used in the input streams to the bosh and initial estimates of remaining variables have been computed by taking overall material and energy balances; the procedure for the same has been discussed in detail in Chapter III.

4.2.6 Constitutive Relationships

In the derivation of model equations, parameters, viz. heat of reaction, rate of reaction, heat transfer coefficients, viscosity of gas, heat capacity etc, have been used extensively. These are specific to a particular gas-solid system handled in the reactor and are normally called as constitutive relationships. The model predictions shall naturally depend upon the accuracy of the values of these parameters. Thus, it is important to calculate these parameters with as much accuracy as possible. In view of their importance, a separate chapter (Chapter V) has been included in the present thesis, where their expressions have been described/derived.

4.3 STEADY STATE MODEL

The dynamic model equations can be easily converted into steady state model equations by setting the accumulation term, i.e. the time derivative ($\partial/\partial t$), equal to zero. Thus, the partial differential equations are converted into ordinary differential equations. Steady state model equations are summarized below.

Component mass balance equations

$$\frac{df_s}{dz} = \frac{(1-\epsilon) A_z}{3 F_s C_{ho}} (R_1 + R_5) \quad (4.46)$$

$$\frac{df_c}{dz} = \frac{A_z (1 - \epsilon)}{F_s C_{co}} (R_2 + R_3 + R_6 + R_8) \quad (4.47)$$

$$\frac{df_L}{dz} = \frac{A_z (1 - \epsilon)}{F_s C_{Lo}} R_4 \quad (4.48)$$

$$\frac{df_{sn}}{dz} = \frac{A_z (1 - \epsilon)}{F_s C_{wo}} R_3 \quad (4.49)$$

$$\frac{dy_{CO}}{dz} = \frac{22.4 A_z}{F_g} \left[R_1 + R_2 (y_{CO} - 2) + R_3 (y_{CO} - 1) + R_4 y_{CO} + R_6 (y_{CO} - 1) + R_7 - R_8 \right] \quad (4.50)$$

$$\frac{dy_{CO_2}}{dz} = \frac{22.4 A_z}{F_g} \left[R_2 (y_{CO_2} + 1) + y_{CO_2} (R_3 + R_6) + R_4 (y_{CO_2} - 1) - R_7 - R_1 \right] \quad (4.51)$$

$$\frac{dy_{H_2}}{dz} = \frac{22.4 A_z}{F_g} \left[R_5 + R_6 (y_{H_2} - 1) - R_7 + y_{H_2} (R_2 + R_3 + R_4) \right] \quad (4.52)$$

$$\frac{dy_{SiO}}{dz} = \frac{22.4 A_z}{F_g} \left[y_{SiO} (R_2 + R_3 + R_4 + R_6) + R_8 \right] \quad (4.53)$$

Energy balance equations

$$\frac{dT_g}{dz} = \frac{22.4 A_z}{F_g q_5} \left[q_1 C_g T_g + q_2 (T_g - T_s) + q_3 \right]$$

$$+ q_4 (T_g - T_{wc}) \quad] \quad (4.54)$$

$$\frac{dT_s}{dz} = \frac{A_z (1 - \epsilon)}{q_g F_s \rho_b} \left[q_6 C_s T_s + q_2 (T_g - T_s) - q_8 - \frac{\beta_3 q_7}{V_B} \right] \quad (4.55)$$

Equations (4.46) to (4.55) give the differential mass and energy balance equations for steady state model. Since the pressure drop equation (4.38) is already in steady state form, it will remain the same. The algebraic equations, the boundary conditions and the constitutive relationships as discussed in Sections 4.2.4, 4.2.5 and 4.2.6 respectively, will also not change and therefore, are considered as such for the steady state model.

4.4 CONCLUDING REMARKS

In this Chapter, a one-dimensional mathematical model of the shaft region of blast furnace has been developed. Equations (4.5), and (4.9) to (4.15) for component material balances, equations (4.29) and (4.33) for energy balances, and algebraic equations discussed in Section 4.2.4 form the mathematical model. This model has also been reduced to steady state model by setting the accumulation term equal to zero. Steady state model equations thus obtained are stated in Section 4.3. In order to study the behaviour and obtain the performance of blast furnace, model equations are to be solved with the initial and boundary conditions (Section 4.2.5) by using appropriate constitutive relationships.

The results of numerical solution of steady state model have been presented and discussed in Chapter VI.

CORRELATIONS FOR PARAMETERS USED IN THE MODEL

5.0 INTRODUCTION

The mathematical model for the shaft region of blast furnace has been developed on the basis of laws of conservation of mass, momentum and energy. In order to predict the performance, the mathematical model is to be solved in conjunction with the constitutive relationships pertaining to the phases and processes occurring in the shaft region. Therefore, the correlations used for physical properties of solid, liquid and gas, heat transfer coefficients, heats of reactions, rates of reactions etc, have been described/derived and discussed in detail in this chapter along with their limitations.

5.1 PROPERTIES OF SOLIDS

In this section the relationships for the volumetric flow rate of burden feed, average diameter, porosity and shape factor of particles, initial concentration of different solid components, surface area of particles, and number of particles per unit bed volume have been derived. The diameter, density, shape factor and porosity of different solid particles used in these relationships, are mentioned in Table A.5.

5.1.1 Volumetric Flow Rate of Burden Feed

The burden feed contains iron ore, sinter, pellets, manganese

ore, coke and limestone. On the basis of their mass flow rates, the volumetric flow rate of burden feed can be calculated by the following equation.

$$F_S = \frac{W_O}{\rho_O} + \frac{W_{OS}}{\rho_{OS}} + \frac{W_{OP}}{\rho_{OP}} + \frac{W_{OM}}{\rho_{OM}} + \frac{W_C}{\rho_C} + \frac{W_L}{\rho_L} \quad (5.1)$$

5.1.2 Average Diameter of Solid Particles

The burden is a mixture of solid particles of different sizes and densities. The average diameter of particles (d_p) in burden can be calculated by using the following relationship. This relationship is derived on the basis of method described by McCabe et al. (1986).

$$d_p = F_S / \left[\sum_i (W_i / \rho_i d_i) \right] \quad (5.2)$$

Where i stands for solid and varies from iron ore to limestone (iron ore, sinter, pellets, manganese ore, coke and limestone).

The iron bearing solids in burden are iron ore, sinter, pellets and manganese ore (Mn Ore). Like d_p , the average diameter of particles of iron bearing solids (d_{oa}) can also be calculated. Thus,

$$d_{oa} = \left[\sum_i (W_i / \rho_i) \right] / \sum_i (W_i / \rho_i d_i) \quad (5.3)$$

where i represents the iron bearing solids.

5.1.3 Average Shape Factor for Solid Particles

The shape factor of particles of solid i (ϕ_i) is defined as follows [Foust et al. (1960)] :

$$\phi_i = \frac{\text{Surface area of sphere with same volume as the particle}}{\text{Surface area of the particle}}$$

The average shape factor of solid particles (ϕ) is derived in terms of average particle diameter (d_p) as follows :

$$\frac{1}{\phi} = \frac{d_p}{F_s} \sum_i (W_i / \rho_i \phi_i d_i) \quad (5.4)$$

Where i represents the solids in the burden, namely iron ore, sinter, pellets, Mn ore, coke and limestone.

5.1.4 Average Porosity of Iron Bearing Solid Particles

The porosity of particles of solid i is defined as follows :

$$\epsilon_i = \frac{\text{Volume of void spaces in the particle}}{\text{Volume of the particle}}$$

Therefore, the average porosity of iron bearing solid particles (ϵ_p) is given by

$$\epsilon_p = \left[\sum_i (W_i \epsilon_i / \rho_i) \right] / \sum_i (W_i / \rho_i) \quad (5.5)$$

where i stands for iron bearing solid particles.

5.1.5 Total Surface Area of Iron Bearing Solid Particles in Unit Volume of Bed

Surface area of particles is required to estimate the rate of gas-solid reactions. Total surface area of iron bearing solid particles per unit bed volume (S_o) is calculated from the individual properties of particles of different solids. Thus,

$$S_o = \frac{6(1 - \epsilon)}{F_s} \sum_i (W_i / \rho_i d_i \phi_i) \quad (5.6)$$

where i stands for iron bearing solid particles, viz. iron ore, sinter, pellets and Mn ore.

5.1.6 Number of Solid Particles in Unit Volume of Bed

It is assumed that the net rate of each reaction within any elemental volume of the bed, is the algebraic sum of the reaction rates at each individual particle present in that volume. Therefore, it is necessary to calculate the number of particles per unit volume of bed of each reacting solid material. The number of particles of solid i in unit volume of bed (N_i) is given by the following equation.

$$N_i = \frac{1.91 (1 - \epsilon) W_i}{F_s \rho_i d_i^3} \quad (5.7)$$

5.1.7 Initial Concentration of Components in Solids

During the development of mathematical model (Chapter IV), the

initial or inlet concentration of a component in solid feed is defined as moles of component present in the solids per unit volume of bed. Thus, the initial concentration of carbon, Fe_2O_3 and CaCO_3 in solid feed, i.e. C_{co} , C_{ho} and C_{Lo} respectively, can be expressed by the following equations :

$$C_{\text{co}} = (1 - \epsilon) W_C t_c / (12.0 F_s) \quad (5.8)$$

$$C_{\text{ho}} = (1 - \epsilon) W_{\text{Fe}_2\text{O}_3} / (159.7 F_s) \quad (5.9)$$

$$C_{\text{Lo}} = (1 - \epsilon) W_L l_{\text{CO}_2} / (44.0 F_s) \quad (5.10)$$

Where

$$W_{\text{Fe}_2\text{O}_3} = W_O v_{\text{Fe}_2\text{O}_3} + W_{\text{OS}} s_{\text{Fe}_2\text{O}_3} + W_{\text{OP}} p_{\text{Fe}_2\text{O}_3} + W_{\text{OM}} g_{\text{Fe}_2\text{O}_3}$$

5.1.8 Heat Capacities of Solids in Burden Feed

Heat capacities of different solid materials present in the burden feed are given by the following equations :

Iron ore

$$(C_s)_O = \sum_i v_i (C)_i \quad (5.11a)$$

Sinter

$$(C_s)_{\text{OS}} = \sum_i s_i (C)_i \quad (5.11b)$$

Pellets

$$(C_s)_{OP} = \sum_i p_i (C)_i \quad (5.11c)$$

Mn Ore

$$(C_s)_{OM} = \sum_i g_i (C)_i \quad (5.11d)$$

Coke

$$(C_s)_C = t_c (C)_c + t_a \sum_i b_i (C)_i \quad (5.11e)$$

Limestone

$$(C_s)_L = \sum_i l_i (C)_i \quad (5.11f)$$

Where i represents the components present in different solid materials. These components are Fe_2O_3 , FeO , SiO_2 , Al_2O_3 , $CaCO_3$, CaO , MgO and MnO_2 . By using the heat capacity of different solid materials, the heat capacity of burden $[(C_s)_B]$ can be written as follows :

$$(C_s)_B = \left[W_O (C_s)_O + W_{OS} (C_s)_{OS} + W_{OP} (C_s)_{OP} + W_{OM} (C_s)_{OM} + W_C (C_s)_C + W_L (C_s)_L \right] / W_B \quad (5.12)$$

Where

$$W_B = W_O + W_{OS} + W_{OP} + W_{OM} + W_L + W_C$$

5.2 PROPERTIES OF GAS MIXTURE

The correlations for viscosity, average heat capacity and thermal

conductivity of blast furnace gas mixture are described in this section.

5.2.1 Viscosity of Gas Mixture

A general method to calculate the viscosity of any gas mixture at any temperature by using the viscosity data of individual gas components has been discussed by Bird et al. (1960). However, this method requires intensive computation and hence, has not been used. Yagi and Muchi (1970b) proposed a relationship to calculate the viscosity of blast furnace gas as a function of temperature, which is as follows :

$$\mu_g = 4.960 \times 10^{-3} T_g^{1.5} / (T_g + 103) \quad (5.13)$$

It is obvious that this relationship does not account for the variations in gas composition from the bottom to top of the blast furnace. Sample calculations of μ_g by both the methods show that the variation is within ± 5 per cent. Besides, Yagi and Muchi (1970b) observed that the use of equation (5.13) did not affect the overall performance of blast furnace appreciably and at the same time, required less computation. In view of this, equation (5.13) has been used in the present work.

5.2.2 Thermal Conductivity of Gas Mixture

Bird et al. (1960) has described a method to compute the thermal conductivity of gas mixture (k_g), which is similar to that of viscosity calculation. But this method is also computationally intensive. They have also stated a relationship for thermal conductivity of polyatomic gases, which makes comparatively approximate predictions for gas mixture of blast furnace. However, this relationship has been used in

the present work for calculating the thermal conductivity of a gas mixture because its use was found satisfactory in the simulations of blast furnace as demonstrated by Ufret et al. (1981). Thus,

$$k_g = \mu_g [C_g + 1.25 R/M_g] \quad (5.15)$$

where

$$M_g = \sum_i y_i M_i \quad (5.15a)$$

and i represents components of gas mixture.

5.2.3 Average Heat Capacity of Gas Mixture

The blast furnace gas, in general, is a gaseous mixture of CO, CO₂, N₂, H₂, H₂O and SiO. The gas composition varies from the top to bottom of the furnace. The average heat capacity of gas mixture may be expressed by using heat capacity and mole fraction of each component. Table A.1 represents the heat capacity of substances as a function of temperature. By using Table A.1, we get following equation for average heat capacity of gas mixture (C_g).

$$C_g = a_3 + b_3 \times 10^{-3} T_g + c_3 \times 10^5 / T_g^2 \quad (5.14)$$

Where

$$a_3 = 6.79 y_{CO} + 10.55 y_{CO_2} + 6.66 y_{N_2} + 6.52 y_{H_2} + 7.17 y_{H_2O} + 7.755 y_{SiO} \quad (5.14a)$$

$$b_3 = 0.98 y_{CO} + 2.16 y_{CO_2} + 1.02 y_{N_2} + 0.78 y_{H_2}$$

$$+ 2.56 y_{H_2O} + 0.57 y_{SiO} \quad (5.14b)$$

$$c_3 = 0.12 y_{H_2} + 0.08 y_{H_2O} - 0.11 y_{CO} - 2.04 y_{CO_2} \\ - 0.505 y_{SiO} \quad (5.14c)$$

5.3 HEAT TRANSFER COEFFICIENT BETWEEN SOLID AND GAS

The heat transfer coefficient between solid and gas (h_{gs}) in the blast furnace is estimated by Ranz's equation [Balakrishnan and Pei (1979), Omori (1987)], which is described as follows :

$$h_{gso} = \frac{k_g}{d_p} \left[2.0 + 0.6 (9 Re_p)^{1/2} (Pr)^{1/3} \right]$$

However, in order to have good agreement with the measured values of variables obtained from operating furnaces, the calculated value of h_{gso} has to be modified. For this purpose, the introduction of a modification coefficient (β_4) is necessary. Thus, we obtain

$$h_{gs} = \beta_4 h_{gso} \quad (5.16)$$

where

$$Re_p = F_g d_p \rho_g / \mu_g \Lambda_z$$

$$Pr = C_g \mu_g / k_g M_g$$

β_4 is an adjustable parameter. It varies between 0.02 and 0.3 as reported by Hatano and Kurita (1982). F_g , ρ_g and Λ_z are given by equations (4.39), (4.40) and (4.43) respectively.

5.4 OVERALL HEAT TRANSFER COEFFICIENT FOR HEAT LOSS THROUGH FURNACE WALL

The overall heat transfer coefficient for heat loss through furnace wall (U) is assumed to have a constant value throughout its inner surface. Thus, the value of U can be calculated in terms of total heat loss through furnace wall (Q_w) as follows :

$$U = Q_w / (A_w \Delta T) \quad (5.17)$$

Q_w is given by equation (3.59). A_w is the curved surface area of the furnace wall and is written as follows :

$$A_w = \pi \left[(D_o + D_b) L_s \operatorname{cosec} \beta_1 + (D_b + D_h) (L - L_b) \operatorname{cosec} \beta_2 + 2 D_b (L_b - L_s) \right] / 2.0 \quad (5.17a)$$

Since the temperature of gas at the inlet of bosh ($T_{g,1}$) is much higher than its temperature at outlet from the top ($T_{g,0}$), therefore, ΔT represents log mean temperature difference (LMTD). Usually the difference between the inlet and the outlet temperatures of cooling water circulated around the wall of the furnace is 2 to 6 °C only [Yagi and Muchi (1970a)]. Therefore, the temperature of cooling water (T_{wc}) may be assumed to be constant throughout. Thus,

$$\Delta T = (T_{g,1} - T_{g,0}) / \ln \left[(T_{g,1} - T_{wc}) / (T_{g,0} - T_{wc}) \right] \quad (5.17b)$$

5.5 HEATS OF REACTIONS

Heat of a chemical reaction depends on the temperature as well as the chemical nature and physical state of each of the reactants and

products. Since in blast furnace, there exists wide variation in temperatures of solids and gases from top to bottom, it becomes necessary to consider the effect of temperature on the heat of reaction. Therefore, in this section, efforts have been made to derive the relationships for heats of reactions as a function of temperature.

Hougen et al. (1964) has recommended the use of Kirchhoff's equation for estimating the effect of temperature on heat of reaction. The reaction is assumed to begin and end with all reactants and products at the same temperature. The Kirchhoff's equation gives the heat of reaction at any temperature, provided that the heat of reaction atleast at one temperature, and heat capacities of each of the reactants and products are known.

The Kirchhoff's equation for any reaction can be written as follows :

$$(\Delta H_R)_{T_2} = (\Delta H_R)_{T_1} + \int_{T_1}^{T_2} \Delta C_p \, dT \quad (5.18)$$

Where

$$\Delta C_p = \sum (C_p)_{\text{products}} - \sum (C_p)_{\text{reactants}}$$

Equation (5.18) has been used for all the chemical reactions considered in the model. For this purpose, the heat capacity of different substances as a function of temperature is taken from Table A.1. The relationships developed for various reactions have been described in the following sections. It may be noted that the temperature of reaction (T) is in K.

5.5.1 Indirect Reduction of Fe_2O_3 by CO

Reaction is exothermic in nature and proceeds as follows :



Relationships for the heat of reaction, $(\Delta H_R)_1$, expressed as kcal per kmol of CO are as follows :

For $298 \leq T \leq 950 \text{ K}$:

$$\begin{aligned} (\Delta H_R)_1 &= -2.0186 \times 10^{-3} T^2 + 1.8453 T + 0.7467 \times 10^5 / T \\ &\quad - 75.8934 \sqrt{T} - 1447.1869 \end{aligned} \quad (5.19a)$$

For $950 \leq T \leq 1050 \text{ K}$:

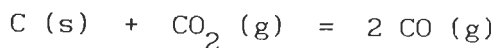
$$\begin{aligned} (\Delta H_R)_1 &= 1.0813 \times 10^{-3} T^2 - 2.3247 T + 1.93 \times 10^5 / T \\ &\quad - 75.8934 \sqrt{T} - 407.9005 \end{aligned} \quad (5.19b)$$

For $1050 \leq T \leq 1750 \text{ K}$:

$$\begin{aligned} (\Delta H_R)_1 &= 0.788 \times 10^{-3} T^2 - 0.8914 T + 1.93 \times 10^5 / T \\ &\quad - 75.8934 \sqrt{T} - 1589.5023 \end{aligned} \quad (5.19c)$$

5.5.2 Solution Loss Reaction

Reaction is endothermic in nature and proceeds as follows :



Relationship for the heat of reaction, $(\Delta H_R)_2$, expressed as kcal per kmol of CO_2 is as follows :

For $298 \leq T \leq 1873 \text{ K}$:

$$(\Delta H_R)_2 = - 1.1 \times 10^{-3} T^2 + 0.10 T - 0.72 \times 10^5 / T + 38929.8952 \quad (5.20)$$

5.5.3 Direct Reduction of Molten FeO

Reaction is endothermic in nature and proceeds as follows :



Relationship for the heat of reaction, $(\Delta H_R)_3$, expressed as kcal per kmol of FeO is as follows :

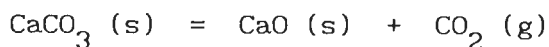
For $T' \leq T \leq 1873 \text{ K}$:

$$(\Delta H_R)_3 = - 0.51 \times 10^{-3} T'^2 - 2.44 T' - 0.99 \times 10^5 / T' + 12.60 T' + 15508.3354 \quad (5.21)$$

Where T' is the temperature at which solid FeO starts to react with the solid carbon.

5.5.4 Decomposition of CaCO_3

Reaction is endothermic in nature and proceeds as follows :



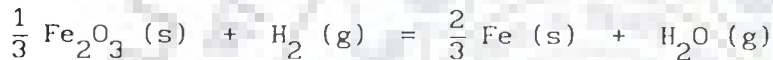
Relationship for heat of reaction, $(\Delta H_R)_4$, expressed as kcal per kmol of CaCO_3 is as follows :

For $298 \leq T \leq 1200 \text{ K}$:

$$(\Delta H_R)_4 = -10^{-3} T^2 - 2.57 T - 2.5 \times 10^5 / T + 44191.7902 \quad (5.22)$$

5.5.5 Indirect Reduction of Fe_2O_3 by H_2

Reaction is endothermic in nature and proceeds as follows :



Relationships for the heat of reaction, $(\Delta H_R)_5$, expressed as kcal per kmol of H_2 are as follows :

For $298 \leq T \leq 950 \text{ K}$:

$$(\Delta H_R)_5 = -1.7187 \times 10^{-3} T^2 - 1.2647 T - 1.1433 \times 10^5 / T - 75.8934 \sqrt{T} + 9928.2890 \quad (5.23a)$$

For $950 \leq T \leq 1050 \text{ K}$:

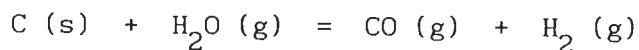
$$(\Delta H_R)_5 = 1.3814 \times 10^{-3} T^2 - 5.4347 T + 0.04 \times 10^5 / T - 75.8934 \sqrt{T} + 10967.436 \quad (5.23b)$$

For $1050 \leq T \leq 1750 \text{ K}$:

$$(\Delta H_R)_5 = 1.0882 \times 10^{-3} T^2 - 4.0014 T - 0.04 \times 10^5 / T - 75.8934 \sqrt{T} + 9785.9445 \quad (5.23c)$$

5.5.6 Water Gas Reaction

Reaction is endothermic in nature and proceeds as follows :



Relationship for the heat of reaction, $(\Delta H_R)_6$, expressed as kcal per kmol of H_2O is as follows :

For $298 \leq T \leq 1873 \text{ K}$:

$$(\Delta H_R)_6 = -1.4 \times 10^{-3} T^2 + 3.21 T - 1.03 \times 10^5 / T + 28292.6832 \quad (5.24)$$

5.5.7 Water Gas Shift Reaction

Reaction is exothermic in nature and proceeds as follows :



Relationship for the heat of reaction, $(\Delta H_R)_7$, expressed as kcal per kmol of H_2O is as follows.

For $298 \leq T \leq 2500 \text{ K}$:

$$(\Delta H_R)_7 = -0.30 \times 10^{-3} T^2 + 3.11 T + 1.89 \times 10^5 / T - 11375.467 \quad (5.25)$$

5.5.8 Reduction of SiO Gas

Reaction is endothermic in nature and proceeds as follows :



Relationship for the heat of reaction, $(\Delta H_R)_8$, expressed as kcal per kmol of SiO is as follows :

For $1473 \leq T \leq 1873 \text{ K}$:

$$(\Delta H_R)_8 = -0.75 \times 10^{-3} T^2 + 2.225 T - 1.495 \times 10^5 / T + 3494.2653 \quad (5.26)$$

5.6 OVERALL REACTION RATES

The rate at which a chemical reaction proceeds, is termed as rate of reaction. It can be expressed on the basis of any of the reactants or products. Thus, the rate of reaction is defined as the number of moles of a reactant or product per unit time per unit volume. The factors that affect the rate of reaction and consequently the performance of reactor, are searched through the chemical kinetics, which depends upon the type of reaction. In blast furnace the reactions are mostly noncatalytic and heterogeneous, viz. gas-solid reactions. Since in these type of reactions, more than one phase is present, the material may have to move from one phase to another. Hence, overall kinetic expression of the reaction will include the rate of reaction as well as other transport processes occurring amongst the phases.

5.6.1 Gas-Solid Reactions

To study the kinetics of single particle gas-solid reaction, most widely used kinetic model is unreacted core model or sharp interface model [Kunii and Levenspiel (1969), Levenspiel (1974), Szekely (1977)]. This model is restricted only to nonporous solids or to the solids

having very low internal porosity. The size of particle remains unchanged during the reaction. In this model the reaction is considered to occur first at the outermost surface of the solid particle. The reaction interface then moves into the solid towards the centre of the particle, leaving behind the reacted shell. Therefore, at any time there exists an unreacted core of solid, which shrinks in size, and a reacted shell, which enlarges during the progress of reaction. Thus, in this model the reaction occurs at the sharp interface between the reacted shell and unreacted core of the solid particle. The movement of a sharp reaction interface inside the particle is known as topochemical inward movement of reaction interface. Yagi and Muchi (1970b) have used unreacted core model with one interface to study the kinetics of reduction of iron oxide (hematite) particles as well as decomposition of limestone particles. In order to determine overall rate expression for these reactions, they visualized following three steps occurring in succession.

- (i) Diffusion of gaseous reactants and products through the gas film surrounding the particle to or from the surface of the solid respectively.
- (ii) The intraparticle diffusion of gaseous reactants and products through the reacted shell from or to the reaction interface, respectively.
- (iii) The chemical reaction at the interface.

It may be mentioned that these steps were first visualized and proposed by Yagi and Kunii (1955) for studying the kinetics of noncatalytic gas-solid reactions based upon unreacted core model.

Yagi and Muchi (1970b) have considered resistances offered by all the above three steps and developed the overall rate expression for iron oxide reduction and limestone decomposition. The resistance due to the gas film diffusion is expressed in terms of Reynolds number and Schmidt number. These numbers depend upon the transport and physical

properties of gases, and the particle diameter. The resistance due to intraparticle diffusion is written in terms of extent of reaction, particle porosity and diffusivity of gas.

The reactions between coke particles and gas behave in a significantly different manner as compared to the iron ore reduction reactions. The blast furnace coke particle is having a large amount of internal porosity. In such a high porous solid particle, the chemical reaction occurs simultaneously at all the gas solid interfaces, both at the outside boundaries and within the particle. But, since the interior of the particle contains much more area than the exterior, therefore, the reaction occurs throughout the porous coke particle. This is in contrast to the unreacted core model, where the reaction is localized at a sharp moving reaction interface. Thus, for highly porous coke reaction, we account for the following three distinct kind of steps, which may cause resistances to overall reaction rate.

- (i) The diffusion of gaseous reactants and products through the gas film surrounding the particle.
- (ii) Intraparticle diffusion of the gaseous reactants from the exterior surface of the particle to an active site on the interior surface of the particle (i.e. inside the pores) and the corresponding outward diffusion of gaseous products.
- (iii) Chemical reaction at the interior surface of the particle.

Further, both the intraparticle diffusion and chemical reaction rates are strongly dependent upon the internal porosity of the coke particle. Yagi and Muchi (1970b) applied this model to solution loss reaction and water gas reaction. They derived the expression for overall reaction rate by taking into account the resistances offered by all the above three steps. It is assumed that the diffusion process through gas film around coke particle takes place in series with the

parallel processes of intraparticle diffusion and chemical reaction inside the particle. The chemical reaction is also assumed to be irreversible and of first order. The resistance due to the gas film diffusion is expressed in terms of diameter of the particle, diffusivity and physical properties of gas. The combined net resistance of intraparticle diffusion and reaction is expressed in terms of effectiveness factor and the rate of reaction. The effectiveness factor is a function of rate constant, diffusivity of gas into the particle, porosity and physical properties of coke particles.

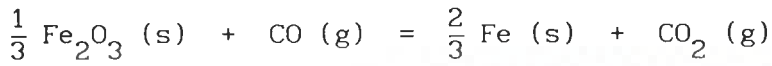
Yagi and Muchi (1970b) in their kinetic model, have reported the overall reaction rates for different chemical reactions occurring in blast furnace, and these have been used in the present work for various reactions considered in the mathematical model with some modifications. However, the equation for overall reaction rate for the reduction of SiO gas, proposed by Taguchi et al. (1982), has been used in place of one used by Yagi and Muchi (1970b).

We have modified the temperature considerations for calculating the diffusion coefficients. Since the velocity of gas in blast furnace is very high, the gas film formed around each type of solid particle, is very thin. Hence, in the present work diffusivity of gases for gas film diffusion is calculated at the arithmetic mean temperature of gas and solid (T_{gm}). In case of intraparticle diffusion for all type of solid particles, the diffusivity of gas is calculated at the temperature of solid (T_s). Temperature of a solid particle is assumed to be uniform throughout the particle volume.

The overall reaction rate equations for chemical reactions are given in following subsections.

5.6.2 Indirect Reduction of Iron Ore by CO

The reduction of iron oxide by CO is described by the following reaction.



The overall reaction rate, R_1 , is defined as follows :

$$R_1 = \text{kmol of CO consumed/m}^3 (\text{bed}).\text{hr}$$

The expression for R_1 is given below.

$$R_1 = S_1 (y_{\text{CO}} - y_{\text{CO}}^*) P / (T_s r_1) \quad (5.27)$$

Where

$$S_1 = 12.1875 S_o$$

$$r_1 = r_{11} + r_{12} + r_{13}$$

$$r_{11} = 1.0 / kf_1$$

$$r_{12} = 0.5 d_{\text{oa}} \{ (1 - f_s)^{-1/3} - 1 \} / D_{s1}$$

$$r_{13} = \{ k_1 (1 - f_s)^{2/3} (1 + 1/K_1) \}^{-1}$$

S_o is given by equation (5.6).

Different rate constants and coefficients used are determined as follows :

Equilibrium constant (K_1)

For $T_s \leq 848$ K :

$$K_1 = \exp (4.91 + 6235 / T_s) \quad ; \quad \text{for } f_s \leq 0.11$$

$$K_1 = \exp (-0.7625 + 543.3 / T_s) \quad ; \quad \text{for } f_s > 0.11$$

For $T_s > 848$ K :

$$K_1 = \exp (4.91 + 6235 / T_s) \quad ; \quad \text{for } f_s \leq 0.111$$

$$K_1 = \exp (2.13 - 2050 / T_s) \quad ; \quad \text{for } 0.111 < f_s \leq 0.333$$

$$K_1 = \exp (-2.642 + 2164 / T_s) \quad ; \quad \text{for } f_s > 0.333$$

Reaction rate constant (k_1)

$$k_1 = 347.0 \exp (-3460 / T_s)$$

Diffusion coefficient of CO

For intraparticle diffusion :

$$D_{CO} = 2.592 \times 10^{-6} (T_s)^{1.78} / P \quad ; \quad \text{for } T_s \leq 848 \text{ K}$$

$$D_{CO} = 2.592 \times 10^{-6} T_s^2 / P \quad ; \quad \text{for } T_s > 848 \text{ K}$$

For gas film diffusion :

$$D_{COg} = 2.592 \times 10^{-6} (T_{gm})^{1.78} / P \quad ; \quad \text{for } T_{gm} \leq 848 \text{ K}$$

$$D_{\text{COg}} = 2.592 \times 10^{-6} (T_{\text{gm}})^2 / P \quad ; \quad \text{for } T_{\text{gm}} > 848 \text{ K}$$

Mass transfer coefficient (kf_1)

$$kf_1 = D_{\text{COg}} \{ 2.0 + 0.55 (\text{Re}_p)^{0.5} (\text{Sc})^{1/3} \} / d_{\text{oa}}$$

Where

$$\text{Re}_p = d_{\text{oa}} F_g \rho_g / \mu_g A_z$$

$$\text{Sc} = \mu_g / (\rho_g D_{\text{COg}})$$

d_{oa} , μ_g , F_g , ρ_g and A_z are given by the equations (5.3), (5.13), (4.39), (4.40) and (4.43) respectively.

Intraparticle diffusion coefficient of CO through reacted shell (D_{s1})

$$D_{s1} = D_{\text{CO}} \epsilon_{\text{vo}} \xi_o$$

Where

$$\epsilon_{\text{vo}} = 0.53 + 0.47 \epsilon_p \quad ; \quad \text{for } 0.15 < \epsilon_p < 0.5$$

$$\xi_o = 0.04 + 0.238 \epsilon_p$$

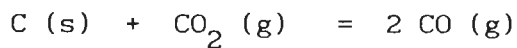
The porosity of iron bearing particle (ϵ_p) is given by equation (5.5).

Equilibrium mole fraction of CO (y_{CO}^*)

$$y_{\text{CO}}^* = (y_{\text{CO}} - y_{\text{CO}_2}) / (1 + K_1)$$

5.6.3. Solution Loss Reaction

The solution loss reaction is described by the following reaction.



The overall reaction rate, R_2 , is defined as follows :

$$R_2 = \text{kmol of } CO_2 \text{ consumed} / m^3 \text{ (bed). hr}$$

The expression for R_2 is given below.

$$R_2 = S_2 P y_{CO_2} / (T_s r_2) \quad (5.28)$$

Where

$$S_2 = 12.1875 \pi d_c^2 N_C / \phi_c$$

$$r_2 = r_{21} + r_{22}$$

$$r_{21} = 1.0 / kf_2$$

$$r_{22} = 6.0 / (d_c \rho_C k_2 Ef_2)$$

N_C is given by equation (5.7).

Different rate constants, coefficients and conditions used are determined as follows :

Conditions

For $y_{CO_2} < 0.1$:

$$y_{CO_2} = 0.1$$

For $y_{\text{CO}_2} = 0$:

$$R_2 = R_1 + R_4 + R_7$$

Reaction rate constant (k_2)

$$k_2 = 2.99 \times 10^{13} \exp(-80000 / R T_s)$$

Diffusion coefficient of CO_2

For gas film diffusion :

$$D_{\text{CO}_2\text{g}} = 2.236 \times 10^{-6} (T_{\text{gm}})^{1.78} / P$$

For intraparticle diffusion :

$$D_{\text{CO}_2} = 2.236 \times 10^{-6} (T_s)^{1.78} / P$$

Mass transfer coefficient (kf_2)

$$kf_2 = D_{\text{CO}_2\text{g}} \{ 2.0 + 0.55 (\text{Re}_p)^{0.5} (\text{Sc})^{1/3} \} / d_c$$

Where

$$\text{Re}_p = d_c F_g \rho_g / \mu_g A_z$$

$$\text{Sc} = \mu_g / (\rho_g D_{\text{CO}_2\text{g}})$$

$$G_g = \frac{F_g \rho_g}{A_z}$$

μ_g , F_g , ρ_g and A_z are given by equations (5.13), (4.39), (4.40) and (4.43) respectively.

Intraparticle diffusion coefficient of CO (D_{s2})

$$D_{s2} = D_{CO_2} \epsilon_c \xi_c$$

Where

$$\xi_c = 0.04 + 0.238 \epsilon_c$$

Effectiveness factor (Ef_2)

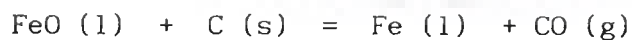
$$Ef_2 = 3.0 (m_2 \coth m_2 - 1) / m_2^2$$

Where

$$m_2 = 0.5 d_c \sqrt{(\rho_c k_2 / D_{s2})}$$

5.6.4 Direct Reduction of Molten FeO

The reduction of molten FeO is described by the following reaction.



The overall reaction rate, R_3 , is defined as follows :

$$R_3 = \text{kmol of FeO} / \text{m}^3(\text{bed}).\text{hr}$$

The expression for R_3 is given below.

$$R_3 = S_3 k_3 (C_{FeO})^2 \tag{5.29}$$

Different parameters used are determined as follows :

Reaction rate constant (k_3)

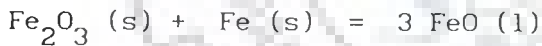
$$k_3 = 4.66 \times 10^4 \exp \left(-53300 / (R T_s) \right)$$

The specific surface area of coke available for the reaction (S_3)

$$S_3 = 0.468 (1-\epsilon) / (\phi_c d_c)$$

Concentration of FeO (C_{FeO})

When the fusion of solids starts, it is assumed that unreacted Fe_2O_3 is fused in the form of FeO according to the following reaction.



Concentration of FeO is expressed by the following equation.

$$C_{FeO} = a_4 / \left\{ (W_{S,1} / \rho_s) + (71.85 a_4 / \rho_w) \right\}$$

Where

$$a_4 = F_{m_{FeO,m}} (1 - f_{sn})$$

$$F_{m_{FeO,m}} = 3 F_{m_{Fe_2O_3}} (1 - f_s) + F_{m_{FeO}}$$

$W_{S,1}$, $F_{m_{Fe_2O_3}}$, $F_{m_{FeO}}$ are given by equations (3.29), (3.57f) and (3.57g) respectively.

Temperature of the reaction

Yagi and Muchi (1970b) have reported that the direct reduction of molten FeO takes place above 1673 K and below this temperature, indirect reduction of iron ore occurs. However, Biswas (1981) has shown that this reaction takes place at 1273 K or above, and below this temperature indirect reduction of Fe_2O_3 takes place. According to Ufret et al. (1981), the reaction takes place in the bosh where temperature is around 1673 K. Hence, in this thesis, the temperature of reaction has been assumed to be an adjustable parameter, which shall be varied between 1273 and 1673 K in simulation to match the experimental data with the predictions.

5.6.5 Decomposition of Limestone

The decomposition of limestone is described by the following reaction.



The overall reaction rate, R_4 , is defined as follows :

$$R_4 = \text{kmol of } CaCO_3 \text{ decomposed} / m^3(\text{bed}).\text{hr}$$

The expression for R_4 is given below.

$$R_4 = S_4 P (y_{CO_2}^* - y_{CO_2}) / (T_s r_4) \quad (5.30)$$

Where :

$$S_4 = 12.1875 \pi d_L^2 N_L / \phi_L$$

$$r_4 = r_{41} + r_{42} + r_{43}$$

$$r_{41} = 1.0 / kf_4$$

$$r_{42} = 0.5 d_L \{ (1 - f_L)^{-1/3} - 1 \} / D_{s4}$$

$$r_{43} = \{ R' k_4 T_s (1 - f_L)^{2/3} / k_4 \}^{-1}$$

N_L can be calculated by equation (5.7).

Different rate constants and coefficients used are determined as follows :

Equilibrium constant (K_4)

$$K_4 = \exp (16.141 - 18887.0765 / T_s)$$

Reaction rate constant (k_4)

$$k_4 = 5.47 \times 10^6 \exp \{ - 40000 / (R T_s) \}$$

Diffusion coefficient of CO_2

$$D_{CO_2} = 2.236 \times 10^{-6} (T_{gm})^{1.78} / P$$

Mass Transfer coefficient (kf_4)

$$kf_4 = D_{CO_2} \{ 2.0 + 0.55 (Re_p)^{0.5} (Sc)^{1/3} \} / d_L$$

Where

$$Re_p = d_L F_g \rho_g / \mu_g A_z$$

$$Sc = \mu_g / (\rho_g D_{CO_2})$$

μ_g , F_g , ρ_g and A_z are given by equations (5.13), (4.39), (4.40) and (4.43) respectively.

Intraparticle diffusion coefficient through reacted shell (D_{s4})

$$D_{s4} = D_{CO_2} \epsilon_{vL} \xi_L$$

Where

$$\epsilon_{vL} = 0.702 \epsilon_L + 0.298$$

$$\xi_L = (\epsilon_{vL})^{0.41}$$

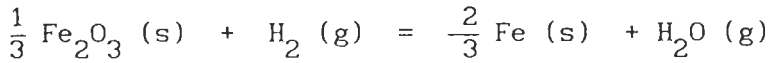
Equilibrium mole fraction of CO_2 ($y_{CO_2}^$)*

$$y_{CO_2}^* = K_4 / P$$

5.6.6 Indirect Reduction of Iron Ore by H_2

The reduction of iron oxide by H_2 is described by the following

reaction.



The overall reaction rate, R_5 , is defined as follows :

$$R_5 = \text{kmol of H}_2 \text{ consumed} / \text{m}^3 (\text{bed}).\text{hr}$$

The expression for R_5 is given below.

$$R_5 = S_1 P (y_{\text{H}_2} - y_{\text{H}_2}^*) / (T_s r_5) \quad (5.31)$$

Where

$$S_1 = 12.1875 S_0$$

$$r_5 = r_{51} + r_{52} + r_{53}$$

$$r_{51} = 1.0 / k f_5$$

$$r_{52} = 0.5 d_{\text{oa}} \{ (1 - f_s)^{-1/3} - 1 \} / D_{s5}$$

$$r_{53} = \{ k_5 (1 - f_s)^{2/3} (1 + 1/K_5) \}^{-1}$$

S_0 is given by equation (5.6).

Different rate constants and coefficients used are determined as follows :

Equilibrium constant (K_5)

For $T_s \leq 848 \text{ K}$:

$$K_5 = \exp (8.883 - 8475 / T_s)$$

For $T_s > 848 \text{ K}$:

$$K_5 = \exp (1.0837 - 1737.2 / T_s)$$

Reaction rate constant (k_5)

For $T_s \leq 848 \text{ K}$:

$$k_5 = 102.78 T_s \exp (-14900 / R T_s)$$

For $T_s > 848 \text{ K}$:

$$k_5 = 82.50 T_s \exp (-15300 / R T_s)$$

Diffusion coefficient of H_2

For intraparticle diffusion :

$$D_{H_2} = 3.960 \times 10^{-6} T_s^{1.78} / P$$

For gas film diffusion :

$$D_{H_2g} = 3.960 \times 10^{-6} (T_{gm})^{1.78} / P$$

Mass transfer coefficient (kf_5)

$$kf_5 = D_{H_2g} \{ 2.0 + 0.55 (Re_p)^{0.5} (Sc)^{1/3} \} / d_{oa}$$

Where

$$Sc = \mu_g / (\rho_g D_{H_2g})$$

Re_p is calculated in the same way as in Section 5.6.2.

ρ_g , d_{oa} and μ_g are given by equations (4.40), (5.3) and (5.13) respectively.

Intraparticle diffusion coefficient of H_2

$$D_{s5} = D_{H_2} \epsilon_{vo} \xi_o$$

ϵ_{vo} and ξ_o are estimated in the same way as in Section 5.6.2.

Equilibrium mole fraction of H_2 ($y_{H_2}^*$)

$$y_{H_2}^* = (y_{H_2} + y_{H_2O}) / (1 + K_5)$$

5.6.7 Water Gas Reaction

Water gas reaction is described by the following reaction.



The overall reaction rate, R_6 , is defined as follows :

$$R_6 = \text{kmol of } H_2O \text{ consumed} / m^3 \text{ (bed).hr}$$

The expression for R_6 is given below.

$$R_6 = S_6 P y_{H_2O} / (T_s r_6) \quad (5.32)$$

Where

$$r_6 = r_{61} + r_{62}$$

$$r_{61} = 1.0 / kf_6$$

$$r_{62} = 6.0 / (d_c \rho_c Ef_6 k_6)$$

S_6 is same as S_2 which is given in Section 5.6.3.

Different parameters used are determined as follows :

Conditions

$$\text{For } y_{H_2O} = 0 :$$

$$R_6 = R_5 - R_7$$

Reaction rate constant (k_6)

$$k_6 = 4.83 \times 10^4 T_s \exp(-17311.0 / T_s)$$

Diffusion coefficient of H_2O

For intraparticle diffusion :

$$D_{H_2O} = 1.500 \times 10^{-6} (T_s)^{1.78} / P$$

For gas film diffusion :

$$D_{H_2O} = 1.500 \times 10^{-6} (T_{gm})^{1.78} / P$$

Mass transfer coefficient (kf_6)

$$kf_6 = D_{H_2O} \{ 2.0 + 0.55 (Re_p)^{0.5} (Sc)^{1/3} \} / d_c$$

Where

$$Sc = \mu_g / (\rho_g D_{H_2O})$$

Re_p is same as given in Section 5.6.3. The values of ρ_g and μ_g are calculated by equations (4.40) and (5.13) respectively.

Intraparticle diffusion coefficient of H_2O in coke (D_{s6})

$$D_{s6} = D_{H_2O} \epsilon_c \xi_c$$

Value of ξ_c is same as used in Section 5.6.3.

Effectiveness factor (Ef_6)

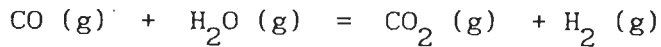
$$Ef_6 = 3.0 (m_6 \coth m_6 - 1) / m_6^2$$

Where

$$m_6 = 0.5 d_c \sqrt{(\rho_c k_6 / D_{s6})}$$

5.6.8 Water Gas Shift Reaction

Water gas shift reaction is described by the following reaction.



The overall reaction rate, R_7 , is defined as follows :

$$R_7 = \text{kmol of H}_2\text{O consumed} / \text{m}^3 \text{ (bed).hr}$$

The expression for R_7 is given below.

$$R_7 = \frac{S_{71} (y_{\text{CO}})^{0.5} y_{\text{H}_2\text{O}}}{r_{71}} - \frac{S_{72} y_{\text{CO}_2} (y_{\text{H}_2})^{0.5}}{r_{72}} \quad (5.33)$$

Where

$$S_{71} = 7.295 \times 10^{11} \epsilon (P/T_g)^{1.5}$$

$$S_{72} = 1.386 \times 10^{10} \epsilon (P/T_g)^{1.5}$$

$$r_{71} = \left[\sqrt{1 + 14.158 P y_{\text{H}_2} / T_g} \right] \exp \{67300 / (R T_g)\}$$

$$r_{72} = (1 + 4.247 P y_{\text{CO}} / T_g) \exp \{57000 / (R T_g)\}$$

5.6.9 Reduction of SiO Gas

For a long time Si content in the hot metal has been used as a measure of the thermal state of blast furnace. Thus, the mechanism of silica reduction and silicon transfer to metal has been a matter of

great concern. Many studies have been made on this aspect of the process. Following two major routes for silicon reduction and transfer have been proposed by research workers.

Direct route

SiO_2 in molten slag transfers silicon directly to the molten metal through the slag-metal reaction.

Indirect route

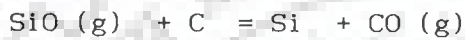
SiO_2 in molten slag or coke ash first form SiO gas and then the silicon transfer takes place via the reaction of SiO gas and carbon in hot metal.

Earlier studies are based on the proposition that the direct route is mainly responsible for SiO_2 reduction [Kay and Taylor (1963), Taylor (1964), Sharma and Ward (1967), Kawai et al. (1972)]. According to Taylor (1964), rate of silicon transfer is directly proportional to the activity of silica in slag. Kay and Taylor (1963) had already developed a method for determining the activity of silica in slag. Kawai et al. (1972) measured the rate of reduction of silica in slag by carbon dissolved in liquid iron under various experimental conditions to examine the effects of slag composition, temperature and slag-graphite interfacial area etc. They further supported the findings of Taylor (1964) and proposed an expression for calculating the rate of silica reduction.

Taguchi et al. (1982) opined that the major part of silicon transfer to metal took place through indirect route. The SiO gas is white gaseous product, which is mainly generated by the reaction of SiO_2 in coke ash with carbon in combustion zone. From there, SiO gas enters the bosh along with tuyere gas. Taguchi et al. (1982) investigated the thermochemistry and kinetic aspects of silicon transfer via SiO gas.

The studies by Taguchi et al. (1982) are found more acceptable as these studies have been verified step by step on experimental and commercial blast furnaces. Therefore, it has been decided to use the work of Taguchi et al. (1982) for calculating the rate of reduction of SiO gas.

It is known that molten iron is never free from carbon. The SiO gas reacts with the carbon present in molten iron in bosh region, where the temperature is more than 1473 K. Thus, Si is absorbed from SiO gas into the metal through the following gas-metal reaction.



The overall reaction rate, R_g , is defined as follows :

$$R_g = \text{kmol of SiO consumed} / \text{m}^3 (\text{bed}).\text{hr}$$

The expression for R_g is given below.

$$R_g = k_g A_{gm} p_{\text{SiO}} \quad (5.34)$$

Different parameters used are determined as follows :

Reaction rate constant (k_g)

$$k_g = 4.77 \times 10^8 \exp(-66500 / R T_g)$$

Effective interfacial area for gas-metal reaction (A_{gm})

$$A_{gm} = 0.34 \sqrt{g} \left(V_m \times \rho_m^2 \sqrt{d_c} / \sigma_m^2 \right)^{1/3}$$

Where

σ_m is the surface tension of metal and is equal to 1.426×10^7 kg/ hr².

V_m is superficial velocity and is expressed as follows :

$$V_m = [(W_{P,1} / \rho_m) + (W_{S,1} / \rho_{sl})] / A_z$$

$W_{S,1}$ and $W_{P,1}$ are given by equations (3.29) and (3.30) respectively.

Values of ρ_m and ρ_{sl} are mentioned in Table A.5.

Partial Pressure of SiO gas (pa_{SiO})

$$pa_{SiO} = P y_{SiO}$$

5.7 CONCLUDING REMARKS

A critical appraisal of this chapter would support the belief that in some modelling studies, constitutive relationships of the system play an important role. Modelling of blast furnace appears to be one such example. With the correlations described for large number of parameters in this chapter, slight omission or error in any one of them, uncertainties associated with the empirical relationships, and assumptions used in their derivations may result in model predictions, which might be far from reality. The extent of deviation naturally depends upon the sensitivity of parameter(s) under consideration. Due to this reason necessity of using the adjustable parameters arises in such studies. These parameters can only be estimated on the basis of actual plant data.

NUMERICAL SOLUTION OF THE MODEL, RESULTS AND DISCUSSION

6.0 INTRODUCTION

One-dimensional mathematical model of the shaft region of blast furnace has been developed in Chapter IV, which is capable of predicting the longitudinal distribution of process variables under steady state as well as unsteady state operation. This chapter describes the numerical solution of steady state model equations. Results thus obtained, would be discussed vis-a-vis results reported in the literature or observed on the blast furnaces operating in steel plants. In this way, the chapter contains three main sections, namely Numerical Solution of the Model, Results and Discussion, and Concluding Remarks about the suitability of the model.

6.1 NUMERICAL SOLUTION OF THE MODEL

Steady state model of the shaft region of blast furnace consists of eleven nonlinear ordinary differential equations, four algebraic equations and a set of boundary conditions. Although differential and algebraic equations have already been derived in the Chapter IV, but in order to recapitulate them, it has been considered necessary to reproduce them below.

Differential equations

$$\frac{df_s}{dz} = \frac{(1-\epsilon) A_z}{3 F_s C_{ho}} (R_1 + R_5) \quad (4.46)$$

$$\frac{df_c}{dz} = \frac{A_z (1 - \epsilon)}{F_s C_{co}} (R_2 + R_3 + R_6 + R_8) \quad (4.47)$$

$$\frac{df_L}{dz} = \frac{A_z (1 - \epsilon)}{F_s C_{Lo}} R_4 \quad (4.48)$$

$$\frac{df_{sn}}{dz} = \frac{A_z (1 - \epsilon)}{F_s C_{wo}} R_3 \quad (4.49)$$

$$\frac{dy_{CO}}{dz} = \frac{22.4 A_z}{F_g} \left[R_1 + R_2 (y_{CO} - 2) + R_3 (y_{CO} - 1) + R_4 y_{CO} + R_6 (y_{CO} - 1) + R_7 - R_8 \right] \quad (4.50)$$

$$\frac{dy_{CO_2}}{dz} = \frac{22.4 A_z}{F_g} \left[R_2 (y_{CO_2} + 1) + y_{CO_2} (R_3 + R_6) + R_4 (y_{CO_2} - 1) - R_7 - R_1 \right] \quad (4.51)$$

$$\frac{dy_{H_2}}{dz} = \frac{22.4 A_z}{F_g} \left[R_5 + R_6 (y_{H_2} - 1) - R_7 + y_{H_2} (R_2 + R_3 + R_4) \right] \quad (4.52)$$

$$\frac{dy_{SiO}}{dz} = \frac{22.4 A_z}{F_g} \left[y_{SiO} (R_2 + R_3 + R_4 + R_6) + R_8 \right] \quad (4.53)$$

$$\frac{dT_g}{dz} = \frac{22.4 A_z}{F_g q_5} \left[q_1 C_g T_g + q_2 (T_g - T_s) + q_3 + q_4 (T_g - T_{wc}) \right] \quad (4.54)$$

$$\frac{dT_s}{dz} = \frac{A_z (1 - \epsilon)}{q_9 F_s \rho_b} \left[q_6 C_s T_s + q_2 (T_g - T_s) - q_8 - \frac{\beta_3 q_7}{V_B} \right] \quad (4.55)$$

$$\frac{dP}{dz} = 2.7887 \times 10^{-15} f_p \left[\frac{1 - \epsilon}{\epsilon^3} \right] \left[\frac{G_g^2 T_g}{d_p P \rho_g} \right], \quad (4.38)$$

where

$$f_p = \frac{150 (1 - \epsilon) \mu_g}{d_p G_g} + 1.75$$

Algebraic equations

$$F_g = F_b \left[\frac{47.4 + 74.6667 \times 10^{-3} w_{st}}{1 - y_{CO} - y_{CO_2} - y_{SiO}} \right] \quad (4.39)$$

$$\rho_g = 1.25 + 0.7143 y_{CO_2} - 1.1607 y_{H_2} - 0.4464 y_{H_2O} + 0.7183 y_{SiO} \quad (4.40)$$

$$\rho_b = \frac{W_B}{F_s} (1 - \epsilon) - 4.0 \left[11.0 C_{Lo} f_L + 3.0 C_{co} f_c \right]$$

$$+ 12.0 C_{ho} f_s + 4.0 f_{sn} C_{wo}] \quad (4.41)$$

$$y_{H_2O} = 74.6667 \times 10^{-3} \frac{F_b \times W_{st}}{F_g} - y_{H_2} \quad (4.44)$$

Besides, the boundary conditions and constitutive relationships have been discussed in Sections 4.2.5 and 4.2.6 respectively. These shall also be used in the numerical solution.

It is obvious that the steady state model forms a nonlinear Boundary Value Problem (BVP) from numerical analysis point of view [Finlayson (1980), Davis (1984)]. Although there are a large number of numerical methods available to solve a BVP, but we have preferred to solve it as an Initial Value Problem (IVP) by using the appropriate numerical method, and matching the calculated and given boundary conditions (within acceptable tolerance) at one of the ends to stop the iteration. This choice has to be made due to the fact, that, the mathematical model possesses many adjustable parameters, which may have to vary during the numerical solution to simulate the plant data. Due to this reason steady state models of the blast furnaces reported in the literature were solved as an IVP by using marching numerical schemes, namely Runge-Kutta-Gill method with matching criteria for boundary conditions at one end to stop the iteration [Koump et al.(1964), Yagi and Muchi (1970b), Togino et al.(1980), Takenaka et al.(1986)].

According to our experience, numerical solution of the model of blast furnace is very sensitive to the adjustable parameters and slight variation in their values might lead to nonconvergence of the numerical scheme adapted to solve it as a BVP. While in case of its solution as an IVP, it is somewhat easier to vary and select the adjustable parameters based upon human judgement and industrial practice, and the numerical simulation could thus be achieved. In other

words one may opine that it is perhaps difficult to develop a general strategy for the selection of adjustable parameters required during numerical simulation. For a particular blast furnace, these may easily be estimated by using the actual plant data and model predictions. Further, necessity to include adjustable parameters in the model would also be discussed later in this chapter.

6.1.1 Runge-Kutta-Fehlberg Formulas

In the present work fourth and fifth order Runge-Kutta-Fehlberg formulas have been used to solve the model equations. Fourth order formula is used to compute the value of dependent variables, while the fifth order formula is utilized to calculate the comparatively better estimates, i.e. so called exact values. This procedure assists in selecting the step-size and is also computationally efficient. The half-step method of selecting the step-size using Runge-Kutta-Gill method requires eleven function evaluations per step, while the procedure mentioned above requires only six - a considerable decrease [Davis (1984)].

Consider the following Initial Value Problem.

$$\frac{dy}{dx} = f(x, y) \quad (6.1a)$$

$$y = y_0 \text{ at } x = x_0 \quad (6.1b)$$

The Runge-Kutta-Fehlberg fourth order pair of formulas is as follows :

$$y_{i+1} = y_i + \left[\frac{25}{216} k_1 + \frac{1408}{2565} k_3 + \frac{2197}{4104} k_4 - \frac{1}{5} k_5 \right] \quad (6.2a)$$

$$y_{i+1}^* = y_i + \left[\frac{16}{135} k_1 + \frac{6656}{12825} k_3 + \frac{28561}{56430} k_4 - \frac{9}{50} k_5 \right]$$

$$+ \frac{2}{55} k_6] \quad (6.2b)$$

In the above equations (6.2a) and (6.2b), error e_{i+1} is proportional to h^5 and h^6 respectively. Expressions for k_1 to k_6 are as follows :

$$k_1 = h f[x_i, y_i] \quad (6.3a)$$

$$k_2 = h f \left[\left(x_i + \frac{1}{4} h \right), \left(y_i + \frac{1}{4} k_1 \right) \right] \quad (6.3b)$$

$$k_3 = h f \left[\left(x_i + \frac{3}{8} h \right), \left(y_i + \frac{3}{32} k_1 + \frac{9}{32} k_2 \right) \right] \quad (6.3c)$$

$$k_4 = h f \left[\left(x_i + \frac{12}{13} h \right), \left(y_i + \frac{1932}{2197} k_1 - \frac{7200}{2197} k_2 + \frac{7296}{2197} k_3 \right) \right] \quad (6.3d)$$

$$k_5 = h f \left[\left(x_i + h \right), \left(y_i + \frac{439}{216} k_1 - 8 k_2 + \frac{3680}{513} k_3 - \frac{845}{4104} k_4 \right) \right] \quad (6.3e)$$

$$k_6 = h f \left[\left(x_i + \frac{1}{2} h \right), \left(y_i - \frac{8}{27} k_1 + 2 k_2 - \frac{3544}{2565} k_3 + \frac{1859}{4104} k_4 - \frac{11}{40} k_5 \right) \right] \quad (6.3f)$$

One may notice easily that the idea responsible for increase in computational efficiency is to use a pair of formulas with a common set of k_i 's [Davis (1984)]. For a system of differential equations, extension of Runge-Kutta-Fehlberg formula is straightforward and can be done by converting the formulas and equations into vector form.

However, its details are not being provided here but given in Appendix B.

6.1.2 Procedure

Step-wise procedure followed for numerical solution is given below.

- a. Check the consistency of given operating data by using overall material and energy balance program.
- b. Compute the values of unknown parameters at the boundaries of shaft by using overall material and energy balance program.
- c. Select the value(s) of adjustable parameter(s).
- d. Start solving the model equations in a marching way from top of the furnace, i.e. the beginning of stack, by using Runge-Kutta-Fehlberg formulas.
- e. Compare two sets of values of parameters at the bottom of bosh; one calculated by overall material and energy balance program and the other predicted by the model. If two sets of values are close to each other within acceptable tolerance, proceed. Otherwise modify the adjustable parameter(s) and go to step d.
- f. Print the results.

6.1.3 Computer Program

Based upon the above procedure, a computer program has been

developed in FORTRAN 77 to solve the steady state model equations. The program consists of about 2000 lines in 21 subroutines, which relate to the calculation of overall rates of reactions, heats of reactions, other constitutive relationships mentioned in Chapter V, functions of system of differential equations of the model, and the computation of variables by Runge-Kutta-Fehlberg formulas. This program has been executed on the NEXUS 3500 (APOLLO 3500) CAD workstation and a typical run takes about 15 min of real time, out of which 26 s is the CPU time.

Main inputs to the computer program include the following :

- Mass flow rates and compositions of all solids in the burden
- Physical properties and characteristics of solid particles
- Temperature of burden
- Composition and temperature of gases leaving the furnace from top
- Composition, temperature and pressure of tuyere gas entering the bosh
- Dimensions of the furnace

Results of the computer program are as follows :

- Longitudinal profiles of the compositions of CO, CO₂ and H₂
- Longitudinal profiles of fractional conversions of Fe₂O₃, FeO, lime, Coke carbon, and SiO gas
- Longitudinal profiles of the temperatures of solid and gas

- Longitudinal profiles of pressure

- Many more results, which may assist in analysing the furnace behaviour and performance.

In order to be brief, it is not desirable to describe the computer program completely or give its complete listing in the thesis. However, complete computer program may be obtained from the author or her supervisors on request.

6.1.4 Selection of Step-size

Step-size used in solving a differential equation is a measure of the accuracy of numerical solution and is also related to the region of stability of the solution. In the present case, many numerical experiments on the simulation of shaft region were conducted with the help of computer program and it was found that a step-size of 0.1 m in height would be adequate for our problem. Error in the computations carried out by the formulas (6.2a) and (6.2b) was less than 1.0×10^{-6} for all the process variables. Therefore, this step-size was selected and used for obtaining results of all the operating data sets.

6.2 RESULTS AND DISCUSSION

This section presents the results obtained for an operating blast furnace by using the developed computer program. Dimensions of the shaft of blast furnace are given in Table A.6 [Tupkari (1985)]. Four operating data sets of this furnace have been taken from the report by Batra (1988) about the Bokaro Steel Plant, Bokaro, India. These are mentioned in Table 3.3. At this juncture, it is necessary to provide the following clarification.

Neither we claim the authenticity of dimensions of the blast furnace considered and its operating data sets, nor support any remark arising out of the discussions of results in the thesis on the performance and productivity of blast furnaces in the Bokaro Steel Plant.

The dimensions and operating data sets of the blast furnace, referred to in the thesis of Bokaro Steel Plant, must merely be viewed as the representative information on a blast furnace, which have been obtained from the literature [Tupkari (1985), Batra (1988)] and do not possess any relevance, whatsoever, to the operating blast furnaces at Bokaro.

First, the boundary conditions for the shaft region of blast furnace were calculated by using the computer program developed and described in Chapter III. These results are summarized in Table 6.1. Thereafter, the computer program for solving the model equations was executed to obtain the results of all the four operating data sets. Prior to the presentation and discussion of results, it is befitting to speak of experiences gained during numerical simulation, and thereby the necessity of using the adjustable parameters.

6.2.1 Experiences with Numerical Simulation and Necessity of Adjustable Parameters

When the computer program was executed with operating data set-1, it was observed that all the processes, viz. reactions, phase transformations, heat exchange etc, got completed upto around 9.8 m height of the furnace from top. In fact, these were supposed to occur upto the total height of 20 m. Besides, the longitudinal profiles of all process variables were not similar to those reported in the

Table 6.1 Boundary Conditions for the Mathematical Model

S.N.	Process variable		Set number			
			1	2	3	4
1	Flow rate of solids ($W_{C,1}$) kg/hr.		46534.06	57170.40	47260.89	43543.74
2	Flow rate of pig iron ($W_{P,1}$), kg/hr		75468.05	86347.68	71371.29	65923.76
3	Flow rate of slag ($W_{S,1}$), kg/hr		22696.63	26104.58	21563.12	19581.71
4	Flow rate ₃ of tuyere gas (F_1), Nm ³ /hr		164180.0	201904.8	165875.3	153701.5
5	Flow rate ₃ of top gas (F_0), Nm ³ /hr		175926.2	213394.5	176493.3	162051.7
6	Composition of tuyere gas, mole fraction	$y_{CO,1}$	0.3602	0.3648	0.3654	0.3653
		$y_{H_2,1}$	0.0280	0.0436	0.0452	0.0452
		$y_{N_2,1}$	0.6014	0.5815	0.5792	0.5795
		$y_{SiO,1}$	0.0104	0.0100	0.0102	0.0100
7	Composition of top gas, mole fraction	$y_{CO,0}$	0.2473	0.2438	0.2536	0.2390
		$y_{CO_2,0}$	0.1653	0.1648	0.1595	0.1685
		$y_{H_2,0}$	0.0262	0.0413	0.0425	0.0429
		$y_{N_2,0}$	0.5612	0.5502	0.5444	0.5496
8	Temperature of tuyere gas ($T_{g,1}$), K		2099.088	2032.608	2046.379	2040.616
9	Temperature of top gas ($T_{g,0}$), K		470.2782	537.2598	508.0406	550.1272

literature [Ufret et al.(1981), Omori (1987)]. Such a behaviour might be due to the assumption of uniform distribution of process variables in the elemental volume at any height z , used in the derivation of model equations. Other plausible reason could be the uncertainties associated with the constitutive relationships of parameters used in the model. Therefore, both the alternatives were explored during simulation.

Process of transfer of heat from ascending gases to the descending solids is very important from the point of view of blast furnace performance. It is controlled by the heat transfer coefficient (h_{gs}) between gas and solids. Research workers [Yagi and Muchi (1970a), Ufret et al.(1981)] advocated the use of an adjustable parameter (say β_4) with h_{gs} , i.e. $\beta_4 h_{gs}$. Hatano and Kurita (1982) have suggested that the value of this adjustable parameter varies from furnace to furnace and in general, lies between 0.02 and 0.3. Further, the heat transfer coefficient for gas-solid heat transfer, and gas-molten metal heat transfer would also be different. Therefore, constant value of β_4 should not be used throughout the shaft. By conducting a large number of numerical experiments, it was found for the furnace under consideration that the values 0.05 and 0.025 of β_4 were adequate for heat transfer from gas to solid, and gas to molten metal respectively, when the h_{gs} was calculated according to the Ranz's equation [equation (5.16)].

In practice, there is likelihood of existence of maldistribution of solids and gases in large diameter moving bed reactors such as the blast furnace. The central portion of the solids may tend to move faster than the region close to the wall. Gas flow maldistribution may also occur if there is a spatial variation in the void fraction or in the diameter of particles that make up the bed. In a physical sense, such nonuniformities may occur owing to the segregation of a charge of solids caused by the feeding arrangements and/or by the breakage of solid particles. The effect of gas and solids maldistribution on the

performance of moving bed reactors with simple reacting systems has been the subject of many research projects in the past [Yagi and Szekely (1977, 1979), Szekely and Proposter (1979), Togino et al. (1980)]. The principal conclusion of all these studies is that the maldistribution of gaseous and solids streams may have a marked and deleterious effect on the performance of moving bed reacting systems.

In the present work, diameter of solid particles in the burden varies from 0.009 to 0.04 m (Table A.5) and the diameter of blast furnace is also large. Therefore, there is every possibility of maldistribution of gas and solids in the furnace. Due to the large diameter, central portion of solids would move faster than the region close to the wall. As radial distributions of the process variables have been neglected in the formulation of the model and all the processes are getting completed upto a height of 0.9 m during numerical simulation, therefore, it was decided to use an adjustable parameter β_5 with the diameter of furnace, i.e. $\beta_5 D_z$. Value of β_5 shall naturally lie between 0 and 1. This parameter would reduce the volume of the furnace and consequently the residence time of solids, which was infact desirable to get all the processes completed within total height of the shaft. This strategy worked well and the longitudinal profiles of process variables thus obtained were in conformity with those reported in the literature [Ufret et al. (1981), Omori (1987)]. Values of β_5 found for all the four operating data sets along with the corresponding residence time of solids are mentioned in Table 6.2.

Once an idea cropped in to increase the mass flow rate of burden feed because this would also reduce the residence time. For maintaining the residence time as given in Table 6.2 with $\beta_5 = 1$, mass flow rates were to be increased 3.5 to 4 times. Consequently, volumetric flow rate of hot air blast increased tremendously. Numerical simulation with these data could not be performed as the pressure of gas became very high, e.g. more than 8 atm, and the

Table 6.2 Adjustable Parameter (β_5) and Residence Time of Solids for Operating Data Sets

Set number	Volumetric flow rate of bed, m^3/hr	Adjustable parameter for diameter D_z , β_5	Residence time of solids in shaft, hr	
			With adjustable parameter	Without adjustable parameter
1	163.9146	0.52	1.568	5.798
2	192.0347	0.50	1.237	4.949
3	160.4319	0.50	1.481	5.924
4	146.5872	0.48	1.494	6.483

computer program started giving Run Time Error, namely raising power to a negative quantity. In view of these computational problems, this idea was not pursued further.

6.2.2 Longitudinal Distribution of Process Variables

Longitudinal distribution of process variables have been obtained for all the four operating data sets by using the computer program. The results thus obtained are presented in the form of plots of process variables versus height. Longitudinal profiles of temperatures, fractional conversions, and mole fractions for all the four operating data sets are given in Figures 6.1 to 6.12 respectively, and discussed in the following subsections. As chemical reactions are frequently cited in the discussion, therefore, one may refer to Section 4.1.2 for their details.

6.2.2.1 Profiles of Temperature of Gas and Solid

The processing of burden feed requires an enormous amount of heat, which is supplied by the hot ascending gases. Heat requirement varies from top to the bottom of furnace due to the occurrence of many chemical reactions and phase transformations at different heights. The variation in heat requirements at different heights establishes the temperature profiles of gas and solid in the furnace.

Figure 6.1 shows the longitudinal profiles of temperature of gas and solid for the operating data set-1. It is evident from the figure that the gas temperature is always higher than the solid temperature throughout the height of furnace, which is a necessary condition for the stable operation of the blast furnace [Reichardt (1927)].

The solids enter the furnace at 303 K, while gases leave it at

560 K. As there occurs no chemical reaction in this temperature range, therefore, the solids get heated. This results in a sharp increase in solid temperature from 303 K to 500 K within 2-3 m height. Rate of heating of solids is not constant with height; it is rapid at the start and reduces progressively because of decreasing $\Delta T (T_g - T_s)$. This zone is generally referred to as preheating zone.

At approximately 2-3 m height, the indirect reduction of iron ore (Fe_2O_3) by CO starts, which is an exothermic reaction. In the derivation of model equations, it has been assumed that for gas-solid reactions, heat of reaction is released to the solid phase only (Sections 4.1.1 and 4.2.2.2). Therefore, the heat of reaction released or consumed during reaction would directly affect the solid temperature.

At this stage it is desirable to refer to the profiles of fractional conversion given in Figure 6.2. It is clear from this figure that upto a height of about 13 m only indirect reduction of Fe_2O_3 occurs. This reduction is mainly due to CO because the reduction of Fe_2O_3 by H_2 takes place at comparatively higher temperature. Although endothermic solution loss reaction starts at about 10 m height, but it does not occur to an appreciable extent. Due to this reason solid temperature goes on increasing and approaches quite close to gas temperature. At this height temperature is approximately 1100 K. Such a portion of the profile, which lies between 3 to 13 m height in the present case, corresponds to the thermal reserve zone.

After 13 m height other endothermic reactions, namely decomposition of lime, indirect reduction by H_2 and water gas reaction, also start taking place. This is apparent from the profiles of fractional conversions of lime, coke carbon and Fe_2O_3 . Due to these endothermic reactions, heat requirement at this level increases enormously. Its effect is evident at 15 m height, where solid temperature reduces appreciably in comparison to continuously

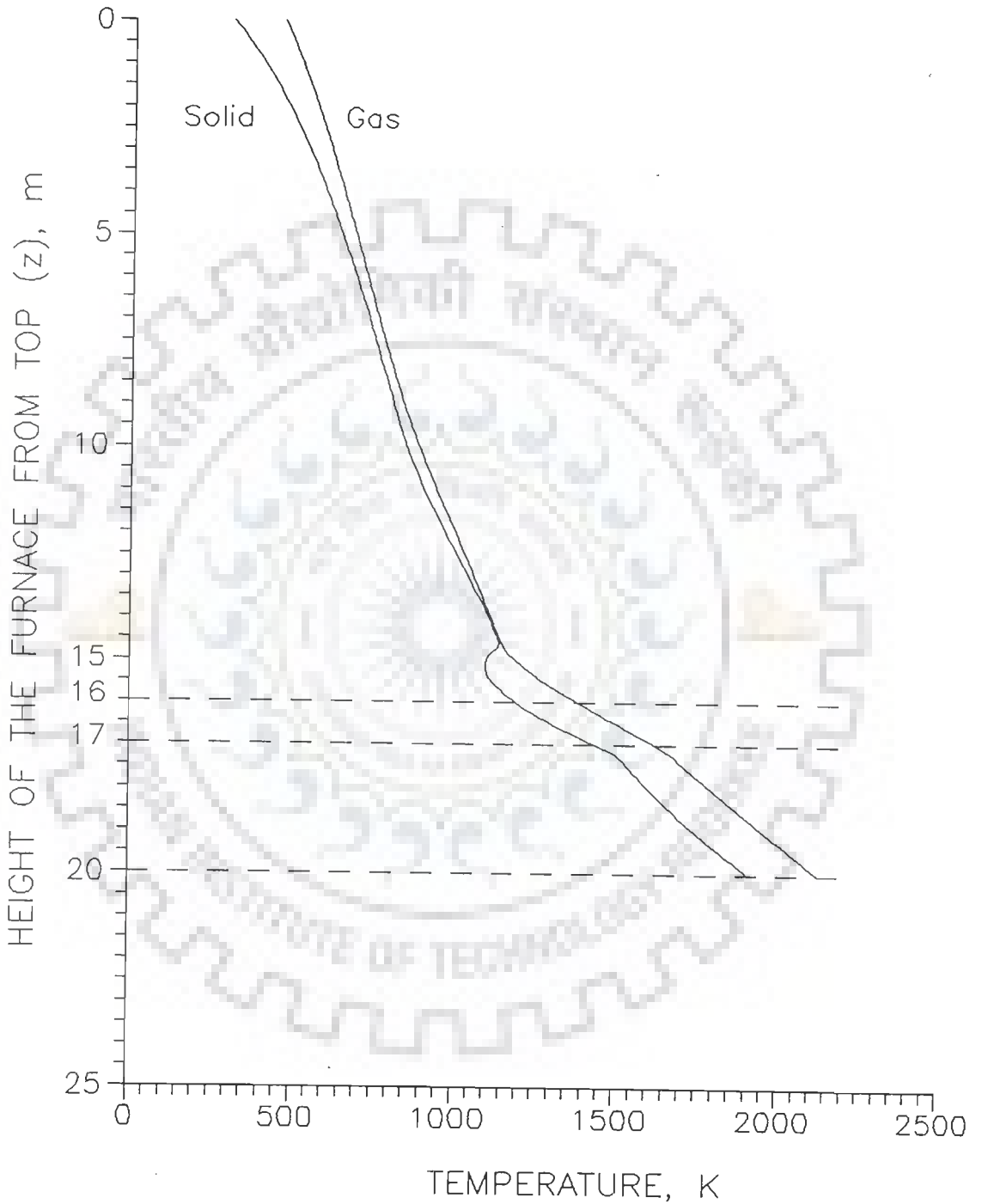


FIGURE 6.1 LONGITUDINAL PROFILES OF TEMPERATURE OF GAS AND SOLID (OPERATING DATA SET-1)

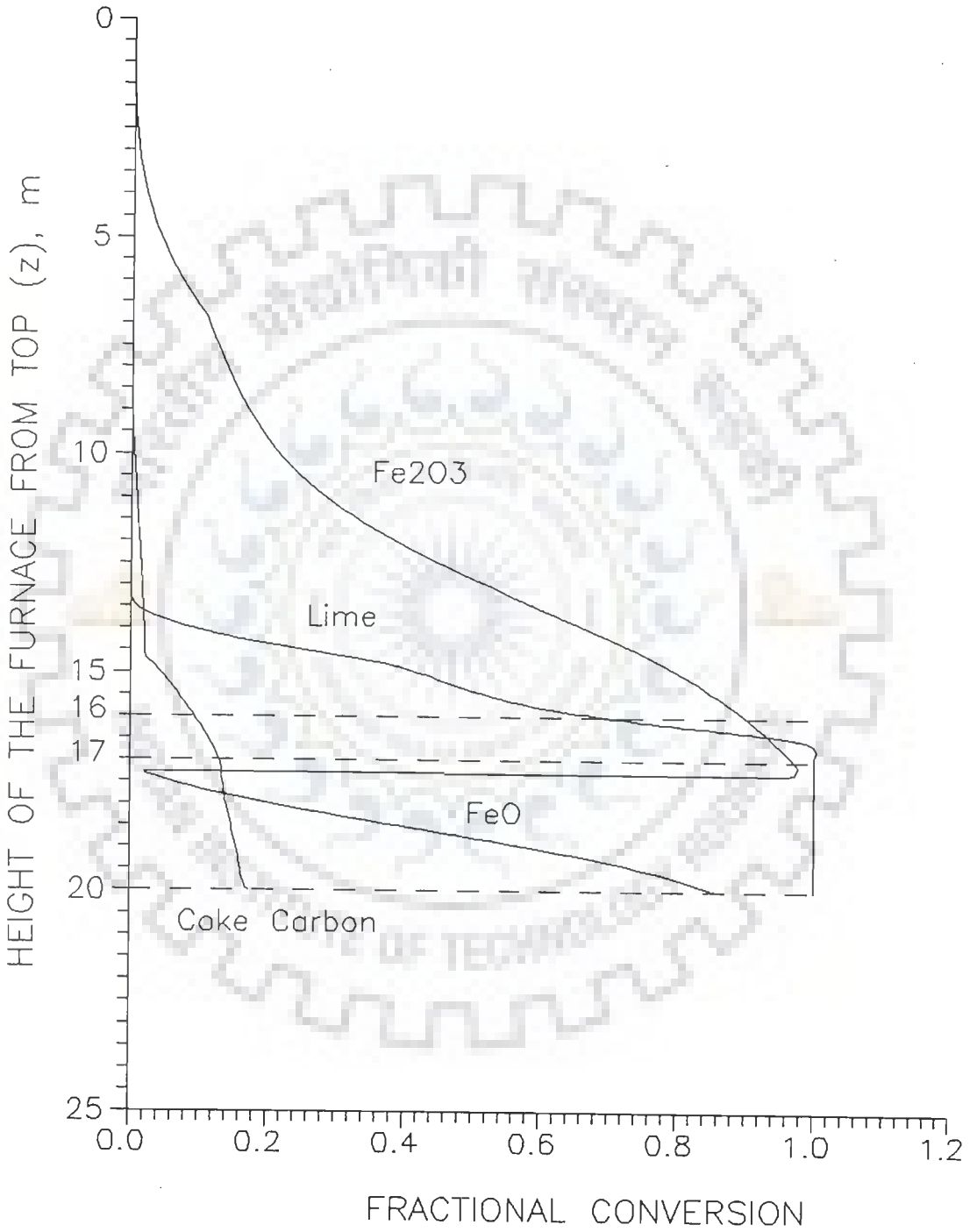


FIGURE 6.2 LONGITUDINAL PROFILES OF FRACTIONAL CONVERSION OF Fe₂O₃, LIME, COKE CARBON AND FeO (OPERATING DATA SET-1)

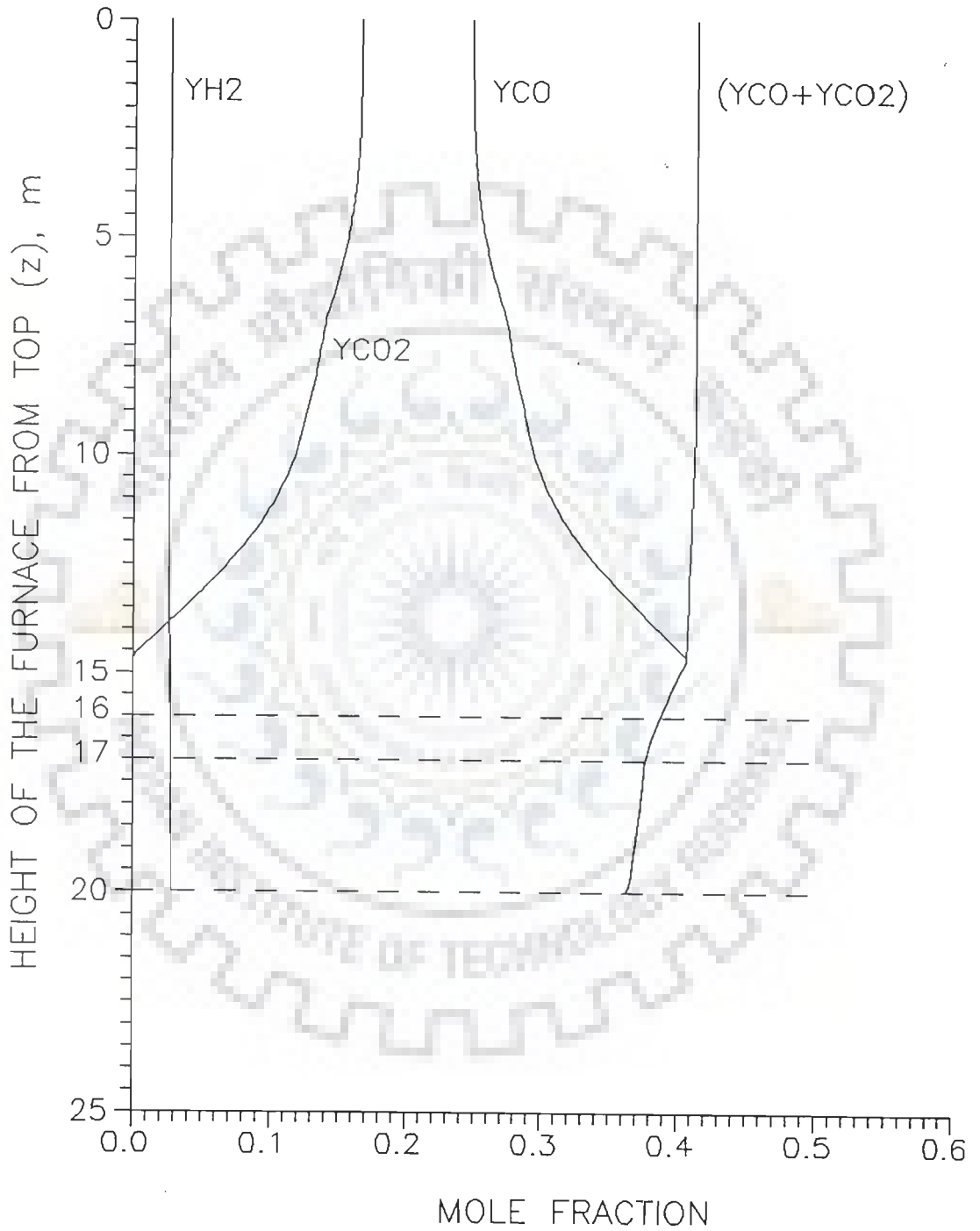


FIGURE 6.3 LONGITUDINAL PROFILES OF MOLE FRACTION OF CO , CO_2 AND H_2 (OPERATING DATA SET-1)

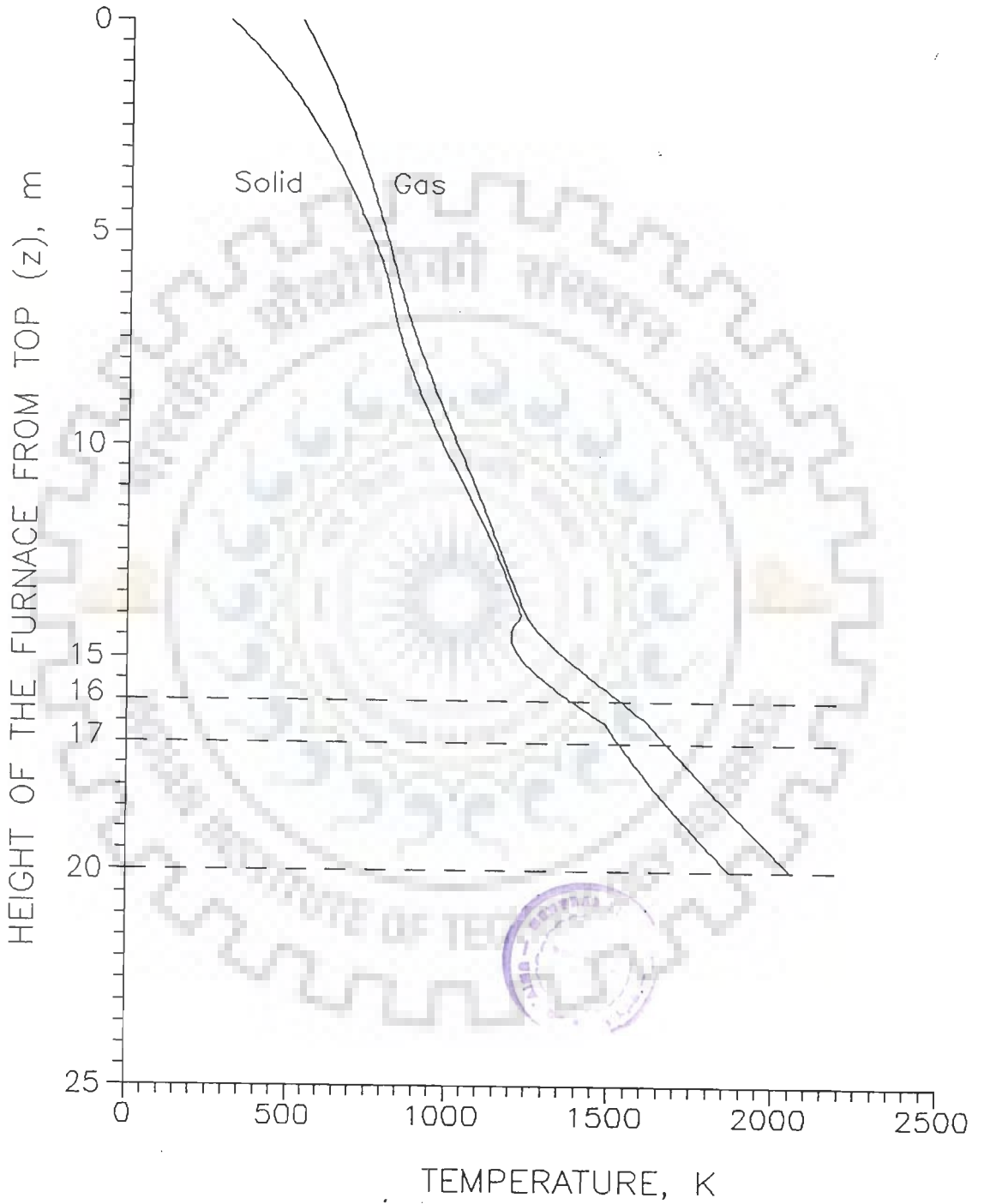


FIGURE 6.4 LONGITUDINAL PROFILES OF TEMPERATURE OF GAS AND SOLID (OPERATING DATA SET-2)

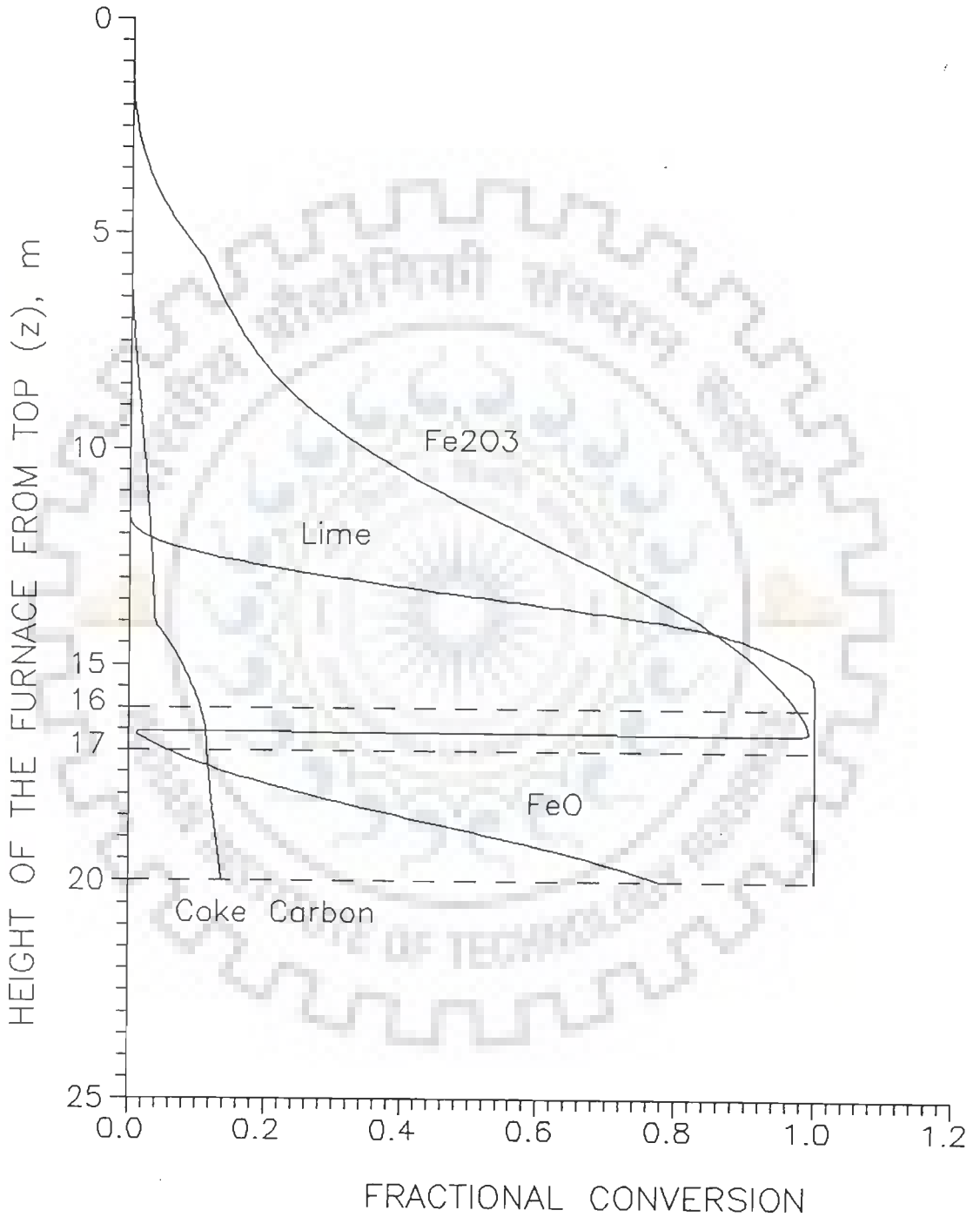


FIGURE 6.5 LONGITUDINAL PROFILES OF FRACTIONAL CONVERSION OF Fe₂O₃, LIME, COKE CARBON AND FeO (OPERATING DATA SET-2)



FIGURE 6.6 LONGITUDINAL PROFILES OF MOLE FRACTION OF CO , CO_2 AND H_2 (OPERATING DATA SET-2)

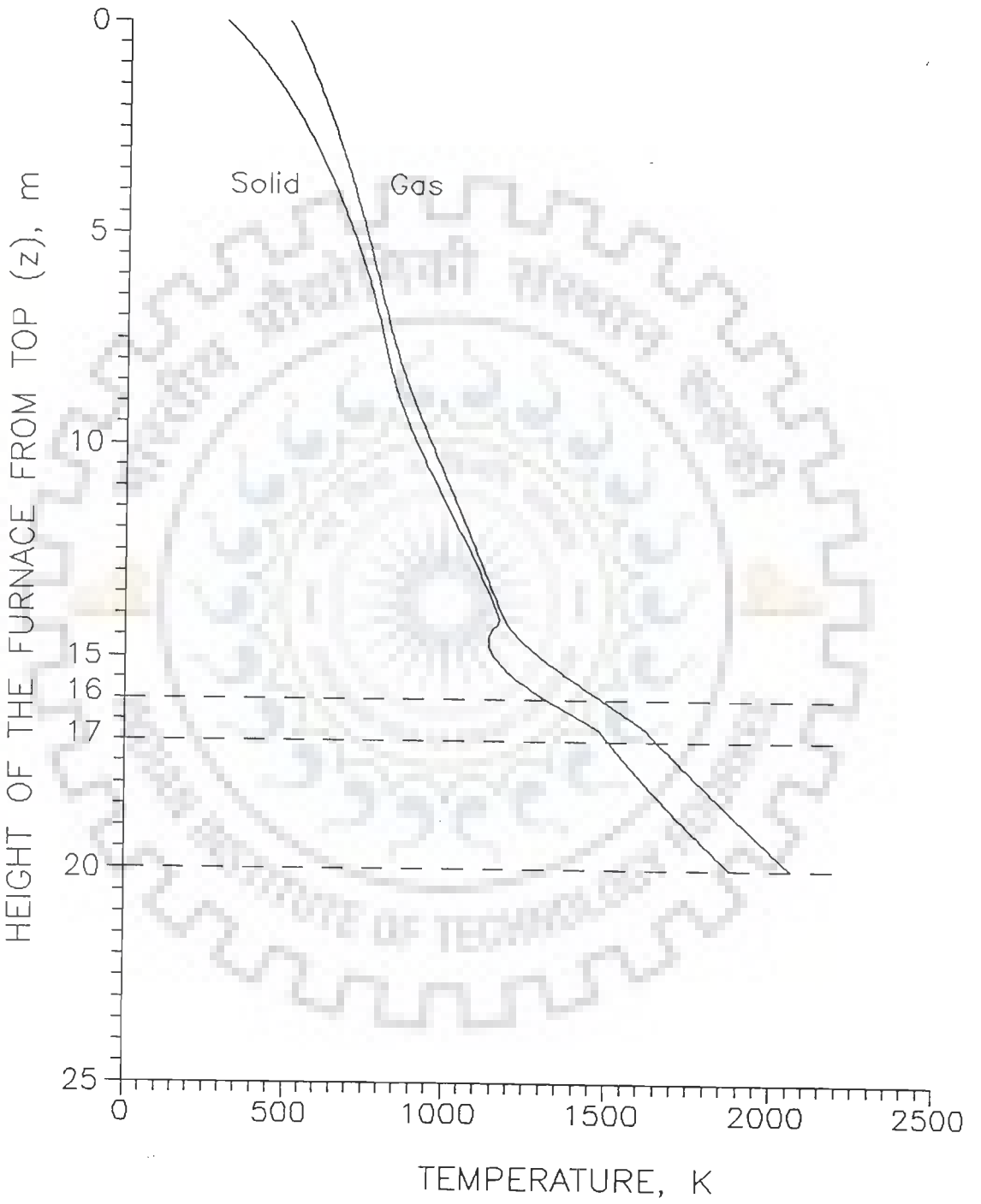


FIGURE 6.7 LONGITUDINAL PROFILES OF TEMPERATURE OF GAS AND SOLID (OPERATING DATA SET-3)

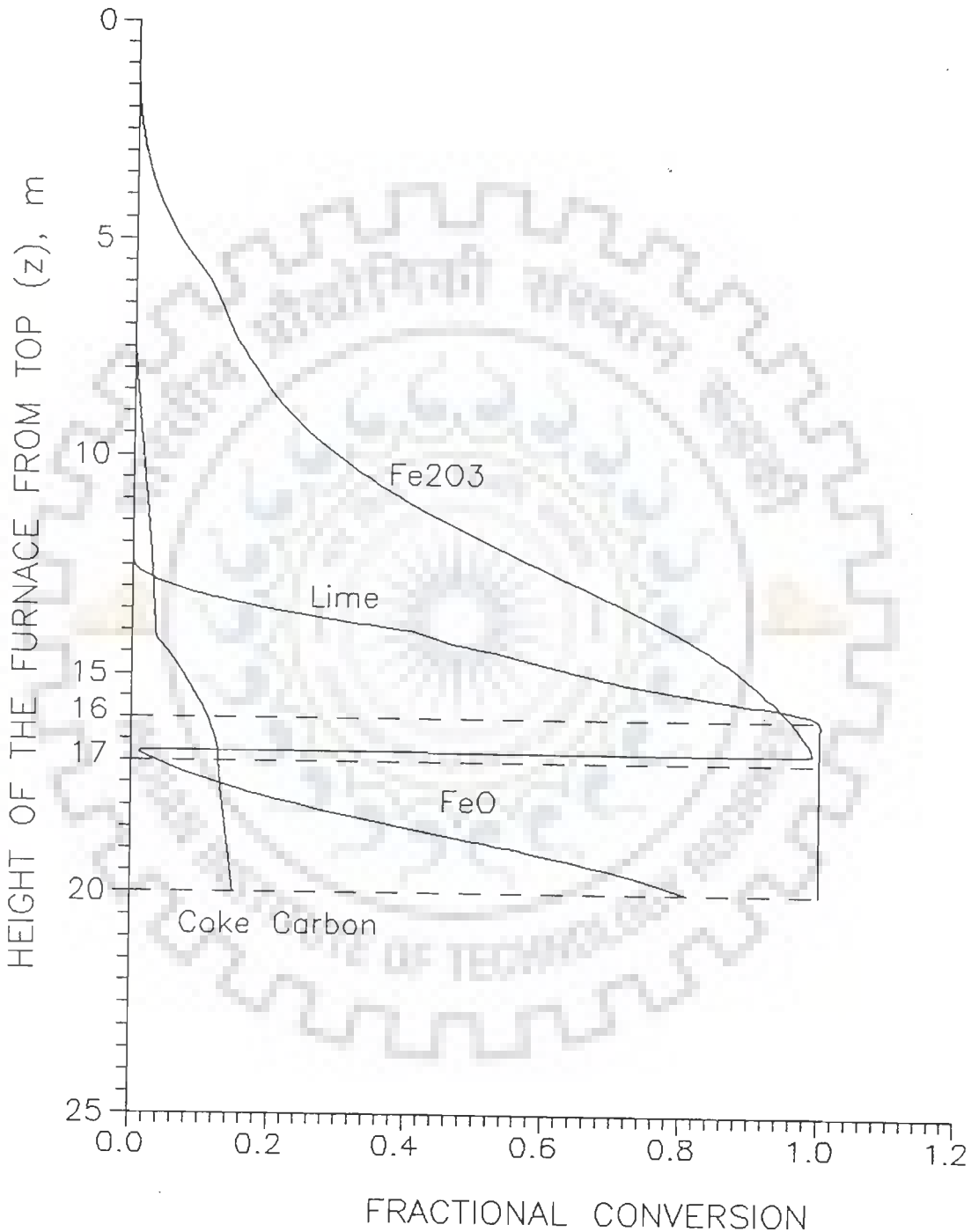


FIGURE 6.8 LONGITUDINAL PROFILES OF FRACTIONAL CONVERSION OF Fe₂O₃, LIME, COKE CARBON AND FeO (OPERATING DATA SET-3)

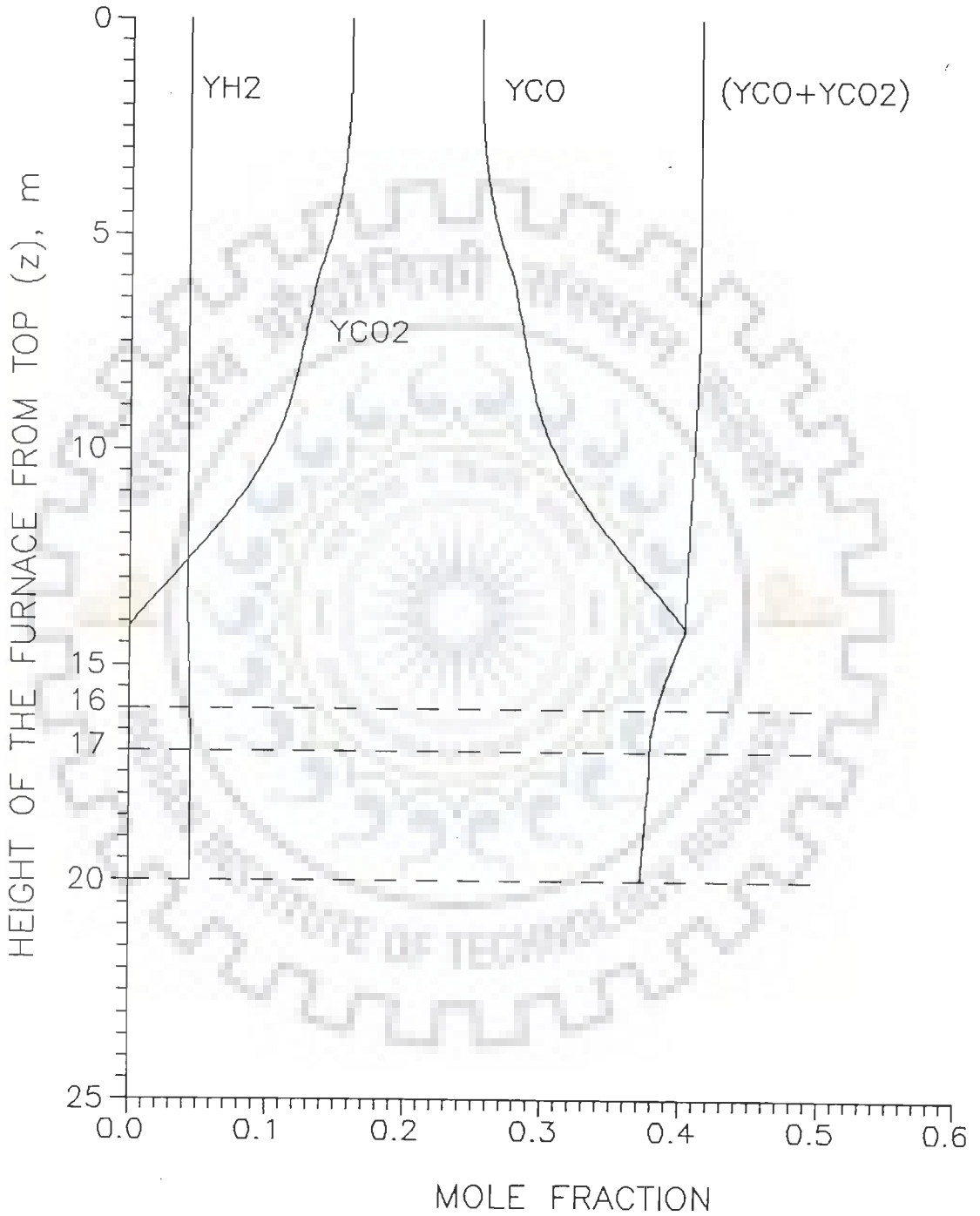


FIGURE 6.9 LONGITUDINAL PROFILES OF MOLE FRACTION OF CO, CO₂ AND H₂ (OPERATING DATA SET-3)

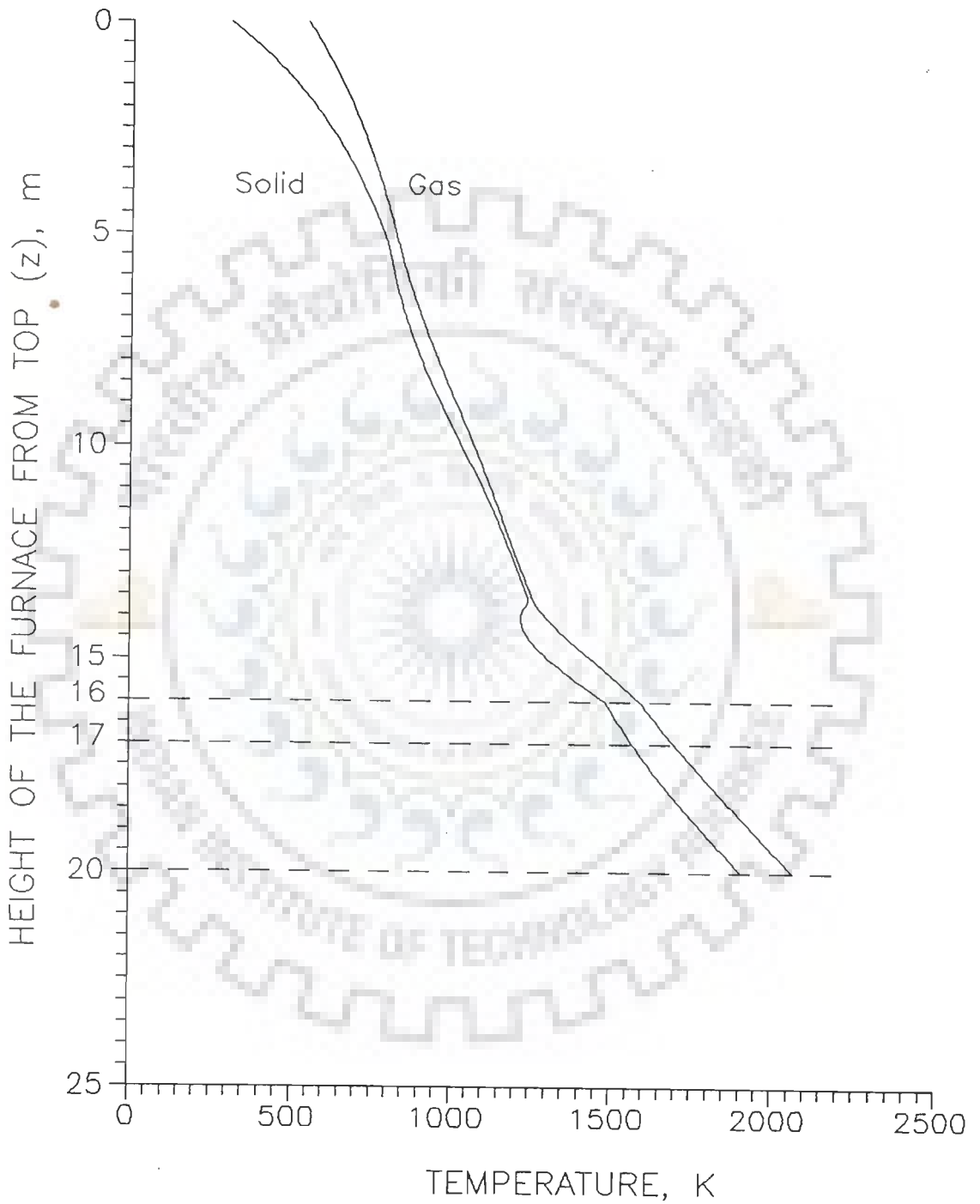


FIGURE 6.10 LONGITUDINAL PROFILES OF TEMPERATURE OF GAS AND SOLID (OPERATING DATA SET-4)

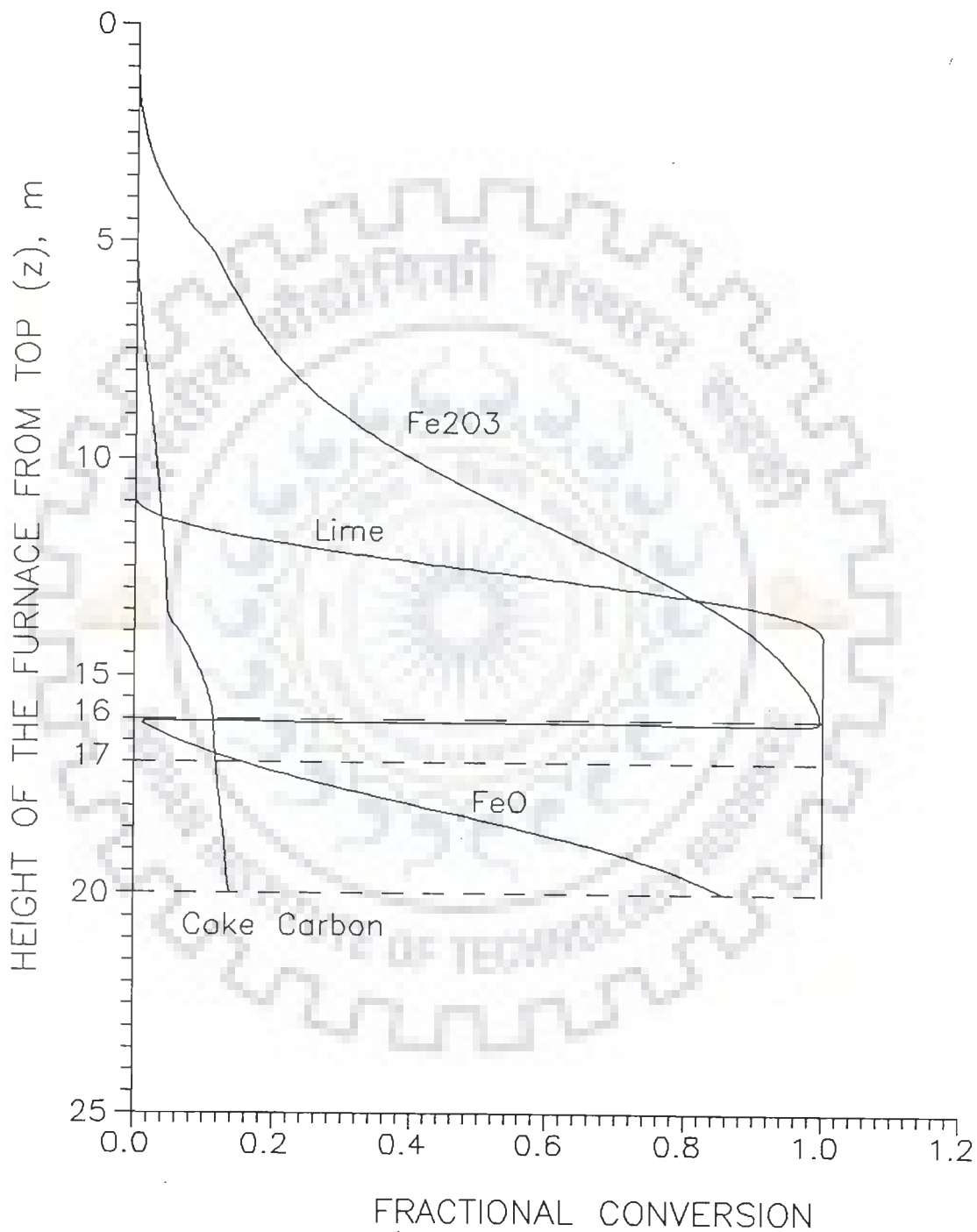


FIGURE 6.11 LONGITUDINAL PROFILES OF FRACTIONAL CONVERSION OF Fe₂O₃, LIME, COKE CARBON AND FeO (OPERATING DATA SET-4)

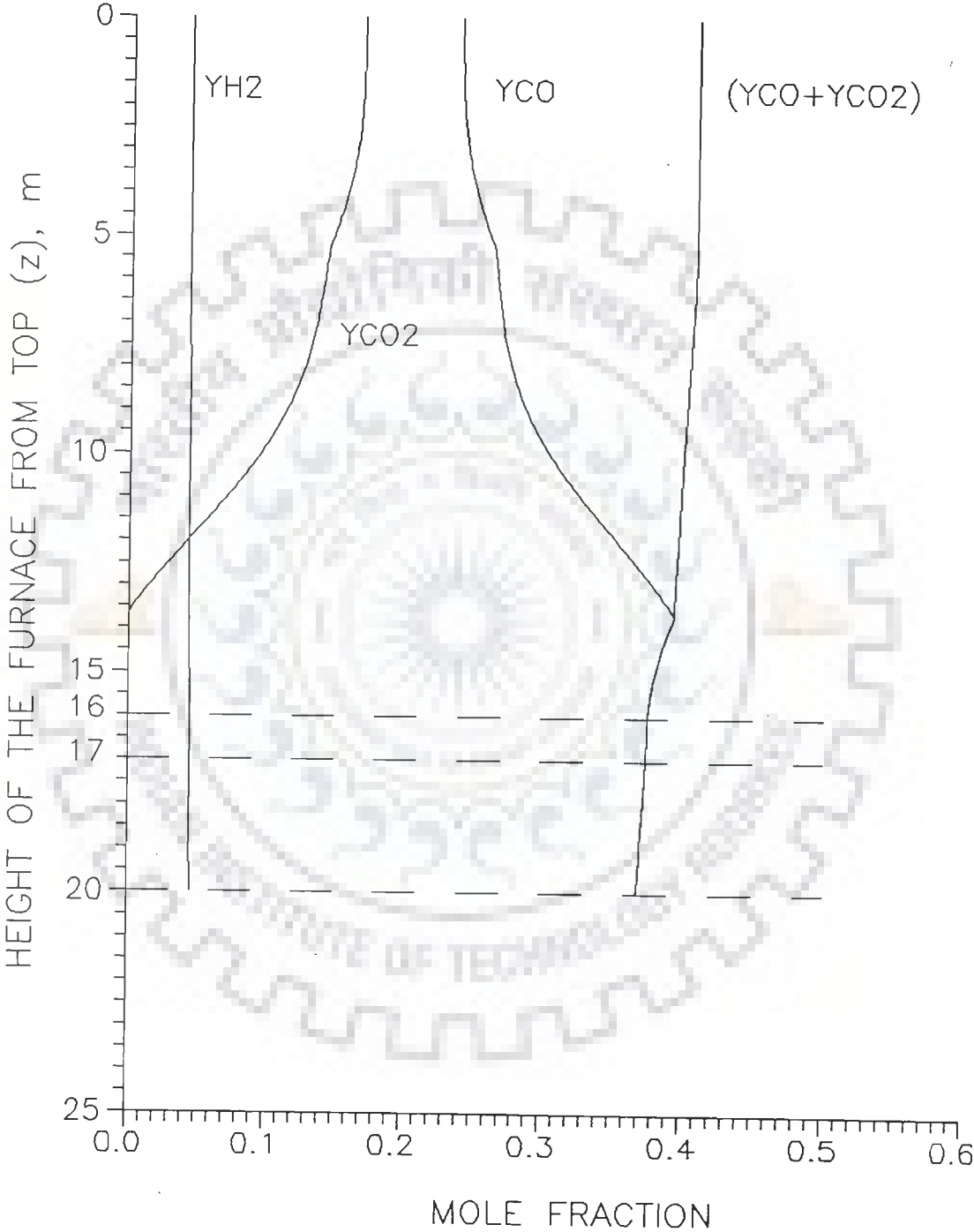


FIGURE 6.12 LONGITUDINAL PROFILES OF MOLE FRACTION OF CO, CO2 AND H2 (OPERATING DATA SET-4)

increasing gas temperature. In order to meet the heat requirement of solids in this region, heat transfer from gas to solid increases significantly. At a height of 17 m, solid temperature is about 1450 K. At this level, the fusion of solids and slag formation start along with endothermic reactions, namely direct reduction of FeO and reduction of SiO. Therefore, a large amount of heat is required for this zone too. This heat requirement is fulfilled mainly by the hot ascending gases, and a small part of it is also supplemented by the heat released during slag formation. The zone where temperature is above 1450 K, is generally referred to as direct reduction and melting zone.

It may be noted that in the derivation of model equation (4.33), the heats of fusion and slag formation per unit of bed volume have been assumed to be constant (Section 4.1.1). This assumption results in approximately parallel profiles of solid and gas temperatures. However, in actual practice heats of fusion and slag formation go on increasing slowly due to the gradual increase in the rate of melting with the downward movement of solids [Strassburger (1969), Biswas (1981)]. It is pertinent to mention that the processes of fusion of solids and formation of slag occur in a complex fashion in the blast furnace and the rates of their occurrence are not available in the literature accessible to us. Due to this reason above assumption was considered in the derivation of model equation.

Temperature profiles of remaining three data sets (Figures 6.4, 6.7 and 6.10) are also similar in nature and may be explained in the same way.

Similar profiles of gas and solid temperatures were also obtained and reported in earlier modelling studies [Yagi and Muchi (1970b), Ufret et al.(1981), and Omori (1987)].

6.2.2.2 Profiles of Fractional Conversion of Fe_2O_3 , Lime, Coke Carbon and FeO

Figures 6.2, 6.5, 6.8 and 6.11 show the longitudinal profiles of fractional conversion of Fe_2O_3 , lime, coke carbon and FeO obtained for the operating data sets 1, 2, 3 and 4 respectively. It is obvious that these profiles show the similar trend for all the data sets. Similar type of profiles of fractional conversion were also reported in earlier modelling studies [Yagi and Muchi (1970b), Ufret et al. (1981), and Omori (1987)].

In the upper part of the shaft upto a solid temperature of 600 K, indirect reduction of iron ore by CO occurs at a slower rate. Therefore, fractional conversion of Fe_2O_3 increases slowly. This rate of reduction enhances above 600 K. As solid temperature rises to 800 K, indirect reduction of H_2 also starts. Due to these two reactions fractional conversion of Fe_2O_3 to Fe increases rapidly from solid temperature 600 to 1150 K, upto about 15 m height. Thereafter, rate of increase slows down due to less availability of reducing gas CO as is evident from the profile of mole fraction of CO in Figure 6.3. Although, the rate of indirect reduction by H_2 is higher at high temperatures, but it does not contribute appreciably to the fractional conversion of Fe_2O_3 in the present sets of data as H_2 gas is available in small quantity only. At about 17 m height, the solid temperature increases to 1450 K. Around this temperature melting of solids start [Biswas (1981), Ufret et al. (1981)]. For this stage, it has been assumed in the model that the unreacted Fe_2O_3 , if remains, gets converted into FeO, because iron oxides exist only as FeO in molten form. Due to this reason the curve for fractional conversion of Fe_2O_3 drops down to zero around 17 m height and the curve for fractional conversion of FeO starts. Above 1450 K fractional conversion of molten FeO to Fe is approximately linear with height.

The decomposition of lime begins to occur in the vicinity of

13.5 m height where solid temperature is around 1000 K. At this temperature the rate of decomposition is very fast. Due to which lime is completely consumed within only 3 m height, which is just above the melting zone. It may be noticed that the fractional conversion of lime increases almost linearly with the height.

Coke carbon is consumed mainly by two reactions, viz. solution loss reaction and water gas reaction. Rate of solution loss reaction is insignificant below 1200 K. Besides, water gas reaction requires H_2O from gases to proceed, which is not available in appreciable quantity; source of H_2O is indirect reduction of ore by H_2 , and it is obvious from Figure 6.3 that it exists only in small quantity. It may be mentioned that according to the assumptions, solid does not contain any moisture or hydrated compound, which could be the potential source of H_2O . Due to these reasons, fractional conversion of coke carbon increases very slowly with height upto 15 m. At this level solid temperature rises to 1200 K. Consequently, the rate of solution loss reaction becomes high. Due to which fractional conversion of coke carbon increases rapidly upto 17 m height and 1450 K temperature. Thereafter, increase in fractional conversion slows down as reduction of molten FeO and SiO gas does not require much quantity of coke according to the conditions prevailing in the bosh.

6.2.2.3 Profiles of Mole Fraction of CO , CO_2 and H_2

Figure 6.3 depicts the longitudinal profiles of mole fraction of CO , CO_2 and H_2 for operating data set-1. These profiles shall be explained from bottom to the top of shaft as tuyere gas enters from the bottom and moves upwards. The tuyere gas contains CO , H_2 and N_2 . In the bosh, i.e. region between 17 and 20 m height, direct reduction of FeO and the reduction of SiO gas along with melting of solids, take place, which are main heat consuming processes. From Figure 6.1, it may be noted that the solids enter the bosh at 1450 K temperature, and as

explained in the preceding section, the solids contain unreacted iron oxides as FeO only.

The direct reduction of FeO, and the reaction of SiO gas with carbon dissolved in pig iron both produce CO gas. Thus, in ascending gases amount of CO increases continuously in the bosh, which results in the increase in its mole fraction. The tuyere gas does not contain CO₂. Besides, CO₂ gas is unstable in the presence of carbon at temperatures above 1200 K [Strassburger (1969), Biswas (1981)]. Therefore, if CO₂ is produced by any reaction, it immediately reacts with coke carbon according to the solution loss reaction and gets converted into CO gas resulting in further increase in CO content. Hence, in the zone where the temperature is more than 1200 K, amount of CO₂ in ascending gases is negligible and equal to zero.

In the bosh, there is no reaction which consumes or produces H₂ gas, so the amount of H₂ remains constant in ascending gases. However, due to the increase in amounts of other components, namely CO, in ascending gases, mole fraction of H₂ decreases as it moves upwards. But, the decrease in its mole fraction is not noticeable in the Figure 6.3 as amount of H₂ in gas is only 2-3 %.

Now consider the zone between 15 to 17 m height, in which temperature of solids varies between 1100 and 1450 K. Reactions occurring in this zone are decomposition of lime, solution loss reaction, water gas reaction, water gas shift reaction, and indirect reduction of iron by H₂. The decomposition of lime, and water gas shift reaction both produce CO₂ gas. At the same time, Figure 6.2 on fractional conversions reveals that the lime is completely decomposed in this zone. As stated earlier, CO₂ gets converted into CO gas via solution loss reaction above 1200 K. Consequently, CO₂ content in ascending gases still remains zero whereas its CO content, i.e. mole fraction of CO, increases continuously.

Further, it is assumed that the solids in the burden feed do not contain moisture or any hydrated compound. Therefore, the amount of H_2 , which is consumed by indirect reduction, gets again produced through the water gas shift reaction and water gas reaction. Thus, the amount of H_2 in ascending gases remains same, but its mole fraction decreases very slowly. Profiles of mole fractions of CO , CO_2 and H_2 in the Figure 6.3 clearly show these trends in this zone.

Now we arrive in the upper part of the shaft, which lies between 2.5 and 15 m height. This zone is known as indirect reduction zone. Indirect reduction of iron ore by CO starts relatively at low temperature while its indirect reduction by H_2 occurs only above 800 K. Due to this reason, indirect reduction by CO begins earlier at a height of 2.5 m. while indirect reduction by H_2 along with water gas reaction starts from 9 m height onwards.

Indirect reduction by CO consumes CO and produces CO_2 . As a result of which amount of CO in ascending gases starts decreasing, thereby increasing the amount of CO_2 . Above 800 K, indirect reduction by H_2 consumes H_2 and produces H_2O , which again forms H_2 via water gas reaction. Thus, these reactions maintain the amount of H_2 constant in ascending gases. Since one mole of CO produces one mole of CO_2 in the indirect reduction by CO , therefore, the summation of mole fractions of CO and CO_2 in ascending gases would also remain constant throughout this zone. This also results into the constant mole fraction of H_2 . Profiles of this zone clearly depicts the occurrence of these phenomena.

In the preheating zone between top to 2.5 m height, solids are only heated, and no chemical reaction occurs. Therefore, the mole fractions of CO , CO_2 and H_2 in ascending gases remain constant as shown in Figure 6.3.

Profiles of the mole fractions of remaining three data sets

(Figures 6.6, 6.9 and 6.12) are also similar in nature and may be explained in the same way. Similar profiles of mole fractions of CO , CO_2 and H_2 were also reported in earlier modelling studies [Yagi and Muchi (1970b), Ufret et al. (1981), and Omori (1987)].

6.2.2.4 Profiles of Per cent Conversion of SiO gas

Figure 6.13 represents the comparison of longitudinal profiles of per cent conversion of SiO gas for all the four operating data sets.

In the Section 5.6.9 reduction of SiO gas has been discussed in detail. It is mentioned there that the SiO gas reacts with carbon dissolved in molten iron in the lower half of the bosh region, i.e. from tuyeres to the middle of bosh. Thereafter, excess SiO gas is oxidized by CO to SiO_2 , which is again mixed with the slag [Taguchi et al. (1982)].

It may be noted from Figure 6.13 that the per cent conversion of SiO gas varies between 5 to 44 for all the data sets. Table 6.3 provides the data on per cent Si content in metal as a result of reduction of SiO gas. These are in conformity with the results reported in the literature [Fukushima (1970)]. Variation in the per cent conversions of SiO gas for all the four data sets may be explained on the basis of pressure and temperature of gas at the bottom of bosh computed by using the model. Perusal of rate equation (5.34) used for SiO gas reduction reveals that it is first order with respect to partial pressure of SiO . In other words, rate is directly proportional to rate constant k_g and partial pressure p_{SiO} (Section 5.6.9). A slight variation in gas temperature changes k_g appreciably due to its exponential dependency on temperature. While change in total pressure at the bottom of bosh would not affect p_{SiO} so strongly due to the following reasons.



FIGURE 6.13 COMPARISON OF LONGITUDINAL PROFILES OF PER CENT CONVERSION OF SiO GAS, OBTAINED WITH VARIABLE HEAT OF REACTION FOR ALL THE FOUR OPERATING DATA SETS

Table 6.3 Percent Si Content in Metal

Set number	$Y_{\text{SiO}_2, 1}$	Per cent conversion	Per cent Si content in metal
1.	0.0104	48.76	1.2368
2.	0.0100	7.94	0.2339
3.	0.0102	5.37	0.1593
4.	0.0100	16.43	0.4819

- (i) p_{SiO} varies linearly with the total pressure.
- (ii) The mole fraction of SiO in tuyere gas ranges between 0.01 and 0.0104 for all the data sets, which is very small [Table 3.6]. Therefore, the temperature, and to some extent pressure of tuyere gas is responsible for the variation in per cent conversion of SiO.

Another feature about this reaction, which needs mention, is the necessity of using an adjustable parameter with its rate equation. In Section 6.1, it is mentioned that the model equations have been solved as an IVP. Therefore, during the numerical solution a particular value of y_{SiO} in ascending gases was to be assumed at a location in the furnace, where gas temperature was about 1673 K. At this temperature rate of reduction of SiO gas was appreciable and should be accounted for in the model equations. In the numerical solution, iterations were stopped when the computed temperatures of gas and solid, and mole fractions of CO and H₂ were matched with those, specified at the bottom of bosh, within acceptable tolerance. However, computed and specified y_{SiO} could not be matched. This naturally forced us to use an adjustable parameter β_8 with the rate constant, i.e. $\beta_8 k_8$. For the present operating data sets, value of β_8 lies between 0.05 and 0.44.

6.2.2.5 Profiles of Gas Pressure

Figure 6.14 shows the longitudinal profiles of gas pressure for all four operating data sets. It may be observed that the gas pressure for all data sets increases almost linearly from 5 m to the bottom of bosh. However, increase in gas pressure from the top to 5 m height is somewhat nonlinear. Due to which, overall profile of gas pressure appears to be curved in shape. This may be attributed to the adjustable parameter β_5 used in the model in conjunction with the diameter of furnace. Since the value of β_5 for all data sets is in

between 0.48 and 0.52, therefore, its use has reduced the diameter considerably, which resulted in relatively more increase in gas velocity. Consequently, the gas pressures predicted by the model are on higher side in contrast to the operating data, because the pressure drop is directly proportional to the square of gas velocity according to the Ergun's equation (4.38). Linear profile of gas pressure between 5 m and bottom of the bosh are in accordance with the profiles reported in earlier modelling studies [Lahiri and Seshadri (1969), Yagi and Muchi (1970b), and Tate (1972)].

It is expected and logical too, that the inclusion of radial distribution of process variables in the model would improve the predictions and show a linear increase in pressure from the top to bottom of the furnace as is generally observed in practice.

6.2.3 Effect of Variation in Heat of Reaction (due to change in temperature) on the Behaviour of Blast Furnace

Figures 6.15, 6.16 and 6.17 represent the profiles of temperature, fractional conversion and mole fraction, respectively, which have been predicted by the model for operating data set-1 with the constant values of heats of reactions. Heats of reactions have been taken at the reference temperature, 298 K, and mentioned in Table 6.4.

In order to observe the effect on longitudinal profiles of process variables, Figures 6.18, 6.19 and 6.20 have been prepared, which consist of the profiles of temperature, fractional conversion and mole fraction for both the cases corresponding to the constant and variable heats of reactions. It may be noted that the effect on all profiles is significant in lower part of the shaft between 15 and 20 m height. In case of temperature profiles, temperature of gas and solid predicted by the model with constant heats of reactions are more than those predicted with variable heats of reactions. This behaviour is

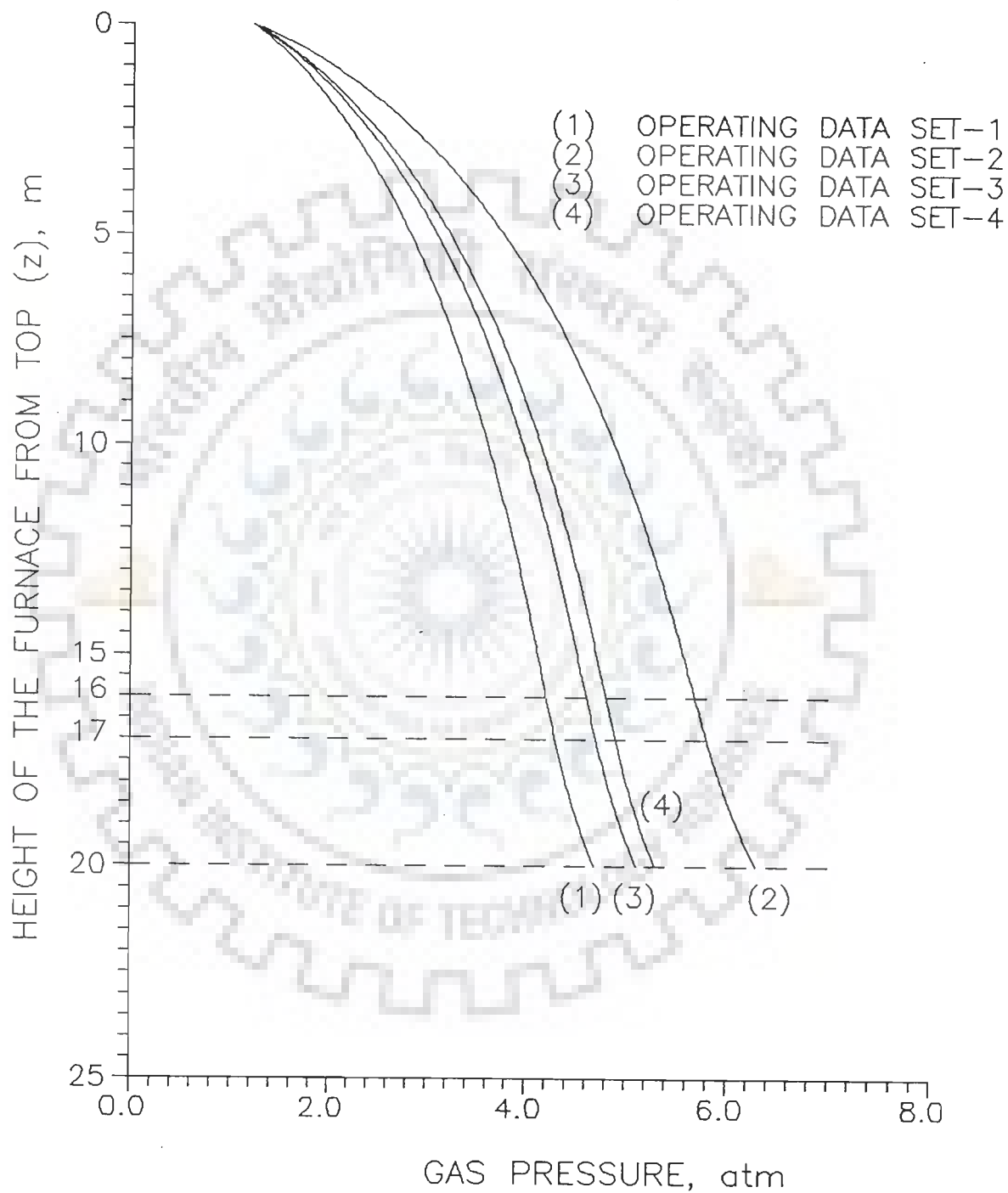


FIGURE 6.14 LONGITUDINAL PROFILES OF GAS PRESSURE FOR ALL THE FOUR OPERATING DATA SETS

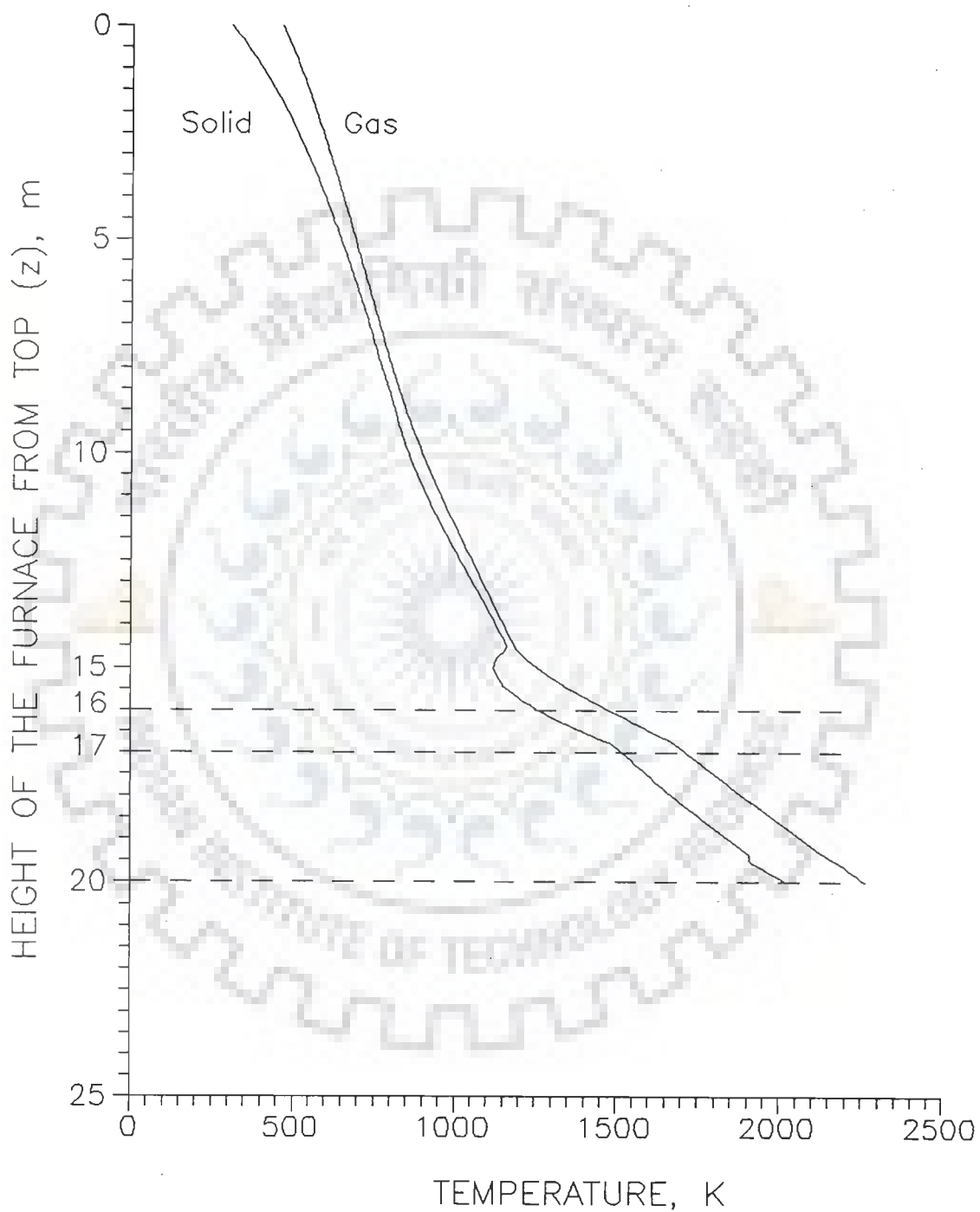


FIGURE 6.15 LONGITUDINAL PROFILES OF TEMPERATURE OF GAS AND SOLID WITH CONSTANT HEAT OF REACTION (OPERATING DATA SET-1)

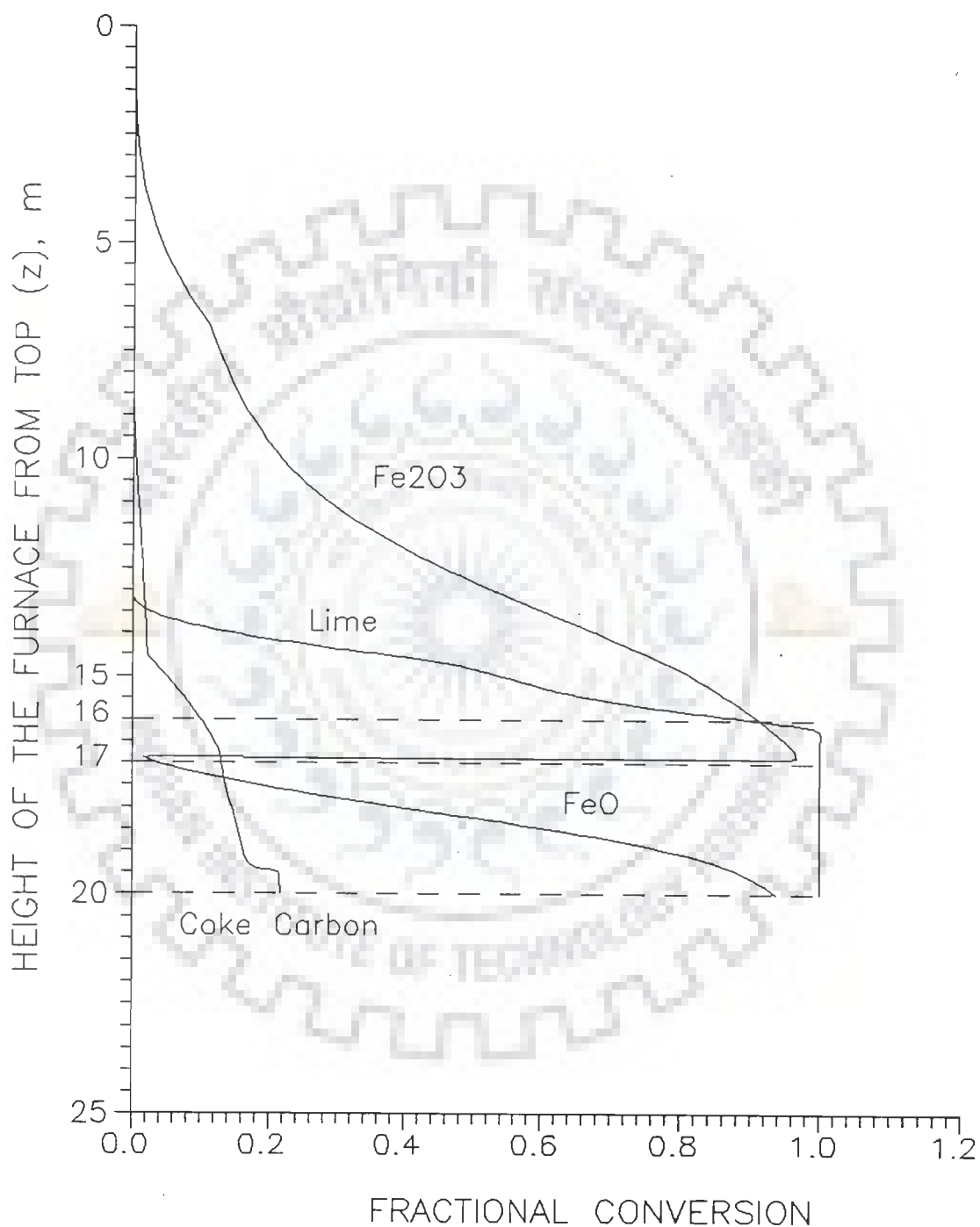


FIGURE 6.16 LONGITUDINAL PROFILES OF FRACTIONAL CONVERSION OF Fe₂O₃, LIME, COKE CARBON AND FeO WITH CONSTANT HEAT OF REACTION (OPERATING DATA SET-1)

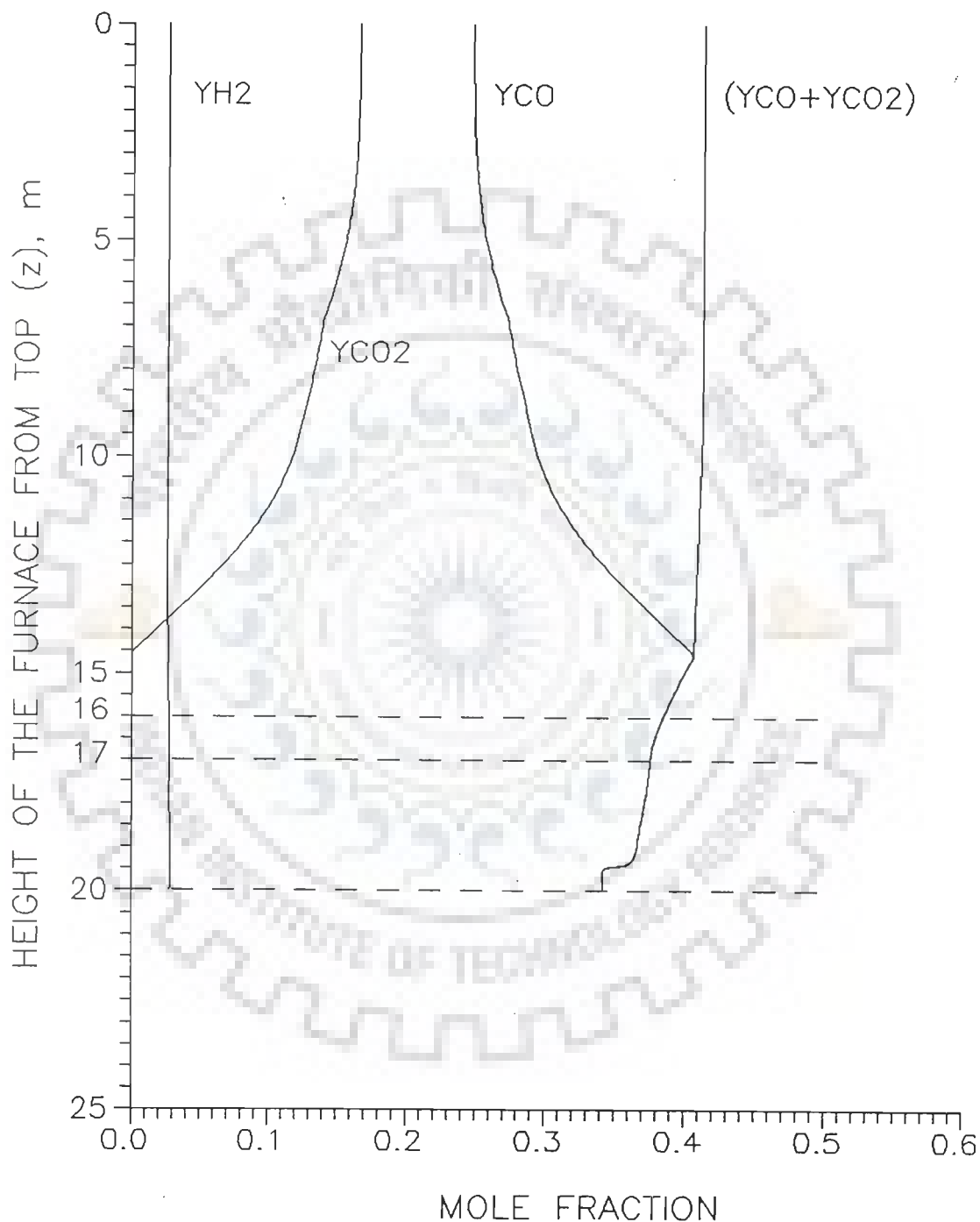


FIGURE 6.17 LONGITUDINAL PROFILES OF MOLE FRACTION OF CO, CO₂ AND H₂ WITH CONSTANT HEAT OF REACTION (OPERATING DATA SET-1)

Table 6.4 Heats of Reactions at Reference Temperature (298 K)

S.N.	Reaction	Heat of reaction
1	Indirect reduction of Fe_2O_3 by CO	-2136.1 kcal/kmol (CO)
2	Solution loss reaction	38620.4 kcal/kmol (CO_2)
3	Direct reduction of molten FeO	25356.8 kcal/kmol (FeO)
4	Decomposition of CaCO_3	42498.2 kcal/kmol (CaCO_3)
5	Indirect reduction of Fe_2O_3 by H_2	7705.0 kcal/kmol (H_2)
6	Water gas reaction	28779.3 kcal/kmol (H_2O)
7	Water gas shift reaction	-9841.1 kcal/kmol (H_2O)
8	Reduction of SiO gas	5042.9 kcal/kmol (SiO)

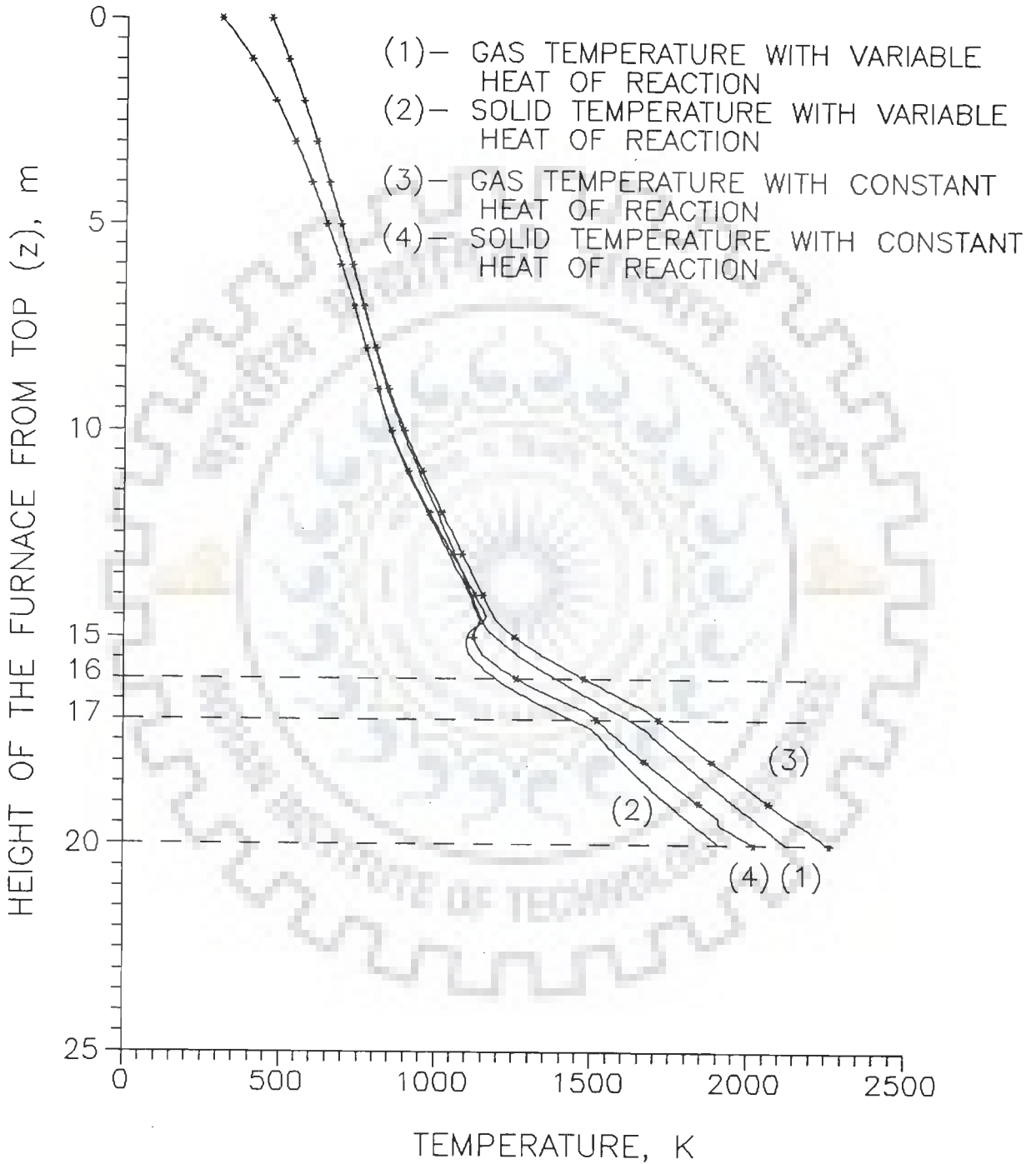


FIGURE 6.18 COMPARISON OF LONGITUDINAL PROFILES OF TEMPERATURES OF GAS AND SOLID, OBTAINED WITH CONSTANT AND VARIABLE HEAT OF REACTION (OPERATING DATA SET-1)

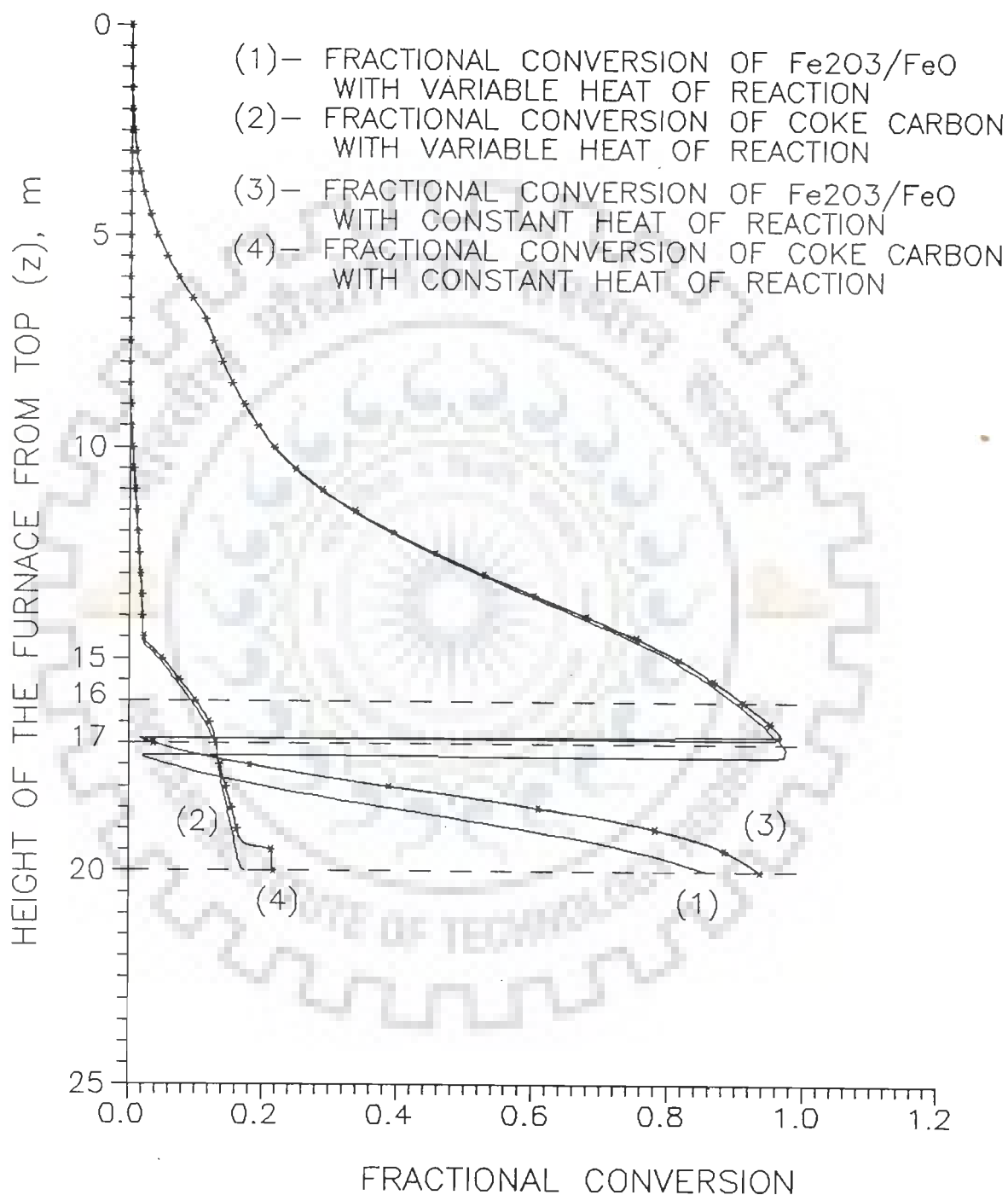


FIGURE 6.19 COMPARISON OF LONGITUDINAL PROFILES OF FRACTIONAL CONVERSIONS OF $\text{Fe}_2\text{O}_3/\text{FeO}$ AND COKE CARBON, OBTAINED WITH CONSTANT AND VARIABLE HEAT OF REACTION (OPERATING DATA SET-1)

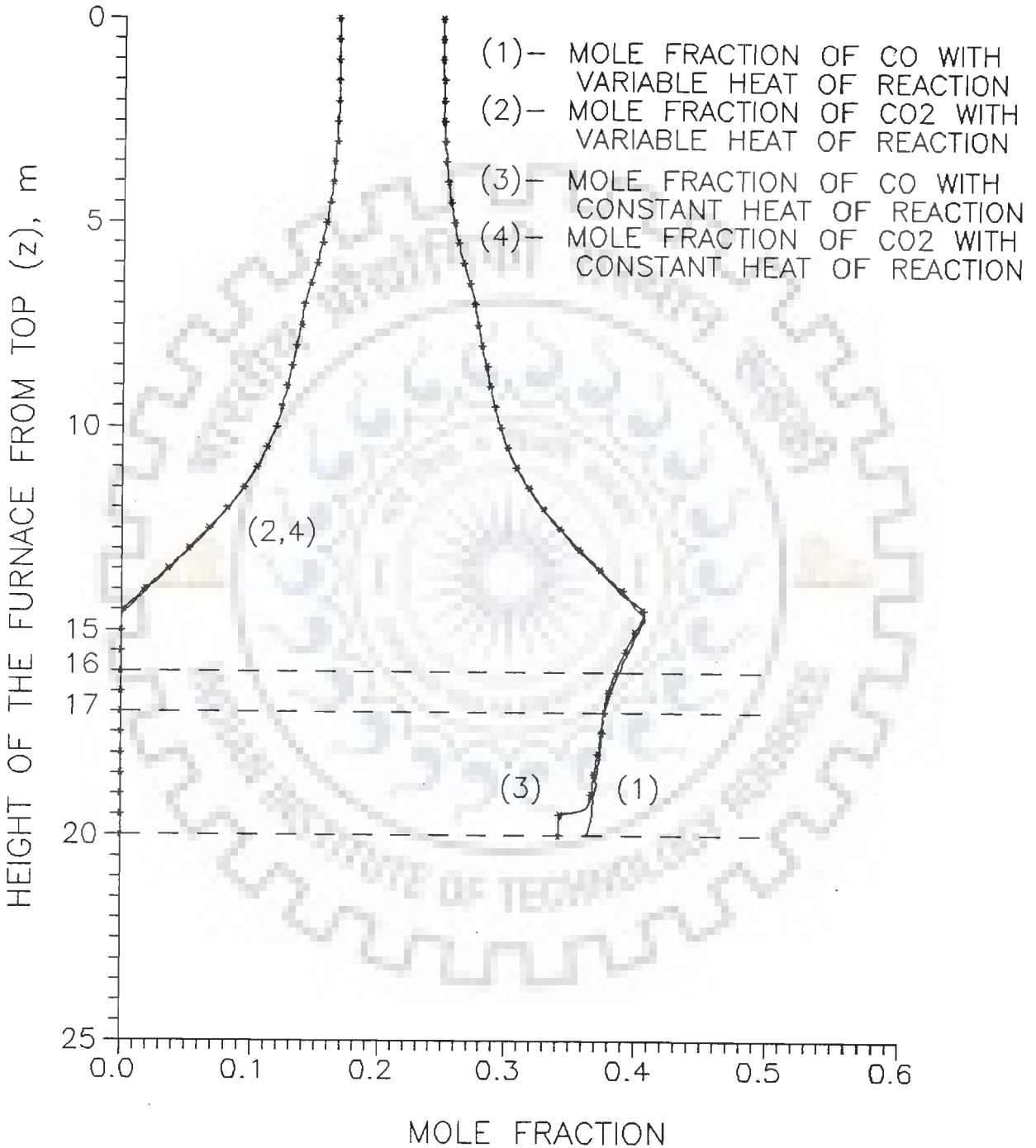


FIGURE 6.20 COMPARISON OF LONGITUDINAL PROFILES OF MOLE FRACTIONS OF CO AND CO₂, OBTAINED WITH CONSTANT AND VARIABLE HEAT OF REACTION (OPERATING DATA SET-1)

understandable because heat of reaction of an endothermic reaction decreases with the increase in temperature [Hougen et al.(1964)]. Therefore, the heat requirement of the furnace for the case of constant heat of reaction shall naturally be more than that calculated for the case of variable heat of reaction.

Increase in temperature affects the overall rates of reactions. As a result of which fractional conversions and mole fractions are bound to be affected. For fractional conversions, effect is visible between 15 and 20 m height (Figure 6.19), while it is only predominant between 19 and 20 m for mole fractions (Figure 6.20). Besides, fractional conversions predicted with constant heats of reactions are on higher side. As a consequence, mole fraction of CO at the bottom of bosh is on lower side for this case.

Figure 6.21 shows the profiles of per cent conversion of SiO gas for two cases under discussion. With variable heats of reactions, per cent conversion is only 44 at the bottom of bosh. While for the case of constant heats of reactions, 100 per cent conversion of SiO gas entering the bottom of bosh, has been achieved upto 19.4 m height only. After this height, this reaction was purposely stopped during computations otherwise it would have disrupted the other profiles. This means that more SiO gas could have been reacted with the molten metal, had it been available there in the ascending gases.

Figure 6.22 depicts the profiles of pressure for two cases. It may be observed that two profiles are almost overlapping each other and so the effect on pressure is insignificant.

In summary, it may be stated that the variation in heats of reactions with temperature affects process variables in lower part of the shaft, i.e. belly and bosh. Therefore, it is advisable to account for this effect in the modelling studies.

6.3 CONCLUDING REMARKS

On the basis of numerical solution of the steady state model equations, experiences during computation, and results obtained, it may be concluded that the developed mathematical model is suitable for studying the behaviour and performance of the shaft region of blast furnace. However, the model consists of several adjustable parameters, which is a common feature of the models of complex systems such as blast furnace. These parameters are to be estimated accurately on the basis of actual plant data, prior to its use for optimization and control purposes.



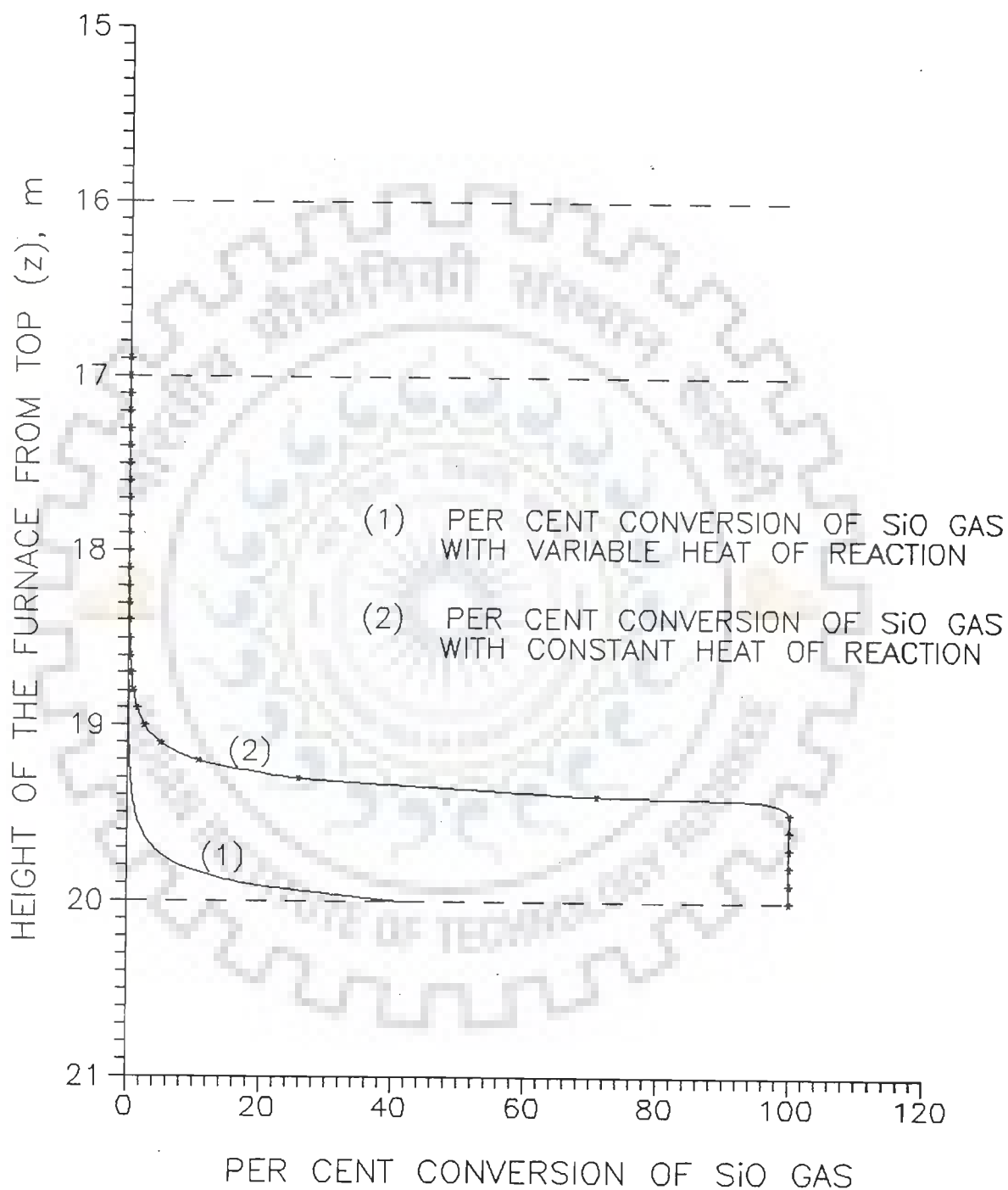


FIGURE 6.21 COMPARISON OF LONGITUDINAL PROFILES OF PER CENT CONVERSION OF SiO GAS, OBTAINED WITH CONSTANT AND VARIABLE HEAT OF REACTION (OPERATING DATA SET-1)

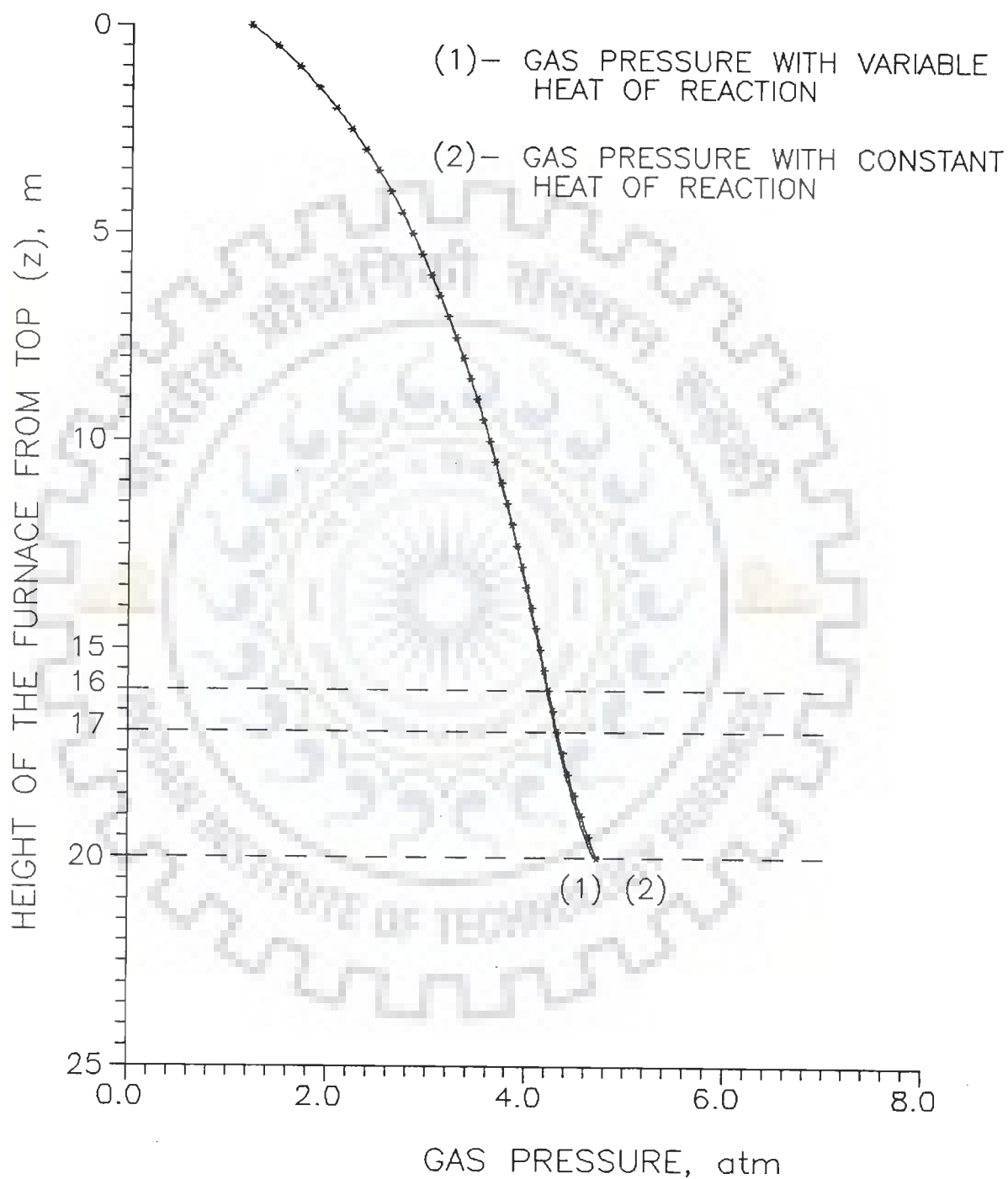


FIGURE 6.22 COMPARISON OF LONGITUDINAL PROFILES OF GAS PRESSURE, OBTAINED WITH CONSTANT AND VARIABLE HEAT OF REACTION (OPERATING DATA SET-1)

CONCLUSIONS AND RECOMMENDATIONS

7.1 CONCLUSIONS

In general, the Mathematical model of a system possesses three components, viz. model equations, boundary and initial conditions, and the constitutive relationships. In order to ascertain its suitability, validation of its predictions is also required with the results reported in literature or actual plant data. Accordingly, the conclusions of the thesis have been organized in separate subsections.

7.1.1 Model Equations

A one-dimensional mathematical model of the shaft region of blast furnace has been developed. This model consists of ten nonlinear partial differential equations (time-dependent convection equations), one ordinary differential equation and four algebraic equations. In the model, eight chemical reactions have been considered. These also include the reaction of SiO gas with carbon dissolved in molten metal, which is responsible for the transfer of Si in pig iron. The model is capable of predicting the behaviour and performance under unsteady state as well as steady state operations. However, the model equations have also been transformed into steady state model equations by setting time derivatives ($\partial/\partial t$) equal to zero. Table 7.1 provides the summary of model equations.

7.1.2 Boundary and Initial Conditions

In order to obtain the boundary conditions, the procedures for computing the material and energy balances of a blast furnace have been developed and programmed. This program calculates the boundary conditions of the proposed mathematical model by using the generally available plant data as inputs, and thus, enhances the utility of the model.

The program also computes mass flow rates, compositions and temperatures of streams, which are difficult to monitor. It may also be utilized to carry out the routine checks on the blast furnace performance in the steel plants.

An empirical correlation [equation (3.13)] has been developed to compute the melting temperature of coke ash for specified Al_2O_3 and SiO_2 contents. This is based upon the $\text{CaO-Al}_2\text{O}_3\text{-SiO}_2$ phase diagram [Muan and Osborn (1965)]. An expression [equation (3.16)] has also been obtained to calculate the molar flow rate of SiO gas formed. It has been shown that the formation of SiO gas results in the reduction of tuyere gas temperature by 150 K, which is in conformity with the observations on Indian blast furnaces [Batra (1988)].

Simplified relationships have been derived for the direct computation of adiabatic flame temperature and top gas temperature by utilizing the method of scaling the variables in polynomial equations, which were formulated as a result of energy balances around appropriate zones of blast furnace. These are as follows :

Adiabatic flame temperature

$$T_1 = \frac{-A_{10} + \sqrt{A_{10}^2 - 4 A_{15} A_9}}{2 A_9} \quad (3.42)$$

Table 7.1 Summary of Model Equations

S.N.	Process Variable	Equations	
		Dynamic model	Steady state model
		partial differential equations (p.d.e.)	ordinary differential equations (o.d.e.)
1	f_s	4.5	4.46
2	f_c	4.10	4.47
3	f_L	4.11	4.48
4	f_{sn}	4.12	4.49
5	y_{CO}	4.9	4.50
6	y_{CO_2}	4.13	4.51
7	y_{H_2}	4.14	4.52
8	y_{SiO}	4.15	4.53
9	T_g	4.29	4.54
10	T_s	4.33	4.55
11	P	o.d.e.	
		4.38	4.38
Algebraic Equations are same for both the models.			
12	F_g	4.39	
13	ρ_g	4.40	
14	ρ_b	4.41	
15	y_{H_2O}	4.44	

A_9 , A_{10} and A_{15} are defined in Section 3.2.1.

Top gas temperature

$$T_{g,0} = \left\{ -E_4 + \sqrt{E_4^2 - 4E_5} \right\} / 2.0 \quad (3.64)$$

E_4 and E_5 are defined in Section 3.2.3.

Expression for tuyere gas temperature has also been derived by taking energy balance around combustion zone, which is given below.

Tuyere gas temperature

$$T_{g,1} = \frac{B_6 T_1 + B_9}{B_8 + B_6} \quad (3.49)$$

B_6 , B_8 and B_9 are defined in Section 3.2.2.

Temperatures, predicted by using the above three equations, are of the same order of magnitude as mentioned in the literature and plant reports. It has also been shown that the tuyere gas temperature is approximately 250 K less than the adiabatic flame temperature. Therefore, it is suggested that the adiabatic flame temperature should not be used in place of tuyere gas temperature in modelling studies.

Further, the solution of steady state model equations yields the initial conditions of the dynamic model, which have been obtained for all the operating data sets. However, the solution of unsteady state model equations was not included in the scope of present doctoral work, therefore, it has not been attempted.

7.1.3 Constitutive Relationships

In the modelling of blast furnace, a large number of constitutive relationships are required. These relationships play an important role and contribute significantly to the quality of model predictions. All the required correlations/relationships have been described in Chapter V.

Besides, correlations for heats of reactions as a function of temperatures have been derived. These are mentioned in Section 5.5 for all the reactions considered in the model.

7.1.4 Numerical Solution of Model Equations and Computer Programs

Steady state model equations form a Boundary Value Problem (BVP), which are generally difficult to solve in comparison to an Initial Value Problem (IVP). Since the developed model consists of many adjustable parameters pertaining to the maldistribution of gas and solids, and uncertainties associated with the constitutive relationships, therefore, the model equations have been solved as an IVP using Runge-Kutta-Fehlberg formula and the iterations have been stopped by matching the calculated and given boundary conditions at one of the ends. It is our experience that this strategy worked very well.

Two computer programs have been developed in FORTRAN 77 ; one for carrying out material and energy balance computations and the other for obtaining the numerical solution of model equations. These programs have been executed on NEXUS 3500 (APOLLO 3500) CAD Workstation. Both the computer programs possess modular structure and are thus not specific to a particular blast furnace. Therefore, these modules may very well be used in future research programmes.

7.1.5 Validation of the Model

A blast furnace of Bokaro Steel Plant has been chosen for validating the model. The information about the dimensions of furnace and four operating data sets have been taken from the book by Tupkari (1985) and report by Batra (1988) respectively.

Table 3.4 provides the comparison of computed results, obtained by Material and Energy balance computer program, with observed data for all the operating data sets.

Predicted and observed data are quite close to each other and maximum variation is about 5 per cent. Besides, all the computed temperatures, namely adiabatic flame temperature, tuyere and top gas temperatures, are of the order of magnitude as reported in the literature. But these temperatures could not be compared with the plant data as measured values were not available.

For all the four operating data sets, longitudinal profiles of process variables, namely temperatures, compositions, fractional conversions and gas pressure, were obtained using developed computer program. Since no plant measurements were available for these parameters, hence, no comparison was possible. However, these profiles of process variables compare very well with those available in literature and their predictions may be justified on the basis of transfer and rate processes occurring in the blast furnace.

The model consists of few adjustable parameters, viz. β_4 , β_5 and β_8 . In the numerical simulation, their values have been assumed on the basis of information available in the literature, but these are to be estimated on the basis of actual plant measurements.

7.1.6 Effect of Variation in Heat of Reaction on the Behaviour of Blast Furnace

In earlier modelling studies, Heats of reactions were taken at reference temperature (298 K) and had been assumed constant throughout the computations. However, it varies with temperature significantly. It has been clearly demonstrated in Section 6.2.3 that the variation in heats of reactions affects the process behaviour significantly in lower part of the shaft, i.e. belly and bosh. Therefore, it is recommended that this variation should be accounted in the modelling studies of high temperature zones of blast furnace, where temperature is expected to be more than 1000 K.

7.1.7 Final Remark

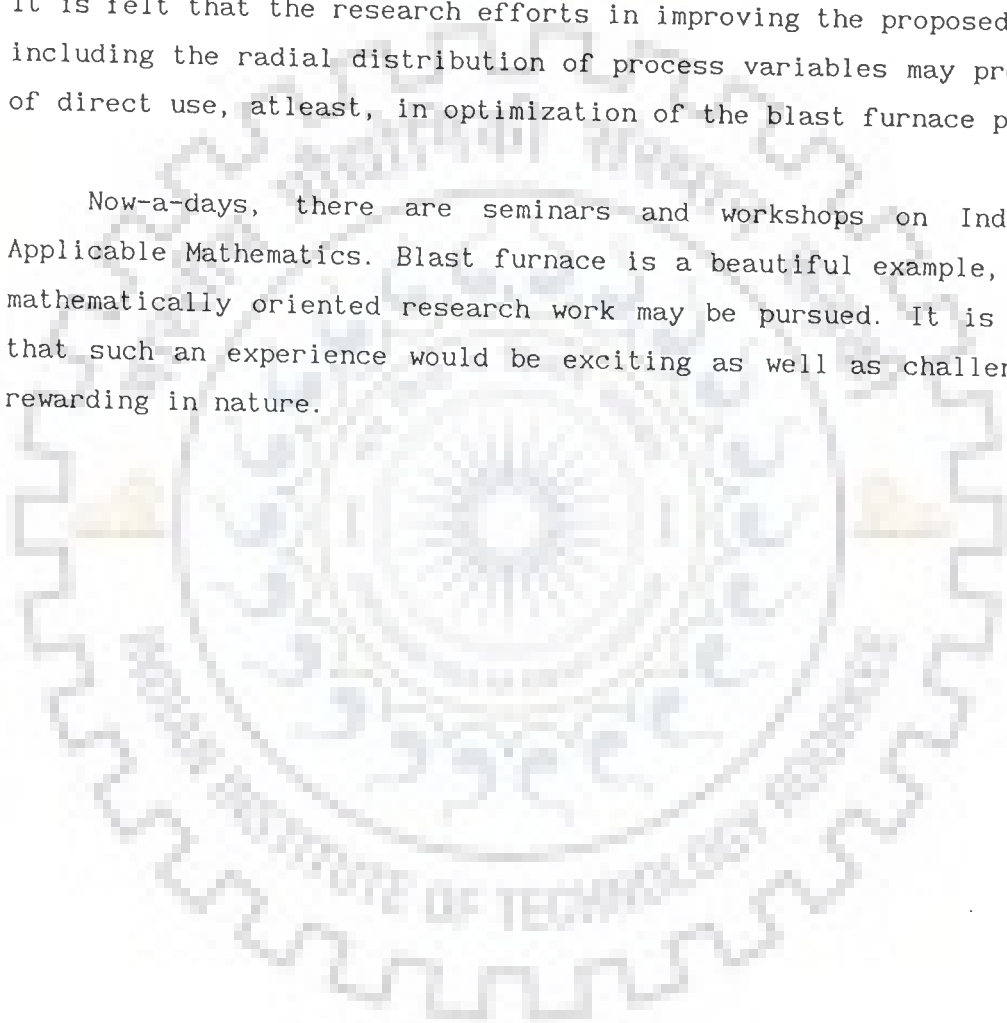
It is our view that the proposed model represents a comprehensive One-dimensional Model of the Shaft region of Blast Furnace. This may be used satisfactorily for the analysis of blast furnace process and optimization of its productivity, provided few plant data could be made available for estimating the adjustable parameters of the model.

7.2 RECOMMENDATIONS FOR FUTURE WORK

One-dimensional mathematical model of a system is comparatively more suitable for implementing advanced control techniques. Therefore, the research work may be pursued by using the proposed model for studying the dynamic behaviour and developing appropriate control strategies for improving the efficiency of the blast furnace and quality of its product.

In the proposed model, radial distribution of process variables have not been considered. But it is well known that the maldistribution of gas and solids exists in the furnace. Although many models based upon longitudinal and radial distributions of process variables have been developed and reported in the literature, but to the best of our knowledge these are not as comprehensive as expected to be. Therefore, it is felt that the research efforts in improving the proposed model by including the radial distribution of process variables may prove to be of direct use, atleast, in optimization of the blast furnace process.

Now-a-days, there are seminars and workshops on Industrially Applicable Mathematics. Blast furnace is a beautiful example, on which mathematically oriented research work may be pursued. It is our view that such an experience would be exciting as well as challenging and rewarding in nature.



REFERENCES

Agarwal, J.C., and W.L. Davis (1963)

The Significance of Fluid Dynamics in The Blast Furnace Stack
Industrial and Engineering Chemistry, Process Design and
Development, 2(1), 14.

Aris, R. (1977)

Re, k and π : a Conversation on Some Aspects of Mathematical
Modelling

Applied Mathematical Modelling, 1, 386.

Aris, R. (1979)

Chemical Reactors and Some Bifurcation Phenomena

Annals of the New York Academy of Sciences, 316, 314

Balakrishnan, A.R., and D.C.T. Pei (1979)

Heat Transfer in Gas-Solid Packed Bed Systems : A Critical Review
Industrial and Engineering Chemistry, Process Design and
Development, 18(1), 30.

Bates, M.P. (1973)

Aerodynamic Model of the Blast Furnace

J. Iron and Steel Institute, 211, 677.

Batra, N.K. (1988)

Assessment of Ironmaking Operations at Bokaro Steel Plant
Department of Metallurgical Engineering, Indian Institute of
Technology, Kanpur, India.

Bird, R.B., W.E. Stewart, and E.N. Lightfoot (1960)

Transport Phenomena

John Wiley & Sons, New York.

Biswas, A.K. (1981)

Principles of Blast Furnace Ironmaking

Cootha Publishing House, Brisbane, Australia.

Bradley, R., R.D. Gibson, and M. Cross (1981)

Case Studies in Mathematical Modelling

Pentech Press, London.

Burnside, H.E.W. (1963)

Predicting the effects of Hydrocarbon Injection on Blast Furnace Operation

Industrial and Engineering Chemistry, Process Design and Development, 2(1), 2.

Chon, M., and M. Tate (1975)

A Mathematical Model of Blast Furnace based on the Assumption of Uniform Distribution of Burden and Gas

J. Iron and Steel Institute of Japan, 61, 935.

Cordier, J.A. (1961)

Blast Furnace Injections

J. Metals, 13 (1), 31.

Davis, M.E. (1984)

Numerical Methods & Modelling for Chemical Engineers

John Wiley & Sons, New York.

Denn, M.M. (1986)

Process Modelling

Longman Scientific & Technical, Essex, U.K.

Doraiswami, L.K., and M.M. Sharma (1984)

Heterogeneous Reactions, Vol.1 : Gas-Solild and Solid-Solid
Reactions

John Wiley & Sons, New York.

Fielden, C.J., and B.I. Wood (1968)

A Dynamic Digital Simulation of the Blast Furnace
J.Iron and Steel Institute, 206, 650.

Finlayson, B.A. (1980)

Nonlinear Analysis in Chemical Engineering
McGraw - Hill, New York.

Flierman, G.A., and J.M. van Langen (1966)

Automation, Amsterdam Session, 105

[Also Published in Monograph by Omori (1987), 108].

Foust, A.S., and Associates (1960)

Principles of Unit Operations

John Wiley & Sons, New York.

Fukushima, T. (1970)

Report of 54th Committee, JSPS,
No.54-1157, July

[Also Published in Monograph by Omori (1987), 552]

Gupta, S.K., V.I. Litvinenko, and E.F. Vegmann (1990)

Iron Ore Processing and Blast Furnace Ironmaking

Oxford & IBH Publishing Co. Pvt. Ltd., New Delhi, India.

Hammond, R.H., W.B. Rogers, and J.B. Crittenden (1987)

Introduction to FORTRAN 77 and the Personal Computer
International Student Edition

McGraw-Hill Book Co., Singapore.

Hatano, M., and K. Kurita (1982)

A Mathematical Model of Blast Furnace with Radial Distribution of Gas, Heat transfer and Reactions Considered

Transactions of the Iron and Steel Institute of Japan, 22, 448.

Hatano, M., Y. Matoba, K. Otsuka, M. Yoshiki, and

T. Miyagi (1982a)

Automatic Control of Hot metal Temperature of Blast Furnace

Transactions of the Iron and Steel Institute of Japan, 22, 534.

Hatano, M., Y. Misaka, Y. Matoba, and K. Otsuka (1982)

A Mathematical Model of Blast Furnace for Control of Hot Metal Temperature

Transactions of the Iron and Steel Institute of Japan, 22, 524.

Hatano, M., and H. Yamoaka (1977)

Tetsu-to-Hagane', 63, S431

[Also Published in Monograph by Omori (1987), 263].

Hatano, M., and H. Yamoaka (1979)

Report to 54th Committee of Japan Society for Promotion of Science

[Also Published in Monograph by Omori (1987), 272].

Hougen, O.A., K.M. Watson, and R.A. Ragatz (1964)

Chemical Process Principles, Part I ; Material and Energy Balance

John Wiley & Sons, New York.

Kawai, Y., K. Mori, and M. Iguchi (1972)

Rate of Reduction of Silica in Slag by Carbon in Liquid Iron

Transactions of the Iron and Steel Institute of Japan, 12, 138.

Kay, A.R., and J. Taylor (1963)

The Silica Reduction Reaction in The Blast Furnace

J. Iron and Steel Institute, 201, 67.

Kubaschewski, O., and C.B. Alcock (1989)

Metallurgical Thermochemistry

Fifth Edition, Volume 24

Maxwell Macmillan International Editions

Pergamon Press, New York.

Koump, V., R.H. Tien, R.G. Olsson, and T.F. Perzak (1964)

Mathematical Simulation of the Stack Region of The Blast Furnace

AIME Metallurgical Society Conference, 32, 125

Gordon & Breach Science Publishers, New York.

Kubo, H., T. Nishiyama, G. Kyoguchi, M. Yasuno, S. Taguchi, and
J. Kurihara (1982)

A Dynamic One-Dimensional Simulation Model of the Blast Furnace
Process

Proceedings of Third Process Technology Conference, on Application
of Mathematical and Physical Models in the Iron and Steel
Industry, Pittsburgh, U.S.A., 3, 39.

Kunii, D., and O. Levenspiel (1969)

Fluidization Engineering

John Wiley & Sons, New York

Kuwabara, M., and I. Muchi (1977)

Mathematical Model of Blast Furnace with Radially Distributed
Burdens

Transactions of the Iron and Steel Institute of Japan, 17, 321.

Lahiri, A.K., and V. Seshadri (1969)

An Analysis of the Blast Furnace Process Based on a Dynamic Model

J. Iron and Steel Institute, 207, 293.

Levenspiel, O. (1974)

Chemical Reaction Engineering

Wiley Eastern Private Limited, New Delhi, India.

McCabe, W.L., J.C. Smith, and P. Harriott (1986)

Unit Operations of Chemical Engineering

McGraw-Hill Book Company, New York.

Miyasaka, N., M. Sugata, Y. Hara, and S. Kondo (1975)

Prediction of Blast Pressure Change by a Mathematical Model

Transactions of the Iron and Steel Institute of Japan, 15, 27.

Muan, A., and E.F. Osborn (1965)

Phase Equilibria Among Oxides in Steelmaking, Sponsored by
American Iron and Steel Institute

Addison-Wesley Publishing Company, Inc., Massachusetts, U.S.A.

Omori, Y. (1987)

Blast Furnace Phenomena and Modelling

Elsevier Applied Science, New York.

[A monograph prepared by Committee on Reaction within Blast
Furnace, The Iron and Steel Institute of Japan.]

Perry, R.H., and C.H. Chilton (1973)

Chemical Engineers' Handbook

Fifth Edition

McGraw-Hill Kogakusha, Ltd., Tokyo, Japan.

Reichardt, P. (1927)

Arch. Eisenhüttenw. 1, 77.

[Also Published in Monograph by Omori (1987), 97].

Ridgion, J.M. (1961)

Blast Furnace Performance with Injection at the Tuyeres

J. Iron and Steel Institute, 199, 135.

Ridgion, J.M. (1962)

Blast Furnace Heat Balance in Stages : Development of a Computer
Program

J. Iron and Steel Institute, 200, 389.

Sharma, S.K., and R.G. Ward (1967)

Kinetics of Silica Reduction by Carbon Saturated Iron
Part II - Reduction of Solid Silica by Carbon in Liquid Iron
J. Iron and Steel Institute, 205, 196.

Staib, C., and J. Michard (1965)

On-Line Computer Control for the Blast Furnace
J. Metals, 17, 33 and 165.

Strassburger, J.H., D.C. Brown, T.E. Dancy, and
R.L. Stepheson (1969)

Blast Furnace Theory and Practice
Gordon and Breach Science Publishers, New York.

Sugiyama, T., H. Sato, M. Nakamura, and Y. Hara (1980)

Tetsu-to-Hagane', 66, 1908

[Also Published in Monograph by Omori (1987), 446]

Szekely, J. (1977)

Reactions Between Porous Solids and Gases
Chemical Reactor Theory, Editors : L.Lapidus & N.R. Amundson
Prentice-Hall, Inc., New Jersey, 269.

Szekely, J., and M.A. Propster (1979)

Theoretical Prediction of Non-uniform Gas Flow Through Simulated
Blast Furnace Burdens

Transactions of the Iron and Steel Institute of Japan, 19, 21.

Taguchi, S., N. Tsuchiya, K. Okabe, H. Kubo, and
K. Ichifuji (1982)

Mathematical Simulation of Silicon Transfer in the Blast Furnace
Proceedings of Third Process Technology Conference on Application
of Mathematical and Physical Models in the Iron and Steel
Industry, Pittsburgh, U.S.A., 3, 25.

Takenaka, Y., Y. Kimura, K. Narita, and D. Kaneko (1986)

Mathematical Model of Direct Reduction Shaft Furnace and its Application to Actual Operations of a Model Plant
Computers and Chemical Engineering, 10 (1), 67.

Tate, M. (1972)

Process Analysis of Blast Furnace

Transactions of the Iron and Steel Institute of Japan, 12, 401.

Taylor, J. (1964)

Silica Reduction Reaction in The Blast Furnace

J. Iron and Steel Institute, 202, 420.

Togino, Y., M. Sugata, and K. Yamaguchi (1980)

Estimation of Lower Limit of Fuel Rate in Blast Furnace by Mathematical Model

Transactions of the Iron and Steel Institute of Japan, 20, 639.

Tupkari, R.H. (1985)

Introduction to Modern Ironmaking

Khanna Publishers, New Delhi, India.

Ufret, C.M., E.L. Christiansen, R.H. Spitzer, and

T.J. Williams (1981)

Mathematical Modelling and Control of the Blast Furnace Process

Report Number 122, Purdue Laboratory for Applied Industrial Control, Purdue University, Indiana.

Von Bogdandy, L. (1971)

A Kinetic and Dynamic Model of the Blast Furnace Process

Proceedings ICSTIC, Supplement Transactions of the Iron and Steel Institute of Japan, 11, 131.

- Yagi, J., and I. Muchi (1970a)**
Improved Mathematical Model for Estimating Process Variables in Blast Furnace
Transactions of the Iron and Steel Institute of Japan, 10, 181.
- Yagi, J., and I. Muchi (1970b)**
Theoretical Estimations on the Longitudinal Distributions of Process Variables in Blast Furnace and on its Productivity
Transactions of the Iron and Steel Institute of Japan, 10, 392.
- Yagi, J., and J. Szekely (1979)**
The Effect of Gas and Solids Maldistribution on the Performance of Moving-bed Reactor : The Reduction of Iron Oxide Pellets with Hydrogen
American Institute of Chemical Engineers Journal, 25 (5), 800.
- Yagi, J., and J. Szekely (1977)**
Computed Results for the Reduction of Iron Oxide Pellets in Moving Beds with Non-uniform Gas and Solids Flow
Transactions of the Iron and Steel Institute of Japan, 17, 576.
- Yagi, J., R. Takahashi, and Y. Omori (1974)**
Process Simulation of Nonisothermal Fixed Bed for Noncatalytic Reactions
Transactions of the Iron and Steel Institute of Japan, 14, 17.
- Yagi, J., K. Takeda, and Y. Omori (1982)**
Two-dimensional Simulation on the Gas Flow and Heat Transfer in the Blast Furnace
Transactions of the Iron and Steel Institute of Japan, 22, 884.
- Yagi, S., and D. Kunii (1955)**
5 th Symposium (International) on Combustion
Reinhold, New York, 231
[Also Published in Levenspiel (1974)]

 PHYSICAL PROPERTIES AND DIMENSIONS

Table A.1 Specific Heat of Substances [Kubaschewski and Alcock (1989)]

S.N.	Substance	Specific heat at constant pressure, kcal/kmol. K, $T = K$	Temperature range, K
1	$Al_2O_3^*$ (s)	$22.08 + 8.971 \times 10^{-3} T - \frac{5.225 \times 10^5}{T^2}$	273 - 1973
2	C^* (coke)	$2.93 + 2.00 \times 10^{-3} T - \frac{1.10 \times 10^5}{T^2}$	273 - 1873
3	$CaCO_3$ (s)	$24.98 + 5.25 \times 10^{-3} T - \frac{6.20 \times 10^5}{T^2}$	298 - 1200
4	CaO (s)	$11.86 + 1.08 \times 10^{-3} T - \frac{1.66 \times 10^5}{T^2}$	298 - 1177
5	CO (g)	$6.79 + 0.98 \times 10^{-3} T - \frac{0.11 \times 10^5}{T^2}$	298 - 2500
6	CO_2 (g)	$10.55 + 2.16 \times 10^{-3} T - \frac{2.04 \times 10^5}{T^2}$	298 - 2500
7	Fe (s)	$8.873 + 1.474 \times 10^{-3} T - \frac{56.92}{\sqrt{T}}$	298 - 1803
8	Fe (s)	10.00	1803 - 1873
9	FeO (s)	$11.66 + 2 \times 10^{-3} T - \frac{0.67 \times 10^5}{T^2}$	298 - 1650
10	FeO (l)	16.30	—
11	Fe_2O_3 (s)	$23.49 + 18.6 \times 10^{-3} T - \frac{3.55 \times 10^5}{T^2}$ 36.0 $31.70 + 1.76 \times 10^{-3} T$	298 - 950 950 - 1050 1050 - 1750

Table A.1 Specific Heat of Substances [Kubaschewski and Alcock (1989)]
(Continued)

S.N.	Substance	Specific heat at constant pressure kcal/kmol. K , $T = K$	Temperature range , K
12	H ₂ (g)	$6.52 + 0.78 \times 10^{-3} T - \frac{0.12 \times 10^{-5}}{T^2}$	298 - 3000
13	H ₂ O (g)	$7.17 + 2.56 \times 10^{-3} T - \frac{0.08 \times 10^5}{T^2}$	298 - 2500
14	MgO* (s)	$10.86 + 1.197 \times 10^{-3} T - \frac{2.087 \times 10^5}{T^2}$	273 - 2073
15	MnO ₂ (s)	$16.60 + 2.44 \times 10^{-3} T - \frac{3.88 \times 10^5}{T^2}$	298 - 780
16	N ₂ (g)	$6.66 + 1.02 \times 10^{-3} T$	298 - 2500
17	O ₂ (g)	$7.16 + 1.0 \times 10^{-3} T - \frac{0.40 \times 10^5}{T^2}$	298 - 3000
18	Si (s)	$5.72 + 0.59 \times 10^{-3} T - \frac{0.99 \times 10^5}{T^2}$	298 - 1700
19	Si (l)	6.12	1700 - 1873
20	SiO (g)	$7.755 + 0.57 \times 10^{-3} T - \frac{0.505 \times 10^5}{T^2}$	298 - 2500
21	SiO ₂ * (s)	$10.87 + 8.712 \times 10^{-3} T - \frac{2.412 \times 10^5}{T^2}$	273 - 848
		$17.09 + 0.454 \times 10^{-3} T - \frac{8.972 \times 10^5}{T^2}$	523 - 1973
22	Slag**	$0.4318 - 0.086 \times 10^{-3} T$ kcal / kg.K	1673 - 1973
23	Pig iron**	0.203 kcal / kg.K	1673 - 1973

* Perry and Chilton (1973)

;

** Yagi and Muchi (1970a)

Table A.2 Heat of Fusion of Substances
 [Perry and Chilton (1973)]

S.N.	Substance	Heat of fusion (Lf), kcal/kmol	Fusion temperature, K
1	Al_2O_3	26000	2318
2	CaO	19000	2980
3	Fe	3560	1803
4	FeO	7700	1650
5	MgO	18500	2915
6	Mn	3450	1493
7	MnO	13000	-
8	Si	9470	1700
9	SiO_2	3400	1743

Table A.3 Heat of Formation of Substances
 [Kubaschewski and Alcock (1989)]

S.N.	Substance	Heat of formation at 298 K, kcal/kmol
1	Al ₂ O ₃ (s)	- 400.90 × 10 ³
2	C (coke)*	2.60 × 10 ³
3	CaCO ₃ (s)	- 288.45 × 10 ³
4	CaO (s)	- 151.90 × 10 ³
5	CO (g)	- 26.4157 × 10 ³
6	CO ₂ (g)	- 94.0518 × 10 ³
7	Fe (s)	0.0
8	FeO (s)	- 63.70 × 10 ³
9	Fe ₂ O ₃ (s)	- 196.50 × 10 ³
10	H ₂ (g)	0.0
11	H ₂ O (g)	- 57.795 × 10 ³
12	MgO (s)	- 143.84 × 10 ³
13	N ₂ (g)	0.0
14	O ₂ (g)	0.0
15	Si (s)	0.0
16	SiO (g)	- 23.5 × 10 ³
17	SiO ₂ (s)	- 205.40 × 10 ³

* Hougén et al. (1964)

Table A.4 Molecular Weight of Substances

S.N.	Substance	Molecular weight	S.N.	Substance	Molecular weight
1	Al	27.00	12	Fe ₂ O ₃	159.70
2	Al ₂ O ₃	102.00	13	H ₂	2.00
3	C	12.00	14	H ₂ O	18.00
4	Ca	40.08	15	Mg	24.32
5	CaO	56.08	16	MgO	40.32
6	CaCO ₃	100.08	17	Mn	54.9
7	CO	28.00	18	MnO	70.9
8	CO ₂	44.00	19	MnO ₂	86.9
9	Fe	55.85	20	N ₂	28.00
10	FeO	71.85	21	O ₂	32.00
11	Si	28.09	22	SiO	44.09
			23	SiO ₂	60.09

Table A.5 Characteristics and Properties of Materials

S.N.	Material	Average particle diameter, m	Porosity of solid particle	Shape factor of solid particle	Density, kg/m ³
1	Iron ore	0.0200	0.40	0.50	2700
2	Sinter	0.0105	0.25	0.50	3525
3	Pellet	0.0102	0.22	0.92	3978
4	Manganese ore	0.0200	0.40	0.50	2700
5	Limestone	0.0090	0.25	0.80	1990
6	Coke	0.0400	0.45	0.72	990
7	Molten FeO	-	-	-	6600
8	Pig iron	-	-	-	6600
9	Slag	-	-	-	2600

Table A.6 Dimensions of the Shaft of Blast Furnace [Tupkari (1985)]

D_o (m)	D_b (m)	D_h (m)	L_s (m)	L_b (m)	L (m)
6.0	9.0	8.0	16.0	17.0	20.0

RUNGE - KUTTA - FEHLBERG FORMULAS FOR SYSTEM OF
ORDINARY DIFFERENTIAL EQUATIONS

This appendix describes the Runge-Kutta-Fehlberg formulas, which have been used to solve the steady state model equations.

Consider the following Initial Value Problem, which consists of n ordinary differential equations.

$$\frac{dy}{dx} = f(x, y) \quad (B.1a)$$

$$y = y_0 \text{ at } x = x_0 \quad (B.1b)$$

Where

$$y^T = [y_1 \quad y_2 \quad \dots \quad y_n] \quad (B.2)$$

$$y_0^T = [y_{10} \quad y_{20} \quad \dots \quad y_{n0}] \quad (B.3)$$

$$f^T(x, y) = [f_1(x, y) \quad f_2(x, y) \quad \dots \quad f_n(x, y)]$$

or

$$f^T = [f_1 \quad f_2 \quad \dots \quad f_n] \quad (B.4)$$

The Runge - Kutta - Fehlberg fourth order pair of formulas is as follows [Davis (1984)] :

$$y_{i+1} = y_i + \left[\frac{25}{216} k_1 + \frac{1408}{2565} k_3 + \frac{2197}{4104} k_4 - \frac{1}{5} k_5 \right] \quad (B.5)$$

$$y_{i+1}^* = y_i + \left[\frac{16}{135} k_1 + \frac{6656}{12825} k_3 + \frac{28561}{56430} k_4 - \frac{9}{50} k_5 + \frac{2}{55} k_6 \right] \quad (\text{B.6})$$

Where

$$k_i^T = [k_{1i} \ k_{2i} \ \dots \ k_{ni}] ; i = 1 \text{ to } 6 \quad (\text{B.7})$$

Expressions for k_1 to k_6 are as follows :

$$k_1 = h f[x_i, y_i] \quad (\text{B.8})$$

$$k_2 = h f \left[\left(x_i + \frac{1}{4} h \right), \left(y_i + \frac{1}{4} k_1 \right) \right] \quad (\text{B.9})$$

$$k_3 = h f \left[\left(x_i + \frac{3}{8} h \right), \left(y_i + \frac{3}{32} k_1 + \frac{9}{32} k_2 \right) \right] \quad (\text{B.10})$$

$$k_4 = h f \left[\left(x_i + \frac{12}{13} h \right), \left(y_i + \frac{1932}{2197} k_1 - \frac{7200}{2197} k_2 + \frac{7296}{2197} k_3 \right) \right] \quad (\text{B.11})$$

$$k_5 = h f \left[\left(x_i + h \right), \left(y_i + \frac{439}{216} k_1 - 8 k_2 + \frac{3680}{513} k_3 - \frac{845}{4104} k_4 \right) \right] \quad (\text{B.12})$$

$$k_6 = h f \left[\left(x_i + \frac{1}{2} h \right), \left(y_i - \frac{8}{27} k_1 + 2 k_2 - \frac{3544}{2565} k_3 + \frac{1859}{4104} k_4 - \frac{11}{40} k_5 \right) \right] \quad (\text{B.13})$$

